UNIVERSITY OF CALIFORNIA, SAN DIEGO

Design of Materials Configurations for Enhanced Phononic and Electronic Properties

A dissertation submitted in partial satisfaction of the requirements for the degree

Doctor of Philosophy

in

Materials Science and Engineering

by

Chiara Daraio

Committee in charge:

Professor Sungho Jin, Co-Chair
Professor Vitali F. Nesterenko, Co-Chair
Professor Prabhakar R. Bandaru
Professor Yu-Hwa Lo
Professor Edward T. Yu

2006

The dissertation of Chiara Daraio is approved, and it is acceptable in quality and form for publication on microfilm:

_____

_____

_____

_____
Co-Chair

_____
Co-Chair

University of California, San Diego

2006

DEDICATION

To my family

TABLE OF CONTENTS

LIST OF FIGURES

LIST OF TABLES

ACKNOWLEDGEMENTS

The present work has been carried out at the University of California, San Diego, within the Materials Science and Engineering Graduate Program. Firstly, I'd like to acknowledge my advisors: Prof. Sungho Jin and Prof. Vitali F. Nesterenko, to whom I'm very grateful for their valuable cooperation, patience, willingness and deep knowledge that made all my PhD work a pleasant and complete learning experience, based on the reciprocal trust and respect over the all walk together till the end of this PhD track. Their guidance and encouragement have deeply affected my life, both personally and professionally, developing in me a profound love for science, academic research and teaching. It has been a real pleasure and an honor being able to learn from them.

I also wish to express my gratefulness to my other committee members for their time and helpful suggestions: Professor Prab Bandaru, Professor Ed Yu and Professor Yu-Hwa Lo.

I cannot forget to thank the support for this program, which came almost entirely from the NSF (Grant No. DCMS03013220) and from the UC Discovery Grants. I'm also grateful for the supplemental support from the Materials Science fellowships that have granted me, in part or in full, the ability to survive in La Jolla.

I also wish to acknowledge the helpful insights of Eric Herbold and his valuable support on the numerical analysis. Dr. Li-Han Chen for the growth of the nanotubes used in this study, grad students Jeonghoon (David) Kim and Joseph AuBuchon and the two undergraduate students that have collaborated on parts of this project: Zolly Hollster and

Sophia Wang. Finally a great acknowledgment goes to Prof. A. Rao at Clemson University for providing the Y-shaped and coiled carbon nanostructures tested.

An important “thank you” goes to my whole family that always encouraged and tolerated my long experience abroad. Especially to my sister that has been close to me all along these years and helped me trough the sometimes difficult choices made despite the seemingly huge geographical distances between us.

Last but not least I’d like to thank my many good friends in San Diego: my second family in the States. Special thanks to my past and present roommates, Elena and GianMarco. Without them all this would have not been possible.

CURRICULUM VITAE

Education

- M.S./B.S., *magna cum laude,* Mechanical Engineering and Metallurgy. University of Ancona, Politecnico delle Marche, Ancona, Italy. December 2001. Final grade 110/110.

- M.S., Materials Science and Engineering, University of California, San Diego. January 2003.

- Ph.D., Materials Science and Engineering. University of California, San Diego. Expected June 16th, 2006. GPA 3.80/4.00.

Ph.D. Dissertation: "Design of Materials Configurations for Enhanced Phononic and Electronic Properties"

Research was conducted on the designing and construction of macro, micro and nano scale structural configurations of materials, and on the study of their phononic and electronic behavior. Variation of composite arrangements of granular elements with different elastic properties in a linear, chain-of-sphere, or Y-junction configurations led to a variety of novel phononic phenomena and interesting physical properties, which can be potentially useful for security, communications, mechanical and biomedical engineering applications. Phononic, mechanical and electronic properties of carbon nanotubes with different atomic arrangements and microstructures were also investigated. Electronic properties of Y-junction configured carbon nanotubes exhibit an exciting transistor switch behavior which is not seen in linear configuration nanotubes.

Advisors: Prof. Sungho Jin and Prof. Vitali F. Nesterenko.

M.S. Dissertation: "Creep fracture fundamentals applied to fracture of Zircaloy".

The fundamental mechanisms of the nucleation and growth of voids in metals and alloys were reviewed and the theories applied to the creep-rupture of zirconium and irradiated Zircaloys. Experimental work focused on the microstructural characterization of pure zirconium, including as received and after tensile and creep testing.

Advisors: Prof. M. Kassner and Prof. E. Evangelista.

Honors and Awards

- Gold Award Winner, MRS Best Graduate Student Contest at the MRS 2005 Fall Meeting, November 2005.
- APS/SCCM travel award recipient, August 2005.
- Materials Science Fellowship (UC San Diego) for the year 2004-2005.
- First Prize Winner for the Rotary Club International Science award, May 2002.
- Jacobs Fellowship (UC San Diego), September 2001.
- Mention of Honor as the youngest degree graduate in mechanical engineering in the university history, Ancona, 2001.
- Special Mention of Honor for Scientific Interest of the Thesis and Publication (Dignita' di Stampa) December 2001.
- Selected as one of the ~40 nation best engineering graduate students by Animal Planet/Discovery Channel TV to participate in the filming of "Chasing Nature" episodes in Australia, October 2005.
- Selected by ESA (European Space Agency) in the Italian students representative for the International Aerospace Conference in Toulouse (FR) in September 2001.
- Italian National basketball team member (juniors) in the year 1994 and 1st division player (1992-1996).

Research Experience

- Lawrence Berkeley National Lab *(March 2003 to present)*
  Guest User at the NCEM (National Center for Electron Microscopy). Intensive TEM (Transmission Electron Microscopy) and FIB (Focused Ion Beam) characterization of nanomaterials. The analysis included a short project collaborating with Prof. R.O. Ritchie on the study of microstructural characterization of bone and dental hard tissue.

- UCSD - University of California, San Diego *(July 2002 to present)*
  Research Assistant. Characterization and electrical measurements of nanomaterials and nanoelectronic devices: carbon nanotubes Y-Junctions, TiO_2 nanotubes, various nanowires, and magnetic nanoparticles. The projects were developed in collaboration with several US institutions. Advisor: Prof. S. Jin.

- Oregon State University – UC San Diego *(October 2000-June 2001)*
  Graduate Student Research Trainee. Mechanical testing and optical and SEM characterization of pure zirconium, aluminum and copper. The work was developed for the Master Thesis. Advisors: Prof. M.E. Kassner and E. Evangelista.

Teaching Experiences

Teaching Assistant, Materials Science and Engineering, U.C. San Diego (2004-2006)

- *"Nanomaterials and Properties"* MATS 253/MAE 267 (Graduate level, three quarters). [In addition to the basic duties, I gave several classroom lectures on nanomaterials microstructures and their analysis.]

- *"Transmission Electron Microscopy"* MATS 240B (Graduate level, one quarter). [In addition to the basic duties, I also covered several classroom lectures on TEM principles and microscopy techniques.]

Publications

Refereed Journal

1. **Daraio, C.**; Nesterenko, V.F.; Herbold, E.; Jin, S. *"Energy Trapping and Shock Disintegration in a Composite Granular Medium"* Physical Review Letters; 96, 058002, 2006.

2. **Daraio, C.**; Nesterenko, V.F.; Herbold, E.; Jin, S. *"Tunability of solitary wave properties in one dimensional strongly nonlinear phononic crystals"* Physical Review E; 73, 026610, 2006.

3. **Daraio, C.**; Nesterenko, V.F. *"Strongly nonlinear waves in a chain of polymer coated steel beads."* Physical Review E; 73, 026612, 2006.

4. Ye, X.R.; **Daraio, C.**; Wang, C.; Talbot, J. B.; Jin, S. *"Room Temperature Solvent-free Synthesis of Monodisperse Magnetite Nanocrystals"* Journal of Nanoscience & Nanotechnology; 6, 3, 852-856, 2006.

5. AuBuchon, J.F.; Chen, L.H.; **Daraio, C.**; Jin, S., "*Multibranching Carbon Nanotubes via Self-Seeded Catalysts*" Nano Letters; 6, 2, 324-328, 2006.

6. Chen, L.H.; AuBuchon, J.F.; Chen, I.C.; **Daraio, C.**; Ye, X.R.; Gapin, A.I.; Jin, S.; Wang, C. M.; "*Growth of Aligned Carbon Nanotubes on Carbon Microfibers by DC Plasma-Enhanced Chemical Vapor Deposition*" Applied Physics Letters; 88, 033103, 2006.

7. Rao, R. ; Chandrasekaran, H.; Gubbala, S. ; Sunkara, M.K. ; **Daraio**, **C.**; Jin, S., Rao, A.M. *"Synthesis of Low-Melting Metal Oxide and Sulfide Nanowires and Nanobelts"* Journal of Electronic Materials; 35, 5, 2006.

8. Park, J.; **Daraio, C.**; Jin, S.; Bandaru, P.R. *"Electrical characterization of the three-way gating capability of Y-junction carbon nanotube transistors"* Applied Physics Letters; (in press) 2006.

9. Oh, S.H.; **Daraio, C.**; Chen, L.H.; Pisanic, T.R.; Finones, R.; Jin, S., "*Significantly Accelerated Osteoblast Cell Growth on Aligned TiO_2 Nanotubes*" Journal of Biomedical & Materials Research; (in press) 2006.

10. **Daraio C.***; AuBuchon, J.F.*; Chen, L.H.; Gapin, A.I.; Jin S. *"Iron Silicide Root Formation in Carbon Nanotubes Grown by Microwave PECVD"*. Journal of Physical Chemistry B; 109, 51, 24215-24219, 2005.

11. **Daraio, C.**; Nesterenko, V.F.; Herbold, E.; Jin, S. *"Strongly nonlinear waves in a chain of Teflon beads"* Physical Review E; 72, 016603, 2005.

12. Bandaru, P.R.; **Daraio, C.**; Jin, S. and Rao, A.M. "*Novel electrical switching behavior and logic in carbon nanotube Y-junctions*" Nature Materials; 4, 663-666, 2005.

13. Nesterenko, V.F.; **Daraio, C.**; Herbold, E.B.; Jin, S. *"Anomalous wave reflection at the interface of two strongly nonlinear granular media"* Physical Review Letters; 95, 158702, 2005.

14. Oh, S.H.; Finones, R. R.; **Daraio, C.**; Chen L.-H.; Jin, S. *"Growth of nano-scale hydroxyapatite using chemically treated titanium oxide nanotubes"* Biomaterials; 26, 4938–4943, 2005.

15. Nalla, R.K.; Porter, A.E.; **Daraio**, **C.**; Minor, A.M.; Radmilovic, V.; Stach, E.A.; Tomsia, A.P. and Ritchie R.O. *"Ultrastructural examination of dentin using focused ion beam cross-sectioning and transmission electron microscopy"* Micron, 36, 672-680, 2005.

16. **Daraio, C.**; Nesterenko, V. F.; Aubuchon, J. F.; Jin, S.; "*Dynamic Nanofragmentation of Carbon Nanotubes"* Nano Letters; 4, 10, 1915-1918, 2004.

17. **Daraio, C.**; Nesterenko, V. F.; Jin, S. *"Highly Nonlinear Contact Interaction and Dynamic Energy Dissipation by Forest of Carbon Nanotubes"* Applied Physics Letters; 85, 23, 5724-5726, 2004.

18. Gothard, N.; **Daraio, C.**; Gaillard, J.; Zidan, R.; Jin S. and Rao, A. M. *"Controlled Growth of Y-Junction nanotubes using Ti-Doped Vapor catalyst"* Nano Letters; 4, 2, 213-217, 2004.

19. AuBuchon, J.F.; Chen, L.H.; Gapin, A.I.; Kim, D.W.; **Daraio, C**; Jin S.H. *"Multiple sharp bendings of carbon nanotubes during growth to produce zigzag morphology"* Nano Letters; 4, 9, 1781-1784, 2004.

20. Srivastava D.; Menon M.; **Daraio, C.**; et al. "*Vacancy-mediated mechanism of nitrogen substitution in carbon nanotubes"* Physical Review B; 69, 15, 153414, 2004.

21. Chen, L.H.; AuBuchon, J. F.; Gapin, A; **Daraio, C**.; Bandaru, P.; Jin, S.; Kim D. W.; and Yoo, I. K.; Wang, C. M. "*Control of carbon nanotube morphology by change of applied bias field during growth"* Applied Physics Letters; 85, 22, 5373-53756, 2004.

22. Gopal, V.; Radmilovic, V. R.; **Daraio, C**.; Jin, S.; Yang, P.; Stach, E. A.; *"Rapid Prototyping of Site-Specific Nanocontacts by Electron and Ion Beam Assisted Direct-Write Nanolithography"* Nano Letters; 4, 11, 2059-2063, 2004.

23. **Daraio, C.**; Nesterenko, V.F.; Rao, A. M.; Jin, S. *"Impact Response by a Forest of Coiled Carbon Nanotubes"* (submitted), 2006.

24. Quist, A.P.; Chand, A.; **Daraio, C.**; Jin, S.; Lal, R. *"An on chip detection system for activity of ion channels in bilayers supported over silicon chip nanopores"* (submitted), 2006.

25. **Daraio, C.**; Nesterenko, V.F.; Herbold, E.B. "*On the interaction of solitary waves with an interface between two strongly nonlinear granular media*" (in progress), 2006.

26. **Daraio, C.** and Nesterenko, V.F. *"Strongly nonlinear wave propagation in two-dimensional force chains"* (in progress), 2006.

27. **Daraio, C.**; Nesterenko, V.F.; Aubuchon, J.; Jin, S. *"Dynamic insulator-metal transition in a strongly nonlinear media"* (in progress), 2006.

28. **Daraio, C.**; Nesterenko, V.F.; Herbold, E.B.; Kim, J.; Wang, S. "*Strongly nonlinear waves in a diatomic chain*" (in progress), 2006

Book Chapters

"Synthesis and patterning methods for nanostructures useful for biological applications" **Daraio, C.**; Jin, S., Chapter 5 of the book "At the Building Block Level: Nanotechnology for Biology and Medicine." By G.A. Silva, Science of Knowledge Press (in progress).

Patents

"Article comprising pulse trapping composite granular medium and methods for fabricating such medium." **Daraio**, **C.**; Jin, S. and Nesterenko, V.F.; U.S. Provisional Application Serial No. 60/758,742 (filed in 2006).

Refereed Conference Proceedings

1. **Daraio, C.**; Nesterenko, V.F.; Herbold, E.; Jin, S. *"Pulse mitigation by a composite discrete medium"*. JOURNAL DE PHYSIQUE IV Proceedings DYMAT 2006, Dijon, France, (in press), 2006.

2. **Daraio, C.**; Nesterenko, V.F.; Herbold, E.; Jin, S. *"Strongly nonlinear waves in polymer based phononic crystals"*. APS – Shock Compression of Condensed Matter, AIP Conference Proceedings, Baltimore (MD), (in press), 2006.

3. Herbold, E.B.; Nesterenko, V. F.; **Daraio, C.** *"Influence of Controlled Viscous Dissipation on the Propagation of Strongly Nonlinear Waves in Stainless Steel Based Phononic Crystals"* APS - Shock Compression of Condensed Matter, AIP Conference Proceedings, Baltimore (MD), (in press), 2006.

4. **Daraio, C.**; Nesterenko, V.F.; Jin, S.; *"Strongly nonlinear waves in 3D phononic crystals"*, APS - Shock Compression of Condensed Matter, 197-200, AIP Conference Proceedings, Portland (OR), 2003.

5. Barrabes, S.; **Daraio, C.**; Kassner, M.E.; Hayes, T.A. and Wang, M.Z. *"Dynamic Restoration Mechanisms and Discontinuous Dynamic Recrystallization in α-Zirconium"*, light Metals 2002, 825-839, T. Lewis ed., Canadian Inst. of Mining, Metallurgy and Petrol. Engineers, Montreal (CA), 2002.

Invited Talks and Conference Presentations

- Caltech - California Institute of Technology, Pasadena, CA, April 2006 (invited).
- NCEM - Lawrence Berkeley National Labs, Berkeley, CA, April 2006 (invited).
- INRS-EMT - University of Quebec, Montreal, Canada, January 2006 (invited).

- MRS - Materials Research Society, Fall Meeting Boston (MA) 2005, *"Analysis of new Y-junction carbon nanotube transistors with novel three-way electrical switching and logic capability"*, Daraio, C.; Bandaru, P.; Jin, S.; Rao, A.M. November 2005, Special Student Award Session (Oral Presentation + Poster).

- APS - Shock Compression of Condensed Matter, Baltimore (MD), 2005. *"Strongly nonlinear waves in polymer based phononic crystal"* Daraio, C.; Nesterenko, V.F.; Herbold, E.B.; Jin, S. August 2005, (Oral Presentation).

- CMRR Research Review, San Diego (CA), *"Nano Island and Nano Pores Arrays by Focused Ion Beam Processing",* Daraio, C.; Jin, S. May 2005, (Oral Presentation).

- UCSD - Research Expo, San Diego (CA) *"Experimental and Numerical Analysis of Interfacial Wave Reflections in Sonic Vacua"*, March 2005, (Poster).

- TMS - Frontiers in Thin Film Growth and Nanostructured Materials, San Francisco (CA), *"Highly Nonlinear Contact Interaction, Dynamic Energy Dissipation and Nano-Fragmentation of Carbon Nanotubes",* Daraio, C.; Aubuchon, J.F.; Nesterenko, V.F.; Jin, S. February 2005, (Oral Presentation).

- APS - Shock Compression of Condensed Matter, Portland (OR), *"Strongly nonlinear waves in 3D phononic crystals",* Daraio, C.; Nesterenko, V.F.; Jin, S. July 2003, (Oral Presentation).

- IAC - International Aerospace Conference, Toulouse (FR), *"Ti-based aerospace fuel containers"*, Latini, V.; Daraio, C.; Evangelista, E. September 2001, (Poster).

Professional Memberships

- MRS - Materials Research Society,
  - Secretary and Vice-President of UCSD Student Chapter in the years 2004-2006

- APS - Applied Physics Society, Topical Group of SCCM

- TMS - The Minerals, Metals & Materials Society

ABSTRACT OF THE DISSERTATION

Design of Materials Configurations for Enhanced Phononic and Electronic Properties

by

Chiara Daraio

Doctor of Philosophy in Materials Science and Engineering

University of California, San Diego, 2006

Professor Sungho Jin, Co-Chair

Professor Vitali, F. Nesterenko, Co-Chair

The discovery of novel nonlinear dynamic and electronic phenomena is presented for the specific cases of granular materials and carbon nanotubes. This research was conducted for designing and constructing optimized macro-, micro- and nano-scale structural configurations of materials, and for studying their phononic and electronic behavior. Variation of composite arrangements of granular elements with different elastic properties in a linear chain-of-sphere, Y-junction or 3-D configurations led to a variety of novel phononic phenomena and interesting physical properties, which can be potentially useful for security, communications, mechanical and biomedical engineering

applications. Mechanical and electronic properties of carbon nanotubes with different atomic arrangements and microstructures were also investigated. Electronic properties of Y-junction configured carbon nanotubes exhibit an exciting transistor switch behavior which is not seen in linear configuration nanotubes.

Strongly nonlinear materials were designed and fabricated using novel and innovative concepts. Due to their unique strongly nonlinear and anisotropic nature, novel wave phenomena have been discovered. Specifically, violations of Snell's law were detected and a new mechanism of wave interaction with interfaces between NTPCs (Nonlinear Tunable Phononic Crystals) was established. Polymer-based systems were tested for the first time, and the tunability of the solitary waves speed was demonstrated. New materials with transformed signal propagation speed in the manageable range of 10-100 m/s and signal amplitude typical for audible speech have been developed. The enhancing of the mitigation of solitary and shock waves in 1-D chains were demonstrated and a new protective medium was designed for practical applications. 1-D, 2-D and 3-D strongly nonlinear system have been investigated providing a broad impact on the whole area of strongly nonlinear wave dynamics and creating experimental basis for new theories and models. Potential applications include (1) designing of a sound scrambler/decorder for secure voice communications, (2) improving invisibility of submarine to acoustic detection signal, (3) noise and shock wave mitigation for protection of vibration sensitive devices such as head mounted vision devices, (4) drastic compression of acoustic signals into centimeter regime impulses for artificial ear implants, hearing aid and devices for ease of conversion to electronic signals and processing, and acoustic delay lines for communication applications.

PART 1

INTRODUCTION

Background on Linear and Weakly-Nonlinear Phononic Crystals

Linear elastic phononic crystals represent a new class of materials with a periodic structure and intriguing acoustic band gap behavior. Most of the papers published on the subject though still present mostly theoretical results and the experimental research is based on periodic structures composed from liner elastic materials. Review papers on this subject are available (see for example Kushwaha, 1996). We describe below some previous results relevant to the proposed project.

Kinra and Ker, 1983 were probably the first authors who experimentally investigated pass and stop bands in periodic particulate composites. Bulgakov and Timchenko, 1984 showed that the periodicity of the medium resulted in the generation of new acoustic modes with a large velocity anisotropy and a large growth rate. The same year Lambert and Tesar performed a study on acoustic structure and propagation in highly porous, layered, fibrous materials. Page and McCulloch, 1986 described the ultrasound propagation in sintered metal powder. They noticed that ultrasonic experiments performed on a 3D percolating system made from sintered powder copper show a rapid increase in the attenuation, corresponding to a sudden decrease in the localization length for vibrations, at wavelength approaching the percolation correlation length.

Parmley, Zobrist, et al., 1995 studied the vibrational properties of a finite one-dimensional string-mass chain. The phononic band structure for a periodically massed string as well as Anderson localized gap modes for a disordered system were found based on the numerical solution of the wave equation.

Vasseur, Djafari-Roubani, et al., 1997 presented theoretical elastic band-structure results for a new geometry of two-dimensional phononic crystals: the boron nitride-like structure. The inclusions and matrix where either fluids or solids: such as carbon or tungsten (or epoxy) fibers in an epoxy (or C or W) matrix, or water cylinders (or mercury) in a mercury (or water) background. They obtained relatively large complete gaps where the propagation, perpendicular to the inclusions, of phonons in the acoustic region is forbidden. These gaps are larger for fluid/fluid than for solid/solid binary composites.

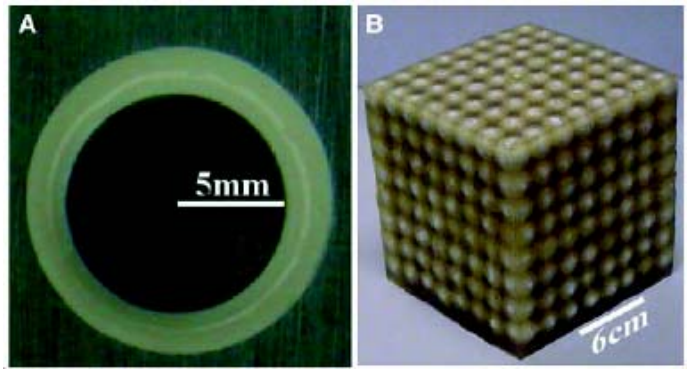

Figure 1. (a) Cross section of a coated lead sphere that forms the basic structureunit; (b) for sonic crystal. (Liu, Zhang, et al., 2000).

Kafesaki, Sigalas, and Garcia, 2000 showed that the transmittivity of wave guides created as rectilinear defects in periodic elastic band-gap materials oscillates as a function

of frequency. Results were presented for a periodic array of Pb and Ag cylinders inserted in an epoxy host, as well as for Hg cylinders in an Al.

Liu, Zhang, et al., 2000 have fabricated “sonic crystals” a few centimeters in size that are capable of blocking out everyday noise. They found that a 2 cm slab of the crystals (Figure 1) can absorb sound that would normally require a much thicker acoustic shield. Liu's team overcame this problem by creating disordered composites of the crystals and, even more interestingly they noticed that the size and geometry of the crystals can be tuned to absorb different wavelengths.

Goffaux and Vigneron, 2001 studied the control of acoustic-frequency gaps by altering the geometry of the system in the particular case of a set of parallel solid square-section columns distributed in air on a square lattice (Figure 2) which they recalled useful to prohibit the specific vibrations in accurate technologies such as transducers or sonar.

Yang, Page et al., 2002 conducted experiments with the same material and also observed a complete band gap. Inside the gap they demonstrated tunneling phenomenon. Potential applications such as ultrasound filters, sound mirrors and novel devices that exploit the anomalous refractive index and focusing properties of sonic crystals (e.g. “superlenses” or “superprisms”) were emphasized.

Weakly nonlinear effects were studied in a one-dimensional lattice with two sites per unit cell, placed respectively in a double quadratic and a parabolic substrate potential were studied by Dinda, Coquet et al., 1990. The phonon stability and phase diagram of this structure, which can represent a possible model of some hydrogen-bonded diatomic chains, were determined.

Lian-Jie and Mora, 1994 proposed an approach for modelling compressional waves in *weakly nonlinear* phononic materials at the microscopic scale. The authors took lattice site movements into account in the phononic lattice solid and name the approach "the phononic lattice solid with fluids (PLSF)" because it could lead to an improved understanding of the effect of solid-fluid interactions in wave propagation problems.

Rice, Torrance and Eikelman 1998 studied the aircraft interior vibroacoustics and the major dissipative mechanism at propeller tone frequencies including nonlinearity of frame covered by glass fibre blankets. Hou, Gong et al., 2001 studied noise effects with respect to the detection of signals and target recognition including non-linearity of signals radiated by the underwater target.

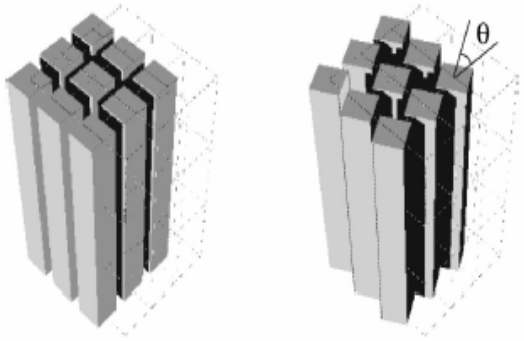

Figure 2. Geometric representation of the two-dimensional periodic systems of solid rods in air. (Goffaux and Vigneron, 2001).

Lisina, Potapov and Nesterenko, 2001 derived a *weakly nonlinear* wave equation for granular media with particle rotations and found formation of microrotational waves. Their approach provided explanation for the generation of the second shear harmonic that

is observed in real solids contrary to the predictions of the continuum nonlinear theory of elasticity.

From this review we can see that *linear* elastic phononic materials represent a very active area of basic research with important applications for the development of band filters for environmental or industrial noise, delay lines, designing vibration free environment and transducers. They also represent a class of man-made materials with evolving understanding of their properties and applications. Their properties are different than the properties of traditional materials and are based on periodic arrangement of components with elastic contrast unavailable in normal conditions. However, the major part of research is performed with "model structures" rather than with "real materials". For example the most favorable configuration for obtaining large acoustic band gaps is a periodic array of water cylinders in mercury. All examples of phononic materials are based on linear wave dynamics in periodic structures. As a result these structures can be tuned only due to awkward rearrangements in the periodic array of components. Also because sound speed of solid materials is in the range 2 – 10 km/s the tunability of band gaps is limited. It is therefore desirable to design and study new materials, which are capable of significant nonlinear tuning by convenient and viable methods.

Background on Strongly Nonlinear Phononic Crystals

In the previous section, the properties of *linear* and *weakly nonlinear* phononic crystals were described. Despite that linear phononic can be considered as a well established area of research, the tunability of phononic devices represents a serious problem. Some attempts are based on the geometrical changes of the periodic structures to tune them into desirable range of frequencies. Nonlinear properties of materials allow to make tunability much simpler based on the dependence of elastic contrast on external action, like pressure, temperature or magnetic fields.

The simplest examples of strongly nonlinear elastic materials are granular materials. By "granular material" we define an aggregate of particles in elastic contact with each other, preferably in linear or network shaped arrangements. The unusual feature of granular state is the negligible linear range of the interaction forces between neighboring particles resulting in zero sound speed in uncompressed material. This makes *linear* and *weakly nonlinear* continuum approach based on Korteveg - de Vries equation invalid and places granular materials in a special class according to their wave dynamics. This was a reason for the introduction of the concept of "sonic vacuum" - the medium where the traditional wave equation is not a basic equation for wave dynamics (Nesterenko, 2001).

If chains of granular materials are placed into a polymer matrix the nonlinear elastic behavior is preserved as manifested by strong dependence of electrical resistivity on local pressure (Jin, Sherwood, et al., 1988; Jin, Tiffel, et al., 1992). This property may potentially result in electroacoustical applications of *strongly nonlinear* phononic crystals

where metal-insulator transition is generated locally by compression in the solitary wave and propagates with nonlinear impulses inside low conductivity body.

Granular materials are highly nonlinear according to a few physically different reasons. For example, Hertz law for compression of two elastic granules (or more general power law) has no linear part even for relatively small displacements in the vicinity of zero compression. Nonlinearity also can be caused by another important reason - structural rearrangements under applied load.

Long-wave equation for *strongly nonlinear* Hertz chain and stationary solutions

As in a case of linear phononics, *strongly nonlinear* phononic materials also have a periodic structure (Figure 3), which is a reason for dispersion phenomena and for band gap in linear case. *Strongly nonlinear* materials of course may exhibit all properties of *linear* materials in the extreme case of small amplitude of elastic waves. Let us consider the main properties of strongly nonlinear systems based on 1-D model presented in Figure 3.

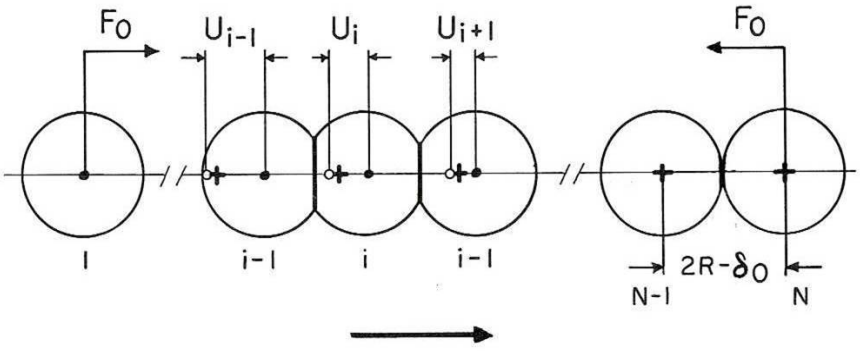

Figure 3. Weakly compressed chain of particles. The crosses represent the initial positions of the particles, the dots correspond to the current positions of spheres, the right end of the chain is undisturbed. The direction of the impulse propagation is shown by arrow (Nesterenko, 2001).

It is very important to notice that the system capable to demonstrate a strongly nonlinear behavior can also work in linear regime. The transition from nonlinear to linear behavior can be managed by the initial "prestress" of the system which can be tuned to be in strongly nonlinear mode for any wave amplitude.

We consider wave propagation in one-dimensional granular material taking into account that elastic particles interact according to the Hertz law (Landau and Lifshittz, 1986). It is assumed that a chain of identical granules with diameter *a* is subjected to constant compression forces *F* applied to both ends and securing the initial displacement δ_0 between neighboring particle centers. The particle equation of motion in descrete periodic chain becomes:

$$\begin{aligned}
&\frac{d^2 u_i}{dt^2} = A\left(\delta_0 - u_i + u_{i-1}\right)^{3/2} - A\left(\delta_0 - u_{i+1} + u_i\right)^{3/2}, \\
&N - 1 \geq i \geq 2 \\
&m = \frac{4}{3}\pi R^3 \rho_0, \\
&A = \frac{E(2R)^{1/2}}{3(1-\nu^2)m}
\end{aligned} \tag{1}$$

here *m* is the mass of the particle, *E* and ρ_0 are the Young's modules and density of particle material, *R* is the granule radius, ν is the Poisson coefficient. It is assumed that the distance between the particle centers does not exceed *a = 2R*, if particles are spherical. After anharmonic and long-wave approximations, Eq. 1 can be transformed into the nonlinear Boussinesq equation and into the Korteweg-de Vries equation (Korteweg-de Vries, 1895), if the change in the displacement δ in a wave is small. The mathematical passages to express Eq. 1 including the anharmonic approximation are included in Appendix I.

A very interesting, non-classical wave behavior appears if the granular material is weakly compressed (Nesterenko 1983, 1992, 2001). It means that the change of the neighboring particle displacements in a wave is much larger than the initial one δ_0,

resulting from the static compression. The principal difference between this case of a "weakly" compressed chain and the "strongly" compressed chain is due to the lack of a small parameter with respect to the wave amplitude in the former case. For long wave disturbance the displacements u_{i-1}, u_{i+1} in Eq. 1 (modified in such way that initial relative displacement δ_0 is included into u_i) can be expanded in a power series according to a small parameter $\varepsilon = a/L$ up to the fourth order. As a result the new wave equation for displacement is obtained:

$$
\begin{aligned}
&u_{tt} = -c^2\left\{(-u_x)^{3/2} + \frac{a^2}{10}\left[(-u_x)^{1/4}\left((-u_x)^{5/4}\right)_{xx}\right]\right\}_x, -u_x > 0,\\
&c^2 = \frac{2E}{\pi\rho_0\left(1-\nu^2\right)},\\
&c_0 = \left(\frac{3}{2}\right)^{1/2} c\xi_0^{1/4}.
\end{aligned}
\tag{2}
$$

It should be noticed that c is not a sound speed in phononic crystals (c_0 is a sound speed). In fact in general this wave equation does not have any characteristic speed of the stationary wave independent on wave amplitude. Linear and weakly nonlinear wave equations are included in the Equation 2. Despite the complex nature of the presented strongly nonliear wave equation, the stationary solutions of Equation 2 can be found in the form $u(x - Vt)$ (Nesterenko 2000, 2001).

The dependence of speed of periodic wave V_p on minimal and maximum strains (ξ_{min}, ξ_{max}, $\xi = -u_x$) can be obtained (Nesterenko, 2001). Solitary wave propagates in this

strongly nonlinear periodic phononic crystal with a speed V_s depending on the minimum ξ_0 and maximum ξ_m strains:

$$\frac{V_s}{c_0} = \frac{1}{(\xi_r - 1)}\left[\frac{4}{15}\left(3 + 2\xi_r^{5/2} - 5\xi_r\right)\right]^{1/2}. \tag{3}$$

The dependence of the phase speed of a soliton on the ratio of soliton amplitude ξ_m to the initial strain ξ_0 is shown in Figure 4 (Nesterenko, 2001). Depending on this ratio ξ_r (ξ_m/ξ_0) a broad change of velocity propagation can be achieved (also sound velocity c_0 can be arbitrary small depending on δ_0).

The existence of a solitary wave as an exact stationary solution of strongly nonlinear wave Eq. 2 is a very interesting fact because this equation is more general than the KdV equation. In a system moving with a speed V_p, the periodic solution is represented by a sequence of humps:

$$\xi = \left(\frac{5V_p^2}{4c^2}\right)^2 \cos^4\left(\frac{\sqrt{10}}{5a}x\right) = \frac{1}{8}\left(\frac{5V_p^2}{4c^2}\right)^2\left[\cos 4\left(\frac{\sqrt{10}}{5a}x\right) + 4\cos 2\left(\frac{\sqrt{10}}{5a}x\right) + 3\right]. \tag{4}$$

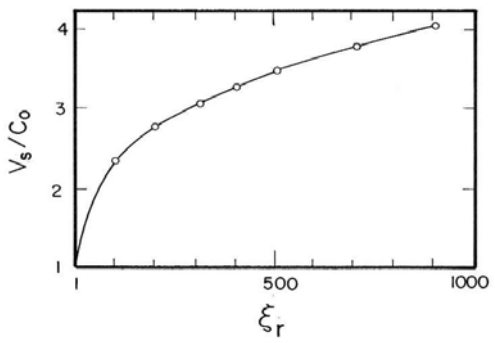

Figure 4. Ratio of the solitary wave speed V_s to the sound speed c_0 in the phononic crystal versus relative strain amplitude ξ_ρ - parameter of nonlinearity (Nesterenko, 2001).

This solution demonstrates that in a strongly nonlinear phononic crystal only two harmonics contribute to a stationary mode of propagation of stationary periodic signal! Solitary shape, if initial prestrain ξ_0 is approaching 0, can be taken as one hump of periodic solution (Eq. 4) with finite wave length equal only five particle diameters. This solitary wave is a supersonic one as well as KdV soliton. The speed of a solitary compression wave is larger than the initial velocity of sound. A unique feature of this solitary wave is the independence of its width on amplitude – the property quite different from the property of weakly nonlinear KdV solitary wave (Nesterenko, 1983, 2001). This qualitative difference is very important for using these solitary waves as information carriers and in signal transformation devices.

The speed of solitary wave V_s has a nonlinear dependence on maximum strain (particle velocity):

$$V_s = \frac{2}{\sqrt{5}} c \xi_m^{1/4} = \left(\frac{16}{25}\right)^{1/5} c^{4/5} \upsilon_m^{1/5} = \left(\frac{8E}{5\pi\rho_0\left(1-\nu^2\right)}\right)^{2/5} \upsilon_m^{1/5}. \quad (5)$$

We may see that the speed of this wave can be infinitely small if the amplitude of the wave is small! It means that using this material as a matrix in NTPCs ((Nonlinear Tunable Phononic Crystals) we can ensure infinite elastic contrast of components, important for monitoring of band gaps. At the same time speed of solitary waves can be considered as constant at any relatively narrow interval of amplitudes due to power law dependence with small exponent. These properties allow using NTPCs as effective delay lines with very low speed of signal.

A practical important result is that the speed of strongly nonlinear solitary wave V_s does not depend on particle size in the granular material. At the same time it depends on elastic properties of particles (E and v) and their density. Strictly speaking Young's modulus E and Poisson coefficient v in the equation for solitary wave speed (Eq. 5) are not properties of bulk of the particle, but of material participating in elastic contact interaction. Thus we can tailor the speed of solitary waves using composite particles. For example, the low speed of solitary waves can be ensured using heavy (for example tungsten) particles coated by materials with low Young's modulus, like polymers.

The presented theoretical results allow us to design strongly nonlinear phononic materials with exceptionally low velocity of signal propagation. Simple estimation based on Eq. 7 shows that it is possible to create materials with nonlinear impulse speed in the interval 10 – 100 m/s corresponding to audible signal. Such material can be used to transform acoustic signals on the space scale comparable to the scale of human auditory

system (ear, nerve pathways and the corresponding part of the brain) which is instrumental in acoustic signal transformation based on nerve system with speed of signal below 100 m/s.

The presented solitary wave solution (soliton with compact support, Wright, 1984; Remoissenet, 1999) describes very well the solitary impulse in an uncompressed chain, as it was verified by computer calculations and in experiments by different authors (Lazaridi and Nesterenko, 1985, Shukla, Sadd, Xu and Tai, 1993, Sinkovits and Sen, 1996, Zhu, Shukla and Sadd, 1996, Coste, Falcon, and Fauve, 1997, Manciu Sen, and Hurd, 1999, Chatterjee, 1999, Sen and Manciu, 1999, Hinch and Saint-Jean, 1999, Coste and Gilles, 1999 and others).

An analytical solution of the form $tanh(f_n)$ for stationary wave in discrete chain, where f_n is represented by series, is presented by Sen and Manciu, 1999. An asymptotic description of the tail of the soliton in discrete chain and a new asymptotic solution for the full solitary wave is found in papers by Chatterjee, 1999. A very interesting idea was proposed by Sen, M. Manciu and F. Manciu, 1999, 2000 to use these strongly nonlinear solitary waves in magnetically aligned1-D granular chains immersed in ferrofluid to generate nanodrops which are impossible to generate in any other way. If this idea will be realized then ink-jet printer of unparallel resolution can be designed.

First experiments with *Strongly Nonlinear* Solitary Waves

The qualitative and quantitative agreement of analytical and numerical results with experiments in *strongly nonlinear* phononic crystals was first observed by Lazaridi and Nesterenko, 1985. One of the remarkable features of "sonic vacuum" is evident - very rapid decomposition of initial impulse on the distances comparable with the soliton width. In fact, in this case the impulse is split after traveling only through 10 (!) first particles (Figure 5).

This remarkable feature of *strongly nonlinear* phononic crystal can be used for controlled impulse transformation in very short transmission lines of different nature. This property can not be obtained through stationary analysis of Eq. 2. This makes nonstationary analysis and establishing some scaling laws very desirable and will be one of the focuses of analytical efforts in this thesis work.

Optical observations of strongly nonlinear solitary wave were reported by Zhu, Shukla and Sadd 1996. It is very interesting that in their experiments solitary waves are formed very fast on the first 7 particles despite of a strong impulse caused by local explosive loading.

Coste, Falcon and Fauve, 1997, Coste and Gilles, 1999 conducted a very detailed quantitative study of the speed and shape of solitary wave at different soliton amplitude. The negligible decay of the soliton in 50 particles chain was found. This is a very important observation for designing of weakly dissipative NTPCs (Nonlinear, Tunable Phononic Crystals) based on 1-D chains.

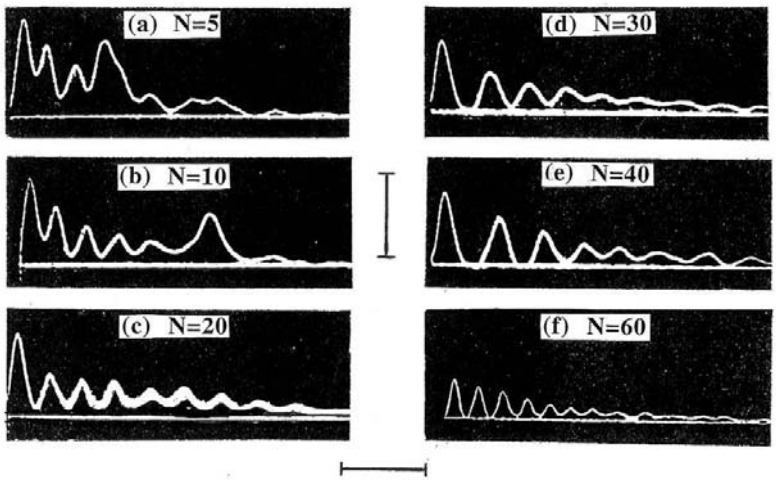

Figure 5. Evolution of the soliton train excited in experiments by striker impact (M_s=10m, u_s=0.5 m/s) with the propagation distance: (a) N = 5, (b) N = 10, (c) N = 20, (d) N = 30, (e) N = 40, (f) N = 60. Vertical scale corresponds to 80 Newton, horizontal scale to 50 μs (a),(b),(c),(d),(e) and 100 μs (f), N is number of particles (Nesterenko, 2001).

It was concluded that experimentally observed shapes of solitons in chains of spheres of different materials are in very good agreement with theoretical solitary solutions (Equations 3, 4 and 5).

It should be emphasized that the relatively low speed of wave 500 m/s detected by Coste et al., 1997 is very unusual for solid materials and corresponds to a disturbance of relatively large amplitude. At the same time the minimum of the propagation speed of a solitary wave was not experimentally established and has been one of the goals of this doctoral research. Theoretically it can be close to zero if the amplitude of disturbance is approaching zero (Eq. 5). Using polymeric and composite particles, for example, we designed NTPCs with speed of solitary wave corresponding to audible signal in the interval 10 – 100 m/s, an order of magnitude less than previously observed in experiments by Coste et al., 1997.

The elastic nonlinear interaction, described by the Hertz law and discreteness of chain are the main reasons for observed wave phenomena. Exponential attenuation of soliton amplitude is found in discrete chains for various coefficient of restitution (Manciu, Sen, and Hurd, 1999). This is important for propagation of impulses with large amplitude accompanied by plastic deformation of contacts (Nesterenko, 1994, 2001).

Impulsive External Force, Fast Decomposition into Solitons

A very attractive property of *strongly nonlinear* phononic crystals is a very fast decomposition of the initial impulse into chain of solitary waves. It is worth mentioning that quick decomposition of the initial impulse into a soliton train close to the entrance is one of the main properties of given *strongly nonlinear* system with nonlinear dispersion (Nesterenko, 2001). The reason for this behavior is connected with the fact that, in comparison with a *weak nonlinear* case, a strong *nonlinearity* does not need accumulation of small disturbances on a long travel distance before substantial changes of input signal appear. In combination with a small speed of the impulse it allows to design devices with small sizes for impulse transformation.

There are no analytical results on nonstationary wave behavior in strongly nonlinear phononic crystals. In the *weakly nonlinear* case the relation between the number of emerging solitons and the initial impulse duration is well established. Experiments are very desirable and were conducted in the course of this research to elucidate this property of *strongly nonlinear* phononic crystals. Nevertheless, the general pictures in these two cases are similar: the longer pulse creates larger number of solitons and their number is proportional to the mass of the striker.

Soliton Interaction with the Interface between Two NTPCs

The behavior of compression pulses at the contact of two NTPCs (Nonlinear Tunable Phononic Crystals) is of fundamental and practical interest. Only one specific case was studied experimentally and numerically (Nesterenko, Lazaridi and Sibiryakov, 1995). An apparent contradiction with traditional acoustics is the existence of the reflected impulse in "light" phononic crystal (despite that acoustic impedances are equal - both are zero) in case when soliton approaches interface from "light" material.

An even more unusual behavior is observed when a symmetric solitary pulse is transformed into a shock-like pulse with subsequent splitting into a soliton train in case of soliton approaching interface from the side of "heavy" phononic material. In this case no reflected impulse in "heavy" phononic crystal is recorded. The observed transformation of the impulses at contact allows such systems to transform external actions into the pulse sequence required. This proposal is focused on designing and processing layered systems containing multiple interfaces between "sonic vacuums" with different properties (densities, particle sizes and elastic constants) or between linear elastic materials and "sonic vacuums". Such materials can be effectively used for impulse transformation on relatively short distances and for pressure induced acoustic transparency.

"Soliton pulse spectroscopy" as a potential method for probing buried objects in granular beds was proposed by Sen, Manciu and Wright, 1998, Manciu, Sen and Hurd, 1999. Elastic wave interacting under some angle with interface of two *liner elastic* materials results in transmitted and reflected waves obeying Snell's law with acoustic

impedance as governing parameter. It should be emphasized that the case of wave reflection from an interface between two *strongly nonlinear* phononic crystals ("sonic vacuums") with different properties or between NTPC and linear elastic media was not investigated. Very unusual behavior due to the absence of acoustic impedance in "sonic vacuum" and strongly nonlinear dispersion may result in observation of new phenomena.

Waves in Two-Particle Periodical Chains

The behavior of a two-particle 1-D periodical chain is qualitatively different from the behavior of a chain with equal particle masses, even in case of linear interaction law. For example, in the former system, for every wave number there are two characteristic frequencies corresponding to the two branches of vibration specter - acoustical and optical. The long-wave approximation analogous to Eq. 2 can be derived using the approach proposed by Dash and Patnaik, 1981 for a weakly nonlinear case. In an extreme case when the mass of one particle is much larger than the mass of another one ($k = m_1/m_2 >> 1$) and both have the same diameter a, this equation has solitary solution only with characteristic space scale of solitary wave $L = 10a$. So, mere redistribution of masses between neighboring particles can result in wider soliton. Computer calculations were used to investigate the behavior of periodical uncompressed diaparticle chains with mass ratio $k = 2, 4, 16, 24, 64$ as well as experiments were conducted (Nesterenko, 2001). Nevertheless, behavior of strongly nonlinear two-mass phononic materials is not studied in details; particularly, the strongly nonlinear analog of an “optical” branch in a linear system is not established. Numerical and experimental efforts were undertaken to investigate properties of two-mass NTPC (Nonlinear, Tunable Phononic Crystal).

Random NTPC (Nonlinear Tunable Phononic Crystals)

The random strongly nonlinear chain of particles has properties quite different from a periodically ordered system. The former does not allow the use of the long wave analytical approach useful for a periodical chain. Important differences between an ordered and a chaotic system of particles were found in numerical calculations (Nesterenko 1992, 2001).

Short impulse loading of random chains was created by the impact of two particles. In comparison with the case of identical particles, excited by the same shape of initial impulse, the perturbation does not decompose into 2 solitons, but has a significantly random character. At the same time it is characteristic that the leading perturbation still resembles the soliton shape, demonstrating the robustness of localization even in highly randomized chains. Of course the leading pulse here is not a stationary one. The important feature is the decay in amplitude even in the absence of dissipative losses (Nesterenko, 2001).

The use of "randomized" strongly nonlinear systems for impulse "randomization" on very short distances is very desirable. At the same time this "randomization" is deterministic because it is described by Newton's laws for finite system of particles and "randomized" signal can be transformed back into initial one if properties of strongly nonlinear system are known. It is very attractive to use this property of "random" system for information packaging into "random" mode with subsequent decoding.

Nonlinear Waves in Power Law NTPCs

Stationary solutions $\xi(x - Vt)$ of wave equation similar to Eq. 2 for general power law interaction were found (Nesterenko, 1992, 1994, 2001). The cases for $n>1$ and $n<1$ represent qualitatively different behaviors of materials. The former represents normal behavior - hardening under increasing of the load and latter represents "abnormal" softening under the load. It is possible that in the different range of the load, the behavior of a real material can be essentially different with switching from $n>1$ to $n<1$.

The solitary wave phase speed V_s approaches sound speed c_0 in case if ξ_m approaches ξ_0. If $\xi_m >> \xi_0$ the compression solitary waves are the basic excitations of strongly nonlinear system characterized by the following dependence of phase velocity V_s on ξ_m, or on maximum particle velocity υ_{max} and characteristic spatial length L_n :

$$V_s = c_n \sqrt{\frac{2}{n+1}} (\xi_m)^{\frac{n-1}{2}} = \left(\frac{2c_n^2}{n+1} \right)^{\frac{1}{n+1}} (\upsilon_{max})^{\frac{n-1}{n+1}},$$
$$L_n = \frac{\pi a}{n-1} \sqrt{\frac{n(n+1)}{6}}. \qquad (6)$$

The phase velocity and the width of these solitary waves are independent of the sound velocity c_0, as opposed to the KdV solitons (where the medium properties in linear description is inherited). Soliton width in numerical calculations for chain shows very close agreement with results of continuum approximation especially for relatively small

values of exponent n (Manciu, Sen and Hurd, 1999). If n = 3/2, these equations are transformed into Eq. 5.

Materials with n<1 represent a different, "abnormal" types of behavior in comparison with n>1. In the former case, sound speed is equal to infinity if $\xi_0 = 0$. The value n <1 stipulates anomalous behavior under compression, i.e. the decrease of its elasticity modules as the deformation grows. Thus in discrete systems with abnormal compressibility, the stationary compression solitary waves are prohibited and instead the rarefaction solitary waves are allowed. No experimental results are available in these systems. At the same time such systems may exhibit very unusual transformation of input signal. A very attractive property of such system is the possibility to design the dependence of the signal speed on the exponent n in the NTPCs (Nonlinear, Tunable Phononic Crystals).

General Case of Nonlinear Discrete Systems

A continuous approximation for general interaction law between particles can be also obtained. It is possible to make some general conclusions about the properties of stationary solutions (if they exist) without finding their concrete forms based on general wave equation (Nesterenko, 1995, 2000, 2001). Particularly the strongly nonlinear compression solitary waves and shock waves (if dissipation is introduced) exist for "normal" phononic crystals ($f''(a\xi)>0$) and rarefaction solitary waves and shocks exist for "abnormal" materials ($f''(a\xi)<0$). For chains with "normal" interaction this result is similar to the condition for solitary wave existence in discrete chain (Friesecke and Wattis, 1994). It explains why continuum approximation for discrete chains is able to support the same solitary solutions.

This general conclusion is very important from a practical point of view because it demonstrates that strongly nonlinear phononic crystals exhibit similar behavior for a general class of nonlinear interaction laws and not only for power law interactions. The practical example of this type of NTPC can be a periodic array of heavy particles (W, WC) or layers embedded into a porous matrix (polymer or aluminum) considered in the following section. It is naturally expected that the porous matrix may exhibit in general a nonlinear behavior which may be enhanced by processing.

Goals of the thesis

A research plan with the aim on developing a fundamental understanding of strongly nonlinear, highly tunable phononic crystal materials was proposed. The program represented a first attempt of synergistic efforts on design, processing and characterization of such materials.

The theses has four major goals: to (1) design *strongly nonlinear*, highly tunable phononic materials based on *strongly nonlinear* wave dynamics; (2) process NTPCs (Nonlinear, Tunable Phononic Crystals) with unique properties including materials with speed of transformed acoustic signal propagation in a manageable regime of 10 -100 m/s; (3) experimentally observe new types of *strongly nonlinear* waves, travelling metal-insulator transitions, pressure induced acoustic transparency and other phenomena; (4) provide fundamental insight into *strongly nonlinear* wave dynamics of NTPC with broad impact in the whole area of strongly nonlinear dynamics.

We explored potential applications of newly designed materials including (1) a sound scrambler/decorder for secure voice communications, (2) improved invisibility of submarines to acoustic detection signals, (3) noise and shock wave mitigation for protection of vibration sensitive devices such as head mounted vision devices, (4) drastic compression of acoustic signals into centimeter regime impulses for artificial ear implants, hearing aid devices for ease of conversion to electronic signals and processing, and acoustic delay lines for communication applications.

Design and Processing of Strongly Nonlinear Tunable Phononic Crystals

One-dimensional chains of aligned particles were the basic components in the design of NTPCs. An important practical result of the theoretical approach presented earlier is that a speed of strongly nonlinear solitary wave V_s (Equations 3, 5 and 6) in such chains depends on the elastic properties of particles (E and v) and the overall density. Thus we tailored the speed of solitary waves using composite particles. Low speed of solitary waves can be ensured using heavy (for example tungsten) particles coated with material with a low Young's modulus like polymer (Young's modulus of polymers can be two order of magnitude smaller than that of steel) (Figure 6). Based on Equation 5 it is easy to show that it is possible to create materials with exceptionally low impulse speed in the interval 10 – 100 m/s in specially tailored granular chains corresponding to signal amplitude initiated by audible signal.

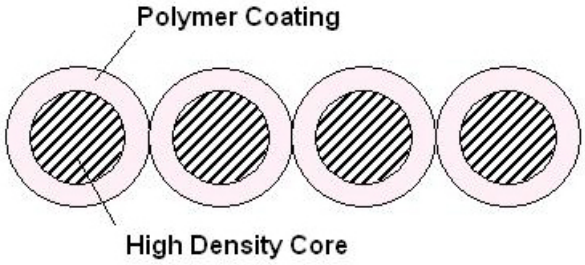

Figure 6. Chain of composite particles for NTPC with very low speed of signal propagation.

The first step in processing of NTPCs was a geometrically assisted assembling of a 3-D system from 1-D particle (composite or homogeneous) chains aligned with the help of elongated holes placed for example in hcp order (Fig. 7). A crucial problem in the designing of such system is to engage all chains simultaneously in case of impulse acting on the top plate. We solve this problem by special structuring of a over plate contacting the chains.

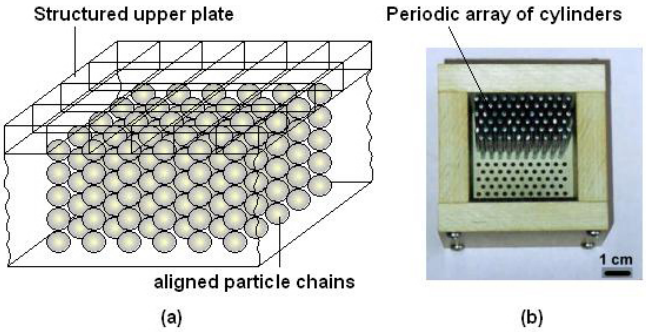

Figure 7. (a) Structure of 3-D NTPC; (b) set-up used to prepare system of holes in polymer for 1-D chains of particles.

The system shown in Figure 7(a) was be used in a few variants. In a basic set-up, which will be used on initial stage of experiments with NTPCs, 1-D chains are placed into the holes in a matrix (Figure 7(b)) and they were not connected with the matrix (which can be solid, porous, metal or polymer).

In another approach, the matrix was connected with particle chains (without affecting their contacts – origin of strongly nonlinear behavior at low amplitude of signal, Figure 8 (a)) modifying the nonlinear interactions between particles with the same sizes. This configuration allowed an enhanced dissipation if the typical frequency of the traveling wave in chains is close to the frequency of maximum dissipation in the matrix.

Important properties of strongly nonlinear system could be realized using arrangement of particles with "random" masses (Figure 8 (b)). Such systems are instrumental in transforming of audible signal into "random" disturbance. The same approach was used to process systems composed of two-mass particles and layered structures composed from particles with different masses (or elastic constants using composite particles).

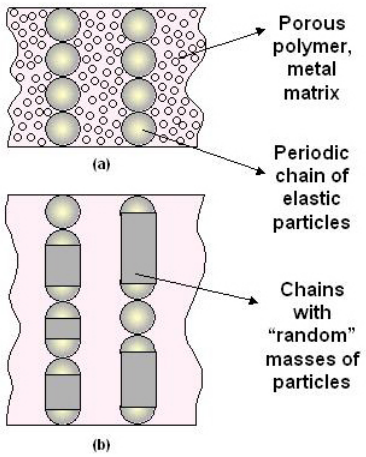

Figure 8. (a) Structure of 3-D NTPC with particles coupled with matrix; (b) system with "random" masses of particles, for example prepared by spot welding of a string of particles aligned in a quartz tube.

Different geometrical arrangement of NTPC could be realized using layers of "heavy" plates connected with "light" intermediate layers of porous material (foam) (Figure 9). In this arrangement the mass is mainly concentrated in heavy plates. Light porous layers (foam, granular materials) play a role of strongly nonlinear springs replacing the contact between particles (plates). As was theoretically demonstrated in previous section, strongly nonlinear behavior of NTPC materials can be induced not only

by direct interactions between particles as is shown in Fig. 8, but also through nonlinear characteristics of light porous intermediate layers as depicted in Fig. 9.

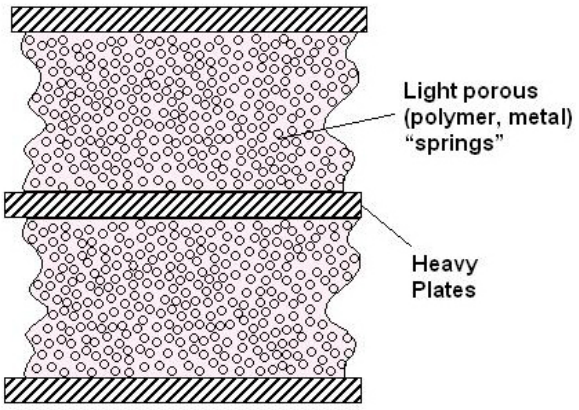

Figure 9. Laminated structure of 3-D NTPC with "heavy" solid layers and nonlinear highly porous (granular) layers.

A way to process this type of NTPC could be using a hollow sphere consolidation process or entrapped gas expansion process based on Hot Isostatic Pressing (HIPing) to ensure relative density below 0.1 of solid density and elastically nonlinear behavior of material. The latter processing for example of Al foam is based on the experimental fact that titanium hydride starts to decompose at temperature 465°C, which is well below the melting point of aluminum alloys (usually above 600°C). Dispersing titanium hydride (or other foaming agent) in solid aluminum using HIPing of powder at temperature below 465°C and then raising the temperature above 465°C allows foam manufacturing with different pore sizes (like closed-cell Alporas foams) (Banhart, 2001). Examples of high-gradient composites with periodic structure of semihollow cylinders in the titanium alloy

matrix were successfully processed for ballistic applications (Nesterenko, Indrakanti, et al., 2000).

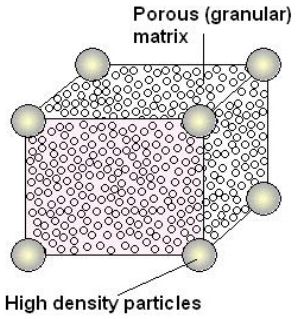

Figure 10. Periodic array of separated particles in granular (porous) matrix.

Another example of tunable NTPC can be realized by placing periodic arrays of noncontacting heavy particles into porous or granular matrix (Fig. 10, were the geometry of the system is similar to Fig. 7(a), only with particles separated by a distance larger than the diameter and then placed into the porous (granular) matrix. The prestressing of porous matrix will result in the change of nonlinear elastic contrast and distances between particles. This allows tunability of band gaps in the three directions based on the variation of two parameters – the elastic contrast of matrix and the distance between embedded particles.

A second step in processing of NTPC (Nonlinear, Tunable Phononic Crystal) could be based on the magnetic alignment and the self-assembly of particles in polymeric matrix similar to the one developed in 1988 by Jin, Sherwood et al., 1988 (Figure 11). This new class of anisotropically conductive materials is based on magnetic alignment of conductive particles in nonconductive matrix materials such as elastomeric or adhesive

polymers. These composites are able to maintain vertically aligned but laterally isolated chains of ferromagnetic metal spheres (Fig. 11).

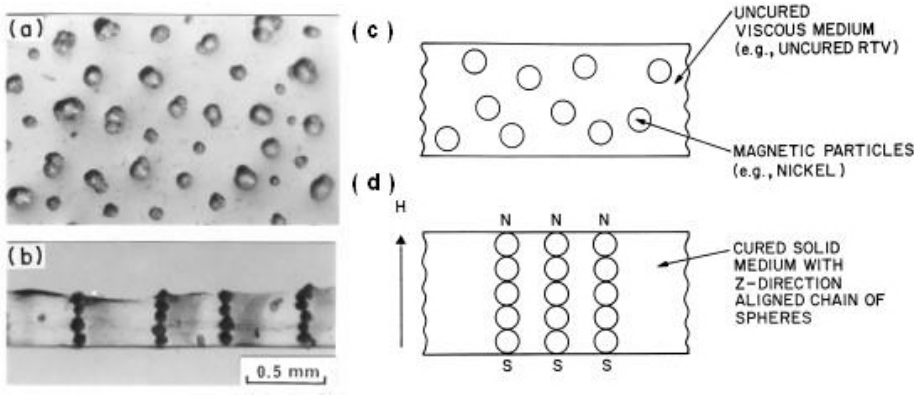

Figure 11. Z-direction aligned magnetic composite: (a), (b) micrographs showing top and cross-sectional view of magnetically aligned conductive polymer; (c) initially mixed state; (d) after alignment and cure.

This approach allowed designing an optically transparent, electrically conductive composite medium (Jin, Tiefel et al. 1992). Such a unique structure can serve as a multi-functional material combining, for example, the NTPC behavior, optical transparency, and sensor characteristics. These authors developed also an in-plane aligned, two-dimensional particle distribution (Jin, Tiefel, Chen, et al. 1993), which may be useful for design of planar NTPCs.

Tunability of NTPC was realized by inducing a static prestress on the particle chains to tune their nonlinear elastic properties like the speed of solitary wave (Eq. 7). The initial prestress, in our experiments, was controlled by magnetic field (Fig. 12(b)), or was obtained in the past by a mechanical application of pressure (Fig. 12(c)) or

controlling the temperature of material (Fig. 13). In Figures 12(b), (c) and Figure 13(a) prestress is shown by bold plane interface between neighboring particles.

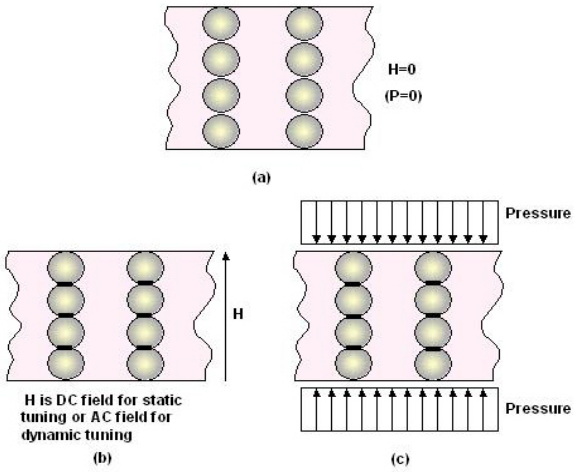

Figure 12. Tuning of initially unstressed NTPC with (a) using magnetic field (b) or mechanical compression (c).

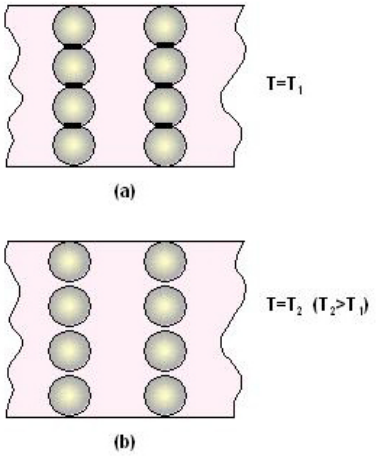

Figure 13. Temperature tuning: (a) initially prestressed NTPC.

In the latter case, chains of particles are placed into a polymer matrix polymerized under the pressure and magnetic field creating residual compression of the system. Due to at least an order of magnitude higher thermal expansion coefficient of polymers to

temperature, temperature dependent expansion of polymer matrix will allow fine tuning of NTPC.

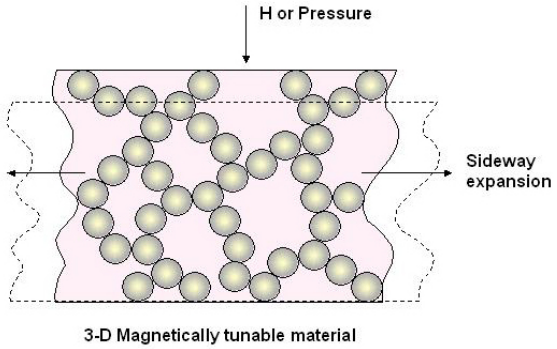

Figure 14. Tuning of complex 3-D network of "force chains" by mechanical action or magnetic field.

Magnetic tunability of NTPC with complex architecture (Jin and McCormack, 1994) is presented in Fig. 14. In this case 3-D network of spherical particles in polymer matrix are magnetically (or mechanically) deformed resulting in the destruction of some "force chains" supporting the mechanical load and changing overall elastic properties. A pressure induced strongly nonlinear softening of NPTC of such structure will not allow propagation of stationary compression pulses causing their dispersion even without energy loss.

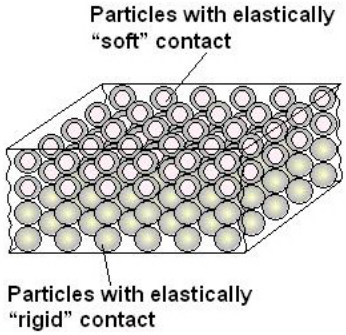

Figure 15. Laminar system of granular materials with pressure-tunable acoustic transparency.

The interesting phenomena of pressure induced transparency (unobstructed propagation of essentially all wave lengths) can be expected in a laminar system which is prepared from layers of granular materials with the same overall density but with very different elastic modulus (for example, particles in one type of layers are coated with thin layer of polymer). One cell of such laminar material is shown in Fig. 15. Due to the different nonlinear elastic contrast, multiple reflection of waves from interfaces can be naturally expected (as experimentally observed by Nesterenko, Lazaridi and Sibiryakov, 1995) reducing acoustic transparency of material. If high enough external pressure is applied to such a system, then the elastic modulus of both types of layers will become close to each other due to decreasing thickness or even removal (squeeze out) of coating material from contacts thus making the nature of the particle contacts in both layers to be essentially the same and eliminating interfaces. This will then eliminate reflection from interfaces and induce acoustic transparency of the system.

We would like to emphasize that NTPC (Nonlinear, Tunable Phononic Crystal) with presented mesostructures combine *strongly nonlinear* behavior in the Z-direction (direction of chains) and linear elastic behavior in perpendicular direction (both tunable) most probably causing very unusual wave dynamics with high potential of discovering new physical effects.

Experiments on wave dynamics in strongly nonlinear tunable phononic crystals

The first step toward the investigation of nonlinear wave dynamics in processed NTPCs was a study of the transformation of single triangular impulse generated using an impedence tube (Bruel and Kjaer System) with relatively small amplitude below 10 atm. Due to the complexity of nonlinear dynamics this approach is the most robust and efficient. It resembles approach resulted in experimental discovery of strongly nonlinear solitary waves in 1-D granular chains (Lazaridi and Nesterenko, 1985, Nesterenko, 2001). Geometric set-up for experiments is shown in Figure 16. It allows a variation of initial impulse amplitude and duration.

This type of loading produces simple boundary conditions and can be easily introduced in numerical analysis. Additional to that, this loading represents an example of blast loading where porous materials were used as blast mitigators (Nesterenko, 2001). One of potential applications of the optimized NTPCs can be also shock (high amplitude sound) mitigation caused by blast.

The set-up shown in Figure 16 will be used for impulse transformation by NTPC with different inner structure in order to establish the basic nature of the propagated signal and its dependence on the initial conditions, duration and amplitude. Impulse attenuation with depth and its transformation will be the focus of our research on the initial stage. Tuning the frequency of signals in chains to maximal damping frequency in polymer (or porous metal, ceramic) matrix will be attempted. Experiments confirming ultra low speed of signal propagation in the interval 10 – 100 m/s will be conducted using composite particles coated with polymer.

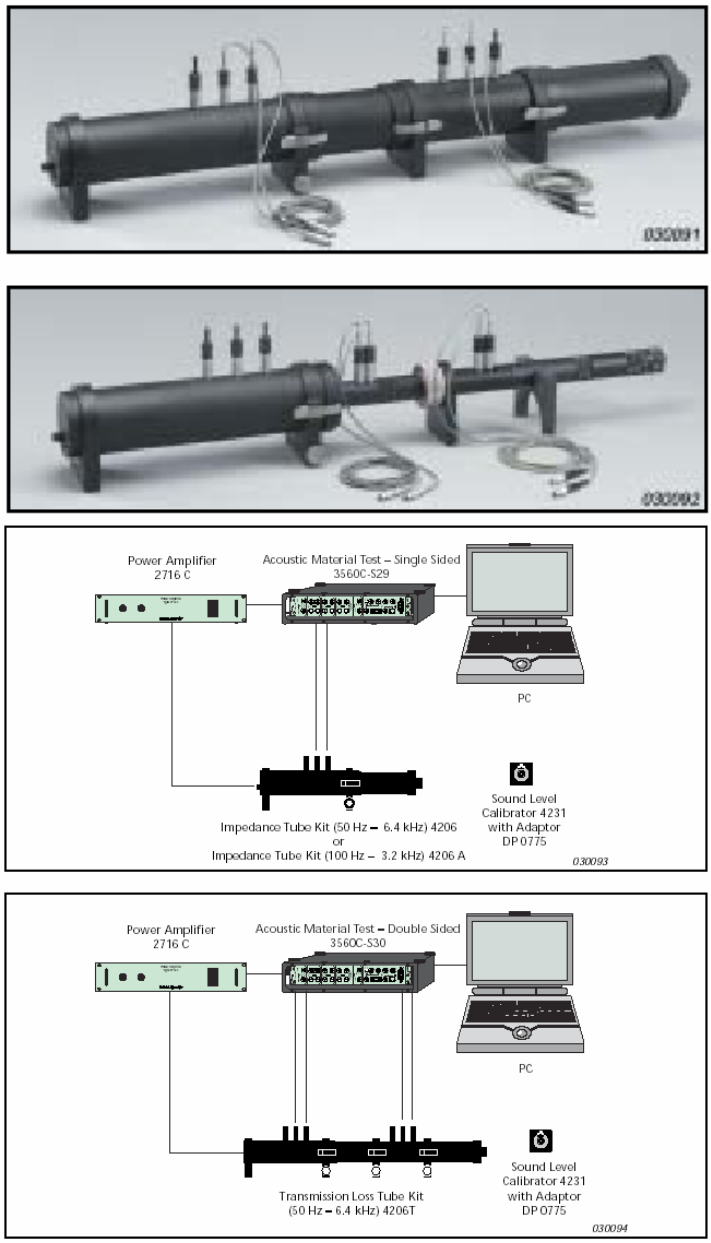

Figure 16. Experimental set-up for impulse loading of NTPCs based on B&K transmission/impedance tube.

The information obtained from the first stage of research with different NTPC will be used to interpret impulse transformation by strongly nonlinear laminar materials

on the second stage of our research. On this stage we expect the observation of a new wave phenomena connected with the interaction of strongly nonlinear waves with the interfaces of NTPCs. Preliminary experiments demonstrated that these materials indeed behave qualitatively differently in comparison with the reflection described by Snell's law in linear acoustics (Nesterenko, Lazaridi and Sibiryakov, 1995). The structure of laminar materials will be optimized to induce scattering and attenuation.

The third stage will be focused on tunability of NTPCs using mechanical and magnetic tools including MEMS devices. Expected pressure induced transparency in laminar granular NTPM will be one of the subjects.

We will explore unique properties of NTPC composed from metal particles in polymer matrix (Elastomeric Conductive Polymer Interconnect (ECPI)). These materials demonstrate highly nonlinear behavior of resistivity under compression (Figure 17, Jin, Sherwood et al., 1988, Jin, Tiefel et al., 1992). Based on the results obtained in the first stage of our experimental research we will explore the possibility to create travelling metal insulator transition (TMIT) induced by single compression solitary wave with some critical amplitude (or train of solitary waves). These phenomena may depend on the signal frequency and should be detected based on the measurement of local conductivity in preselected 1-D chain.

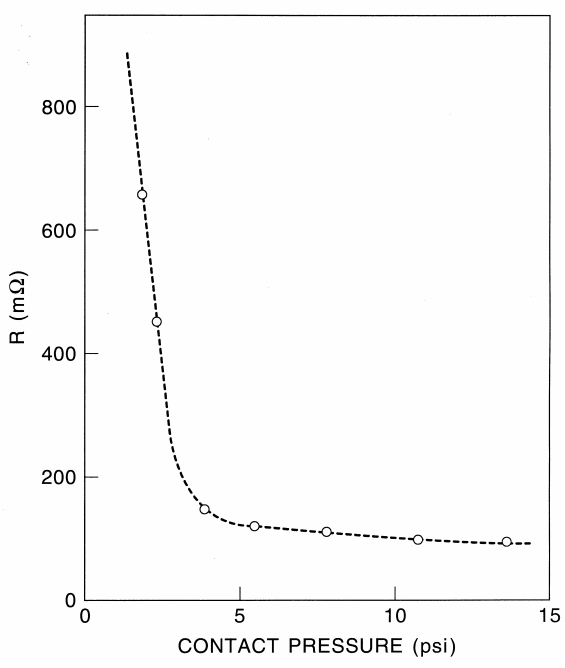

Figure 17. Electrical resistivity decrease under compression in Elastomeric Conductive Polymer material.

The mechanism of these new phenomena is shown in Figure 18. The train of TMITs is expected if the train of solitary waves is excited in the ECPI. It is practically impossible to induce TMIT effect in other materials using acoustical signal. At present, we can not identify a definite application of this unique effect. We will try to do so it in the course of our research.

Interaction of more complex waves generated by a loud speaker with NTPCs (including "random" system) will be also conducted with a goal to optimize delay lines, impulse coding/decoding, and sound transformation and absorption.

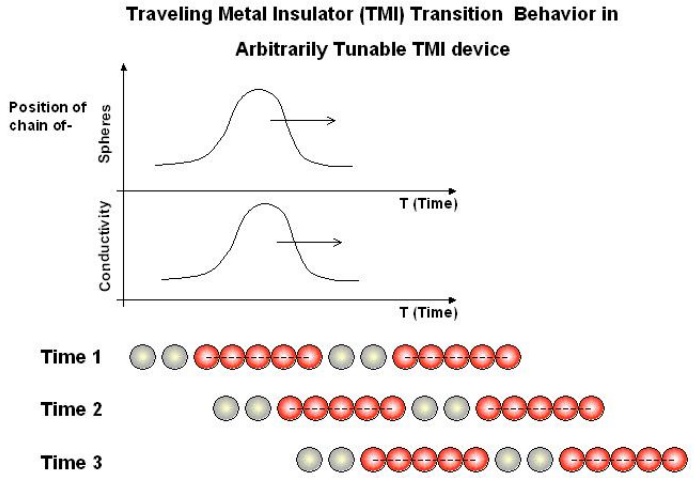

Figure 18. Traveling Metal Insulator Transition phenomenon which is likely to happen due to localized compression in solitary wave in Elastomeric Conductive Polymer.

One interesting feature of the proposed NTPCs should be emphasized. Based on their geometry they may exhibit not only strongly nonlinear properties but also high anisotropy. In the direction parallel to the periodically arranged chains of particles and perpendicular to these 1-D chains, band gaps are highly probable and our efforts will be concentrated mainly on the tunability of this band gaps based on the changing of nonlinear elastic contrast. Fine tunability of NTPCs with temperature and magnetic field will be especially emphasized.

PART 2

ONE DIMENSIONAL ANALYSIS

The study of strongly nonlinear wave propagation in one-dimensional chains of spherical beads representing the simplest model of granular materials has received much attention in recent years (Nesterenko, 1983, 1992, 1993, 1994, 1995, 2001, Lazaridi, 1985, Gavrilyuk, 1993, Shukla, 1993, Zhu, 1997, Coste, 1997, 1999, Manciu, 1999, 2001, Remoissenet, 1999, Hinch, 1999, Hong, 1999, 2001, 2005, Chatterjee, 1999, Hascoet, 2000, Sen, 2001, Arancibia-Bulnes, 2002, Rosas, 2003, 2004, Reigada, 2003, Daraio, 2003, 2004, 2005, Musienko, 2004, Kastner, 2004). One of the distinguished properties of these materials is the existence of a qualitatively new solitary wave with a finite width that is independent of solitary amplitude. This solitary wave was first discovered in 1983 analytically and numerically (Nesterenko, 1983) and later in 1985 it was observed in experiments. *Strongly* nonlinear wave dynamics is a new area of interest, which is a natural extension of *weakly* nonlinear wave dynamics described by the Korteweg-de Vries equation. Initially "strongly" precompressed, strongly nonlinear granular chains may behave as weakly nonlinear systems similar to the one considered in the Fermi-Pasta-Ulam paper (Fermi, 1965). In contrast to weakly nonlinear systems, the behavior of strongly nonlinear uncompressed granular chains exhibit qualitatively new features (Nesterenko, 1992, Hascoet, 2000, Sen, 2001, Reigada, 2003, Musienko, 2004, Kastner, 2004, Daraio, 2006). Novel applications might arise from understanding the basic physics of these 1-D systems. Sound focusing devices (tunable acoustic lenses and

delay lines), sound absorption layers and sound scramblers are among the most promising engineering applications.

Non-classical, strongly nonlinear wave behavior appears if the granular material is “weakly” compressed. In this case, the amplitude in a wave is significantly higher than the forces caused by initial precompression. The anharmonic approximation based on the small parameter (ratio of wave amplitude to initial precompression) is not valid. The principal difference between the strongly nonlinear case and the "strongly" compressed weakly nonlinear chain is due to the lack of a small parameter with respect to the wave amplitude in the former case. Long wave equation for particle displacement u in this case is expressed in Eq. 2 (on page 30). Here E, ρ, and ν are the bulk elastic modulus, density, and Poisson ratio of the particles in the chain. The particle diameter is a and ξ_0 is the initial strain in the system (phononic crystal). It should be mentioned that constant c is the same order of magnitude as the bulk sound speed in the particle material and not the sound speed in the phononic crystal. Instead parameter c_0 corresponds to a long wave sound speed related to initial strain ξ_0. This equation for high amplitude pulses (or for negligible precompression) has no characteristic wave speed that is independent on amplitude. The regularized equation and the equation for a general interaction law can be found in (Nesterenko, 2001). Despite its complex nature Eq. 2 has simple stationary solutions with unique properties that are similar to the stationary solutions for the discrete chain even though some differences due to the relatively short width of solitary wave exist. The solitary wave speed V_s in a “sonic vacuum” can be closely approximated by one hump of a periodic solution with finite length (L) equal only five particle diameters (see Eq. 4).

The concept of "sonic vacuum" was introduced to emphasize the fact that in an uncompressed chain (ξ_0=0) sound speed is equal to zero. The solitary wave speed V_s has a nonlinear dependence on maximum strain ξ_m, the particle velocity υ_m and the force between particles F_m:

$$V_s = \frac{2}{\sqrt{5}} c \xi_m^{1/4} = \left(\frac{16}{25}\right)^{1/5} c^{4/5} \upsilon_m^{1/5} = 0.68 \left(\frac{2E}{a\rho^{3/2}\left(1-\nu^2\right)}\right)^{1/3} F_m^{1/6} \ . \tag{7}$$

In a weakly compressed chain a supersonic solitary wave (V_s > c_0) with an amplitude much higher than the initial precompression propagates with a speed V_s, which can also be closely approximated by one hump of the periodic solution corresponding to zero prestress.

The speed of a wave in a "sonic vacuum" can be infinitesimally small if the amplitude of the wave is also small. It is interesting that a strongly nonlinear system supports solitary waves that are composed from a constant strain and only two harmonics (with wave length about 2.5*a* and 5*a* correspondingly) (see Eq. 4). The existence of this unique wave was verified analytically, numerically and in experiments (Lazaridi, 1985, Hinch, 1999, Coste, 1999, Chatterjee, 1999, Nesterenko, 2001, Hascoet, 2000, Sen, 2001). This solitary wave can be considered as a soliton in a physically reasonable approximation, though small amplitude secondary solitary waves were observed in numerical calculations after collision of two identical solitary waves. The ratio of the largest amplitude of the secondary wave to the amplitude of the original wave is about

0.02 (Manciu, 2001). This solitary wave is of a fundamental interest because Equation (2) is more general than the weakly nonlinear KdV equation, which describes behavior of various physical systems (Remoissenet, 1999) and the former includes the latter.

The solitary wave speed V_s in a chain with finite prestress ξ_0 due to applied static precompression for tuning can be written in terms of normalized maximum strain $\xi_r=\xi_m/\xi_0$ or force $f_r=F_m/F_0$:

$$V_s = c_0 \frac{1}{(\xi_r - 1)} \left\{ \frac{4}{15} \left[3 + 2\xi_r^{5/2} - 5\xi_r \right] \right\}^{1/2} = \\ = 0.9314 \left(\frac{4E^2 F_0}{a^2 \rho^3 (1-\nu^2)^2} \right)^{1/6} \frac{1}{\left(f_r^{2/3} - 1 \right)} \left\{ \frac{4}{15} \left[3 + 2f_r^{5/3} - 5f_r^{2/3} \right] \right\}^{1/2}. \quad (8)$$

It is important to mention that V_s can be significantly smaller than the bulk sound speed in the material composing the beads and can be considered approximately constant at any narrow interval of its relative amplitude f_r. The described properties of strongly nonlinear waves might allow the use of "sonic vacuum" based materials as effective delay lines with exceptionally low speed of signal propagation. The estimation based on Eq. (7) with Young's modulus E=600 MPa, Poisson's ratio ν=0.46 and density $\rho=2.2\cdot10^3$ kg/m^3 (DuPont) of PTFE shows that it is possible to create materials with an impulse speed below 100 m/s, which corresponds to a particle velocity of 0.2 m/s or smaller. This signal speed in condensed soft matter is below the level of sound speed in gases at normal conditions. In this chapter experimental results on pulse propagation in PTFE chains of spheres are presented in accord with the main conclusions of the outlined strongly

nonlinear theory. The speed of the signals is in the range of 88 m/s to 168 m/s. Uniformly compressed discrete chains are considered in numerical analysis and in experiments. It is shown that the solitary wave speed generated by an impact of a piston with the same velocity increases with precompression. Also, the tendency of the impulse to split into a train of solitary waves decreases and the solitary wave width increases. Gravitationally loaded discrete chains are considered in numerical calculations in the papers (Hong, 1999, 2001, Sen, 2001).

It should be noticed that particles with Hertzian contacts serving as strongly nonlinear springs are not the only way of discovering a "sonic vacuum" type system. Any power law interaction between particles ($n>1$) results in a similar behavior. Also, any general strongly nonlinear interaction laws support solitary waves with finite length for the long wave approximation. Different physical systems can be designed with properties suitable for the realization of "sonic vacuum" type behavior. For example, a forest of vertically aligned carbon nanotubes exhibits strongly nonlinear but non Hertzian type force interaction with spherical particles which can be used for assembling strongly nonlinear phononic crystals (Daraio, 2004).

One dimensional strongly nonlinear granular chains are, therefore, "sonic vacuum" (SV) type systems that support a new type of solitary wave with parameters determined by the interaction force (Nesterenko, 1983; Lazaridi, 1985 and Nesterenko, 2001). These solitary waves are qualitatively different from the well known weakly nonlinear solitary waves of the Korteweg-de Vries equation (Korteweg, 1895, Remoissenet, 1999) which were first discovered experimentally by Russel (Russel, 1844). The concept of a SV was proposed to emphasize the uniqueness of the types of materials

that do not support sound waves without initial prestress (Nesterenko, 1994, 2001). The unique property of these materials is that a single parameter (the prestress) is able to tune the response from a linear to a strongly nonlinear regime. One of the main features of strongly nonlinear solitary waves is that the speed is strongly influenced by interrelated potential and kinetic energies.

Nonlinear dynamic properties can be extended to other designed metamaterials including the propagation of electrical or other types of signals. Interesting applications of this new area of wave dynamics have been proposed e.g. for the creation of nanodroplets (Sen, 1999). It is interesting that a power law interaction with n=3, corresponding to a physical system of particles on an unstretched string in transverse vibrations supports periodic harmonic waves and solitary waves with a linear dependence of maximum strain on speed.

Chains of 2 mm diameter beads

The first one dimensional system tested is described in Fig. 19. In this system composed of steel bearing beads of 2 mm diameter, single and trains of strongly nonlinear solitary waves were excited by short duration impacts and their propagation was investigated (Daraio, 2004).

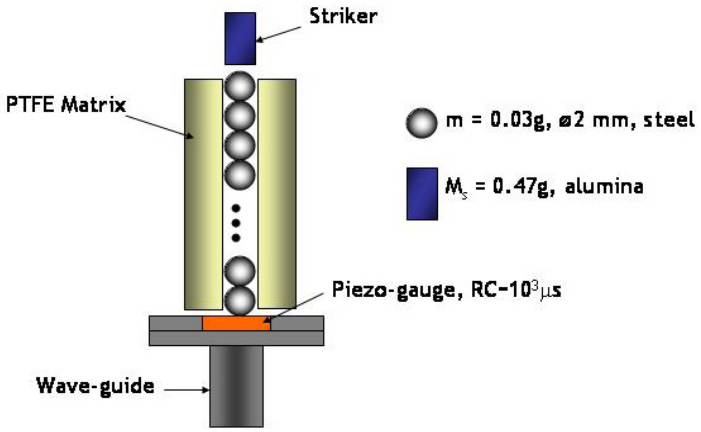

Figure 19. Set-up for testing of 1-D chain.

Solitary wave with speed of propagation below sound speed in the air and reflection from the boundary of two "sonic vacuums" with different architecture were detected. For testing, we also processed a 3-D phononic crystal (Fig. 20) based on a silicon matrix filled with an array of one-dimensional chains.

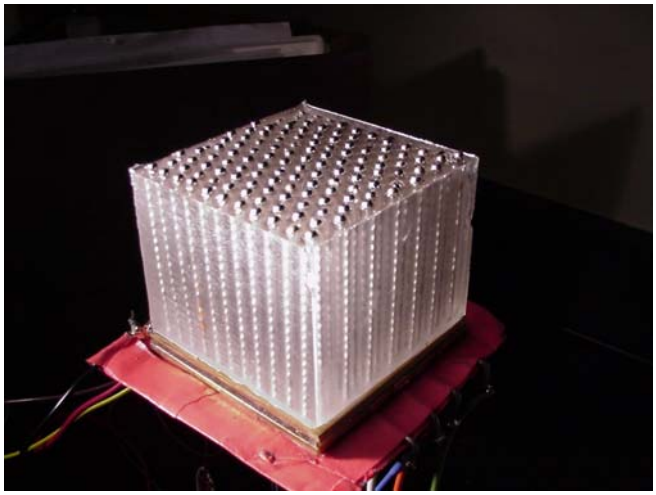

Figure 20. 3-D phononic crystal

In experiments we measured the force between the bottom plate and the last particle in the chain resting on this plate (Fig. 19). For the 3-D crystal, piezoelectric gauges of different diameters were placed under the all area of the crystal allowing supporting either one or seven chains altogether. They were connected with a wave guide - a long steel rod with a length about 20 cm embedded into the massive steel block. The typical time of the electric circuit of the gauge was $RC=10^3$ μs which was enough to ensure a good quality of signals with characteristic period up to 100 μs. The gauges were calibrated using impact with the parallel detection of acceleration. The one dimensional testing was the performed in chains of balls placed in PTFE (Teflon) or Silicon matrixes which have a very low elastic modulus to investigate how matrix may influence wave propagation in the chains.

A remarkable feature of a "sonic vacuum"-type system is evident: the very rapid decomposition of the initial impulse on distances comparable with the soliton width (Fig. 21).

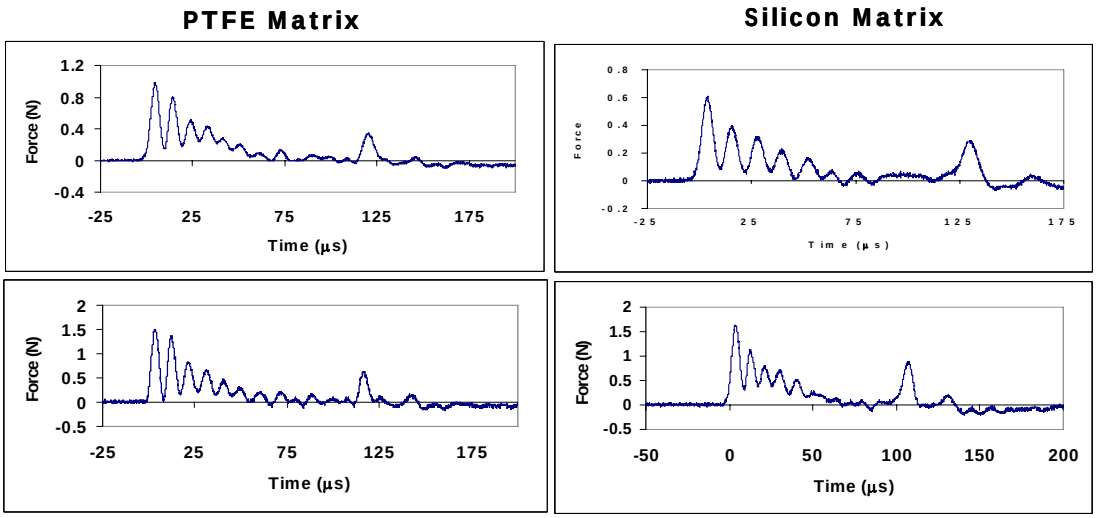

Figure 21. Impulses in a 1-D chains (20 steel particles with diameter 2 mm embedded into different matrixes) under identical loading by alumina striker (mass 0.47 g, velocity 0.4 m/s (top Figures) and 0.6 m/s (bottom Figures).

In facts, the impulse is split after traveling only through 20 first particles. This example also demonstrates that "short" duration impact on highly nonlinear ordered periodic systems (lattices) may result in a chain of solitary waves instead of intuitively expected shock wave. Increase of the duration of impact results in shock wave impulse with oscillatory structure where the leading pulse can be of KdV type for weakly nonlinear chain or compacton-like for strongly nonlinear case (Remoissenet, 1999). This property of *strongly nonlinear* phononic crystal can be used for controlled impulse transformation in very short transmission lines.

Single solitary wave can be generated in the strongly nonlinear chains under impact of a particle (or piston) with a mass equal or smaller than mass of particle in the chain. Earlier experiments were conducted with amplitudes of solitary waves about 10 N. It is important to determine the possibility of extending the lower range of wave amplitudes and speeds supported by these chains. For this reason we conducted

experiments on single chains of 20 stainless steel beads with 5 mm diameter chains by impact of a single 2 mm diameter particle.

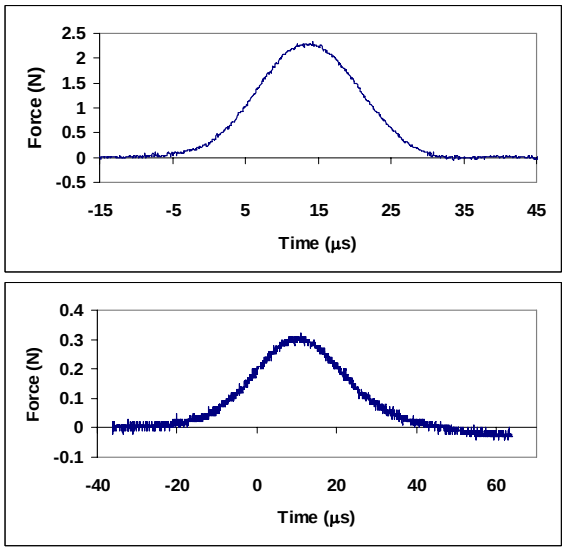

Figure 22. Solitary wave with amplitude significantly larger than gravitational prestress (top) and comparable to gravitational prestress.

The wave signal was detected with the amplitude 2.5 N and 0.3 N. It is very important that based on the amplitude of the signal (Eq. 5) a speed of solitary waves are equal 350 m/s and 317 m/s correspondingly, which is below sound speed in air.

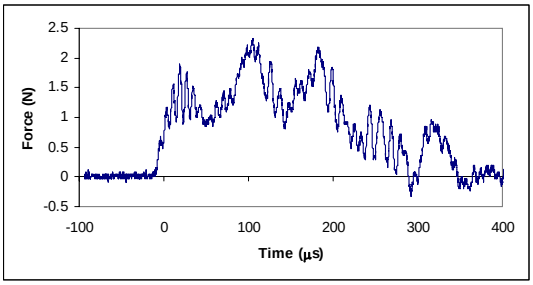

Figure 23. 3-D results for the 7 central chains with steel cover top plate with thickness 3 mm, u_s = 0.4m/s, M_s = 5.3g, striker is a steel ball with mass.

Preliminary experiments with the 3-D material were conducted using the central part of our phononic crystal (Fig. 20). Seven chains were supported by the same plate placed on the top of piezogauge. The recorded signal (Fig. 23) corresponds to their collective action: it has oscillatory front and waves reflected from the cover plate back to the gauge are evident.

Polymer based 1-d systems

Strongly nonlinear waves in a chain of Teflon beads

For this study, one dimensional "sonic vacuum" type phononic crystals were assembled from a chain of polytetrafluoroethylene (PTFE, Teflon) spheres with different diameters in a Teflon holder. It was demonstrated for the first time that this polymer-based "sonic vacuum", with exceptionally low elastic modulus of particles, supports the propagation of strongly nonlinear solitary waves with a very low speed. These solitary waves can be described using classical nonlinear Hertz law despite the viscoelastic nature of the polymer and high strain rate deformation of the contact area. The experimentally measured speeds of solitary waves at high amplitudes are close to the theoretically estimated values with a Young's modulus of 1.46 GPa obtained from shock wave experiments. This is significantly higher than the Young's modulus of PTFE from ultrasonic measurements. Trains of strongly nonlinear solitary waves excited by an impact were investigated experimentally and were found to be in reasonable agreement with numerical calculations based on Hertz interaction law though exhibiting a significant dissipation.

One dimensional phononic crystals were assembled filling a PTFE tube (with inner diameter 5 mm) with chains of 11 and 21 PTFE balls (McMaster-Carr catalogue) with diameter a=4.76 mm and mass 0.1226 g (standard deviation 0.0008 g) (Fig. 24). Different numbers of particles were used to clarify the stages of impulse transformation and interaction with the wall. A chain assembled from 18 PTFE particles with smaller

diameter a=2.38 mm and mass equal to 0.0157 g (standard deviation 0.0003 g) in a PTFE tube with inner diameter of 2.5 mm was also tested. Using two different sizes of beads helps to understand the behavior of the investigated polymeric material in the contact area at different stresses, strains and strain rate, which is dependent on the particle size. Scaling down the particle sizes is important for future applications in different devices (i.e. biomedical application, imaging, sound scrambling, etc.). Waves of different amplitude and durations were excited by impacting the top of the chain with strikers of different mass and velocities.

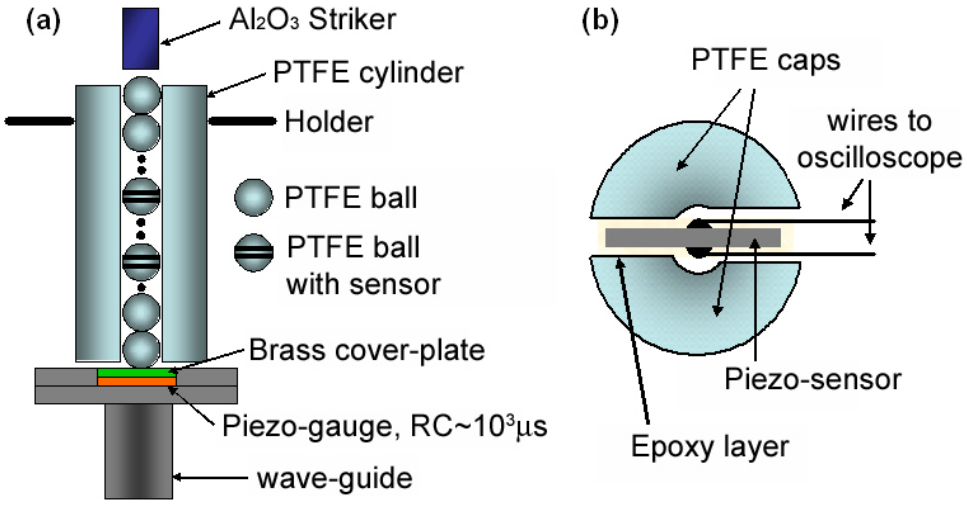

Figure 24. (a) Experimental set-up for testing of 1-D strongly nonlinear phononic crystals with PTFE beads; (b) Schematic drawing of a particle with embedded piezo-sensor.

The experimental set-up for measurements of soliton speed, duration and force amplitude together with the measurements of reflected pulse from the wall is presented in Fig. 24. It includes three calibrated piezo-sensors (RC ~ 10^3 μs) connected to a Tektronix oscilloscope. Two lead zirconate titanate based piezo-gauges (3 mm side plates with thickness 0.5 mm) with nickel plated electrodes and custom microminiature wiring,

supplied by Piezo Systems, Inc., were embedded inside two PTFE particles similar to (Nesterenko, 1995, 2001, Job, 2005). The particles with embedded sensors consisted of two PTFE caps with a total mass $2M$=0.093 g and a sensor with a mass m=0.023 g glued between these caps. Including glue, the total mass of the sensor was equal to 0.116 g (Fig. 24(b)), which was very close to the mass of the PTFE particle 0.123 g. This design allows a calculation of the speed of solitary wave simultaneously with measurement of the forces acting inside the particles.

A third piezo-gauge, supplied by Kinetic Ceramics, Inc., was bonded with epoxy on electrode foils for contacts and reinforced by a 1 mm brass plate on the top surface. The sensor assembly was then placed on the top surface of a long vertical steel rod (wave guide) embedded at the other end into a steel block to avoid possible wave reverberation in the system (Fig. 24(a)). This sensor was calibrated by using the impact of a single steel ball, which provides similar conditions of loading as in our measurements. Initial velocity and linear momentum conservation law were used for calibration. The area under the force-time curve measured by the gauge was integrated from the beginning of impact up to the point of maximum force and compared with linear momentum of particle at the beginning of impact. The sensors in the two particles were calibrated by comparison with the signal from the sensor at the wall. This was done using a controlled, relatively long, simultaneous loading of the internal sensor and the sensor in the wall by an impact of a massive piston.

The introduction of a particle with a different mass (particle with a sensor) in the chain of particle of equal masses results in wave reflections investigated in (Manciu, 1999, Hascoet, 2000, Sen, 2001). It was suggested to use reflected signals for detection

of buried inclusions (Sen, 2001). In numerical calculations, a slightly lighter particle with mass 0.116 g was introduced into the chain of particles with mass 0.123 g producing wave reflections that would be too small to detect experimentally. Attenuating soliton like pulse in a chain of random particles was considered in (Nesterenko, Manciu, 2001).

To interpret the signal measured in the experiments we considered the particle with an embedded sensor as a rigid body (Fig. 25(a)). The forces on the sides of the contacts of the particle (F_1 and F_2) can be easily related to the forces acting on both sides of the sensor (F_3 and F_4):

$$F_3 = \frac{F_1 + F_2}{2} + \frac{F_1 - F_2}{2}\frac{m}{2M + m}, \qquad F_4 = \frac{F_1 + F_2}{2} - \frac{F_1 - F_2}{2}\frac{m}{2M + m} \quad . \tag{9}$$

From Equation (9) we can see that the average of the compression forces, F_3 and F_4, (considered positive) is equal to the average value of forces F_1 and F_2, $F \equiv (F_1 + F_2)/2$ acting on the particle contacts. It should be mentioned that in numerical modeling the particles are considered rigid bodies and only contact forces F_1 and F_2 are taken into consideration. The time dependence of forces on the particle contacts were calculated numerically and their average values are presented in Fig. 25(b).

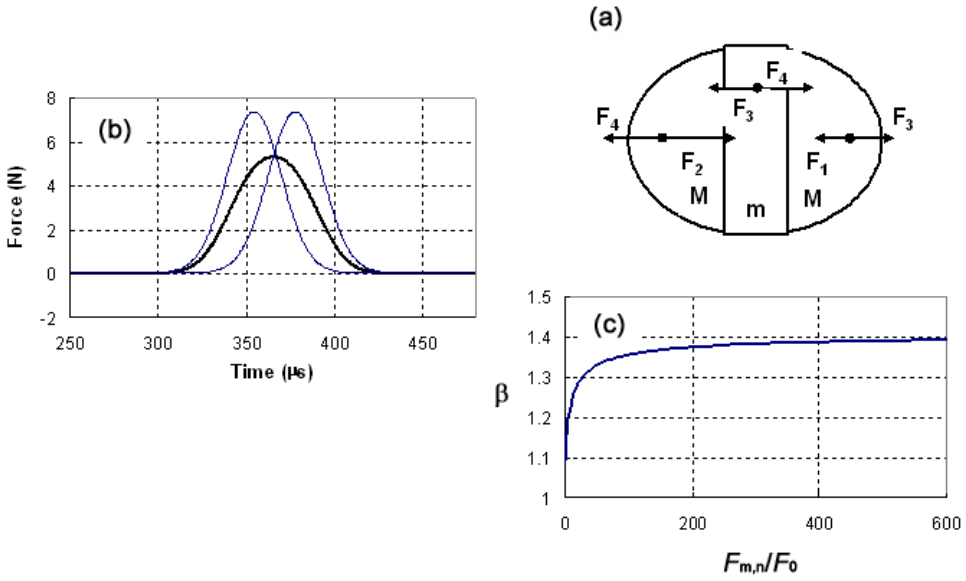

Figure 25. (a) Schematic drawing showing the forces acting on the different parts of particle with embedded sensor; (b) Numerical calculation showing the forces vs. time obtained for the two contacts of the particle with embedded sensor (left and right curves correspondingly for F_1 and F_2) and average of the previous two (central curve) representing the average force acting on the sides of the sensor; (c) Dependence of the coefficient β found in numerical calculations on normalized averaged dynamic force amplitude in solitary wave, $F_{m,n}/F_0$ with respect to static precompression.

In the case of m<<M, the forces on each side of the sensor (Equation (9)) are very close to the average forces on the particle contacts (Nesterenko, 1995, 2001). In our case the forces F_3 and F_4 deviate from their average value by less than 20% in the vicinity of signal "shoulders", and are seen from the time dependence of contact forces in Fig. 25(b). It should be noted that at the moment when averaged force F is maximum it is equal to the corresponding forces F_3 and F_4 (Fig. 25(b), Equation (9)). Comparison of averaged force and contact forces (Fig. 25(b)) reveals that averaging reduces the maximum amplitude of the force and increases the duration of the pulse. This averaged curve is

used for comparison with experimental results based on sensors embedded in the particles.

To relate the maximum value of average compression force $F_{m,e}$ measured by the embedded sensor to the value of maximum force at the contact between neighboring particles (Fig. 25(a)), we used a coefficient β determined in numerical calculations. It represents the ratio of the dynamic force on the particles contacts to the maximum average of dynamic forces $F_{m,n}$ acting on the two contacts of the given particle in the solitary wave. Relating the two forces facilitates the use of Equations (3) and (4) with experimental data. The dependence of β on the relative force amplitude of a solitary wave is presented in Fig. 2 (c). This coefficient has negligible dependence on elastic moduli of PTFE particles (<1% in investigated range of a solitary wave amplitude and relevant range of elastic modulus from 600 MPa to 1460 MPa). It should be mentioned that the investigated range of relative amplitudes of dynamic force and static precompression represents a strongly nonlinear regime of system behavior resulting in relatively short length solitary waves. The coefficient β is about 1 in the linear regime when the amplitude of the dynamic force is much smaller than the initial precompression and the solitary waves are very long in comparison with a particle diameter.

The maximum compression force on the contact between two particles (F_m) adjacent to the sensor embedded in the particle was calculated using an equation:

$$F_m = \beta F_{m,e} + F_0, \tag{10}$$

where $F_{m,e}$ is the maximum averaged dynamic compression force measured experimentally by the gauge embedded in the particle (it is represented by $F_{m,n}$ in numerical calculations) and F_0 is the gravitational precompression.

Pulses of different durations and amplitudes in the 1-D phononic crystals were generated by impact of an alumina (Al_2O_3) cylinder (0.47 g), a PTFE ball with a diameter of 4.76 mm (mass 0.123 g) or a stainless steel bead with a diameter of 2 mm (mass 0.036 g) onto the top particle of the chain. Single solitary waves can be generated by an impactor with a mass equal to the mass of the beads in the system which is physically equivalent to the application of δ–function force. To generate a single solitary wave in a chain of 21 PTFE beads, we used the same bead as the striker (m=0.123 g). Sensors were placed in the 9th and 5th ball from the bottom and in the wall at the end of the chain.

The theoretically predicted speed of solitary waves in strongly nonlinear phononic crystals has a strong dependence on the amplitude represented by Equations 7 and 8 for "sonic vacuums" and for precompressed chains respectively. This is shown in Fig. 26(a) together with the corresponding numerical calculations of the soliton speed for discrete chains. The curves based on the long wave approximation (Equations 3 and 4) and the numerically calculated values practically coincide. In experiments (solid dots in Fig. 26(b)), the solitary wave speeds for different amplitudes were obtained by dividing the distance between the sensors by the measured peak-to-peak time interval. The corresponding force amplitude in the solitary wave was found based on the measurements of gauges embedded inside the particles. The $\log_{10}F_m$-$\log_{10}V_s$ curves presented in Fig. 26 are based on these measurements.

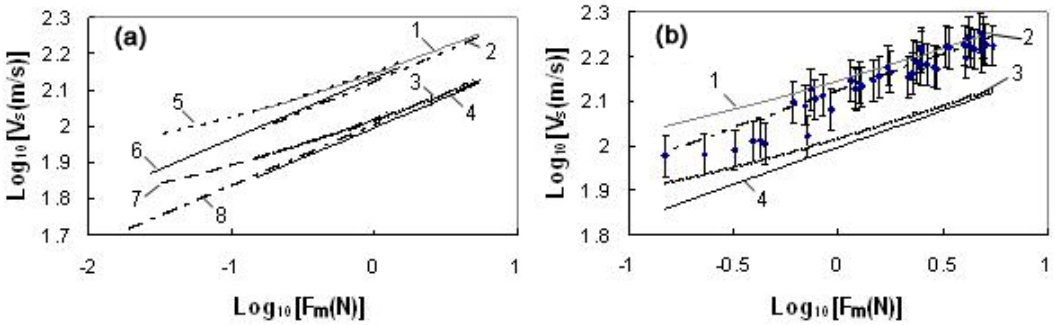

Figure 26. Dependence of the velocity of solitary wave on amplitude. (a) Comparison of numerical results for a discrete chain and analytical data obtained from long wave approximation. Curves number 1 and 3 represent the long wave approximation for gravitationally pre-compressed systems (Equation 8) at E=1460 MPa and E=600 MPa respectively; curves 5 and 7 represent the corresponding numerical calculation. Curves 2 and 4 are the theoretical curves based on Equation 7 for a "sonic vacuum" with a Young's modulus equal to 1460 MPa and 600 MPa respectively. Curve number 6 and 8 represent the corresponding numerical calculations for these cases. (b) Comparison of the experimental values (shown by solid dots) with the curves obtained from the long wave approximation (curves 1-4).

Accuracy of the measurements of amplitude of solitary waves was in the range of 15% to 30 % for large and small amplitudes. The larger errors being due to the higher signal to noise ratio at low amplitudes. In experiments the accuracy of the speed measurement can be estimated within 10 % due to the uncertainty in the sensors alignment (about 1 mm for each sensor).

Table 1. Experimental data for amplitude, speed, duration and normalized width of solitary wave in the PTFE chain composed of particles with diameter 2R=4.76 mm. Numerical data for discrete chains are also presented for comparison.

	Experimental data			Numerical Results		
F_m, [N]	Duration [μs]	V_s [m/s]	$L/2R$	V_s [m/s]	$L/2R$ (at 0.2%)	$L/2R$ (at 4%)
5	153	168	5.4	190	5.4	4.0
2	164	152	5.2	164	5.7	4.1
0.6	233	106	5.2	137	6.2	4.3
0.1	326	97	6.6	109	7.8	5.3
0.06	360	88	6.7	103	8.6	5.7

After measuring the speed and duration of the propagating pulse, the widths of solitary waves were calculated for the corresponding force amplitudes (Table 1). The same data obtained from numerical analysis of discrete chains with PTFE elastic modulus 1.46 GPa based on the averaged forces on the particle contacts are also shown with solitary width truncated at the level 0.2% and 4% of the solitary wave amplitude.

Experimental results for forces measured by sensors embedded into the particles and into the wall corresponding to a 2.0 m/s impact velocity are shown in Fig. 27(a). The zero time in all experiments corresponds to the start of recording triggered by the signal. In numerical calculations presented in all figures the zero time corresponds to the moment of impact.

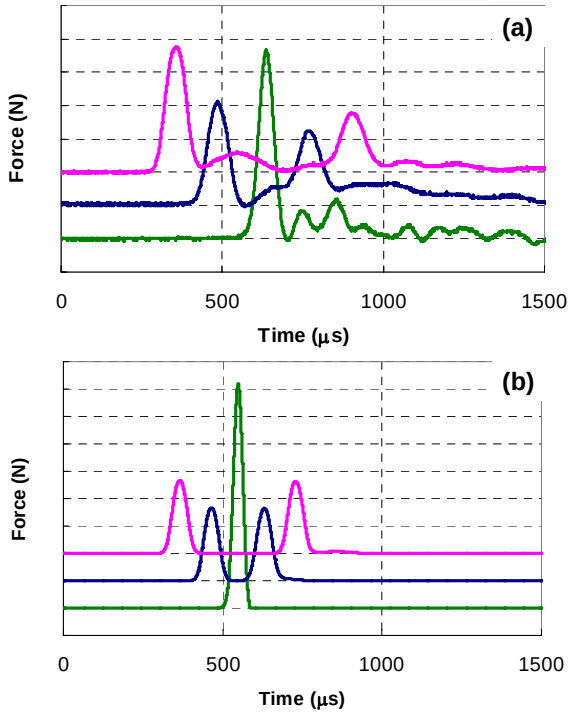

Figure 27. Solitary waves in PTFE chain generated by PTFE ball-striker with a velocity of 2 m/s: (a) incident, reflected solitary waves and force on the wall detected experimentally in the chain of 21 PTFE beads with diameter 4.76 mm. The curves represent force vs. time detected by the sensor embedded into the 9th ball from the wall (top curve), and by the sensor in the 5th ball from the wall (middle curve) and at the wall (the vertical scale is equal to 0.5 N); (b) numerical calculations for a discrete chain under conditions corresponding to experimental conditions in (a). Curves represent the average value of the forces acting on the top and bottom contact of each sensor. Grid scaling on the vertical axes is 2 N.

One of the distinguished features of strongly nonlinear "sonic vacuum" type system is the fast decomposition of shock type pulse caused by impact on a short distance from the impacted side (Nesterenko, 2001). To check if the PTFE based strongly nonlinear phononic crystal exhibits this property, the impact by striker with a larger mass (Al_2O_3 cylinder 0.47 g) was employed to create a longer initial shock pulse in chains of different lengths. This impact results in an incoming pulse shape at the entrance of the system with the rise time equaling 50 μs and an initial decay with the characteristic

exponential behavior $A\exp-0.0185t$, where the time (t) is measured in microseconds, starting from the peak of the signal with amplitude A. The total duration of the incident signal is equal to 370 μs. The result for the short chain composed of 11 PTFE particles is presented in Fig. 28(a).

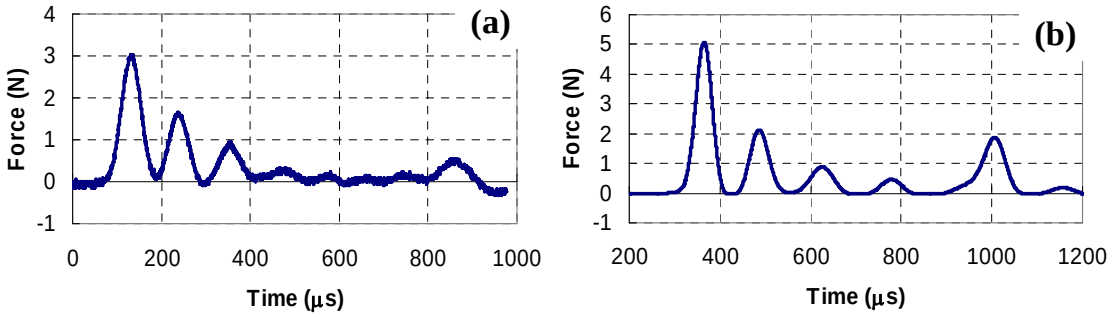

Figure 28. Experimental and theoretical results demonstrating that a short chain of PTFE beads with a diameter 4.76 mm supports a train of solitary waves induced by the alumina striker with a mass equal four times the mass of the particle. (a) Force detected in experiment by the sensor mounted at the wall supporting an 11 PTFE particle chain, striker velocity 0.44 m/s, vertical scale is 1 N. (b) Numerical calculations corresponding to experimental conditions in (a), including gravitational precompression; vertical scale is 1 N, elastic modulus 1.46 GPa.

It is important to note that if exponential curves are drawn through the solitons maxima, corresponding to the force history at given point (in Fig. 28 this point corresponds to the wall), they will depend on the position of the sensor due to the dependence of soliton speeds on amplitude. Exponential decays corresponding to experimental data and numerical calculations at the wall are $A_e\exp-0.0067t$ and $A_n\exp-0.0059t$ (time is measured in microseconds). Absolute values of coefficients in these exponents are about three times smaller than in the incident pulse (0.0185) due to the dependence of soliton speeds on amplitude. Despite the evident attenuation in

experiments ($A_e < A_n$) the corresponding exponents for envelope curves in experimental data and numerical calculations are close to each other. This suggests that the attenuation of the solitary waves is not strongly dependent on their amplitudes at the investigated range of amplitudes.

A chain of smaller diameter PTFE particles (2.38 mm) was also investigated to determine the diameter-dependence of strongly nonlinear behavior of PTFE-sphere-based "sonic vacuum" and dissipative properties. It should be mentioned that based on Hertz law the radius of the contact area is decreasing with particle radius under the same force. The experimental results are presented in Fig. 29(a) for short duration of shock loading (impact by a 2 mm diameter steel ball with a mass about 2.3 times that of the PTFE particle) and for relatively long duration of impact induced by a PTFE ball with a diameter 4.76 mm and mass 0.123 g (Fig. 29(c)).

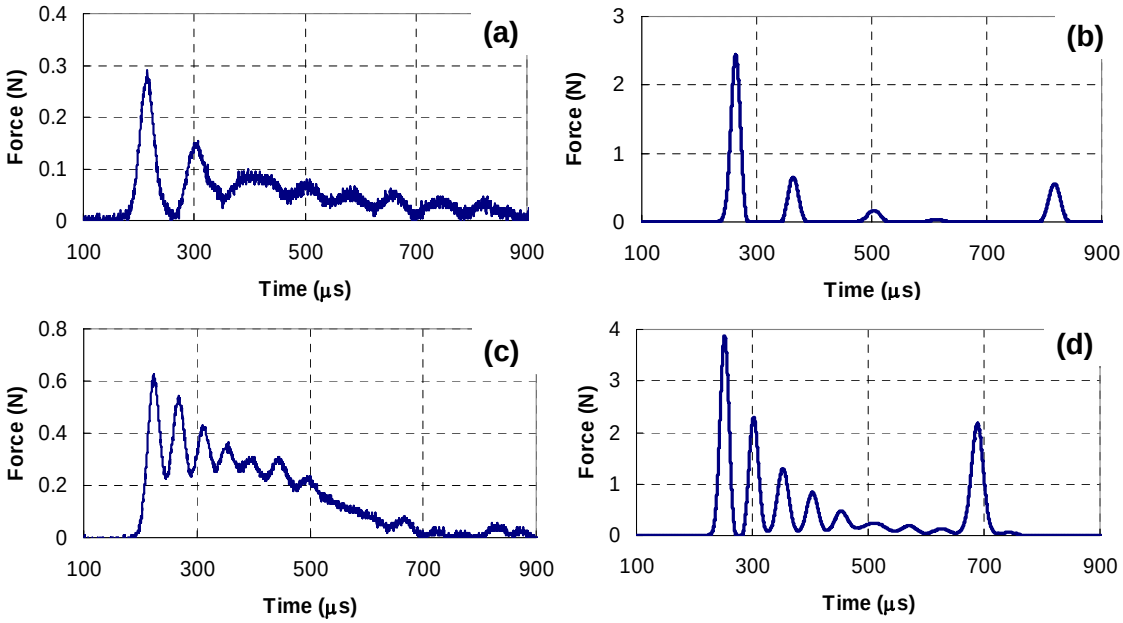

Figure 29. The experimental and theoretical results demonstrating that a PTFE chain of smaller particles with 2.38 mm diameter supports the solitary waves and oscillatory "shock" waves modified by dissipation in experiments. (a) The leading solitary wave with an oscillatory tail detected at the wall generated in a chain of 18 smaller PTFE balls (0.016 g) (the velocity of 2 mm diameter steel ball impactor (0.036 g) was 0.89 m/s); (b) Numerical calculations corresponding to experimental conditions in (a), including gravitational precompression, elastic modulus 1.46 GPa; (c) Oscillatory "shock" wave detected at the wall generated in a chain of 18 PTFE balls, impacted at velocity 0.89 m/s with a 5 mm diameter PTFE ball (0.123 g); (d) Train of solitary waves detected in numerical calculations corresponding to experimental conditions in (c), including gravitational precompression, elastic modulus 1.46 GPa.

Numerical Analysis

It was shown previously (Coste, 1997, 1999, Nesterenko, 2001) that wave propagation in 1-D system of linear elastic beads can be described considering particles as rigid bodies connected by nonlinear springs according to Hertz law (Eq. 7) for contact interaction of spheres (Hertz, 1881, Timoshenko, 1987).

$$F = \frac{2E}{3\left(1-\nu^2\right)}\left(\frac{R_1 R_2}{R_1 + R_2}\right)^{1/2}\left[\left(R_1 + R_2\right) - \left(x_1 - x_2\right)\right]^{3/2} \tag{11}$$

A system of second order differential equations was reduced to the first order equations (Nesterenko, 2001) and numerical calculations were performed using Matlab.

For comparison with experiments we calculated an average compression force $F=(F_1+F_2)/2$ for solitary waves based on the compression forces on the particle contacts (F_1,F_2). Both of these plots are shown in Figure 25(b). In these calculations Hertz law was used for PTFE particle interaction. We used different values of elastic modulus and Poisson ratio equal to 0.46 (Ehrenstein, 2001, DuPont). Interaction between the flat wall and last particle was also described by Hertz law with an elastic modulus of 115 GPa and Poisson ratio of 0.307 for red brass (Cu_{85}-Zn_{15}). Hertz law was also used to calculate the interaction between the alumina impactor (E=416 GPa, ν=0.231) and the first PTFE particle. No dissipation was included in numerical analysis. Gravitational force acting on particles causing initial nonuniform precompression in the chain increasing toward the wall was included in calculations. The linear momentum (before interaction with a wall)

and energy were conserved with a relative error of 10^{-12}% and 10^{-8}%. Results of the numerical calculations for the experimental set-up and conditions are shown in Figs. 25(b), (c), Fig. 26, see corresponding curves, Fig. 27(b), Fig.28(b), and Fig.29(b), (d).

PTFE is a polymeric viscoelastic material with a strong strain rate sensitivity (Zerilli, 2002) and exceptionally low elastic modulus (Ehrenstein, 2001). At normal conditions Young's and flexural moduli for PTFE are in the range of 400 – 750 MPa and Poisson's ratio is 0.46 (Ehrenstein, 2001, DuPont, Gondret, 2002). This property can be very attractive for ensuring a very low speed of soliton propagation and tunability of the system. But it is not evident that a chain formed from this type of beads will support strongly nonlinear solitary waves as for chains made from typical linear elastic materials like stainless steel (Lazaridi, 1985, Coste, 1997, 1999). In particular, the role of dissipation and deviation from linear elastic law (Zerilli, 2002) for PTFE under high strain and high strain rate deformation in the contact area with high gradients of strain is the primary concern. In the present study, the strains obtained were up to 0.06 based on estimation of maximum compressive stresses in the center of contact on the order of 80 MPa at a maximum force approximately equal to 5 N. The typical strain rates were approximately $4x10^2$ s^{-1} and the compressive strains at the center of contact were about 0.06 decreasing to zero at a distance about 170 micrometers.

The beads made from Nylon with elastic modulus six times larger than that for PTFE demonstrated a Hertz type interaction law (Coste, 1999). Chains made of these beads supported propagation of strongly nonlinear solitary waves with amplitudes in the range 1-33 N. In our experiments we extended range of amplitudes of solitary waves toward far smaller amplitudes by more than order of magnitude, down to 0.03 N.

Dynamic behavior of "sonic vacuum" type systems at such low amplitudes is very interesting especially in view of potential practical applications related to noise reduction in audible acoustic range, acoustic lenses and delay lines, and for investigation of validity of Hertz law at very low displacements.

Furthermore, one of the distinguished features of "sonic vacuum" systems is a strongly nonlinear dependence of solitary wave speed on amplitude and precompression (Equations (7) and (8)) which are the important factors in imparting a tunability of various properties of these systems, for example in delay lines or acoustical lenses. The dependence of the solitary wave speed on the amplitude (F_m), based on Equations (8) and (7), is shown in Fig. 26(a) and (b) (curves 3 and 4 respectively) with an elastic modulus equal to 600 MPa (AcraBall Manufactoring Co. Product catalogue). Numerical calculations based on the results for a discrete chain are also shown in Fig. 26(a) at the same value of elastic modulus (see curves 7 and 8). It is clear that theoretical and numerical approaches result in very close values of speeds at the given interval of amplitudes. For the low amplitude solitary waves in experiments (Fig. 26(b)), it was observed that gravitational precompression results in a noticeable deviation from the above curves. Comparison of the solitary wave profiles and speeds in a discrete chain and in a continuum approximation for different nonlinear interaction laws are considered in (Hascoet, 2000, Rosas, 2004).

It is evident that there is a large difference between experimental values of soliton speed obtained in numerical calculations and in long wave theory for large amplitudes of force if the value of Young's modulus was taken as 600 MPa (AcraBall Manufactoring Co. Product catalogue). The difference between experimental speeds at high amplitude

and predicted values based on the long wave approximation (or on numerical calculations) will be even more dramatic, if 400 MPa is used for the PTFE elastic modulus (Gondret, 2002).

It should me mentioned that the dependence of shock wave speed u_s on particle velocity u_p in polymers (Hugoniots in $u_s(u_p)$ coordinates) extrapolated to bulk sound speed results in significantly higher values than the sound speed at normal conditions measured using ultrasonic technique. This well known discrepancy indicates a rapidly varying change of compressibility at low values of shock amplitudes (Carter, 1995). For PTFE, the extrapolated value of bulk speed c_b from Hugoniot gives a value of 1.68 km/s in comparison with 1.139 km/s from ultrasonic measurements. Using c_b=1.68 km/s from extrapolated Hugoniot measurements and Poisson ratio 0.46, we obtained a value of Young's modulus equal to 1.46 GPa based on relations for elastic solids (Fung, 1965). Ultrasonic data for the same material gives a value of the elastic modulus equal to 704 MPa. The calculated theoretical and numerical data for solitary wave speed versus amplitude using elastic modulus of 1.46 GPa are presented in the Fig. 26(a) (see curves 1, 2, 5 and 6). When comparing the analytical data (curves 1-4 in Fig. 26(a) and (b)) with the experimental data (in Fig. 26(b)) we can see that there is a better agreement between the experimental results and the calculated speed of solitary waves at high amplitude at 1.46 GPa and disagreement at low amplitudes.

Calculations with elastic modulus of 1000 MPa results in a reasonable correspondence between experimental data and calculation at the lower range of investigated force amplitudes of solitary waves. This suggests that the elastic modulus of PTFE is likely to be stress and strain rate dependent.

In a “sonic vacuum”, solitary wave length does not depend on amplitude; it depends on the behavior of the interaction force (Hascoet, 2000, Nesterenko, 2001). In the case of a power law Hertz interaction (n = 3/2) this length is equal to five particles. The properties of solitary waves were used to establish validity of Hertz law for different materials (Coste, 1999). Measuring solitary wave speeds and durations in our experiments allows straightforward calculation of solitary wave widths corresponding to different amplitudes (see Table 1).

In the experiment corresponding to Fig. 27(a), for example, the speed of the leading solitary wave (with amplitude about 2 N) was measured using 5^{th} and 9^{th} particles from the wall and was found to be 152 m/s. The estimation based on the peak to peak measurements between the sensor in 5^{th} particle and the wall gave a similar value. The duration of solitary wave was about 164 microseconds resulting in the length of solitary wave equal to 5.2 times the diameter of the PTFE particle (Table 1). This is very close to the predicted length of solitary wave in long wave approximation equal to 5 particle diameters. The measurements of averaged force using sensors embedded into the particle results in a slightly longer pulse in comparison with pulse duration based on the contact forces (Fig. 25(b)).

It is clear from the experimental data that the widths of solitary waves with relatively large amplitude are close to the predicted value of 5 particle diameter based on Hertz interaction law. Numerical analysis of a solitary wave in a “sonic vacuum” demonstrated that the energy contained in 5 particles is equal to 99.999996% of the total energy of the solitary wave. The distribution of velocities of particles in a solitary wave including more than 5 particles was analyzed in (Chatterjee, 1999, Sokolow, 2005). It

should be mentioned that these widths do not depend on the elastic modulus. The widths of the solitary waves tend to be wider at lower amplitudes of propagating signals (Table 1). This may be due to the influence of gravitational precompression being closer to the impulse amplitude which drives the system away from the strongly nonlinear limit, producing broader solitary pulses tending to the weakly nonlinear regime described by the solitary waves of the KdV equation. Numerical calculations performed in this work demonstrated a similar dependence of solitary widths with the amplitudes (Table 1).

It is evident from the comparison between Fig. 27(a) and Fig. 27(b) that numerical calculations of the behavior of a discrete system and experimental results are in close agreement with respect to the signal amplitudes and time durations between corresponding pulses. It is noted, however, that the amplitude of the reflected solitary wave recorded by the sensor inside the 9^{th} bead is significantly smaller than the amplitude of the incident wave. This is apparently due to the presence of dissipation in experiments, which was not taken into account in numerical calculations and will be addressed in future research.

From the preceding discussions it is apparent that a chain of low modulus PTFE beads also supports the propagation of strongly nonlinear solitary wave, which is yet another realization of the "sonic vacuum" type phononic crystals with exceptionally low speed of signal.

Another remarkable feature of a "sonic vacuum" type system is the very fast decomposition of longer initial pulse into a train of solitary waves. Apparently this phenomenon can be obscured by the strong dissipation in the system. To check if this property is also demonstrated by a chain of PTFE particles, we used a striker mass

(m_s=0.47 g) that was higher than the mass of the particles in the chain to create a longer incident pulse. Usually the number of solitary waves with significant amplitude is comparable to the ratio of the striker mass to the mass of the beads in the chain.

The results of this experiment are shown in Fig. 28. It is evident that this Teflon-based "sonic vacuum" also demonstrates very fast decomposition of initial impulse on a distance comparable with the soliton width (Fig. 28(a), (b)) and a clear tendency of signal splitting is very noticeable already after only 10 particles. The mass of the striker was chosen to be about four times that of the particles in the chain, expecting a decomposition of the initial triangular pulse into a train of four solitary waves. It should be mentioned that the number of solitary waves may be significantly larger if smaller amplitudes are included (Hascoet, 2000, Sokolow, 2005). This example also demonstrates that a “short” duration impact on highly nonlinear “sonic vacuum” type ordered periodic systems results in a train of solitary waves instead of intuitively expected shock wave. An increase of the duration of impact results in a shock wave impulse with an oscillatory structure where the leading pulse can be of the KdV type solitary wave for weakly nonlinear chain or strongly nonlinear soliton with finite width for the strongly nonlinear case**.** Similar qualitative agreement of the experimental results and numerical calculations was found for all investigated conditions of impacts.

Previous experimental work with chains of steel beads, acrylic disks and spheres, glass, brass and nylon beads validated the prediction of strongly nonlinear solitary wave as stationary solutions of strongly nonlinear wave equation (Equation (2)). In those cases, the amplitude of the maximum force in the solitary wave was at least 3 times greater (1 N for Nylon beads) than the one obtained in this paper for PTFE beads (0.03

N). This and the higher elastic modulus of Nylon resulted in higher speeds of signal propagation (the minimum reported speed was 235 m/s for Nylon beads (Coste, 1999)). Furthermore, PTFE is a very versatile visco-elastic material. It is widely biocompatible, has a very low friction coefficient, and a very low elastic modulus which ensures applicability in a large variety of engineering solutions. As a result, we were able to experimentally achieve a speed of signal propagation of 88 m/s for a force amplitude of 0.06 N (Table 1), which is more than two times smaller than the speed of solitary wave detected for nylon beads and more than 3 times smaller than the sound speed in the air at normal conditions. In principle, a "sonic vacuum" type media of different structure (Hertzian and non Hertzian) can support solitary waves with indefinitely small amplitude and speed of propagation. In the future, it is not unreasonable to expect that a "sonic vacuum" type system which supports detectable solitary waves with force amplitude similar to the one investigated in this paper with a speed of the order of magnitude of 10 m/s or lower could be designed using new materials with tailored elastic properties.

Finally, it is important to investigate the influence of particle size on the system behavior for application purposes. In fact, a smaller size of particles composing the PTFE based strongly nonlinear system results in different stresses and strain rate conditions in the contact area which may affect the system behavior. We conducted experiments with smaller diameter PTFE balls (2.38 mm) to check the validity of the strongly nonlinear theory. Experimental and numerical results are presented in Fig. 29. In the experiments, pulses were generated by impact of a 2 mm diameter steel ball (0.036 g, Fig. 29(a), (b) and a 5 mm diameter PTFE ball (0.123 g, Fig. 29(c), (d)) at velocity 0.89 m/s. Numerical calculations did not account for the effects of dissipation. It is

evident that the smaller diameter PTFE particles do support the "sonic vacuum" type behavior, although in this case the effect of dissipation appears to be more significant. Influence of dissipation on dynamics of solitary waves in strongly nonlinear discrete systems was considered in (Manciu, 2001, Rosas, 2003). The effect of dissipation is likely to be responsible for the tail present after the 2nd solitary waves formed in experiments (Fig. 29(a)), and delays the solitary wave splitting in experiments in comparison with numerical results (compare Fig. 29(a) to (b) and Fig. 29(c) to (d)).

The propagation of impulses in one dimensional strongly nonlinear phononic crystals assembled from PTFE spheres was investigated for different conditions of loading and geometrical parameters. It was demonstrated, for the first time, that the chains of PTFE beads with different diameters support the Hertzian behavior with very low signal propagation speed due to its exceptionally low Young's modulus and despite viscoelastic nature of PTFE. Single solitary waves and decomposition of the signal into trains of solitary waves with amplitude more than one order of magnitude smaller than previously reported were observed. Small amplitude solitons broke the "sound barrier" having a speed of propagation well below sound speed in air. Single solitary waves and trains of strongly nonlinear solitary waves were excited by impact were investigated experimentally and were found to be in reasonable agreement with numerical calculations based on Hertz interaction law with Young modulus 1000 MPa for the lower amplitudes and 1460 MPa for higher amplitudes of signals, both being significantly higher than its value at normal conditions.

Strongly nonlinear wave dynamics in a chain of polymer coated beads

Strongly nonlinear phononic crystals were assembled from a chain of Parylene-C coated steel spheres in a polytetrafluoroethylene (PTFE) holder. This system exhibits strongly nonlinear properties and extends the range of materials supporting "sonic vacuum"-type behavior. The combination of a high density core and a soft (low elastic modulus) coating ensures a relatively low velocity of wave propagation. The beads contact interaction caused by the deformation of the Parylene coating can be described by classical nonlinear elastic Hertz theory with an effective value of the elastic modulus equal to 15 GPa for the contact interaction. Strongly nonlinear solitary waves excited by impacts were investigated experimentally and compared to chains composed of uniform steel beads. Fracture of the polymer coating was detected under relatively large pulse amplitude.

Coating a high density particle such as the steel beads considered in this study with a soft polymeric layer might ensure a better control of impulse transformation and propagation characteristics allowing applicability in a large variety of engineering solutions. The results obtained from these analyses may lead to applications in sound focusing devices (acoustic lenses), very short transmission delay lines, sound and shock absorption layers and sound scramblers. Granular beds composed from iron particles are used for designing systems able to transform impacts from heavy strikers and contact explosion (Nesterenko, 2001). The soft coating is important for delaying and reducing the amplitude and wave speed in the medium adjusting, for example, the protective granular barrier to a wider spectrum of dynamic loads. Parylene-C is a very versatile

visco-elastic material, widely biocompatible, with a very low friction coefficient, and low elastic modulus. Its properties, combined with the wide commercial availability of Parylene-C thin film coating, allowed it to be suitable for the assembling of strongly nonlinear systems. To the best of our knowledge no other results on the pulse propagation in chains composed of coated particles were previously published.

For the theoretical treatment, we consider that the particle's stainless steel core with radius R' behaves as a rigid body and the depth of the deformed contact zone is smaller than the thickness of the coated layer Δ. In the initial conditions the beads have all point contacts with their neighboring particles and the particles interaction is limited only to the deformation of their coating. Finally we assume that the time of the particle interaction is significantly longer compared to the time of the wave propagation inside the particle ensuring the application of a quasistatic interaction law with constant value of elastic modulus. Under these assumptions using the Hertzian expression of force between the granules (Hertz, 1881),

$$F = \frac{2E}{3\left(1-\nu^2\right)}\left(\frac{R'+\Delta}{2}\right)^{1/2}\left(2\left(R'+\Delta\right)-\left(x_2-x_1\right)\right)^{3/2} \tag{12}$$

we obtain the following equation of motion for a one dimensional chain of identical uniform coated beads (Fig. 30) similar to the one presented in (Nesterenko, 2001):

$$\ddot{u}_i = A(\delta_0 - u_i + u_{i-1})^{3/2} - A(\delta_0 - u_{i+1} + u_i)^{3/2}, \tag{13}$$

where

$$A = \frac{E\, a^{1/2}}{3(1-\nu^2)M},\ a = 2(R'+\Delta)$$

and $$M = m_{ss} + m_p = \frac{4}{3}\pi R'^3 \rho_{ss} + \frac{4}{3}\pi\left((R'+\Delta)^3 - R'^3\right)\rho_p .$$

Here δ_0 is the initial displacement between particles due to the static precompression, E is the elastic modulus and ν is the Poisson's coefficient of Parylene-C, Δ represents the Parylene coating thickness**.** The diameter of the particles is a, the mass M (m_{ss} is the mass of the stainless steel core and m_p is the mass of the coating) and the displacement of the i-th particle is u_i.

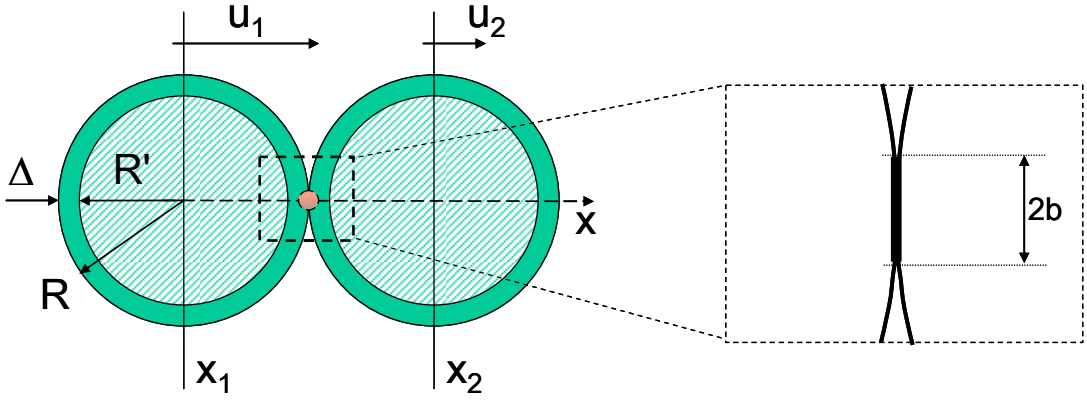

Figure 30. Schematic diagram showing the contact interaction area between two Parylene coated particles. The inset shows an enlargement of the contact interaction area.

When a weak precompression is applied to the system the long wave equation for the particle displacement u is presented in Eq. 2.

Here ξ_0 is the initial strain in the system. It should be noticed that c does not represent the sound speed in the chain, while c_0 corresponds to the long wave sound speed at initial strain ξ_0 in the system. Equation 2 for high amplitude pulses (or for negligible precompression) has no characteristic wave speed. In this case, despite their complex nature, Eqs. 2 and 13 support supersonic solitary waves with finite length equal to only five particle diameters.

In the leading approximation, the force F_{m} between particles in a discrete chain is related to the maximum strain ξ_{m} in the solitary wave as follows:

$$F_{\mathrm{m}} = \frac{4E}{3\left(1-\nu^2\right)}\left(R'+\Delta\right)^2 \xi_m^{3/2} \ . \tag{14}$$

Also, we know that for a solitary wave in "sonic vacuum" the speed is equal:

$$V_s = \frac{2}{\sqrt{5}} c \xi_m^{1/4} \ . \tag{15}$$

Combining Eq. 14 and Eq. 15 we obtain the relation between the solitary wave speed and the maximum force between particles:

$$V_s = \frac{2}{\sqrt{5}}\left(\frac{E\, a^{7/2}}{3\left(1-\nu^2\right)}\right)^{1/3} \frac{F_m^{1/6}}{\sqrt{M}} \ . \tag{16}$$

It's evident that the speed of this wave has a nonlinear dependence on the maximum strain ξ_{m} or force F_{m} and can be infinitesimally small if the amplitude of the wave is small. For chains composed of uniform beads of different materials the existence of this

solitary wave was verified in numerical calculations and in experiments (Nesterenko, 1983, Lazaridi, 1985, Shukla, 1993, Coste, 1997, 1999).

The addition of significant initial precompression on the system is known to modify the wave propagation behavior, for example due to the presence of gravitational precompression in the vertical alignment of the chains or due to the added prestress by another external source. The speed of the solitary wave V_s in a chain of coated beads with applied static precompressive force (F_0) is derived in a similar way as in (Daraio, 2005) for uniform particles:

$$V_s = \left(\frac{2}{15}\right)^{1/2}\left(\frac{3E^2F_0a^7}{M^3\left(1-\nu^2\right)^2}\right)^{1/6}\frac{1}{f_r^{2/3}-1}\left(3+2f_r^{5/3}-5f_r^{2/3}\right)^{1/2}. \quad (17)$$

The speed V_s has a nonlinear dependence on the maximum force $f_r=F_m/F_0$ but can be considered approximately constant at any relatively narrow interval of its amplitude due to the small exponent present in the power law. Equation 16 can be obtained as a limit of Eq. 17 when the precompressive force (F_0) is approaching zero.

The force dependence on displacement may still obey the equation similar to Hertzian theory (Eq. 12) even if the depth of the deformed area is comparable or larger to the thickness of the coating. In this case the elastic modulus E in Eq. 17 represents an effective elastic modulus for the contact interaction of the composite particles and can be different from the elastic modulus of the coating.

If the dependence of contact force on displacement between composite particles can be approximated by a general power law with exponent different from the Hertzian

value 1.5, an equation similar to Eq. 17 can be derived with different exponents and coefficients based on the Eq. 1.127 in (Nesterenko, 2001). It should be mentioned that the width of the solitary wave is related to the value of the exponent in the power law dependence of the contact force on displacement. The properties of strongly nonlinear solitary waves were used to identify the contact interaction law between the beads made from different materials.

We assembled strongly nonlinear chains from steel bearings balls (diameter of 4.76 mm and 2.48 mm) coated with a 50 μm thick layer of Parylene-C polymer (AcraBall Inc.) via vaporization processes (Fig. 31(a)). The properties of Parylene-C provided by the manufacturer are the following: Young modulus, E = 2760 MPa, density = 1289 Kg/m^3, Poisson's coefficient v = 0.388 (AcraBall Manufactoring Co. Product catalogue). The yield strength (Y) of thin films of Parylene-C is reported to be at 59 MPa (Shih, 2004).

Parlylene-C is a polymeric viscoelastic material with a low elastic modulus. It is widely used in different areas from electronic to biomedical applications. Its properties can be very attractive to ensure a low speed of soliton propagation and a good tunability of the system. At the same time it is not evident that a chain formed from this type of composite beads would support strongly nonlinear solitary waves based on Hertzian interaction, as for example chains made from uniform linear elastic materials like steel (Coste, 1997, Nesterenko, 2001, Job, 2005). In particular, the role of dissipation and deviation from the linear elastic law under high strain rate deformation (~10^2 – 10^3 s^{-1}) can influence the contact interaction and the wave dynamics. Additionally, the geometrical constrains introduced by the stiffer steel core, interfacial phenomena between

the Parylene coating and the steel core, for example due to the weak adhesion, may contribute to the contact deformation and dissipation and affect the dynamic behavior of the chains. Chains of beads made from Nylon (Coste, 1999) with elastic modulus ~23% larger than Parylene-C and chains made of PTFE (Daraio, 2005) with a nominal elastic modulus ~5 times smaller than Parylene-C demonstrated the validity of the Hertz type interaction law and supported propagation of strongly nonlinear solitary waves.

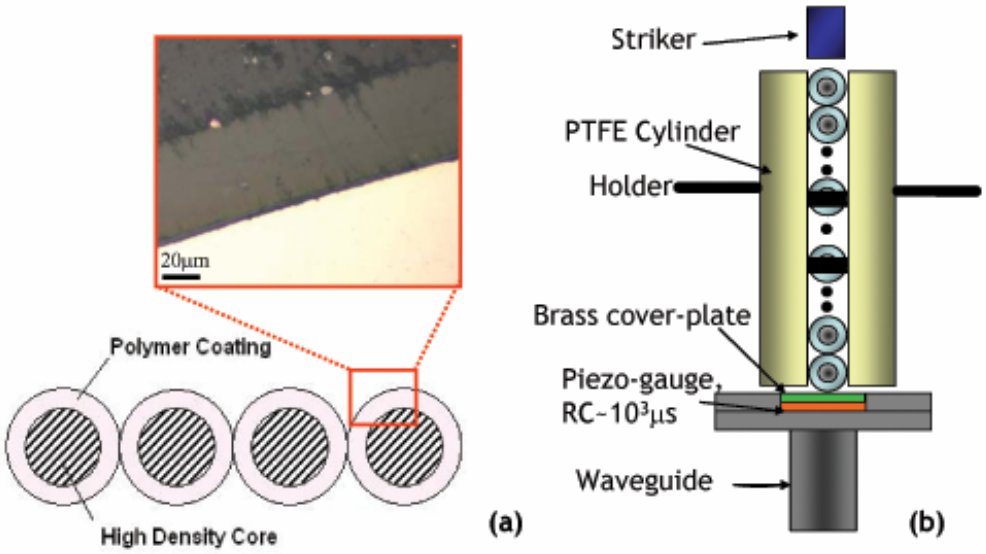

Figure 31. Experimental set-up for testing of 1-D strongly nonlinear chains. (a) schematic diagram of the chain and optical micrograph showing the Parylene-C polymer coating (b) set up used for the single chain testing, showing the particles with embedded sensors shown by a black central bar.

One dimensional chains were assembled from 21 Parylene-C coated steel beads (with diameter a=4.86 mm and mass 0.44 g) vertically aligned in a PTFE (polytetrafluoroethylene) holder with inner diameter 5 mm (Fig. 31(b)). Pulses of different durations and amplitudes were generated by impact of an alumina (Al_2O_3) cylinder (0.47 g and 1.23g) on the top particle of the chain from different heights.

In the described set-up we included three calibrated piezo-sensors (RC~10^3μs) connected to a Tektronix oscilloscope similar to (Daraio, 2005). Two lead zirconate titanate based piezo-gauges with Nickel electrodes and custom microminiature wiring (Piezo Systems, Inc.) were embedded inside two of the Parylene-C coated particles. The original beads were cut into two parts and the wired piezo-elements were glued between the steel parts. The total mass of the assembled beads with sensors was approximately equal to the mass of the original particle (0.44 g) to preserve the uniformity of the chain. This design ensured a precise calculation of the speed of signal propagation simultaneously with the measurement of the forces acting in the particles. The speed of propagation of the main pulse in the chains was calculated dividing the distance between the sensors by the peak to peak time interval. The accuracy of the speed measurement can be estimated about 10 % due to the uncertainty in the sensors alignment ($\pm$1 mm for each sensor).

A third piezo-gauge (Kinetic Ceramics, Inc.) was bonded with epoxy on the electrode pads for contacts and reinforced by a 1 mm brass plate on the top surface. This wall-sensor was then placed on the top surface of a long waveguide (vertical steel rod) ending into a steel block to avoid possible reverberations in the system. It was calibrated using linear momentum conservation law during single impact by a steel ball. Sensors embedded in the particles were calibrated by comparison with the signal from the sensor at the wall under simultaneous impact loading.

To compare the experimentally measured speeds of the solitary waves at different amplitudes with the theoretical prediction derived from the long wave approximation (Eqs. 16 and 17) we ran a series of experiments at different striker velocities.

The dynamic behavior of the chains composed of Parylene-C coated beads and steel beads was initially tested in conditions usually resulting in exciting single solitary waves. This is observed when the mass of the striker is close to the mass of one bead. The experimental results corresponding to a chain composed of 21 Parylene-coated beads (4.86 mm diameter, 0.44 g mass) are shown in Fig. 32(a). It is apparent that under these conditions of loading a single pulse is mainly excited, as expected. In comparison to the bare steel beads case (Fig. 32(b)) the composite particles showed some additional solitary like small amplitude pulses, following the main pulse, especially noticeable in the first (uppermost) gauge record. Probably this is related to the complex behavior of the coating on the beads composing the system affecting the contact forces between particles.

In Fig. 32(a) the speed of the main pulse is 197 m/s, being significantly below the level of sound speed in gases at normal conditions. Its duration was about 130 μs and width equal ~5.3 particle diameters being close to the length of the stationary solution of Eq. 2 based on Hertz interaction law for weakly compressed chains. Similar widths of solitary wave close to 5 particles diameters were observed at larger amplitudes of solitary waves. This allows us to conclude that the Parylene-C coated beads chain supports the propagation of strongly nonlinear solitary waves with Hertzian exponent 1.5. A higher value of exponent could be expected at larger forces due to the presence of stiffer core which should result in shorter length of solitary wave. Hertz law is derived for linear elastic materials. Nevertheless Hertzian exponent 1.5 was observed for viscoelastic materials like Nylon (Coste, 1999) and PTFE (Daraio, 2005).

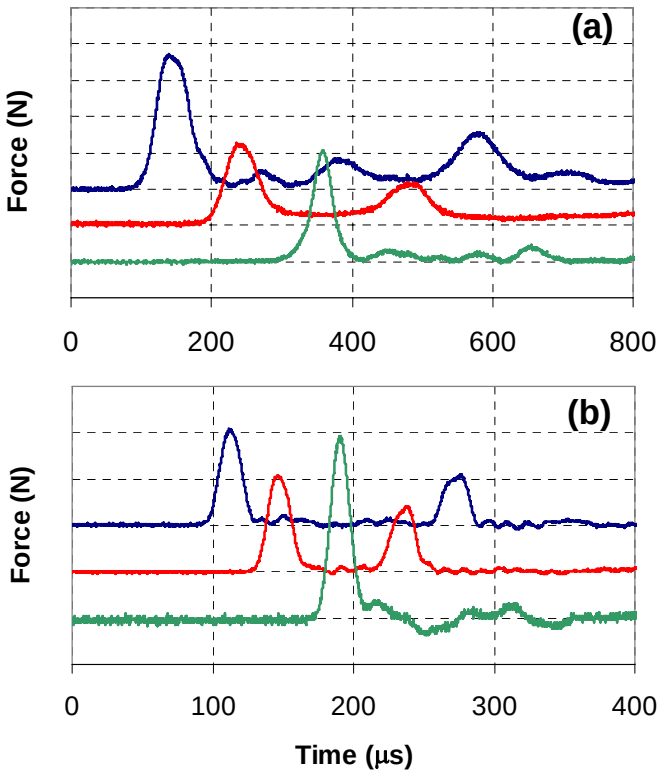

Figure 32. Pulses generated in chains composed of (a) Parylene-C coated steel balls (4.86 mm diameter) and of (b) bare stainless steel balls (4.76 mm diameter) for comparison of their amplitudes, speed, width and attenuation. In both chains sensors are placed in the 9th ball from the bottom (top curves), 5th ball from the bottom (middle curves) and at the bottom wall. The velocity of striker (0.47 g Al_2O_3 cylinder) was 0.44 m/s. The scale of the vertical axis is 1 N for (a) and 5 N for (b).

It's worth noticing that the amplitude of the solitary waves traveling through the chains (especially in the Parylene-C based system) might be heavily affected by the presence of dissipation. Its effects will be addressed in our future research.

It is interesting to compare the behavior of the polymer coated beads with a chain of bare steel beads (Fig 32(b)) of similar diameter (equal to the diameter of the steel core of the coated beads) and under the same type of loading (same impact striker and same velocity). Steel beads are well known to support strongly nonlinear waves in one

dimensional chains. It is evident from comparison between Fig. 32(a) and 32(b) that the behavior of the coated and the not coated beads differs dramatically in the speed of the propagating pulse (578 m/s for steel beads versus 197 m/s for composite beads). Although, both chains are forming a solitary pulse with width close to 5 particle diameters which is similar to the length of a stationary solution of Eq. 2 for particles interacting according to Hertz law. Reducing the amplitude of the signal traveling through the system to ~0.25 N we were able to achieve solitary waves speeds in the chain composed of Parylene-C coated beads down to ~130 m/s, which is more than two times smaller than the smallest speed of a solitary wave detected for solid nylon beads and it is comparable with the one obtained with solid PTFE particles. In principle such media can be designed to support solitary waves with indefinitely small amplitude and speed of propagation. It is reasonable to expect detectable solitary waves with a speed within the order of magnitude of 10 m/s or lower, useful for example in acoustic delay lines and shock pulse mitigation devices.

It is interesting to follow the dependence of the solitary wave speed on amplitude and compare it with the results from long wave approximation (Eq. 17). The agreement between these approaches was previously demonstrated for strongly nonlinear chains of beads made from different materials (Coste, 1997, 1999, Daraio, 2005).

The experimental results (solid diamonds) and theoretical curves for Parylene are shown in Fig. 33(a), where the bottom curve corresponds to the long wave approximation with elastic modulus provided by manufacturer 2.76 GPa (AcraBall Manufactoring Co. Product catalogue). It is evident that there is a large discrepancy between the experimental pulse's speed values and the lower theoretical curve (Eq. 17). The

experimental data can be described by shifting the theoretical curve up using an increased effective elastic modulus of the composite beads, this was obtained with the value E=15 GPa (see Fig. 33(a), upper curve).

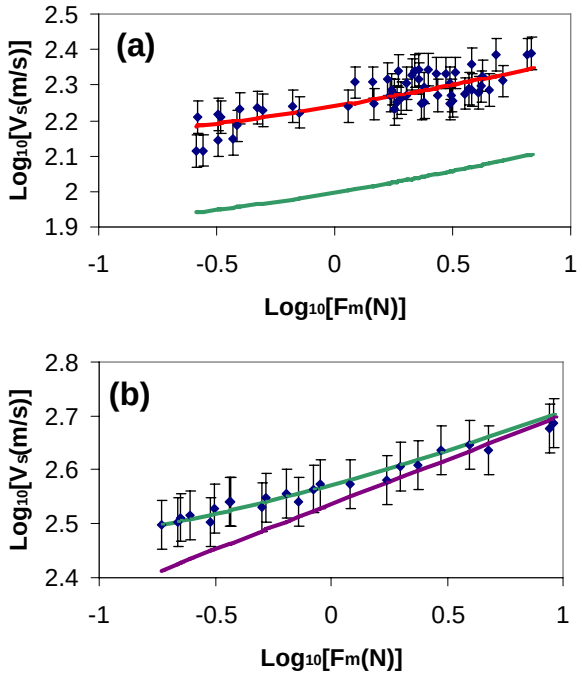

Figure 33. Dependence of the wave speed on the amplitude of the solitary wave in the chains assembled from coated spheres (a) and from stainless steel beads (b). (a) Experimental vales (solid dots) and theoretical curves corresponding to the long wave approximation including gravitational preload. The lower curve corresponds to a value on elastic modulus E=2.76 GPa, the upper curve matching the experimental values corresponds to E=15 GPa. (b) Experimental values obtained in a uniform stainless steel chain with the long wave approximation at E=193 GPa for a "sonic vacuum" (lower curve) and for a gravitationally precompressed chain (upper curve).

The increased value of effective elastic modulus of contact interaction can be due to the high strain, strain rate deformation of Parylene and also due to the geometrical constrains caused by the rigid core because the value of the contact radius is comparable

or larger than the thickness of the coating. The strain rate in the deformed coating was in the interval 10^2-10^3 s^{-1}. It should be mentioned that elastic moduli of polymers are very sensitive to the conditions of testing. For example, measurements of the elastic modulus of Parylene-C based on membrane deflection measurements gave a significantly higher value of 4.75 GPa (Shih, 2004) than one provided by manufacturer.

In Fig. 33(a) the value of the elastic modulus for the contact interaction of the composite particles matching the experimental data is ~5.4 times higher than the value for Parylene provided by the manufacturer. A similar difference was observed also for another polymer based granular material in (Daraio, 2005) where the elastic modulus of PTFE appeared to be ~3 times higher than its nominal value (and matched the Young's modulus extrapolated from the Hugoniot measurements (Carter, 1995)). It is likely that in polymer-based strongly nonlinear systems the effective elastic modulus for the contact interaction might be stress and strain dependent due to the properties of polymers (Job, 2005).

Further research on the value of elastic modulus of Parylene-C coating under conditions of dynamic deformation and validity of Hertz approximation for contact law of polymer coated beads is necessary to clarify the observed increase of contact stiffness.

Results for the pulse traveling in the bare stainless steel beads chain are presented in Fig. 33(b). In this case the curves represent the long wave approximation at E=193 GPa for steel in the "sonic vacuum" (lower curve) and in the gravitationally precompressed case (upper curve) agreeing with experimental data. Gravitational precompression was included into the Eq. 17 similarly to (Daraio, 2005).

In both investigated systems (Parylene coated and steel beads), the theoretical estimate appears to be strikingly close to the experimental results in the whole investigated range, especially taking into account that no adjustable parameter was used in the theoretical consideration for stainless steel beads and a constant effective elastic modulus was used for the contact interaction of the composite particles (though significantly increased in comparison with the manufacture's value for Parylene).

We may conclude that chains of polymer coated beads with a high density core support the propagation of a strongly nonlinear solitary wave, being another realization of a "sonic vacuum" type system with an exceptionally low speed of signal as observed in chains of beads made from other polymeric materials like Homalite, Nylon or PTFE (Shukla, 1993, Zhu, 1997, Coste, 1999, Daraio, 2005).

Another feature of the strongly nonlinear systems without dissipation is the very fast decomposition of a relatively long initial pulse into a train of solitary waves. This type of pulse can be created using a striker with a mass higher than the mass of the particles in the chain (0.44 g). We used a striker with a mass m_s=1.23 g. Apparently this property may be obscured by the strong dissipation in the polymer based viscoelastic systems. The number of solitary waves with significant amplitude in which the longer initial pulse is expected to decompose throughout the chain is comparable to the ratio of the striker mass and the mass of the beads in the chain (~3 in this particular experimental set-up). The results of this experiment for a Parylene coated beads chain and for a chain made from bare stainless steel beads are shown in Fig. 34.

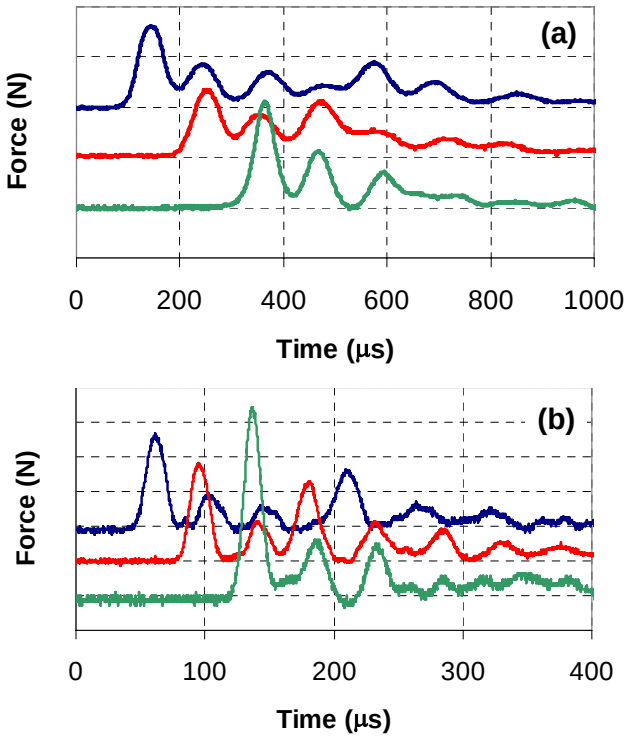

Figure 34. Train of solitary waves generated in a 21 particles chain composed of (a) Parylene-C coated steel balls (4.86 mm diameter) chain and (b) bare stainless steel beads (4.76 mm diameter) chain for comparison. Sensors are placed in the 9th ball from the bottom (top curve), 5th ball from the bottom (middle curve) and at the bottom wall. The velocity of striker (1.23 g Al_2O_3 cylinder) was 0.44 m/s. Y-axis scale is 1 N for (a) and 5 N for (b).

It is evident that the polymer-based strongly nonlinear chain demonstrates a clear tendency to quickly decompose the initial impulse in a train of 3 solitary waves on a distance comparable with the soliton width (Fig. 34(a)) as it is also the case for the much less dissipative stainless steel based system (Fig. 34(b)). In both cases the impulse appears to be almost completely split at the wall, after traveling through only 21 particles, despite the significant difference in pulse speed. Previous experimental work with chains of steel, glass, brass, Homalite, Nylon and PTFE beads validated the prediction of the existence of strongly nonlinear solitary waves as stationary solutions of the wave

equation (Eq. 2). At the same time, it is evident that the bare stainless steel chain supports a more pronounces splitting of the initial pulses into a train of solitary waves. This is most probably related to the higher dissipation in the contact area between the Parylene coated particles. The presence of an increased dissipation in the coated beads is evident from the faster decay of the pulses and the larger overlap of the peaks in the train. The presence of an increased viscous dissipation might contribute to a delay in the signal splitting, as observed in (Herbold, 2006) for a chain of particles immersed in liquids of different viscosities (oil and glycerol).

It is important to investigate the influence of the particle size on the system's behavior for application purposes. Reducing the diameter of the Parylene-C beads may result in different stresses and strain rate conditions at the contact area affecting the behavior of the system specifically increasing the dissipation, as it was observed in a chain of PTFE beads. We conducted experiments with smaller diameter steel balls (2.38 mm) coated by a 50 μm Parylene-C layer (total bead diameter is 2.48 mm). Experimental results are presented in Fig. 35.

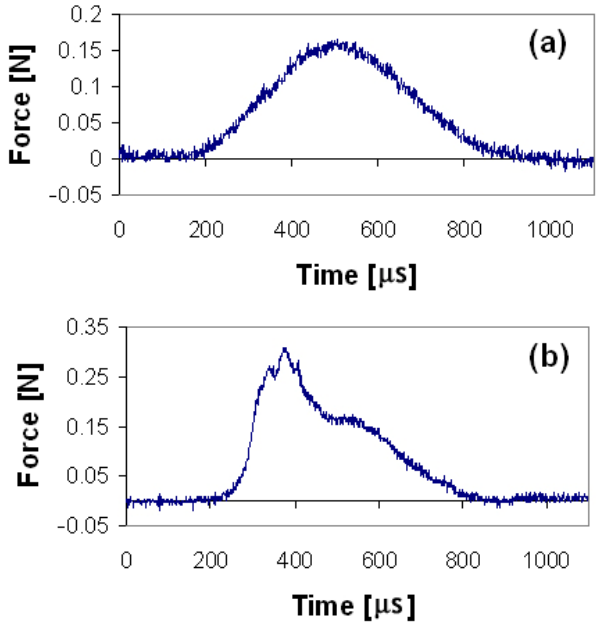

Figure 35. Pulse generated by a single solitary wave (a) and the shock like nonstationary pulse (b) detected on the wall supporting a chain of 22 smaller ParyleneC balls (2.48 mm diameter, m=0.04 g). (a) Impact at velocity 0.89 m/s with 2 mm diameter steel ball (0.036 g); (b) Impact at velocity 0.89 m/s with a 4.76 mm diameter PTFE ball with larger mass 0.123 g.

The sensor in this particular set-up was placed only at the wall for simplicity. Impacts were generated using a 2 mm diameter steel ball (0.036 g, Fig 35(a)) and a 4.76 mm diameter PTFE ball (0.123 g, Fig 34(b)) at velocity 0.89 m/s with no pre-compression acting on the chains (other than the practically negligible gravitational loading due to vertical set-up). It appears that the smaller diameter Parylene-C coated particles tend to form a single solitary wave when impacted by a striker of the same mass as a bead (Fig. 35(a)). This is a typical feature of the "sonic vacuum"-type behavior. When impacted by a striker with higher mass the effect of dissipation appears to delay the solitary wave splitting (Fig. 35(b)).

Parylene can be plastically deformed even at room temperature (Sadeghipour, 1994); this restricts the amplitude of the pulses that can be treated based on the elastic approach. Further details on the extended analysis on the theory of elasticity applied to coated particles can be found in Appendix II. Cracking of the coating layer was seldom observed at higher dynamic force amplitude ranges (≥3 N). Despite this, we observed a consistent behavior in terms of the wave speed dependence on amplitude (Fig. 33(a)). Typical cracks morphology is depicted in Fig. 36. The development of median cracks before the Hertzian cracks is evident. We explain this phenomenon in analogy to the behavior of polymers under spherical indentation (Sadeghipour, 1994). Finite element studies demonstrated that under significant displacements in the contact area the polymeric material is pushed outward causing hoop tensile stresses just outside the contact zone. In our experiments, the median cracks appeared prior to any ring cracks around the contact area, in agreement with the numerical results in (Sadeghipour, 1994). We may expect that under very large contact forces and high strains in the contact area, the steel core might come into direct contact increasing the stiffness of the system therefore increasing the speed of signal propagation.

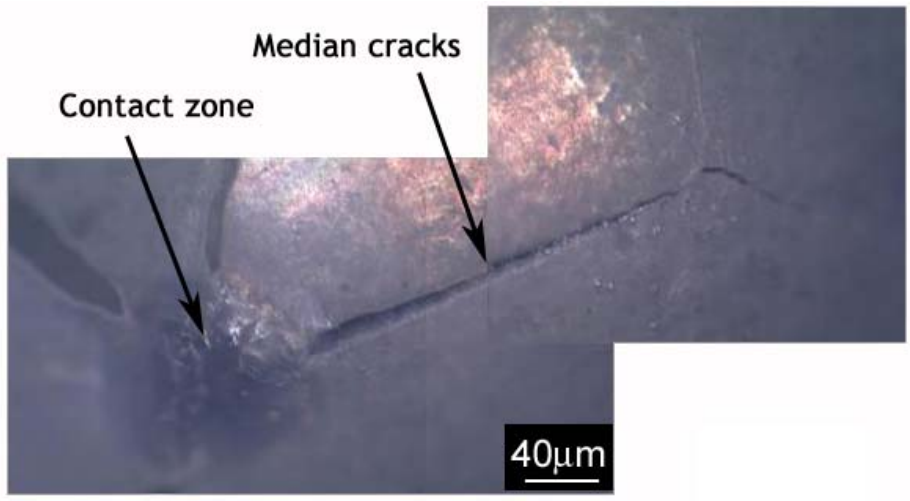

Figure 36. Typical four median cracks originating away from the deformed contact zone (related to the area with radius *b* depicted in Fig. 1) observed after high amplitude dynamic testing with a maximum force on the level of ~3 N. Note that they appear before the Hertzian ring cracks which are supposed to originate on the outside area of the contact zone.

Chains composed of steel beads of different diameters coated by a 50 μm layer of Parylene-C were assembled and investigated under different conditions of impact loading. It was demonstrated that chains of composite particles with a "hard" core and a "soft" interacting contact do support the Hertzian type of interaction and the formation of single and trains of strongly nonlinear solitary waves. The "soft" interacting coating enabled a low signal propagation speed due to the low elastic modulus of the contact interaction and supported the formation of strongly nonlinear solitary waves despite its viscoelastic nature. The formed solitary waves had a speed of propagation well below sound speed in air. Decomposition of the incoming signal into trains of solitary waves was observed only for the larger diameter beads. At relatively high amplitudes of solitary waves we observed the formation of median cracks prior to the formation of ring Hertzian cracks.

Tunability of solitary wave properties in one dimensional strongly nonlinear phononic crystals

As mentioned earlier, strongly nonlinear systems composed of arrays of beads permit the unique possibility of tuning the wave propagation behavior from linear, to weakly nonlinear and further to strongly nonlinear regimes. Through simple noncontact magnetically induced static compression it is possible to tune the wave propagation response of the system from the strongly nonlinear to the weakly nonlinear regime. This allows a fine control of the propagating signal shape and speed with an adjustable static compressive force. Novel applications in different areas may arise from understanding the basic physics of these tunable strongly nonlinear 1-D systems, especially at a low magnitude range of stresses corresponding to signals used in ultrasonic diagnostics or in the audible range. For example, tunable sound focusing devices (acoustic lenses), tunable acoustic impedance materials, sound absorption layers and sound scramblers are among the most promising engineering applications.

The non-classical, strongly nonlinear wave behavior appears in the chain if the system is "weakly" compressed with a force F_0 (Nesterenko, 2001). The term "weakly" is used when the static compressive force (F_0) is very small with respect to the maximum force in a wave. A supersonic solitary wave that propagates with a speed V_s with a force magnitude much higher than F_0 can be closely approximated by one single positive pulse of the periodic solution corresponding to a zero static force (or ξ_0=0). This exact solution has a finite length equal to only five particle diameters for a Hertzian contact interaction. In the continuum approximation the solitary wave speed V_s has a nonlinear dependence

on the maximum strain ξ_m, which translates to a nonlinear dependence on the maximum force F_m on the contacts between the particles in discrete chains. The speed of a solitary wave V_s has a nonlinear dependence on the normalized maximum strain $\xi_r=\xi_m/\xi_0$ in the continuum approximation or, equivalently, the normalized force $f_r=F_m/F_0$ in the discrete chain with beads of diameter a, bulk density ρ, Poisson's ratio ν and Young's modulus E (Eq. 8).

The sound speed c_0 in a chain statically compressed with a force F_0 can be deduced from Eq. 8 at the limit for $f_r=1$ as

$$c_0 = \left(\frac{3}{2}\right)^{1/2} c\ \xi_0^{1/4} = 0.9314\left(\frac{2E}{a\rho^{3/2}\left(1-\nu^2\right)}\right)^{1/3} F_0^{1/6}, \tag{18}$$

where the constant c is:

$$c = \sqrt{\frac{2E}{\pi\rho\left(1-\nu^2\right)}}. \tag{19}$$

Equation 8 also allows the calculation of the speed of weakly nonlinear solitary waves (f_r is slightly larger than 1) which is the solution of the Korteweg-de Vries equation.

When f_r or ξ_r are very large (i.e. F_0 (ξ_0) is approaching 0) Eq. 8 reduces to the Eq. 7 for solitary wave speed V_s in "sonic vacuum" (Gavrilyuk, 1993) for continuum approximation and discrete chains respectively.

The term "sonic vacuum" is used for strongly nonlinear systems without a linear part in the force displacement relation between particles in which no characteristic sound speed is present. For simplicity only the leading approximation was used to connect

strains in the continuum limit and forces in discrete chain in Eqs. (8) and (7). The apparent similarity between Eq. 18 and Eq. 7 is striking (and can be misleading) because these equations describe qualitatively different types of wave disturbances. Equation 18 represents the speed of a sound wave with an infinitely small dynamic force magnitude in comparison with the initial precompressive force and with a long wave length. This wave is the solution of the classical linear d'Alambert wave equation. Equation 7 corresponds to the speed of a strongly nonlinear solitary wave with a finite width of 5 particle diameters and a ratio of solitary wave dynamic force magnitude to initial precompression equal infinity. This solitary wave is the solution of the strongly nonlinear wave equation. A strongly nonlinear compression solitary waves exist for any general power law interaction between particles with an exponent in the force dependence on displacement $n>1$ (Hertz law is a special case when $n=3/2$). The exponent n determines the width of the solitary wave and the dependence of its speed on the maximum strain. The corresponding equations for the speed and width of these solitary waves in the continuum approximation were first derived in (Nesterenko, 1992). The results of numerical calculations for discrete chains can be found in (Rosas, 2004). A general type of strongly nonlinear interaction law also supports the strongly nonlinear compression or rarefaction solitary waves depending on an elastic "hardening" or "softening" behavior.

It is possible to find from Eqs. 7,8,18,19 that the speed V_s of a solitary wave propagating in a one dimensional granular chain can be significantly smaller than the sound speed in the material composing the beads and can be considered approximately constant in any narrow interval of its relative magnitude f_r due to the small exponent in

the power law dependence. The signal speed of strongly nonlinear and linear compression waves in this condensed "soft" matter can be below the level of sound speed in gases at normal conditions as was experimentally demonstrated for PTFE (polytetrafluoroethylene) based sonic vacuum (Daraio, 2005). The described properties of strongly nonlinear waves may permit the use of these materials as effective delay lines with an exceptionally low speed of the signal.

In stainless steel based chains, previous experimental and numerical data regarding the dependence of the solitary wave speed on the force magnitude exists for only relatively large magnitudes of dynamic forces (20 N – 1200 N) (Coste, 1997,1999) and 2 N – 100 N (Job, 2005) and for large diameter of stainless steel beads – 8 mm and 26 mm respectively. To characterize the behavior of stainless steel based strongly nonlinear systems at force magnitudes closer to the magnitude of the signals used in ultrasonic diagnostics we extended the range of experimental data to a lower force magnitude range down to 0.1 N in a chain of beads with a smaller diameter of 4.76 mm. Scaling down of the size of the beads is important for the assembling of practical devices.

The speed, duration and dynamic force magnitude in propagating and reflected pulses from the wall were measured using the experimental set-up presented in Fig. 37. One dimensional PTFE based phononic crystals were assembled in a PTFE cylinder, with inner diameter 5 mm and outer diameter 10 mm. The cylinder was filled vertically with chains of 20 and 52 PTFE balls (McMaster-Carr) with diameter a=4.76 mm and mass 0.1226 g (standard deviation 0.0008 g) (Fig. 37(a)). PTFE has a high strain rate sensitivity (Zerilli, 2002) and an exceptionally low elastic modulus in comparison with metals (Ehrenstein, 2001, DuPont), which ensures a very low speed of soliton

propagation. To compare the properties of the system (signal speed, tunability) 20 stainless steel beads (316 steel, McMaster-Carr catalogue) with diameter a=4.76 mm and mass 0.4501 g (standard deviation 0.0008 g) were assembled in the same PTFE cylinder.

A magnetic steel ball, with diameter a=5.0 mm and mass 0.5115 ± 0.0001 g, was then placed on top of the PTFE or stainless steel chain to magnetically induce a precompression equal to the weight of the magnet (Fig. 37(a)). This experimental set up allows the tunability of interfacial properties, as for example in laminar composite systems made from chains of different materials (Daraio, Nesterenko, 2005).

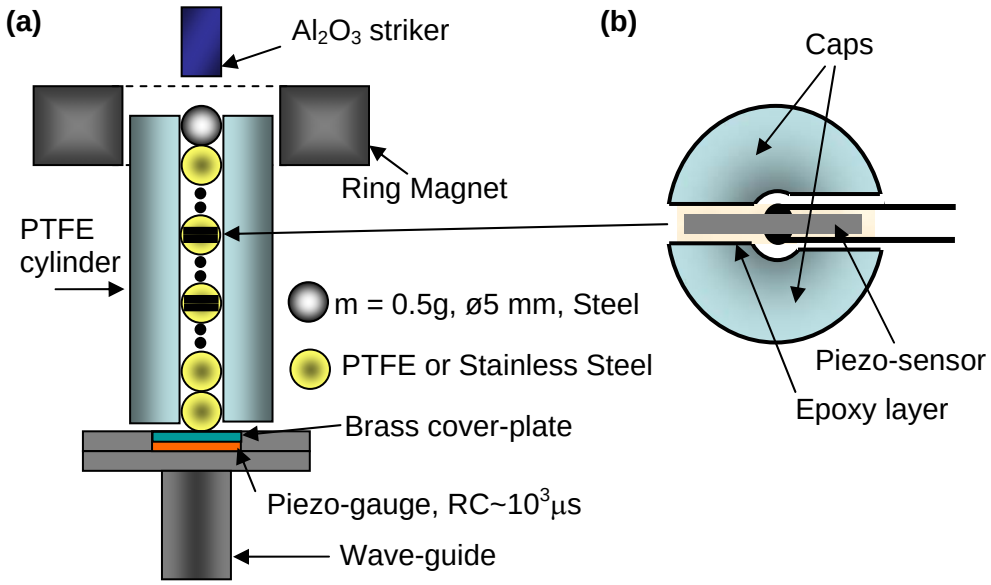

Figure 37. (a) Experimental set-up for testing of strongly nonlinear 1-D chains, the magnetic particle on the top is used for the tuning of the system behavior through exerting a compressive force on the chain equal to the mass of the magnet. The smaller black circles identify a continuation of the similar particles. (b) Schematic drawing of a particle with embedded piezo-sensor.

Three calibrated piezo-sensors (RC ~10^3 μs) were connected to a Tektronix oscilloscope to detect force-time curves. Two piezo-gauges made from lead zirconate titanate (square plates with thickness 0.5 mm and 3 mm side) with Nickel plated electrodes and custom microminiature wiring supplied by Piezo Systems, Inc. were embedded inside two of the PTFE and two steel particles in the chains similar to (Daraio, 2005). The wired piezo-elements were glued between two top parts cut from original beads (Fig. 37(b)). The calculation of the signal speed is based on the time interval between the maxima of the signals detected by the two gauges separated by a known distance (in most cases equal to 5 particle diameters) simultaneously with the measurement of the force acting inside the particles. The speed of the pulse was related to the averaged force magnitude between the two gauges representing the magnitude of the contact force.

A typical PTFE particle with an embedded sensor consisted of two similar caps (total mass $2M$=0.093 g) and a sensor with a mass m=0.023 g glued to them. The total mass of these particles was equal to 0.116 g, which is close to the mass of the original PTFE particle (0.123 g). In theory, the introduction of a particle with a different mass in a chain of particles of equal masses results in weak wave reflections, as observed in (Manciu, 1999, Hascoet, 2000, Sen, 2001). Numerical calculations with a single particle in the chain with a mass 0.116 g embedded into the chain of particles with mass 0.123 g created negligible effects of wave reflections. Therefore such small deviation of the sensor mass from the particle mass (<6%) in both the PTFE and stainless steel chains was neglected in the following numerical calculations and thus, the chains were considered uniform for simplicity.

The third piezo-gauge, supplied by Kinetic Ceramics, Inc., was bonded with epoxy on two electrode foils for contacts and reinforced by a 1 mm brass plate on the top surface. This sensor was then placed on the top of a long vertical steel rod (wave guide) embedded at the other end into a steel block to avoid possible wave reverberation in the system (Fig. 37(a)). The sensor embedded in the wall was calibrated using the conservation of linear momentum during a single impact by a steel ball as in (Daraio, 2005). Sensors in the particles were calibrated by comparing their signal with the signal from the sensor at the wall under a controlled, relatively long, simultaneous impact loading.

Considering the particles with an embedded sensor as rigid bodies, the forces on the top and bottom of the piezoelectric plate can be easily related to the forces acting on the corresponding contacts of the sensor. This simplification allowed a direct comparison of the force-time curves obtained in experiments with the average of the contact forces derived in the numerical calculations. The forces acting on both sides of the sensor deviate symmetrically from the average value of the contact forces if attenuation is negligible. When the measured force reaches its maximum ($F_{m,e}$) it is equal to the corresponding forces on the contacts of the particle and on both sides of the piezoelement.

To relate the maximum value of the dynamic force measured by the embedded sensor $F_{m,e}$ and the value of the maximum contact force between neighboring particles F_m, which is present in the equations for solitary wave speed (Eq. 8, 18, 19), we used the coefficient β found numerically as explained Eq. 10.

Strongly nonlinear sonic vacuum type materials allow a significant change of speed of propagation using an initial static compressive force, which make them qualitatively different from the linear systems. The tunability of the signal propagating through the chains was achieved by adding a magnetically induced preload. In contrast, previous investigations used a preloading of the system through the mechanical application of the load using a wire with attached weights or contact interaction between the last particle and the frame. The former type of preloading allows application of a constant external force to the end magnetic particle independently from its displacement. This was difficult to achieve in the previous attempts especially if the dynamic displacement of the end particle was comparable to its initial displacement due to the preloading. This case would change boundary conditions in an uncontrollable way. The proposed magnetically induced static precompression ensures fixed boundary conditions which are used in numerical calculations and even allows the additional possibility of a fine tuning of the preload which can be time dependent. A Neodymium-Iron-Boron ring magnet (internal and external diameters 11.43 mm, 53.34 mm respectively, with mass 242.2 g ($\pm$ 0.1 g) from Dexter Magnetics Technologies) was placed around the PTFE cylinder containing the chain and held in place by the magnetic interaction with the magnetic steel particle placed on the top of the chain (Fig. 37(a)). Throughout the whole chain the static compressive force induced by the weight of the magnet was 2.38 N additional to nonuniform gravitational preload. This particular set up was chosen to allow an easy noncontact control over the variation of the static preload by slight axial movements of the magnetic ring or by the use of ring magnets of different masses. A

higher level of magnetically induced precompression in experiments (4.25 N) was achieved by adding mass to the magnet.

Nonmagnetic alumina (Al_2O_3) cylinders (0.47 g and 1.2 g) were used in experiments to generate pulses of different durations and force magnitudes in the 1-D phononic crystals, by controlled impacts on the top particle of the chain. Waves of different magnitudes were excited with different velocities of the striker impacts.

Numerical Analysis

For a comparison with experiments, numerical calculations were performed using Matlab. Particles were treated as rigid bodies connected by nonlinear springs according to Hertz law as in the earlier investigations. The validity of the Hertzian interaction for a system composed of PTFE beads was extensively studied and demonstrated in (Daraio, 2005). As mentioned earlier, to compare numerical results and experimental data, we calculated an average compression force for solitary waves based on the corresponding compression forces on the particle contacts. The parameters used in numerical calculations to represent the materials properties are listed in Table 2.

The coefficient β in Eq. 10 is determined numerically as $\beta=F_{d,n}/F_{m,n}$, where $F_{m,n}$ is the maximum value of the force obtained numerically by averaging, at each time step, the dynamic forces on the contacts between adjacent particles and $F_{d,n}$ is the magnitude of these dynamic contact forces. $F_{m,n}$ is analogous to $F_{m,e}$ in experiments.

The dependence of the coefficient β as a function of the normalized force magnitude in a solitary wave $F_{m,n}$ ($F_{m,n}$ / F_0) is shown in Fig. 38. The same coefficient was introduced earlier for PTFE based systems. The coefficient β is independent of the elastic modulus, but varies with respect to the force magnitude of the solitary wave approaching one when $F_{m,n}$ is close to zero. This dependence was taken into account when calculating the value of dynamic contact force from measured values by gauges inside particles for both PTFE and stainless steel cases.

The nonuniform static precompression resulting from the gravitational loading of the particles in the vertical chains was included in calculations and added to the

magnetically induced prestress. The numerical calculations included the presence of the magnetic bead at the top of the chain in all cases. Energy and linear momentum (before interaction with the wall) were conserved with a relative error of 10^{-8} % and 10^{-12} %. Dissipation was not included in the current numerical analysis.

Table 2 Parameters used in numerical calculations to represent the properties of the materials composing the strongly nonlinear media tested experimentally.

	Elastic modulus [GPa]	Poisson ratio	Density [Kg/m^3]
PTFE beads	1.46	0.46	2200
Stainless steel beads	193	0.30	8000
Red-brass (wall)	115	0.31	8750
Alumina (impactor)	416	0.23	3900

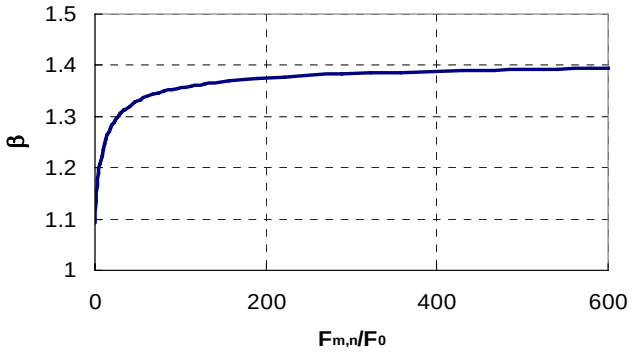

Figure 38. Plot representing the β-coefficient for solitary waves found in numerical calculations for the stainless steel case, as a function of the normalized maximum averaged dynamic force on the contacts ($F_{m,n}$ is corresponding to $F_{m,e}$ measured by embedded gauges in experiments).

The force magnitude of the solitary waves was measured with accuracy in the range of 15% to 30%. The larger error at lower magnitudes is attributed to the higher signal to noise ratio. The accuracy of the speed measurements can be estimated within 10% due to the uncertainty in the sensors alignment (about 1 mm for each sensor).

Typical results of the experiments for a chain of 52 PTFE beads capped by the magnetic steel particle are shown in Fig. 39(a) and (c). In these experiments, the impulse loading was generated using a 0.47g Al_2O_3 cylinder with a velocity of 0.89 m/s impacting the top of a magnetic particle.

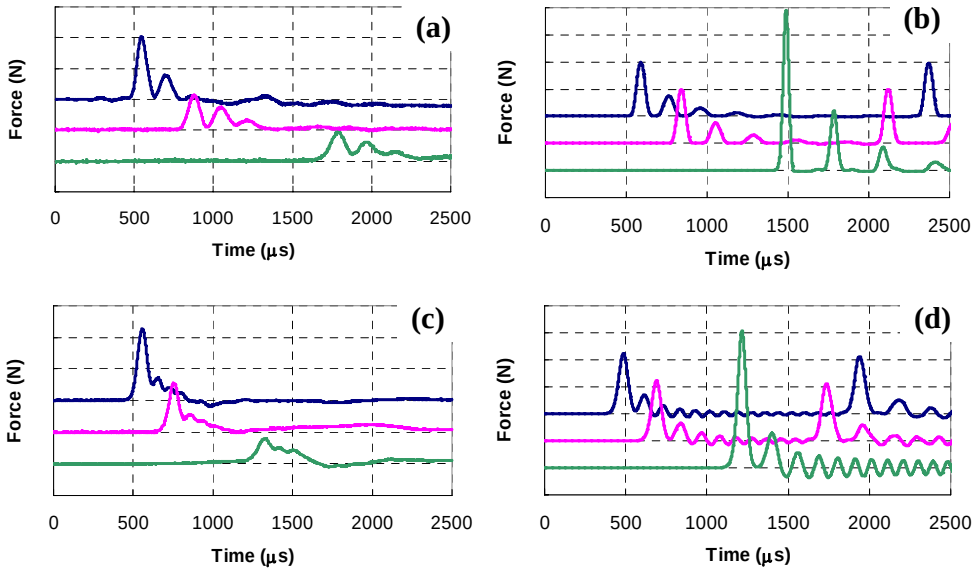

Figure 39. Experimental and numerical results corresponding to a chain of PTFE beads with and without magnetically induced precompression. (a) Forces detected in experiment by the sensor in the 20th ball from the impacted side (top curve), by the sensor in the 29th ball (middle curve) and at the wall (bottom curve) without magnetic pre-compression, vertical scale is 0.5 N per division; (b) Numerical calculations of averaged dynamic contact forces between particles and at the wall corresponding to the signals detected by the sensors in (a), without magnetic precompression but including gravitational preload, vertical scale is 2 N per division; (c) Forces detected in experiment with static magnetically induced precompressive force equal 2.38 N, vertical scale is 1 N per division; (d) Numerical calculations corresponding to experimental conditions in (c) including forces due to gravitation and magnetic precompression, vertical scale is 2 N per division.

Internal sensors were placed in the 20th and 29th beads from the top magnetic particle and the third piezo-gauge was embedded in the wall. The zero time in experiments corresponding to Fig. 39(a),(c) is arbitrary chosen, and the zero time in numerical calculations (Fig. 39(b),(d)) corresponds to the moment of impact.

The obtained experimental profiles and corresponding numerical results for a gravitationally loaded chain are presented in Fig. 39(a),(b). In this weakly compressed state, the Teflon-based "sonic vacuum" demonstrates the typical fast decomposition of an

initial impulse over a distance comparable to the soliton width similar to the trains observed in a shorter 21 particle chain (Fig. 28). In Fig. 39(a) the duration of the leading solitary wave pulse was equal to 170 μs. The speed of its propagation, based on the time interval between the signal's maxima measured by the two embedded sensors, was 129 m/s. These values result in a solitary wave width equal to 4.6 particles diameters. This agrees reasonably well with the solitary wave width predicted in long wave theory for a chain of particles interacting according to Hertz law (5 particles diameter). These parameters allow one to evaluate the characteristic strain rates for PTFE at the contact area equal to $4x10^2$ s^{-1}. The experimental results (Fig. 39(a),(c)) agreed reasonably well with the numerical calculations under the same testing conditions (Fig. 39(b),(d)) as well as other investigated impact conditions although dissipation is apparent especially at the bottom of the chain (Fig. 39).

Results of numerical calculations demonstrated that magnetically induced static compressive force under a similar type of impact caused a qualitative change of the signal shape from a train of solitary waves in a weakly compressed case (Fig. 39(b)) to a few solitary waves with a periodically oscillating tail (Fig. 39(d)). In experiments (Fig. 39(c)) the periodic oscillatory tail was not observed, which may be due to the dissipation caused by the interaction between the wall of the holder and the particles as well as dissipation on the contacts.

One of the most interesting consequences of the noncontact magnetically induced static force applied to the chain is a significant change in the speed of the signal propagation. In Fig. 39(a-d) the pulse excited by the same impact resulted in an increased speed from a value of 129 m/s for the gravitationally loaded chain to 222 m/s for the

magnetically preloaded system. This means a ~70% control over the initial "natural" signal speed of the investigated strongly nonlinear system. The solitary wave speed in only gravitationally loaded PTFE chains is about two times smaller than the speed of a solitary wave in the chain of nylon beads with magnitude 1 N due to a smaller elastic modulus of Teflon in comparison with Nylon. This is in agreement with theoretical dependence of speed on elastic modulus (Eq. 8).

Interestingly, in numerical calculations the dynamic force magnitudes of the incident pulses in the magnetically precompressed chains are close to the one observed in the only gravitationally loaded chains (compare corresponding curves in Fig. 39(b) and (d)). Meanwhile, the dynamic force magnitude on the wall in the magnetically precompressed chains in numerical calculations is noticeably smaller than the one in the former case (see bottom curves in Fig. 39(b) and (d)). This shows that the static compressive force can significantly reduce the maximum of the dynamic force acting on the wall though this phenomenon was not observed in the experiments probably due to the decrease of dissipation in the magnetically precompressed chain.

In experiments an impact by the same striker with the same velocity on the gravitationally and magnetically preloaded PTFE chains resulted in an increase of force magnitude by 2 times in the incident pulses (compare corresponding curves in Fig. 39(a) and (c)). This is probably due to the significant decrease of dissipation related to the increase of the stiffness and to the reduction of the relative displacement between the particles under similar conditions of loading at higher precompression. The delayed splitting observed in Fig. 39(c) also contributes to the larger amplitude of the leading pulse.

The low magnitude precursor under magnetic precompression was noticeable especially in the wall gauge (Fig. 39(c), bottom curve). This may be due to the propagation in front of the leading solitary wave of a high speed disturbance with the speed of sound in solid PTFE through the central cylindrical column created when the initial precompression flattens the contact area between spherical particles. This phenomenon is not included in the numerical approach and requires further investigation.

Table 3 shows a summary of the typical results for the magnitude of the dynamic contact forces F_d and corresponding velocities V_s obtained in experiments. A comparison of 5 representative values obtained experimentally with the corresponding values obtained in numerical calculation and with the theory of long wave approximation for given values of F_d are included for clarity.

Table 3. Comparison of experimental values of the solitary wave speeds V_s with the corresponding values obtained in numerical calculation and with the theoretical values from long wave approximation.

Only Gravitational Precompression						Magnetic and Gravitational Precompression					
erimental Data		Numerical Results		Long Wave Approximation		Experimental Data		Numerical Results		Long Wave Approximation	
N]	V_s [m/s]	$F_{d,n}$[N]	V_s [m/s]	F_d [N]	V_s [m/s]	F_d [N]	V_s [m/s]	$F_{d,n}$ [N]	V_s [m/s]	F_d [N]	V_s [m/s]
5	168	5.7	184	5.7	182	5.7	241	5.8	228	5.8	230
3	166	4.3	177	4.3	174	4.5	235	4.5	224	4.5	227
3	167	3.3	170	3.3	167	3.4	230	3.2	220	3.2	223
5	163	2.6	163	2.6	161	2.6	221	2.6	218	2.5	221
1	143	2.0	159	2.0	155	2.0	223	2.0	215	2.0	220

The force data presented in the experimental part of the table (F_d) represents the average of the maximum value of the force at the two contact points ($F_{d,e}$) extracted from the magnitudes of the corresponding signals of the two embedded gauges with force magnitudes $F_{m,e}$, (where $F_{d,e} = \beta F_{m,e}$). The solitary wave speeds related to F_d were obtained by dividing the distance between the sensors (placed in integer intervals of 5 particle diameters) by the measured peak-to-peak time interval. To calculate the speed of a solitary wave corresponding to the given contact force magnitude F_d in the long wave approximation we used Eq. 8 where the total force F_m is the sum of F_d plus F_0 caused by initial precompression (gravitational or gravitational plus magnetic).

The speed of a solitary wave in the long wave approximation is slightly lower than in the numerical calculations for a gravitationally loaded discrete chain at the same magnitude of dynamic force F_d (see left side of Table 3). The opposite tendency is

characteristic for the case where additional magnetically induced loading is applied (see right side of Table 3). In both cases the difference between the long wave approximation and a discrete chain is actually very small, which agrees with the results of Rosas, 2004.

It should be noted that the speeds of the solitary wave at the investigated range of dynamic force magnitudes (which is about 2 times higher than the initial precompression force) in the magnetically precompressed chain is slightly higher than the speed of the sound in the system c_0 =211.2 m/s evaluated from Eq. 19.

The comparison of the shapes of the leading pulses detected experimentally and the stationary solitary waves obtained in separate numerical calculations including a larger number of particles is shown in Fig. 40.

From Fig. 40 we can see that the shape of the leading pulses in experiments is close to the shape of the stationary solitary waves in the numerical calculations despite that in experiments these pulses were not completely separated from the oscillatory tail at the given distances of the sensors from the impacted end of the chain.

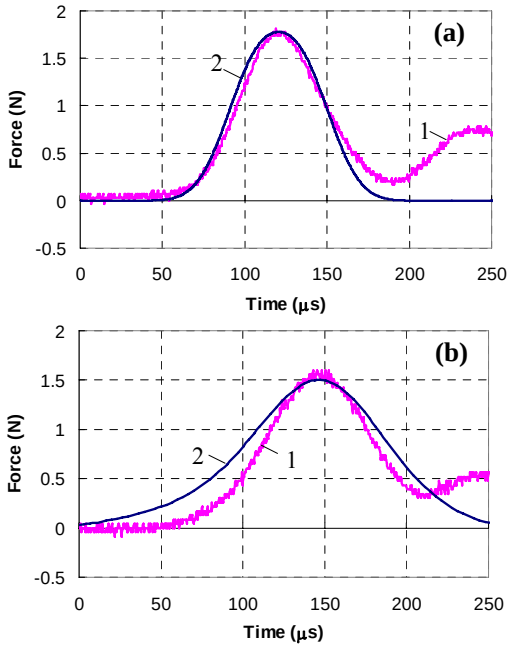

Figure 40. The leading pulses obtained in experiments (curve (1)) and stationary solitary waves found in numerical calculations (curve (2)) with the same force magnitude. (a) PTFE chain under gravitational precompression and the stationary solitary wave calculated in a "sonic vacuum", (b) Magnetically precompressed PTFE chain and the stationary solitary wave calculated in a uniformly precompressed chain with force 2.38 N. In both cases the PTFE chain was composed of 52 particles and a sensor was embedded into the 21st particle from the top, a magnetic steel particle was positioned on the top and the impactor was the 0.47 g Al_2O_3 cylinder.

It should be mentioned that, in the magnetically precompressed chains the splitting of the incident pulse into a train of solitary waves is delayed especially when the dynamic force magnitude of the pulse is smaller than or comparable to the initial static compressive force. At a relatively small value of their ratio the strongly nonlinear solitary wave becomes close to the soliton solution of the Korteweg-de Vries wave equation with a width infinitely increasing with dynamic force magnitude decreasing to zero. Detailed analysis of the depth for solitary wave stabilization depending on the relative magnitude of the solitary wave force and the initial precompressive force can be

found in (Arancibia-Bulnes, 2002). In the numerical calculations, the leading solitary pulse was formed being completely separated from the oscillatory tail in the vicinity of the 950th particle from the impacted end (curve 2 in Fig. 40(b) corresponds to the 980th particle in the chain included in the numerical calculations). This may explain why the stationary solitary pulse in numerical calculations is wider than the width of the nonstationary leading pulse in the magnetically precompressed chain experimentally detected at the 20th particle (Fig. 40(b)). The corresponding increase of the width of the leading pulse when it propagates inside the magnetically precompressed chain was observed in our numerical calculations.

Figure 41 shows the comparison of the experimental results with the theoretical values obtained from the long wave approximation, and the numerical data for discrete chains of both gravitationally (lower curves and experimental points) and magnetically precompressed (2.38 N) systems (upper curves and corresponding experimental points). It is known that the theoretically predicted speed of solitary waves in strongly nonlinear chains has a strong dependence on the magnitude represented by Eq. 8 for precompressed chains. The curves based on the long wave approximation (curves 2 and 4) are very close to the one obtained in numerical calculations (curves 3 and 5). It should be mentioned that this agreement is obtained when only the leading approximation was used to connect strains in the continuum limit and forces in discrete chain in Eqs. 8 and 7. Experimental data obtained with an increased precompression (4.25 N, not shown in Fig. 41) also followed the general trend prescribed by long wave approximation.

At higher force magnitudes in the solitary wave the agreement between the theoretical data and experiments is better than at lower magnitude for the weakly

(gravitationally) precompressed chain. We attribute this behavior to the dependence of the elastic modulus of the dynamically deformed PTFE on strain (and strain rate) on the particle contact.

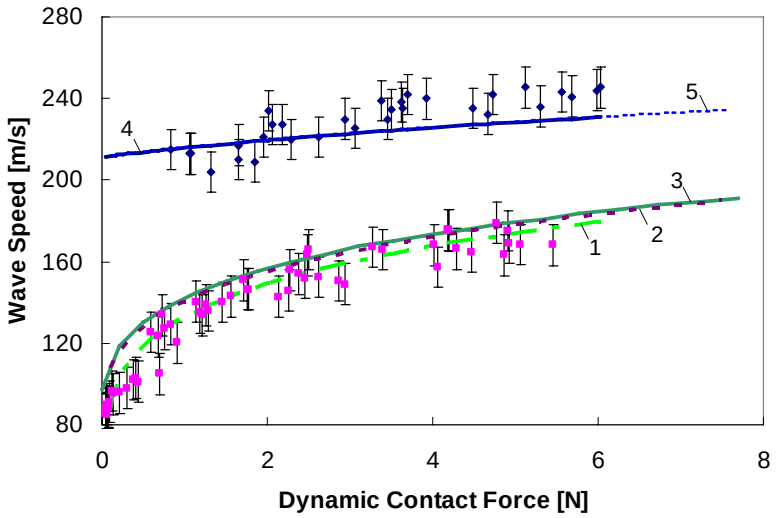

Figure 41. Dependence of the solitary wave speed on the magnitude of the contact dynamic force for gravitationally loaded and for magnetically tuned chains composed of PTFE beads. The experimental values for corresponding curves are shown by solid squares and dots. Curve 1 represents the long wave approximation for the "sonic vacuum" using an elastic modulus for PTFE equal to 1.46 GPa. Curves 2 and 4 are the theoretical curves based on Eq. 8, and the corresponding numerical calculations for the discrete chains are represented by curves 3 and 5.

It should be mentioned that the solution obtained with the long wave approximation (Eq. 8) for a solitary wave refers to a uniformly compressed chain with a static force F_0. The gravitational force, though, results in a nonuniform chain compression. To apply the solution from the long wave approximation to the gravitationally preloaded and magnetically tuned chains to calculate V_s, we used a constant value of F_0 equal to the value of compressive force at the midpoint between the

sensors. In the numerical results the local wave speed was calculated taking into account the nonuniform gravitational compression. The small difference observed when comparing the two approaches (compare curves 2 to 3 and 4 to 5 in Fig. 41) demonstrated that they are in a very good agreement in this range of static and dynamic forces. Even the "sonic vacuum" approximation (where the gravitational preload is excluded, Eq. 7) agrees reasonably well with the cases where gravitational compressive forces were taken into account (compare curve 1 with 2 and 3) for larger magnitudes of dynamic contact force. At magnitude of dynamic contact forces close to zero, there is a significant difference between the "sonic vacuum" and the gravitationally precompressed chains. The speed of the wave in sonic vacuum tends to zero at very low magnitude of dynamic contact forces, while in the gravitationally loaded chains it tends to the value of the corresponding sound speed c_0 = 92.6 m/s with a dynamic elastic modulus for PTFE taken equal to 1.46 GPa (Eq. 18). The numerical data also demonstrated the same limit for c_0. In the low magnitude range the experimental data is below the long wave approximation and numerical curves. This may be due to the less than 1.46 GPa dynamic elastic modulus of PTFE at smaller strains (and strain rates).

The increase of the sound speed c_0 in the PTFE chain under the added magnetically induced precompression (2.38 N) in comparison with only gravitational preload (0.017 N, c_0 = 92.6 m/s) is about 128% at practically the same density. This results in a corresponding change of acoustic impedances.

The agreement between the speeds in the magnetically tuned system and the estimated theoretical values means that the equations for the dependence of the solitary wave speed based on the nonlinear continuum approximation can be a reasonable

foundation for the design of "sonic vacuum" type devices based on PTFE beads. The speed of the solitary wave at the minimum investigated dynamic force magnitude in the magnetically precompressed chain (limit at F_d approaching zero for curves 4 and 5 for long wave approximation and numerical calculations respectively) is very close to the speed of the sound in the system c_0 = 211.2 m/s (estimated based on long wave approximation Eq. 18).

In the experiments with magnetically induced static precompression the maximum total force (8.4 N) was larger than in the gravitationally precompressed chain. Additionally PTFE was loaded differently in comparison with the weakly compressed chain even when the maximum forces were the same. As mentioned, the elastic modulus of PTFE chains was selected to have a constant value of 1.46 GPa from the extrapolation of the Hugoniot data (Carter, 1995). Despite a difference in the loading conditions at this large strain the higher value of the elastic modulus (compared to the ultrasonically measured elastic modulus at normal conditions) is able to describe the experimental data. Further research on the value of elastic modulus of PTFE under conditions of dynamic deformation and the application of Hertz law is necessary to clarify the observed behavior. The dependence of PTFE's elastic modulus on contact strain may cause a deviation of the contact law from a Hertzian type behavior.

To compare the predictions of the long wave theory for the tunability of strongly nonlinear systems and relate it with the variation of the elastic modulus of the beads, we measured the parameters of the solitary waves in a stainless steel based system under the same magnetically induced precompression. Stainless steel particles have more than two orders of magnitude difference in the elastic modulus (193 GPa) with respect to PTFE

(1.46 GPa). The experimental results of previous research (Lazaridi, 1985 Coste, 1997, 1999, Job, 2005) are in excellent agreement with the predictions of the long wave theory and with the results of numerical calculations for chains composed of stainless steel beads. The addition of a prestress in chains composed of steel beads was also examined by Coste, 1997 but for a range of force magnitudes much higher than the one presented in this study. This paper extends the investigation to multiple solitary waves in contrast to single solitary wave in (Coste, 1997).

Experimental and numerical results for chains composed of stainless steel beads are shown in Figs. 42 and 43. Solitary waves in the chain of stainless steel beads also demonstrated a significant increase of speed with added magnetically induced prestress of 2.38 N. For example, in experiments the leading solitary pulse presented in Fig. 42(a) had a speed of 580 m/s in the gravitationally precompressed chain then increased to 688 m/s with the addition of magnetic precompression in Fig. 42(c). This behavior was also observed in the numerical calculations (Fig. 42(b), (d)).

Similar to the PTFE based chains, the numerical calculations in the stainless steel based system did not show any change of the dynamic force magnitudes of the incident solitary pulses with the application of the initial magnetically induced precompression (see Fig. 42(b), (d)). This behavior is different than the one observed in experiments, where the added precompression did change the magnitude of the incident pulse (compare Fig. 42(a) and (c)). This difference can be explained by the reduction of dissipation in the precompressed chain in experiments.

It is interesting that a tendency toward a delay of the splitting into a solitary wave train in experiments was observed when the force magnitude of the incident pulse was increased which may be due to the dissipation increase with magnitude of the pulse.

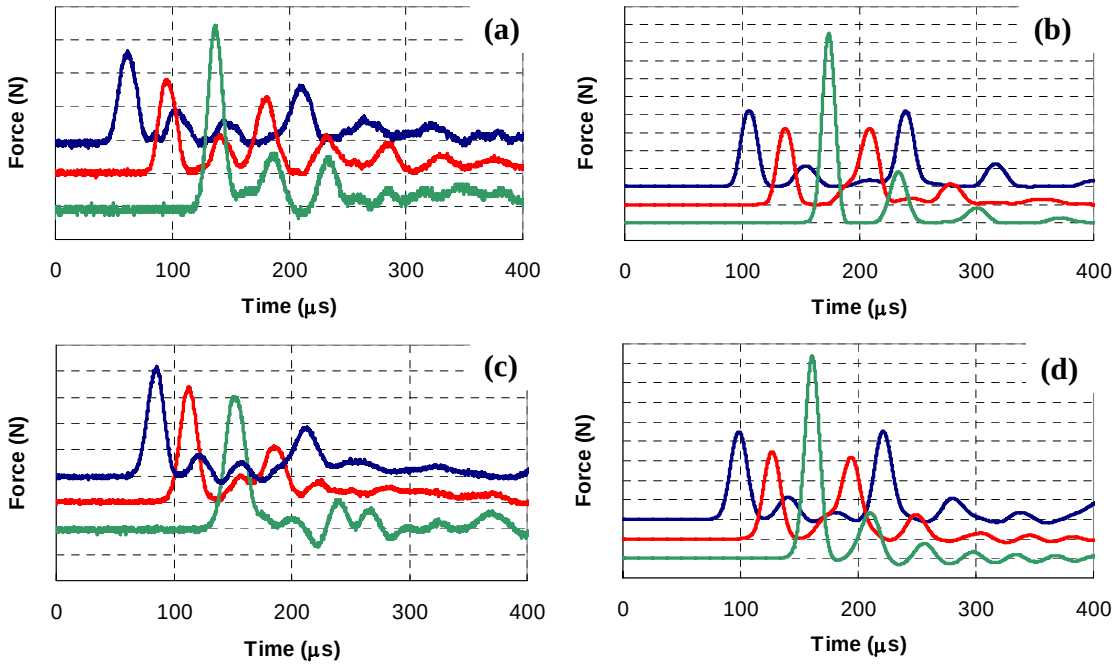

Figure 42. Experimental and numerical results on a chain of 21 stainless steel (316) beads with and without magnetic precompression impacted by an alumina striker with a mass equal to 1.2 g and initial velocity equal to 0.44 m/s. (a) Force detected in experiment by the sensor in the 9th ball from the wall (top curve), by the sensor in the 5th ball (middle curve) and at the wall (bottom curve) without magnetic pre-compression; (b) Numerical calculations corresponding to experimental conditions in (a), including gravitational precompression; (c) Force detected in experiment with magnetic pre-compression equal 2.38 N; (d) Numerical calculations corresponding to experimental conditions in (c), including gravitational and magnetic precompression. Vertical scale is 5 N per division for all figures (a-d).

A slight change of the propagating pulse shape was observed in the magnetically precompressed stainless steel chain. The reduced time interval between the maxima of the incident solitary waves in experiments and in numerical calculations (Figs. 42(c) and

(d) respectively) demonstrates a significant delay of the pulse splitting. This effect in stainless steel based chains is less noticeable than in PTFE (see Fig. 39(c) and (d)) which may be due to the smaller speed of signal propagation in the PTFE chains. Also, in the stainless steel case, no increase of the wall's pulse magnitude was detected, contrary to the PTFE based chains. The larger difference between the elastic constant of the wall and that of the PTFE chain can be the cause of this phenomenon.

Figure 43 shows the comparison of the experimental results with the theoretical values for solitary wave speed versus dynamic force magnitude obtained from the long wave approximation (Eq. 8), of both gravitationally (curve 1 and experimental points) and magnetically precompressed systems (curve 2 and corresponding experimental points). The curves corresponding to the stainless steel system extend to a wider range of magnitudes and velocity and the scale is therefore wider than in Fig. 41 for PTFE chains. The curves based on the long wave approximation and the numerical results coincide for both gravitationally and magnetically precompressed chains. When the dynamic force magnitude approaches zero in the magnetically plus gravitationally precompressed chain (F_0=2.44 N), the pulse speed is seen to approach the sound speed (c_0= 539.6 m/s) derived from the long wave approximation (Eq. 18). The change of the sound speed c_0 in the stainless steel chain under the added magnetically induced precompression (2.38 N) in comparison with the system under only the gravitational preload (0.062 N, c_0=292.6 m/s) is about 84% at practically the same density, resulting in the corresponding change of acoustic impedances.

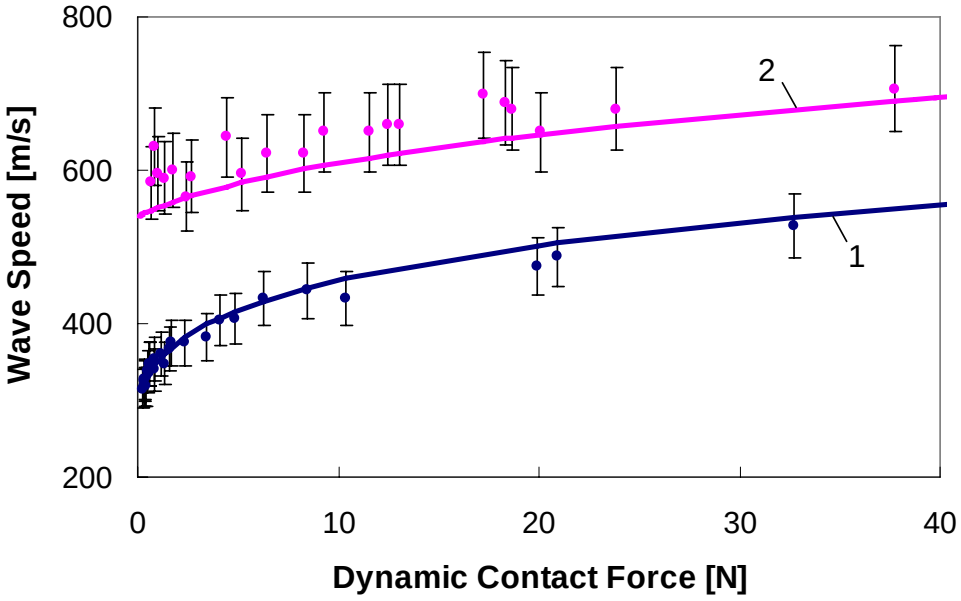

Figure 43. Dependence of the velocity of a solitary wave on the magnitude of the dynamic force for both a gravitationally loaded and magnetically tuned stainless steel chain. Experimental values for corresponding curves are shown by solid dots. Curves 1 and 2 are the theoretical curves based on Equation 8, corresponding numerical calculations for discrete chain practically coincide with curves 1 and 2 based on the long wave approximation.

These results show that stainless steel particles under the same static precompressive force demonstrate a higher absolute increase of the solitary wave speed when compared to the PTFE system (compare Fig. 41 and 43) both in experiments, theory and in numerical calculations. Because the PTFE system is elastically much softer, this result can appear counterintuitive. This behavior of the solitary wave speed with static preloading is due to the fact that, in general, a smaller displacement under the same precompression is outweighed by the larger elastic modulus of stainless steel.

These properties of strongly nonlinear phononic crystal can be used for controlled impulse transformation in relatively short transmission lines as well as in tunable acoustic focusing lenses.

In conclusions, one-dimensional strongly nonlinear phononic crystals were assembled from chains of PTFE (polytetrafluoroethylene) and stainless steel spheres with gauges installed inside the beads. Trains of strongly nonlinear solitary waves were excited by an impact. A new method of preloading phononic crystals via magnetic precompression was successfully demonstrated for one dimensional strongly nonlinear systems based on two qualitatively different materials – elastic (stainless steel) and viscoelastic (PTFE) beads having more than two orders of magnitude difference in their elastic moduli. This novel method of precompression ensured well controlled boundary conditions and the possibility of a time-dependent fine tuning of the signal speed. The change of the sound speed in these systems under the investigated magnetically induced precompression in comparison with the gravitational preload only is 84% and 128% for stainless steel and PTFE chains respectively at practically the same density. They result in the corresponding change of acoustic impedances.

Both systems were investigated for different conditions of loading under the tunable unobtrusive magnetic prestress. A significant tunability of the speed of the signal was achieved over the "natural" uncompressed strongly nonlinear system. The change of the solitary wave speed with prestress in experiments is described very well by the results of the long wave approximation and the numerical data.

The initial preloading significantly reduced dissipation in the experiments in both PTFE and stainless steel based systems. A decrease of the reflected wave force

magnitude on the wall was observed in numerical calculations for PTFE system. A delay of the splitting of the solitary waves under prestress was observed in experiments and in numerical calculations.

The solitary wave properties obtained in the long wave approximation are a reliable tool in the designing of sonic vacuum based devices.

Analysis of waves interaction with interfaces

Another intriguing property of the strongly nonlinear materials is the reflection of the solitary waves at the interface between two SV-type materials (Nesterenko, 2001, Vergara, 2005), from imperfections (Manciu, 1999) or from a wall (Job, Vergara, 2005). Based on the former, the novel concept of impulse trapping inside a protecting granular laminar layer has been proposed (Hong, 2002, 2005, Daraio, 2006).

The passage of a solitary wave through the interface of two SV type systems from a region of particles with a higher elastic modulus (or higher mass) to a region of lower elastic modulus (or lower mass) results in the impulse decomposition into a train of solitary pulses. The reflection from light and heavy inclusions was earlier proposed as a technique for nondestructive identification of impurities in a granular medium (with implications in the analysis/detection in geological or biological fields).

In the studies presented we investigated experimentally and numerically some new interesting properties of interfacial interaction of strongly nonlinear solitary waves propagating in different systems.

Interface reflection in a 5 mm - 2 mm steel beads system

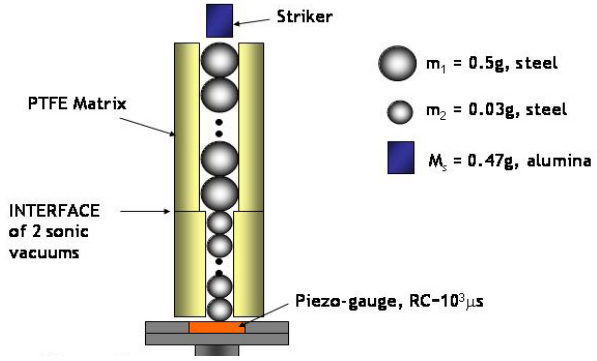

Figure 44. Set-up for the testing of reflection from interface of "sonic vacuums".

The first type of interface testing between 2 strongly nonlinear systems was performed on the interface between two "sonic vacuums" (SV-type) systems composed of stainless steel beads of different diameter (5 mm and 2 mm) and mass (0.5 g and 0.03 g) as illustrated in Fig. 44. From the comparison of the signals arriving at the bottom sensor (wall of the system) it is apparent that the impulses marked by arrows (Fig. 45) correspond to the reflection of the wave, originated on the bottom of the system, from the interface of two strongly nonlinear chains. Because the system is strongly nonlinear this reflection may not be described in terms of linear acoustics impedances.

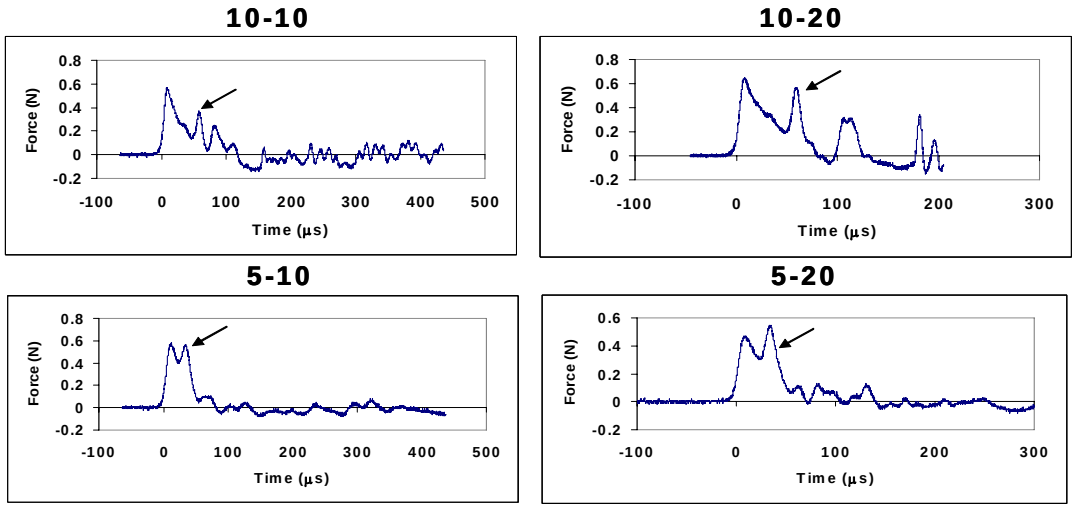

Figure 45. Wave reflection (shown by the arrows) from the interface of strongly nonlinear chains.

Anomalous wave reflection at the interface of two strongly nonlinear granular media

Here we present the first experimental and numerical observation of strongly nonlinear wave interaction with the interface of two SV-type systems resulting in anomalous reflected compression and transmitted rarefaction waves when the magnetically induced prestress is applied.

We propose a new method of noncontact precompression based on the magnetic interaction of the first magnetic particle in the chain with a Nd-Fe-B ring magnet placed outside the chain as described earlier and in (Daraio, 2005). The added magnetically induced static precompressive force (2.38 N) is practically independent of the motion of the magnetic particle.

In experiments we placed a chain of 20 nonmagnetic stainless steel (316 type) particles (plus a magnetic particle on the top) with diameter a=4.76 mm and mass 0.4501 g above 21 PTFE (polytetrafluoroethylene) beads with diameter a=4.76 mm and mass 0.1226 g. The elastic moduli and Posson's ratios for PTFE and stainless steel were equal to 1.46 GPa (Daraio, 2005) and 193 GPa, 0.46 and 0.3 respectively. Piezogauges measuring the compression force were placed in the 8^{th} and 4^{th} particle above the interface and in the 4^{th} and 8^{th} particle below the interface.

The equations of motion used in numerical calculations are similar to those described earlier. The intrinsic MATLAB ODE45 solver was used with a time step of 0.8 microseconds. No restitutional losses were taken into account. The linear momentum and energy were conserved with a relative error of 10^{-12}% and 10^{-8}%.

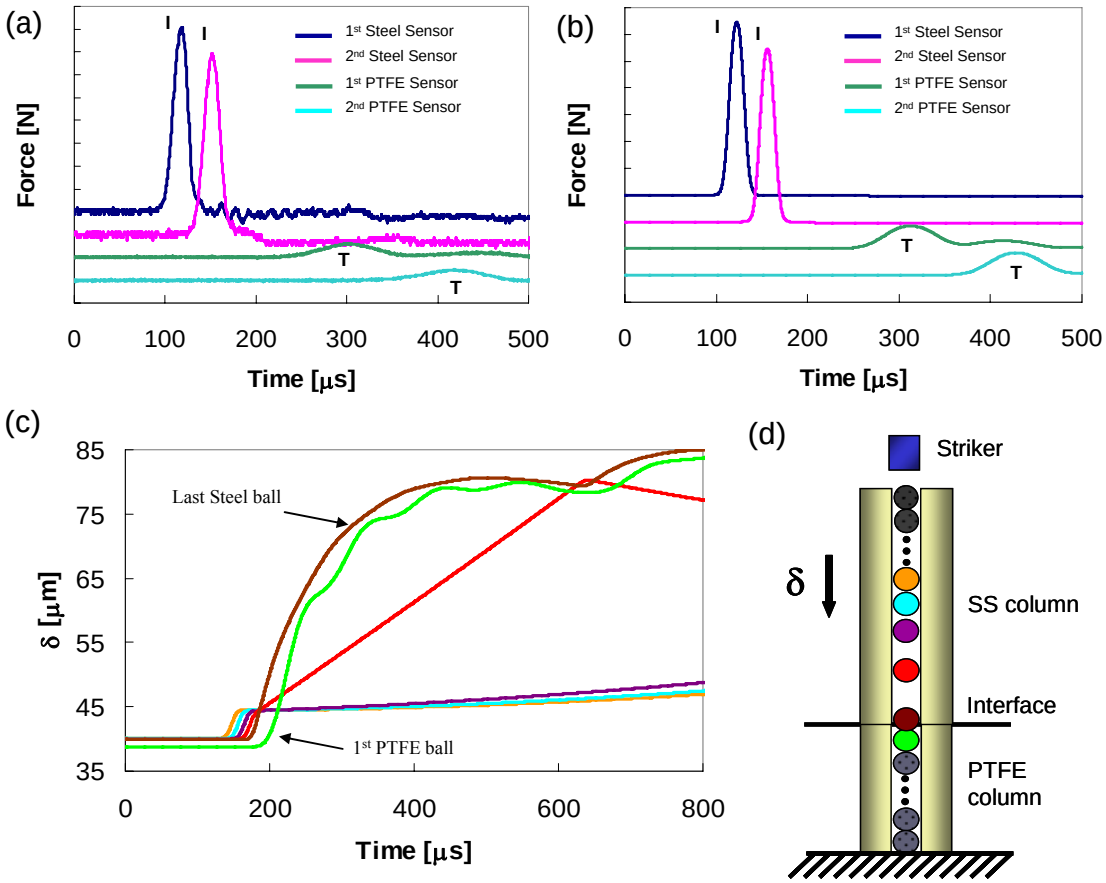

Figure 46. Incident pulse (I) interaction with the interface of the two SVs composed of 20 stainless steel and 21 PTFE beads. (a) Experimental data. (b) Numerical simulation of (a), vertical scales 1N (a) 2 N (b) per division. (c) Displacements (δ) of beads adjacent to the interface. (d) The relative positions of particles 600 μs after the impact.

The curves obtained in numerical calculations represent the averaged compression forces on the contacts of each particle, except curves in Fig. 48(a) and (c) where the contact forces between particles are shown. The displacement (δ) of each particle is calculated from the equilibrium positions with no external load.

The results without magnetic precompression are presented in Fig. 46. A solitary wave ("I") was excited in the system by an impact of an alumina cylinder with a mass of 0.47 g and velocity of 0.44 m/s. This single solitary wave generates multiple pulses ("T")

in the PTFE chain after the interaction with the interface. No reflected compression wave is detected in experiments or numerical calculations (Fig. 46(a) and (b)).

The mechanism explaining the practically complete energy transfer into the PTFE chain and the absence of a reflected compression wave is illustrated by the numerical results in Fig. 46(c). The slopes of the displacement-time curves represent the velocity of the corresponding particles. It is evident that a series of gaps (Fig. 46(d)) open between the stainless steel particles in the vicinity of the interface. Therefore a "fracture wave" is propagating into the stainless steel chain similar to the one originating when the solitary wave arrives at the free surface (Hinch, 1999) due to high gradients of particle velocities. Gap openings are also observed in: a 1-D granular chain in the process of solitary wave collision, which are related to the generation of secondary solitary waves (Manciu, 2000, 2002 Sen, 2003) and in 2-D numerical simulations of the transmission of the static force (Goldenberg, 2005), and it is related to the subharmonics and noise excitation in the transmission of the acoustic wave in granular media (Tournat, 2004).

The gap's opening and closing introduce an entirely new time scale in the system which is determined by the size of the gaps and particle velocities instead of the time of flight determined by particle diameter or length of the chain and signal speed.

The strongly nonlinear particle's interaction results in a high gradient of particle velocity in the incident wave that translates into a high gradient of velocity near the interface with the last stainless steel particle absorbing the main part of the energy. The zero tensile strength of the chain ensures the uni-directional energy transfer to the PTFE chain without sending any tensile wave back to the stainless steel chain. Thus, the

observed behavior is due to a double nonlinearity: a strongly nonlinear compression part of the interacting force and a zero tensile strength of the system.

At the moment when the process of energy and linear momentum transmission into the PTFE chain is practically complete, only a very small portion of the impactor's kinetic energy (about 0.16%) is reflected and the second steel particle is rebounding from the interface with a velocity of 0.018 m/s. Without the gravitational precompression this particle rebounds much later with a velocity significantly smaller (0.0009 m/s) than in the previous case. This indicates that the reflected energy can be increased with the initial precompression.

The sequence of pulses in the PTFE chain are generated by the decelerating interfacial stainless steel particle, which is demonstrated by the kinks of decreasing amplitude on the displacement curve of the first PTFE particle in Fig. 46(c).

The application of the magnetically induced precompression resulted in a completely different reflection of the strongly nonlinear pulse from the interface (compare Fig. 46(a) with Fig. 47(a) and Fig. 46(b) with Fig. 47(b)). In this case the compression pulse is propagating into the steel chain followed by an oscillatory rarefaction wave (Fig. 47(a) and (b)). The acoustic impedance of the stainless steel chain is about one order of magnitude higher than that of the PTFE chain.

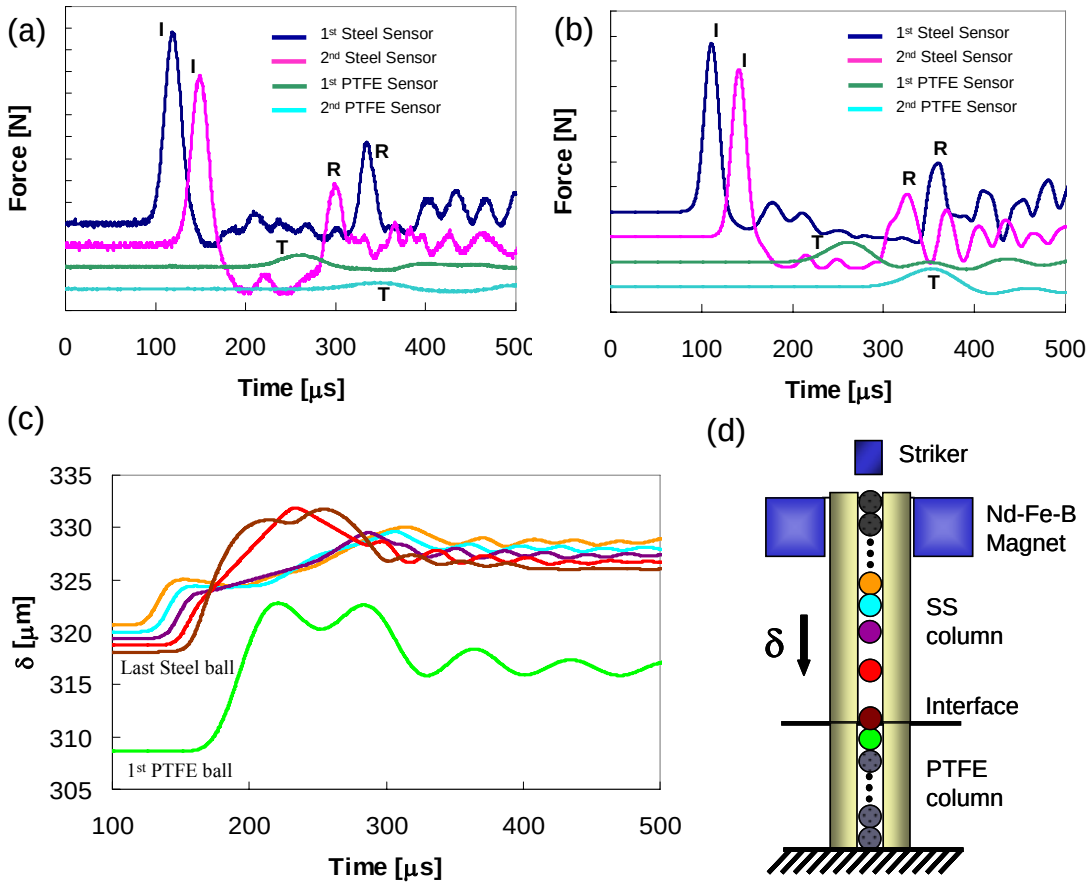

Figure 47. Anomalous pulse reflection from magnetically preloaded interface of two sonic vacua in a configuration similar to Fig. 46. (a) Experimental data. (b) Numerical simulation of (a); vertical scales 1N (a) and 2 N (b) per division. (c) Displacements (δ) of the stainless steel and PTFE beads adjacent to the interface related to the beginning of the formation of the rarefaction wave and anomalous reflected compression waves. (d) Relative positions of particles about 200 microseconds after the impact.

In the linear approach the incident compression solitary wave should result in a rarefaction wave propagating back from the interface into the stainless steel chain, it is indeed noticeable from the coordinated change of sign of the slope in the displacement curves starting from the 4th stainless steel particle from the interface (Fig. 47(c)). Additional to the expected reflected rarefaction wave we observed experimentally and numerically anomalous reflected compression waves (R) (Fig. 47(a) and (b))!

Based on the measurements of compression force inside particles (Fig. 47(a)) the leading reflected pulse in experiments has an amplitude (total contact force F_m including initial preload F_0) of about one half of the amplitude F_m of the incident wave. The relation between measured compression force inside particles and maximum contact force F_m is discussed in (Daraio, 2005). It should be noted that the contribution of the incident rarefaction wave to the reflected compression wave, based on the acoustic impedance ratio, can not bring the force above the initial precompression. Also, the leading transmitted (T) compression pulse in PTFE chain is followed by unexpected rarefaction pulses (Fig. 47(a) and (b)).

We may say that a superimposed static precompression on the interface of two sonic vacua made this interface visible based on the reflected signal in contrast to the uncompressed case. A peculiar characteristic of the leading reflected compression wave is related to its delayed time of arrival (about 90 microseconds) at the gauges in experiments and calculations based on the distance from the interface and the speed of the incident and reflected compression pulses (Fig. 47(a) and (b)).

When the leading reflected compression wave is formed, at 500 microseconds after the impact, the energy transferred to the PTFE chain is about 86% of the combined kinetic energy of the striker and the energy supplied by the magnetic force at the early stage of the motion of the first particle (about 25 microseconds). This contrasts with the previous case where almost all of the kinetic energy of the striker (over 99%) was transferred into the PTFE chain. It may be appropriate to name this dramatic change of reflectivity triggered by the initial precompression (zero and 14% reflected energy respectively) the “acoustic diode” effect.

The reflected compression waves were formed mainly by the rebounding motion of the last stainless steel particle due to the resistance of the PTFE beads. This phenomenon is a clear manifestation of the discrete nature of the system and can not be captured in a continuum approximation similar to the fracture of a chain in the vicinity of impacted end (Nesterenko, 1983, 2001) or the formation of secondary solitary waves (Manciu, 2000, 2002, Sen, 2003). The particles in the vicinity of the interface are self organizing into a state close to the original precompressed state (Fig. 47(c)).

As in the previous case (Fig. 46(c)), the stainless steel interfacial particle serves as the main energy transformer from the stainless steel chain to the PTFE chain (Fig. 47(c)). Again, a "fracture-wave" follows the rarefaction wave that is propagating from the interface back into the stainless steel chain. In the case of stronger precompression the gaps are closed rather quickly assisting the formation of reflected compression pulses. The opening and closing of gaps introduce a new time scale which is much shorter than in the previous case due to the significantly smaller size of the opened gaps and larger velocities of the particles moving into the gaps (compare Figs. 46(c) and 2(c)).

Initial precompression in a counterintuitive manner triggers the generation of a reflected compression wave and does not suppress the process of gaps opening and closing but instead makes it faster. Their characteristic opening and closing also participate in the process of wave reflection in this case (Fig. 47(c) and (d)). This indicates that the response of the interface between two SVs can be qualitatively tuned by the applied static preloading.

The gap openings between the stainless steel particles in the vicinity of the interface in the investigated set-up has a threshold on the amplitude of the incident wave

detected in numerical calculations. This threshold amplitude of contact force F_m is approximately equal to 4.3 N, which is larger than the static preload at the interface 2.473 N. The anomalous reflected compression wave was generated at this amplitude even when no gap openings were detected. This shows that the anomalous reflected compression wave is due to the changing direction of the velocity of the last stainless steel particle.

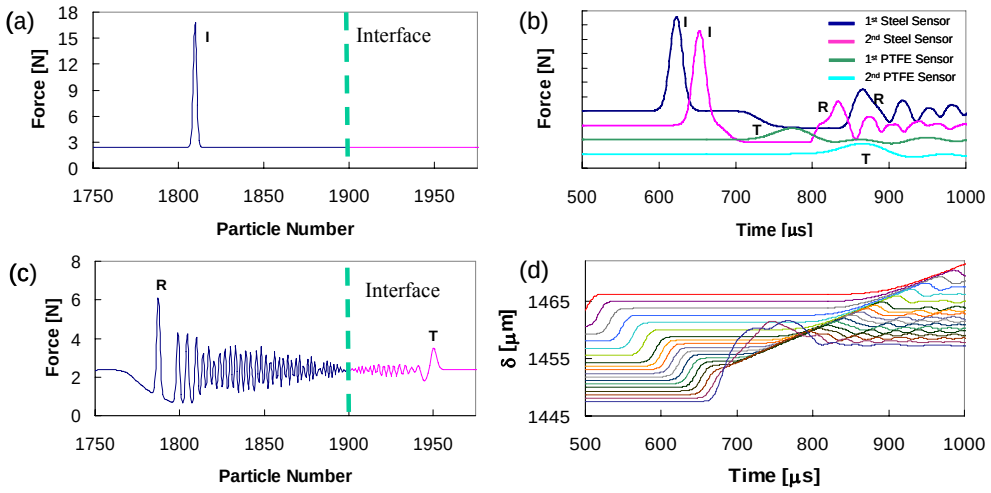

Figure 48. (a) Incident solitary wave (I). (b) The forces inside the stainless steel particles corresponding to the positions of the gauges in experiments close to the interface, vertical scale is 2 N per division (compare Fig. 48(b) with Fig. 47(a),(b)). (c) The reflected rarefaction wave, anomalous compression solitary wave (R) and trailing pulses in the stainless steel chain and transmitted compression pulse (T) with the rarefaction pulse and oscillatory tail in the PTFE chain. (d) Displacements of the stainless steel beads adjacent to the interface.

After the interaction, an expected reflected rarefaction wave formed close to the interface in the stainless steel chain and was followed by a compression pulse and an oscillatory tail (Fig. 48(b) and (c)). The amplitude of the first reflected compression

pulse (Fig. 48(b)) and the behavior of the displacements of the particles adjacent to the interface (Fig. 48(d)) were very similar to our experiments and numerical calculations for a smaller number of particles where the incident rarefaction wave was present (Figs. 47(b) and (c)). This clearly indicates that the observed anomalous reflected compression pulse and trailing oscillatory tail are caused by the incident solitary wave.

The reflected compression solitary wave is a nonlinear wave with a speed apparently higher than the speed of the head of the reflected rarefaction wave and oscillating tail. It becomes the leading reflected pulse about 1000 particles from the interface as was found in separate numerical calculations with 25000 stainless steel and 1000 PTFE particles. It is interesting that only one anomalous reflected compression solitary pulse was able to overcome the head of the reflected rarefaction wave, with amplitude F_m decreasing by about 40% during this process. As a result, the reflected signal at a relatively large distance from the interface (larger than 1000 particles) is composed of three essential elements in the following order: leading anomalous reflected compression solitary wave, a rarefaction wave and an oscillatory tail. On later stages the oscillatory tail overcomes the head of the rarefaction wave leaving only a leading reflected compression solitary wave and an oscillatory tail. The leading transmitted compression pulse in the PTFE chain is followed by an unexpected rarefaction wave and an oscillatory tail (Fig. 48(c) and (d)), also evolving into a leading transmitted compression solitary wave and an oscillatory tail.

Similar experiments and numerical analysis (Fig. 49) were performed on the same system using an interfacial particle with a flat bottom side as a contact between the steel and PTFE portions of the system. The flat interface was introduced to assure a Hertzian

type of interaction in experiments and to monitor the wave propagation behavior when interfacial properties of the system have changed.

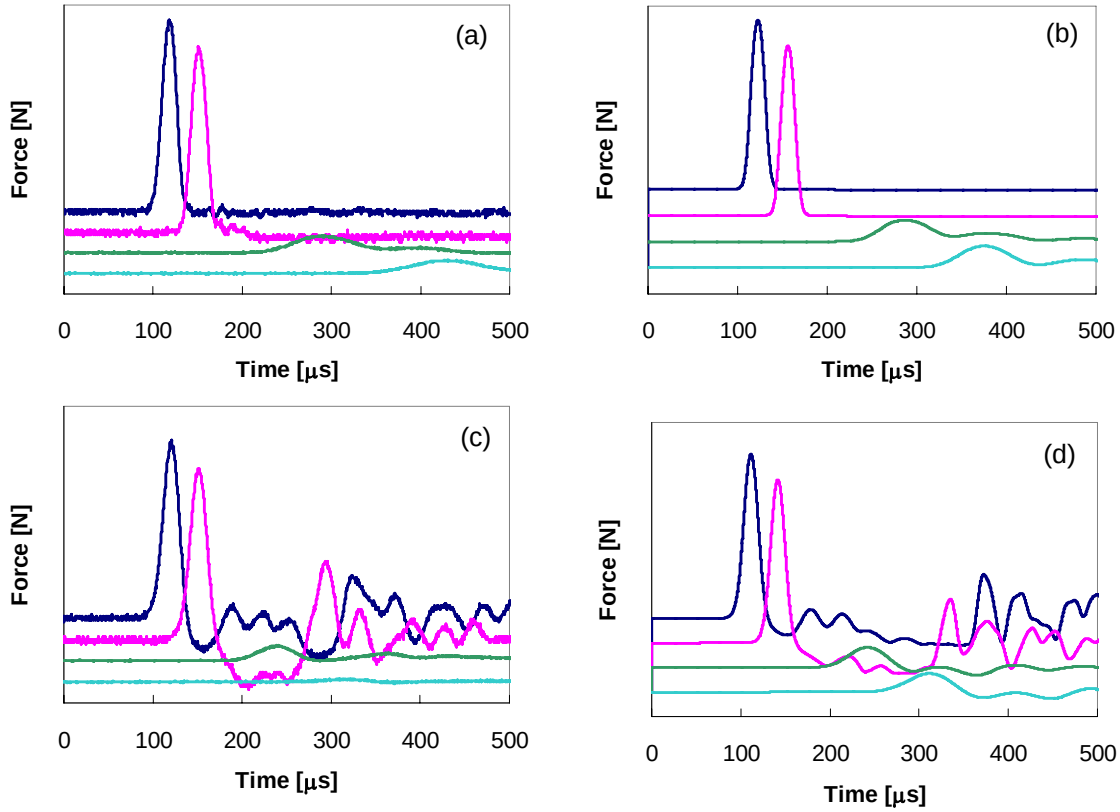

Figure 49. Pulse interaction analogous to Figs. 46 and 47 obtained experimentally and numerically in a system having a flat surface of stainless steel particle at the interface between the steel and PTFE portions. (a) Experimental results in the only gravitationally preloaded system, (b) numerical calculations corresponding to (a). (c) Experimental results in the gravitationally and magnetically preloaded system, (d) numerical calculations corresponding to (c).

The replacement of the last bead of the stainless steel chain with a bead of equal mass but flat bottom interface resulted in similar results under the same testing conditions. Only small wave propagation variations seem to appear, showing consistency of the anomalous reflection results even with a planar interface.

In summary we observed a strong sensitivity to the initial precompression of the reflected and transmitted energy from the interface of the two granular media, when the incoming solitary pulse reaches the interface from the "heavier" side of the chain under static precompression. This phenomenon can be named the "acoustic diode" effect. It can be employed for designing tunable information transportation lines with the unique possibility to manipulate the signals delay and reflection at will, and decompositions/scrambling of security-related information. It can also be used for identification of such interfaces (e.g. geological multilayer structure consisting of dissimilar granular materials) and for optimization of shock protection layers composed of uniquely combined composite granular media with layers of different particle sizes (masses) and elastic constants.

In the experiment corresponding to Figure 50 the soft/lighter (PTFE beads, 0.123 g and E=1.46 GPa (Daraio, 2005)) portion of the chain was placed on top and the hard/heavier (316 steel beads, 0.45 g and E=193 GPa (Daraio, 2006)) portion of the chain at the bottom (inverted setup as compared to the one described earlier). The data corresponding to the wave behavior the non-magnetically precompressed chain is presented in Fig. 50(a) and the one obtained from the statically prestressed chain is shown in Fig. 50(b).

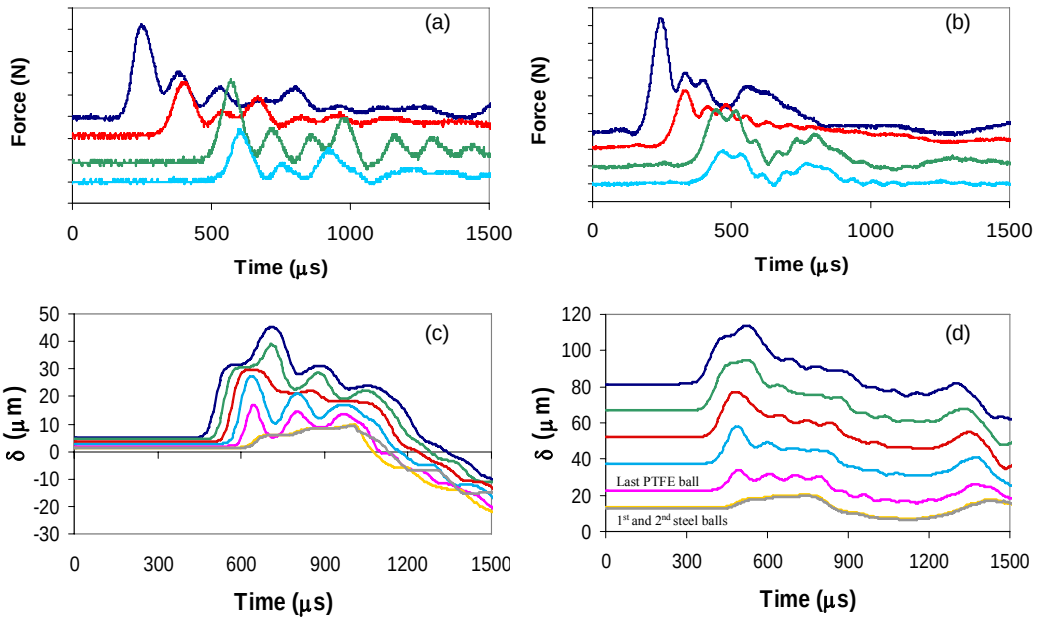

Figure 50. Pulse interaction with the interface of the two SVs composed of particles with different masses and elastic moduli with incident pulse coming from the "soft" section. The corresponding sections are composed from 20 PTFE and 21 stainless steel beads. An additional magnetic steel particle is added on the top of the PTFE chain to allow magnetic precompression. In (a) and (b) the curves corresponds to sensors placed in the 14th particle, the 18th particle, the 25th particle and 28th particle. (a) Experimental data with no static precompression. (b) Experimental data with added static precompression, vertical scales 0.2 N per division in (a) and (b). The Al_2O_3 striker (0.47 g) impact velocity is 0.44 m/s in both cases. (c) Displacements of the PTFE and stainless steel beads adjacent to the interface of the two SVs under only gravitational precompression. (d) Same as (c) but under gravitational and magnetic precompression.

Figure 50(c) and (d) show the displacement (δ) vs. time (t) curves relative to the motion of the last 5 PTFE particles before the interface and the first 2 stainless steel beads after the interface, when testing under only gravitational precompression and under gravitational plus magnetically induced precompression correspondingly.

Under the investigated conditions of impact a train of 4 solitary waves is quickly emerging at the vicinity of the impacted end (the mass of impactor and the mass of the end magnetic particle were about 4 times the mass of the beads in the chain). This is a

typical feature of strongly nonlinear systems. The interaction of the incident pulse with the interface generates both transmitted and reflected waves detected by the gauges in the PTFE and the steel chains. A good agreement between experimental data and the numerical analysis is observed. Magnetically induced preloading significantly increased the speed of solitary waves in PTFE and steel chains. A less pronounced splitting of the initial pulse into the train of solitary waves is evident both in experimental and numerical data although the character of the reflection was qualitatively the same. Again, a reasonable agreement is observed between the experimental and numerical data. We did not observe a qualitative change of the reflectivity under the applied precompression when the wave approached the interface from the PTFE side.

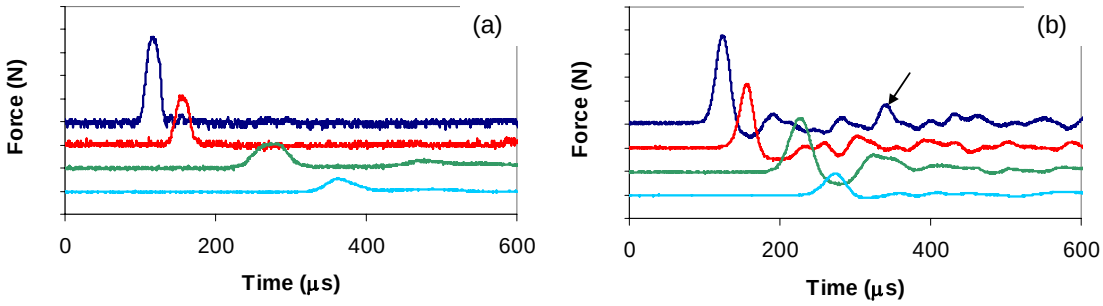

Figure 51. Pulse interaction with the interface of two SVs with similar masses of the particles with large difference in elastic moduli with incident pulse coming from "rigid" section. The system is composed of 20 stainless steel particle on top and 21 Parylene-C coated beads at the bottom. An additional magnetic steel particle is added on the top of the stainless steel chain. In all figures sensors are placed in the 14th particle (8th particle from the interface), the 18th particle (4th from interface), the 25th particle (4th Parylene-C coated from the interface), and 29th particle (8th Parylene-C coated from the interface). (a) Experimental data with only gravitational preload; (b) experimental data for gravitationally and magnetically (2.38 N) precompressed chains. The vertical scale of the first two curves is 2 N per division and for the bottom two 0.4 N Impact was by alumina cylinder with mass 0.47 g, velocity 0.77 m/s. The arrow shows the presence of the anomalous reflected wave as observed in Fig. 2(c).

An additional set of experiment to understand the phenomena of wave propagation behavior through a hard/soft interface was performed placing the chain of steel beads on the top of a chain composed of Parylene-C coated beads (see Fig. 51). The peculiarity of this interface stems from the fact that the steel beads and the parylene coated beads have the same mass (0.45 g) but very different elastic modulus (2.76 GPa for the Parylene-C coated beads).

The testing of the system composed of steel and parylene-C coated steel beads arranged in a setup analogous to Figs. 46 and 47 showed that the variation of the elastic modulus of the beads above and below the interface is sufficient to generate the anomalous reflected pulse. Figure 51(b) shows the effects of precompression on the single solitary pulse propagation through such system. The black arrow points at the anomalous reflected wave detected by the sensors in the stainless steel portion of the chain, after the interaction with the Parylene-C bottom section.

Energy trapping and shock disintegration in a composite granular medium

Here we report the first experimental observation of impulse energy confinement and the resultant disintegration of shock and solitary waves in one dimensional strongly nonlinear composite granular materials. The chains consist of alternating ensembles of beads with high and low elastic moduli (more than two orders of magnitude difference) of different masses. The trapped energy is contained within the "softer" sections of the composite chain and is slowly released in the form of weak, separated pulses over an extended period of time. This effect is enhanced by using a specific group assembly and precompression.

Granular matter has many known applications but it is difficult to understand its intrinsic dynamic properties due to the strong nonlinearity of forces between particles and complex contact-force distributions between grains (Nesterenko, 2001, Goldenberg, Corwin, Majmudar, 2005). In the past, the design of shock protectors focused mainly on the wave transformation provided by layered systems or the enhanced energy dissipation in porous media (Benson, 2001, Nesterenko, 2003). Yet an entirely different way of protecting materials is through the confinement of an impulse in a particular region of the shielding medium called a *"granular container"* using a series of sections with particles interacting according to different contact forces and masses as predicted by theoretical analysis (Hong, 2002, 2005) but not experimentally demonstrated.

The idea of the impulse confinement in our case is based on the anomalous features of an incident wave interacting with an interface between the two different

granular media (stainless steel and PTFE) (Nesterenko, 2005). It was shown that a solitary wave passing through the interface between a stainless steel and PTFE chain from the stainless steel side transmits all of its energy through the interface into the PTFE section. Furthermore the transmitted signal disintegrates into a sequence of solitary waves (see Fig. 1(c) in (Nesterenko, 2005)). On the other hand, when a solitary wave approaches the same interface from the PTFE side, numerical calculations and experiments have shown that a significant part of the incident pulse's energy is reflected back into the PTFE side. The amplitude of the reflected solitary wave is ~75 % of the incident wave's amplitude and the pulse transmitted to the stainless steel chain decomposes into a train of three solitary waves. In this study we tested experimentally and numerically a granular system composed of sections of stainless steel and PTFE beads with a constant overall number of particles and a fixed ratio between them. We introduced multiple interfaces between sections to enhance the wall's protection efficiency. A material with a similar dynamic behavior can also be made from a different combination of structural elements with strongly nonlinear interactions.

To create the granular system for pulse trapping and protection of the wall, we used a constant total number of 32 beads with diameter ~4.76 mm, of which 22 were the high-modulus, large mass stainless steel beads (non-magnetic, 316 type) and 10 were the low-modulus, small mass PTFE (polytetrafluoroethylene) beads (Daraio, 2005). The mass of the 316 stainless steel bead was 0.45 g, with a density of 8000 kg/m^3, Young's Modulus of 193 GPa and the Poisson ratio equal to 0.3 (ASM Metals Handbook). The mass of a PTFE bead was 0.123 g, the density 2200 kg/m^3, the elastic modulus was 1.46 GPa, and a Poisson ratio 0.46 (Daraio, 2005, DuPont, Carter, 1995). Three piezo-sensors

were embedded inside the particles as described in (Nesterenko, Daraio, Daraio, 2005) allowing the calculations of the time-of-flight for determining the pulse speed. A fourth sensor was embedded in the wall at the bottom of the chain as in (Daraio, 2004). The particles were assembled in a vertical PTFE holder. Pulses were generated with a 0.47 g Al_2O_3 rod striker for the single solitary wave type loading and with a 63 g Al_2O_3 rod for the shock-type loading with various velocities. In order to tune the properties of this new granular protector, a magnetically induced non-contact compressive force (2.38 N) was applied as described earlier.

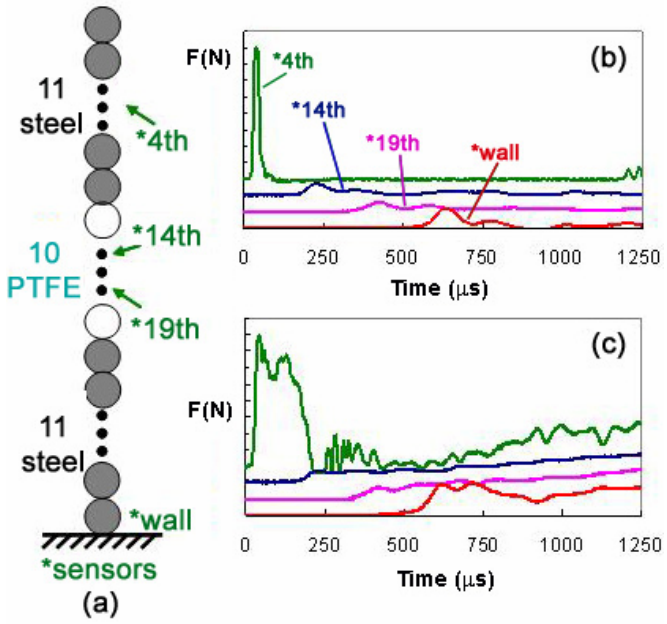

Figure 52. Trapping of a solitary- and a shock-pulse in the granular protector with a single central PTFE section. (a) Schematic diagram of the stainless steel and PTFE bead's geometrical arrangement used for testing with indicated sensors. (b) Experimental data corresponding to the solitary-type loading. The striker here was an Al_2O_3 cylinder of 0.47 g with an impact velocity of 0.44 m/s. (c) Experimental data corresponding to the shock-like loading with shock amplitude similar to (b) excited by an Al_2O_3 striker (63 g). The y-axes scale is 1 N per division for (b) and (c).

First, a granular protector with a single central PTFE section was tested (Fig. 52(a)). Here 11 stainless steel beads were placed at the top of the chain, 10 PTFE beads in the middle and 11 steel beads at the bottom, forming a softer central section of the chain. The corresponding impulse behavior is presented in Fig. 52(b,c) for incident solitary and shock-like waves.

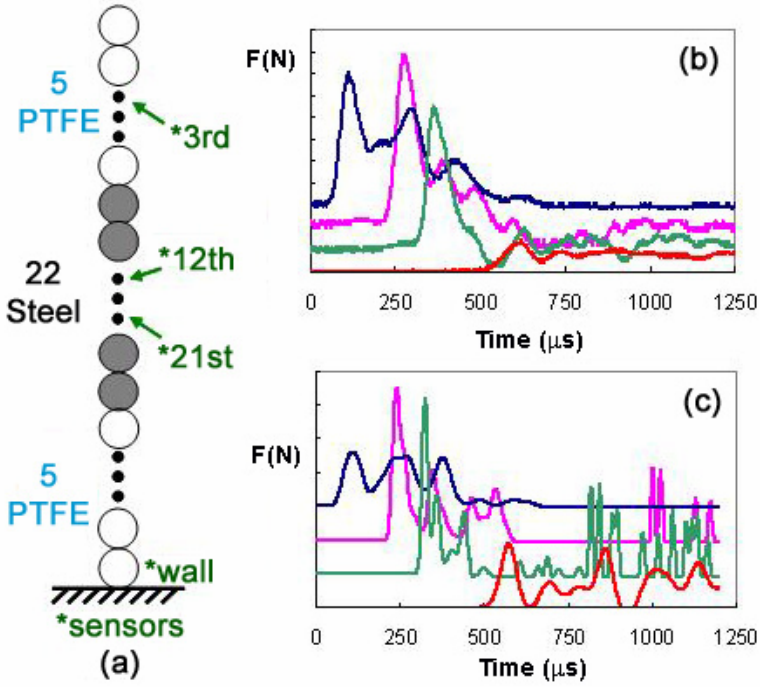

Figure 53. Trapping of a solitary pulse in the granular protector with a single stainless steel central section. The striker was an Al_2O_3 cylinder of 0.47g with an impact velocity of 0.44 m/s. (a) Schematic diagram of the stainless steel and PTFE beads geometrical arrangement used for testing with indicated sensors. (b) Experimental data corresponding to the solitary-type loading. The y-axes scale for all curves is 0.2 N per division. (c) Numerical data corresponding to (b). The y-axes scale is 1 N per division.

To qualitatively compare the experimental results with the granular containers proposed in (Hong, 2005), similar tests were conducted exchanging the particle's positions. In this case 5 PTFE particles were set on the top and bottom sections of the chain and the 22 stainless steel beads were positioned in the middle (Fig. 53(a)). This

configuration can be compared to half of the granular container presented in the Fig. 2(c) in (Hong, 2005). The experimental and numerical results are presented in Fig. 53 (b) and (c).

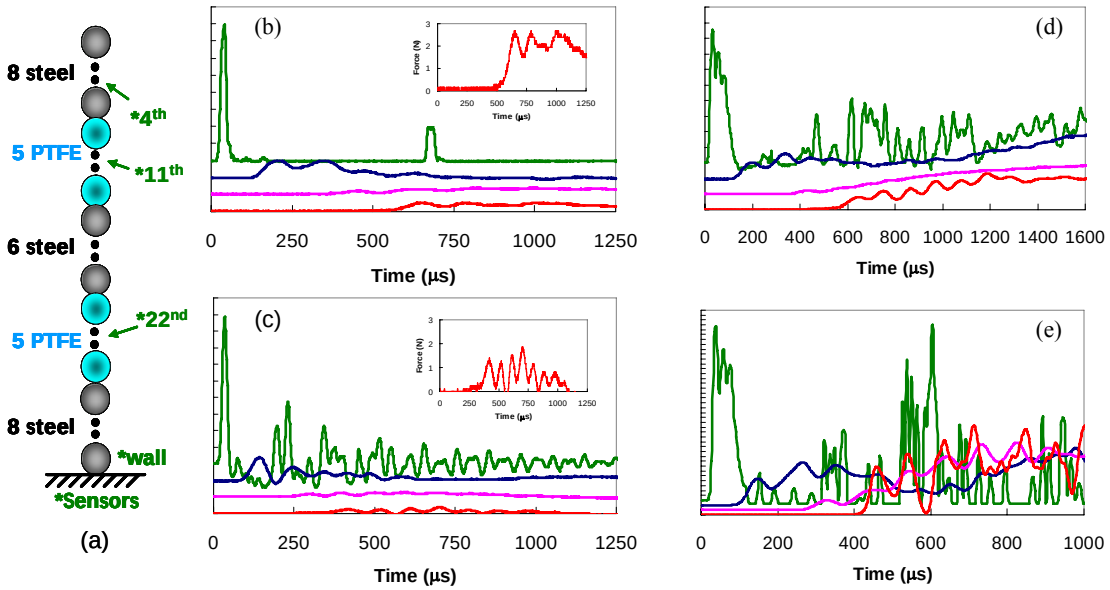

Figure 54. Solitary pulse trapping in the composite granular protector with two PTFE sections without and with additional precompresion. (a) Schematic diagram of the arrangement of the stainless steel and PTFE beads with indicated sensors. (b) Experimental results for only gravitationally loaded system obtained with an Al_2O_3 striker (0.47 g) at 0.44 m/s. (c) Experimental results including a magnetically induced precompression; all other conditions as in (b). The y-axes scale is 1 N per division. Insets in (b,c) show the pulse behavior at the wall for the gravitationally loaded and the magnetically tuned system. Note the significantly moderated impulse shape arriving on the wall in (b) and (c): the strong incident impulse (first curve) disintegrates into a very weak series of pulses delivered over a much longer period of time (bottom curve). (d) Shock pulse trapping obtained experimentally by the impact of an Al2O3 rod (63 g) striking with a velocity of ~0.17 m/s. The y-axes scale is 1 N. (e) Numerical analysis corresponding to (d).

The granular protector with two PTFE sections (Fig. 54(a)) configuration consisted of the same overall number of stainless steel and PTFE beads, but divided into

two sections of 5 PTFE particles interposed between the stainless steel beads creating a larger number of interfaces in comparison with the Figs. 52(a) and 53(a).

Numerical analysis of the discrete chains was performed for all the set-ups described to calculate force-time curves as well as the total energy trapped and released by the granular containers. The numerical simulations were run similar to earlier using the equation of motion for the grains with Hertzian contact and identical conditions of impact striker and velocity. The presence of the gravitational precompression (caused by the vertical orientation of the tested chain) was taken into account in the numerical analysis although it has a weak effect at the investigated pulse amplitudes. The effects of dissipation were not included in the calculations and will be addressed in future studies.

In the case of the granular protector with a single PTFE central section, the trapping of the incident solitary pulse in the softer region is clearly evident in experiments (Fig. 52(b)) and matched well with the numerical calculations. The experimental data clearly demonstrates that the incident solitary pulse (~40 μs long and 8 N in amplitude) is quickly transformed by the PTFE portion of the chain to a much longer signal and it is decomposed into a train of pulses arriving at the wall with a much lower amplitude in experiments.

We would like to point out that the processes of impulse transformation and confinement, corresponding to the arrangement represented in our Fig. 52(a) (Steel-PTFE-Steel), are similar to the one presented in (Hong, 2002) (see Fig. 3 there). Specifically, it was observed: (a) a complete transmission of the energy of the incident solitary wave into the PTFE section without any wave reflected back in the steel section (see also Nesterenko, 2005); (b) a significant reflected pulse propagating back into the

PTFE section when the incident pulse arrives from the PTFE side of the interface; (c) the disintegration of the transmitted impulse into a train of solitary waves was observed in both cases.

The solitary wave speed in the steel section of the chain is 357 m/s. The experimental data (Fig. 52(b)) shows that the signal speed drops down to 137.4 m/s when the pulse passes through the first interface into the PTFE section. This slowing down can be attributed to the drastically lower elastic modulus of PTFE (1.46 GPa) compared to steel (193 GPa), which enables the pulses to remain mostly trapped in the softer section of the chain for a relatively long time "bouncing" back and forth between the two interfaces releasing the energy of the impact in both directions very slowly.

The first and largest impulse reaching the wall in Fig. 52(b) has an experimentally measured amplitude significantly smaller (about 5 times) than the one measured in independent experiments in a uniform steel chain under identical impact conditions and the same number of particles. In the numerical calculations the reduction is also very significant being 3 times smaller (amplitude 6.7 N) than the wall amplitude of ~20 N in a uniform stainless steel chain of beads. The difference between the experimental data and numerical results is most likely due to dissipation not being included in the numerical calculation, which underestimates the total extent of signal amplitude reduction. It also demonstrates that the dissipation present in the experiments can significantly enhance the protection against incident solitary waves. The trapped pulses reflected from the bottom of the central soft section have an amplitude comparable to the incoming pulses in the PTFE section, demonstrating that a significant amount of the total energy remains

confined in the softer central portion of the chain, slowly leaking out only a small amount at each rebound (~28% after the first rebound).

The performance of the granular protector with a single PTFE central section against shock wave type loading is shown in Fig. 52(c). To the best of our knowledge its trapping in a granular container was not investigated before theoretically or experimentally, though shock-like loading is very important in practical applications. A shock wave is a qualitatively different type of pulse in comparison with solitary wave. It is usually characterized by a longer duration which may affect the reflection and transmission at the interfaces. The results of numerical calculations for both types of incident waves (solitary and shock), showed similar tendencies in the impulse behavior which qualitatively agreed with the experimental results.

To compare this particle's arrangement to one proposed in (Hong, 2005) we exchanged the particle's position as described in Fig. 53(a). This new arrangement, still preserving the total number of beads and the ratio between them, may be qualitatively compared to the design of one half of the granular container presented in the Fig. 2(c) in (Hong, 2005). It is evident from the numerical calculations that this arrangement dramatically improved the efficiency of the wall's protection reducing the pulse amplitude reaching the wall from 6.7 N observed in the previous case down to ~2 N in Fig. 53(c). A similar trend is observed in experiments where the amplitude of the signal reaching the wall drops from ~1 N in Fig. 52(b) to ~0.2 N in Fig. 53(b) when impacted with the same striker and velocity.

To investigate the influence of the particle arrangement in our system and to enhance the protection efficiency, we reorganized the PTFE beads as shown in Fig. 54(a)

increasing the number of interfaces. Here we alternated steel and PTFE portion of the chains with a periodicity 8-5-6-5-8, where the two 5-particle sections are composed of PTFE beads only. This geometry resulted in a much better protection of the bottom wall in comparison to the first case studied (compare Fig. 54(b) with Fig. 52(b)) by more efficiently trapping most of the incoming pulse and releasing its energy more slowly. In this case the amplitude of the force calculated numerically at the wall was 3.4 times less (2.4 in experiments) than the one detected in the granular protector with a single PTFE section and ~10 times less than the one observed in an all-steel chain (not shown). The discrepancy between the numerical and experimental case is probably due to the enhanced effects of dissipation at higher signal amplitudes. However, there exists a qualitative agreement of the wave behavior in experiments and numerical calculation for solitary-type loading.

In this set-up, the first (uppermost) PTFE section works very efficiently trapping a larger amplitude of the pulse and transforming the 40 μs long incoming solitary pulse (from the steel section) into a much longer and delayed train of signals with an overall duration over 1000 μs. Numerical calculations of the energy contained in the PTFE sections confirmed the higher efficiency as a protector: the granular protector with two PTFE sections traps most of the potential energy for a longer time when compared to the single PTFE section and achieves equal wall protection efficiency when compared to the setup presented in Fig. 53.

It was previously reported that the wave behavior and the reflection from the interface of two strongly nonlinear systems is strongly affected by an initial precompression causing the phenomenon of the “anomalous reflection” of a compression

solitary wave. This is because an anticipated combination of pulses contains a solitary-like reflected rarefaction pulse which is not supported by the equations of motion as a stationary wave. This rarefaction pulse, formed very close to the interface, quickly disintegrates into a complex pattern of waves.

To explore the influence of the precompression we tested the more efficient granular protector with two PTFE sections under a magnetically induced precompression. This resulted in an evident increase of the speed of the signal propagation and in the creation of an anomalous reflected wave on the first steel sensor (uppermost curve) followed by a series of multiple reflected pulses (compare Figs. 54(b) and 54(c)). The introduction of the preload significantly reduced the force impulse acting on the wall, facilitating the splitting of the signal into a train of low-amplitude waves (see insets in Fig. 54(b) and 54(c)).

The physical explanation for such an increase in the pulse confinement in the softer region of the chain is related to the self assembly of gaps at the interfaces causing a complex "rattling" among the interfacial particles combined with the reflection of the pulse from the interfaces of the soft and rigid regions. These gaps allow the two softer regions of the chain to keep the energy trapped longer, therefore enhancing the protection of the wall. Moreover when the signal propagates through the first interface, a "fracture wave" is formed and propagates back into the stainless steel chain. The presence of these open gaps is counter intuitively enhanced by the static precompression and is responsible for the introduction of a new time-scale in the system as well as the formation of an anomalous reflected wave at the interface under precompression (top curve of Fig. 54(c)). As a result, the gaps delay the wave reflection and propagation, and enhance the

reflections from the heavy/light interfaces. In this case the total energy trapped in the softer sections remains almost constant within the investigated time. Furthermore the superimposed force transforms the pulse arriving at the wall in a series of well separated pulses, delaying the total momentum reaching the bottom wall. This behavior is very useful as a mean to protect an object from incoming impacts by providing longer distances of pulse traveling within the protector region, thus additionally causing the impact to lose its energy due to dissipation.

The granular protector with two PTFE sections was also tested for the trapping of shock pulses (Fig. 54(d) and 54(e) without and with magnetic precompression correspondingly). To generate such pulses we used an Al_2O_3 rod (63 g) as a striker impacting the first steel bead. The signal reaching the wall was dramatically transformed from an oscillatory, fast-ramping shock loading into a long, slowly increasing series of pulses. This trapped and transformed pulse is likely to be much less damaging to the protected object (the end wall in these experiments).

Results of the numerical calculations indicated a similar trend as in the experiments. The data demonstrates that under shock-type loading the softer sections of the chain do not appear to trap energy, thus only acting as pulse transformers, as opposed to the energy trapping of incident solitary waves.

Calculations were also performed for a chain composed of one-by-one alternating stainless steel and PTFE beads. In this case the chain responded as a homogenized “two-particle system” without the creation of reflected pulses, thus drastically reducing the efficiency of the protector.

In conclusion, we demonstrated experimentally and numerically the efficiency of soliton-like and shock-like pulse trapping and disintegration in a composite granular protector and proved that its efficiency depends on the particle's arrangements. The introduction of a magnetically induced precompression divided the signal reaching the wall into a series of subdivided pulses reducing the total force impulse even further. The shock-disintegrating principles demonstrated here can be utilized for practical three dimensional composite structures used for protection against explosive and impact pulses.

TWO DIMENSIONAL ANALYSIS

Diamond shaped wave-guide

We report the first experimental observation of strongly nonlinear solitary pulses propagating in a two dimensional system. This represents an important step toward the understanding of the signal propagation in the "force chains" present in the three dimensional granular media. The system consists of a double Y-shaped guide in which high- and low-modulus chains of spheres are arranged in various geometries. We observed fast splitting of the initial pulse, rapid chaotization of the signal and sharp bending of the propagating acoustic information. Pulse and energy trapping was also observed in composite systems assembled from hard- and soft- particles in the branches.

Granular assemblies, common in our everyday life, have many known applications but they present fundamental difficulties in the understanding of their intrinsic dynamic properties due to the strong nonlinearity and complex contact-force distributions between the grains under static and quasi-static loading (Blair, 2001, Goldenberg, Corwin, Majmudar, 2005). Their three dimensional structural features include filamentary force chains, i.e. chains of granules with preferred contacts for force/pulse transmission, which may be relevant also to characterize the behavior of matter in a glassy state. The experimental study of the pulse propagation in these force chains is essential for a better understanding of the response to dynamic impulse propagation in a three-dimensional system.

A simplified model for such chains can be obtained with a two-dimensional arrangement of the beads (granules) forming planar bi- and trifurcations. Here we describe the first experimental observation of strongly nonlinear solitary waves propagating inside a two dimensional double Y-junction (diamond shaped) guide for a composite granular medium. Uniform systems assembled from PTFE and stainless steel beads are studied and chains composed by a combination of these beads and Parylene-C coated steel spheres are also considered for exploring possible applications as signal scrambling and pulse trapping devices.

One dimensional model systems were proposed earlier to experimentally and theoretically demonstrate the propagation of strongly nonlinear waves in steel and polymer-based chains of spheres and to introduce the concept of impulse trapping.

The passage of a strongly nonlinear solitary wave from a one dimensional chain of beads through a 2-D bifurcation is a matter of interest on its own. Recently, the study of the strongly nonlinear behavior at the interface between two strongly nonlinear media has recently received increasing attention for the discovery of interesting new dynamical aspects arising from the self-organization of the granules in close proximity to the interface. It was shown that a solitary wave crossing the interface of two SV type systems from a region of particles with a higher elastic modulus (or higher mass) to a region of lower elastic modulus (or lower mass) results in the impulse decomposition into a train of solitary pulses. In the zero or weakly precompressed case, the number of pulses composing the train is proportional to the ratio of the difference in the mass of the particles at the two sides of the interface. In this case, no reflected wave from the interface was observed propagating back into the stiffer region. In contrast, when the

solitary wave in SV passes from the softer (lower elastic modulus) region to the stiffer region, it divides its energy into 2 portions. In this case, no impulse disintegration beyond the interface was observed. A solitary wave traveling along a one dimensional chain is expected to have a similar behavior when encountering a split interface, keeping into account also the energy and momentum redistribution between the beads in the two branches of the bifurcation.

To create the two dimensional system of beads, we used a total 132 beads of uniform diameter, ~4.76 mm, composed of different materials: the high mass, high elastic modulus steel (non-magnetic, 316 type) beads; the small mass, low-modulus PTFE (polytetrafluoroethylene) beads and the high mass, low elastic modulus Parylene coated steel beads with slightly larger diameter (4.86 mm). The properties of the materials composing the beads used in this study are summarized in Table 4.

Table 4. Properties of the materials composing the strongly nonlinear media tested experimentally.

	Elastic modulus [GPa]	Poisson ratio	Density [Kg/m^3]
Stainless steel beads [17]	193	0.30	8000
PTFE beads [18]	1.46	0.46	2200
ParyleneC coating [16,19]	15	0.38	1289

The beads where arranged in an horizontal PTFE guide with cylindrical grooves of ~5 mm in diameter carved in a double Y-shape (diamond-like) with a bifurcation angle of 60° between the two branches (see Fig. 55(a) for a schematic). The described holder was positioned horizontally (parallel to the table-top) to exclude the action of precompressive gravitational forces on the beads and create a pure SV system. The beads

were carefully positioned in the grooves with point contact between them and the filled holder was then covered by a transparent PVC plate to avoid vertical misalignment of the beads during impulse propagation and to allow careful positioning of the beads. Such geometry was chosen to demonstrate the capability of splitting the solitary waves through a bifurcation and the "bending" of the traveling pulses at angles of 120°.

Four calibrated piezo-sensors were embedded inside particles in the system as described earlier allowing the time-of-flight calculations of the signal's speed and the tailoring of their shape. Pulses were generated with a swinging pendulum with spherical steel strikers of different masses (0.45 g and 5.33g) dropped from various heights.

The first set of experiments was performed on a uniform system composed of all stainless steel and all PTFE beads as described in Fig. 55(a). Each one of the 4 sensors connected to the oscilloscope was positioned in one of the branches of the system to monitor the shape and duration of the solitary waves propagating before and after the bifurcated interface. The systems were excited with strikers having masses equal to 0.5 g for the PTFE based system and 5.33 g for the stainless steel system. According to the theory we expected the formation of trains of solitary waves on the first stem of the system with a number proportional to the striker/particle mass ratio (i.e. ~4 solitary waves in the PTFE case and ~10 solitary waves in the stainless steel case). The results obtained experimentally are shown in Fig. 55(b) for the PTFE based system and in Fig. 55(c) for the stainless steel based set-up. The exact position of the sensors in each test is labeled on the respecting curves. The same set up but different strikers were utilized to study the behavior of single solitary waves propagating in the uniform system and

interacting with the bifurcated interface. In this case we used a PTFE bead to strike the PTFE based chain and a stainless steel particle for the steel based systems.

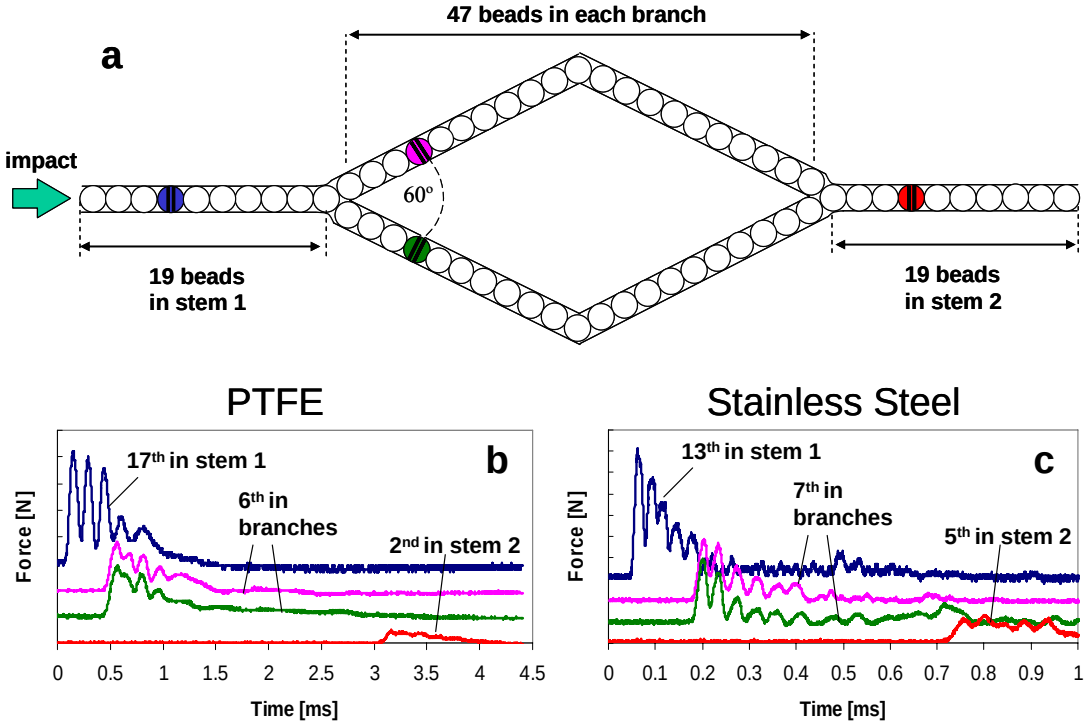

Figure 55. Trains of strongly nonlinear waves propagating in the diamond-shaped holder filled with uniform types of beads. (a) Schematic diagram of the geometrical arrangement used for testing with indicated sensors. (b) Experimental data corresponding to the train of solitary waves excited by a 0.45 g striker in a PTFE based system. The y-axes scale for all curves is 0.2 N per division. (c) Experimental data corresponding to the train of solitary waves excited by a 5.33 g striker in a stainless steel based system. The y-axes scale for the top 3 curves is 2 N per division and 0.4 N per division for the last (bottom) curve.

The remaining sets of experiments were performed on composite systems where one of the branches after the Y-shaped bifurcation was filled with polymer based (low modulus) particles and the remaining section of the system was composed of stainless steel (high modulus) beads. The testing was done to analyze the behavior of strongly

nonlinear SV-systems with a completely new type of interface interaction. This set up is important to understand the fundamental mechanisms governing the responses of force chains in three dimensional systems and also to create practical devices for signal phase-shifting, pulse scrambling and energy trapping within one of the diamond branches.

The first of such experiments is described in Fig. 56. Fig 56(a) shows a schematic diagram of the particles arrangement and Fig. 56(b) depicts the experimental results obtained when a 0.45 g striker was used to create a single solitary wave in the first stem of the system.

The last system tested was composed of a stainless steel and parylene coated stainless steel beads arranged similarly to the previous case. The schematic diagram representing this experiment is shown in Fig. 57(a), and the experimental results for a single solitary wave and a train of solitary waves excited in the system are shown in Fig. 57(b) and (c) correspondingly.

The behavior of a train of solitary waves in a uniform system interacting with a bifurcated interface and later merging back into a single chain is presented in Fig. 55(b) and 55(c) for PTFE and stainless steel beads correspondingly. A system composed of a uniform type of beads like the one presented in this experiment is the simplest to analyze because the wave propagation behavior can be predicted using the conservation laws of momentum and energy of the particles before and after the interface, simply knowing the masses and initial velocity of the beads in the system. This case is analogous to the well known behavior of a billiard ball hitting with velocity v_p the center of two other balls of equal mass and properties at rest on a plane. In this case the amplitude and speed of the solitary wave traveling in each branch after the bifurcation is expected to be one half of

the incoming pulse. In our experiments, the top-most curve in Fig. 55(b) represents the passage of a train of 5 solitary waves recorded by the sensor embedded in the 17th PTFE bead of the first stem. It is evident that even in this first section of the system the solitary waves are not yet completely separated in the proximity of the bifurcation. In addition no reflected signal is present after the train interacts with the bifurcated interface. After the train passes through the split interface two remarkably similar trains of pulses proceed through the system (with same amplitude, shape, duration and velocities) accordingly to what expected from the theory. The reduction of the solitary wave's amplitude to ~1/2 of the incoming pulse affected also the splitting of the solitary waves in the train, slowing down the separation between the pulses and the speed of the pulse propagation according to Eq. 7. The reduction of this pulse speed has been calculated from the initial 129.8 m/s in the stem to 114.5 m/s in the two branches. The presence of dissipation observed in earlier studies for polymer based granular systems has to be taken into consideration when estimating the solitary wave's speed according to Eq. 7 because the amplitude of the solitary waves traveling along the branches will decay, causing the train of waves to further delaying their approach to the second interface. The behavior of the trains of solitary waves in the fifth particle of the final stem of the system is shown in the fourth (and bottom) curve in Fig. 55(b). It is evident that the two split trains of solitary waves traveling in the two branches later recombine after the second bifurcated interface into one single train again. Unfortunately due to the presence of dissipation in the system the waves composing the train do not seem well separated although the simultaneous arrival is clearly shown and separated peaks of the solitary-like pulses composing the train are still evident. The absence of any reflected pulse and the ability of the two split trains to

recombine into one also demonstrates the capability of the acoustic information propagating in the system to undergo 150° and 120° bends without major losses throughout their traveling along the branches. Similar results were observed in Fig. 55(c) for a stainless steel based system. Here the speed of signal propagation before and after the interaction with the bifurcated interface has been calculated at 516.1 m/s for the incoming pulse down to 408 m/s in the branches. These calculated values for both the PTFE and stainless steel based systems agree very well with the experimental values derived from the time-of-flights measurements between the sensors.

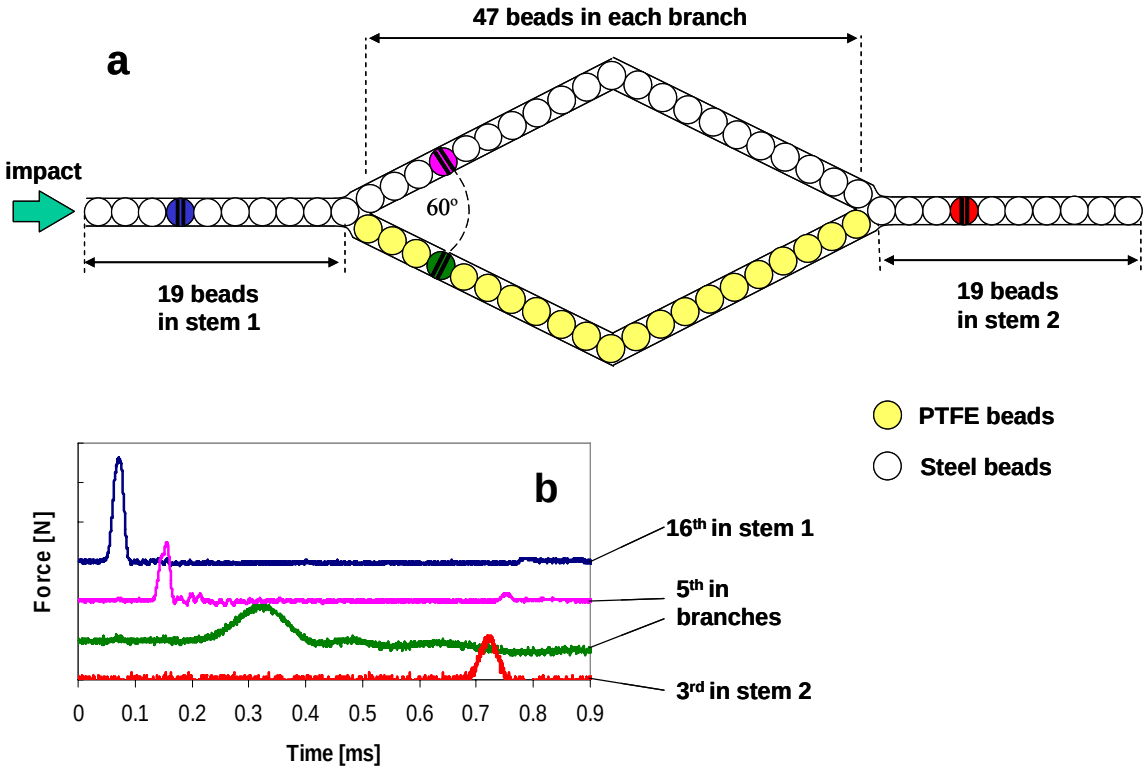

Figure 56. Single strongly nonlinear waves propagating in the diamond-shaped holder filled with stainless steel and PTFE beads. (a) Schematic diagram of the geometrical arrangement used for testing with indicated sensors. (b) Experimental data corresponding to the train of solitary waves excited by a 0.45 g striker. The y-axes scale for the top two curves is 2 N per division, while it is 0.2 N per division for the two lower curves.

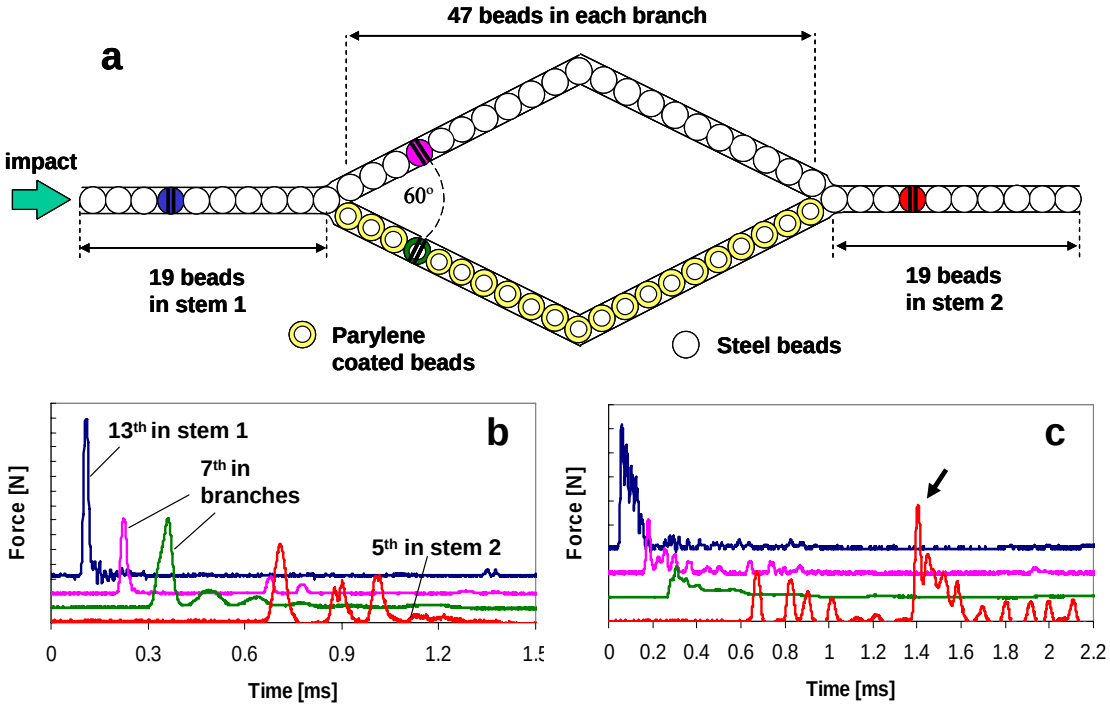

Figure 57. Trains of strongly nonlinear waves propagating in the diamond-shaped holder filled with uniform types of beads. (a) Schematic diagram of the geometrical arrangement used for testing with indicated sensors. (b) Experimental data corresponding to the train of solitary waves excited by a 0.45 g striker in a PTFE based system. The y-axes scale is 2 N for the two top most curves, 0.4 N per division for the third curve and 0.1 N for the bottom curve. (c) Experimental data corresponding to the train of solitary waves excited by a 5.33 g striker in a stainless steel based system. The y-axes scale for the top 3 curves is 5 N per division and 0.5 N per division for the last (bottom) curve.

The behavior of a single solitary wave traveling in a composite system is presented in Fig. 56. In this case, a single solitary wave is excited on the initial stem using a single stainless steel bead as a striker. According to Eq. 7, the so formed solitary wave has a speed of 450.6 m/s. Once the pulse reaches the interface, it splits into two parts: one single solitary wave that continues to propagate in the branch composed of stainless steel beads identical to the stem (see the second curve from the top in Fig.

56(b)), and another part that splits into a train of ~4 solitary waves in the PTFE branch (third curve in Fig. 56(b)). The speed of the single solitary pulse traveling in the stainless steel based branch of the system is calculated at 407.9 m/s. The speed of the leading pulse of the train of solitary waves formed in the PTFE section is 102 m/s. It is interesting to notice that the train of solitary waves in the PTFE section have a much longer duration and smaller amplitude if compared with the solitary waves traveling in the steel section and the pulses seem to never appear to leave the PTFE branch. In the time interval studied in facts only the solitary wave in the steel section proceeds till the 4^{th} sensor in the second stem after undergoing one 120° and one more 150° turn. The train of solitary waves formed in the softer PTFE section remains trapped and seem to "bounce" back and forward within its region, similarly to the behavior observed in (Daraio, 2006), until it disappears due to the effects of dissipation.

The final set of experiments describes the dynamic behavior in a composite system similar to the previous case assembled from stainless steel and Parylene coated stainless steel beads (see Fig. 57(a)). The results are shown in Fig. 57(b) and 57(c) for a solitary wave and a train of solitary waves respectively. This case study is very interesting because it presents for the first time the interface response of a very unique system composed of two chains of particle with the same mass but very difference elastic properties at the contacts. In this case, when a single solitary wave formed in the initial steel stem propagates through the first bifurcated interface it appears evident that, similarly to the PTFE composite case, the signal splits into two parts: one composed of a single solitary-like pulse in the bare stainless steel branch (see second curve from the top in Fig. 57(b)); and the other one composed of a train of 4-5 solitary-like pulses that

propagates in the Parylene coated section (third curve in Fig. 57(b)). The splitting of the single solitary wave at the interface between the steel and polymer coated sections of the system was fairly unexpected (having particles composed of basically identical masses) but can be explained by some complex dynamic response of the elastically softer polymeric coating. In this case two small reflected pulses are visible in the second curve of Fig. 56(b) and they are believed to be related to some undesired reflection of the pulses from the two 120° "bends" and are probably due to the imperfect initial positioning of the beads in the system.

The speed of the solitary wave propagating in the first stem of the system has been calculated at 568.6 m/s according to Eq. 7 and at 502.6 m/s and 172.4 m/s for the stainless steel and Parylene coated branches respectively. These calculated values agree reasonably well also with the speed of pulses extrapolated from time-of-flight measurements between the sensors with accuracy within the 10% range. The pulse presented in the bottom curve of Fig. 57(b) represents the response of the 4^{th} sensor in the system, placed after the merging of the two branches in the 5^{th} bead of the final stem. The signal recorded show a first, leading solitary-like pulse which corresponds to the arrival of the solitary pulse from the bare steel branches and three more peak delayed of few hundreds of microseconds which are not clearly identified. The anomalous pulses in facts appear too early to be related to the arrival of the pulses (not shown) from the Parylene coated branch, which instead reach this sensor, as expected, ~1 ms after the first leading pulse from the steel branch. It is interesting to notice that no pulse trapping within the Parylene coated branch seemed to appear, although the fact might have been obscured by the presence of dissipation affecting especially the softer sections of the

system. These results are relevant to underline the presence of self phase-shifting in the system and they suggest possible applications of such structures as delay lines, pulse scramblers and chaotization devices.

Analogous results were obtained when testing the same beads configuration exciting a train of solitary pulses in the first stem of the system (see Fig. 57(c)). In this case, the 4th curve shows clearly the separate arrival of the train of waves from the steel branch (at ~0.6 ms from the triggering time) and from the Parylene coated section, marked in the figure by a black arrow at ~1.4 ms from the triggering time.

Finally, in this work we studied the dynamic behavior of inter-particle forces in a two-dimensional granular medium analogous to the typical force-chains present in granular materials. We demonstrated experimentally the ability to bend, split, scramble, trap and delay single and trains of soliton-like pulses in a two dimensional composite granular system. We were able to decrease the size of the system that splits the initial pulse into a train of separate waves. The presented results represent a model system for the behavior of pulses propagating through force-chains in three dimensional arrangements of granular materials and provide a better understanding of the behavior of the two dimensional systems. In addition, we analyzed for the first time the behavior of a pulse propagating through the interface between steel and polymer coated steel beads and showed the unexpected decomposition of a single solitary wave into a train of ~4-5 separated pulses.

The principles demonstrated here can be utilized for the design of practical two and three dimensional composite structures. Among the foreseen application are: delay lines, scramblers for secure communications, protecting gear and signal phase shifters.

THREE DIMENSIONAL ANALYSIS

Tunable acoustic properties of granular materials

Impedance tube measurement system

The preliminary studies on three dimensional arrangements of granular materials were performed on a Bruel and Kier (B&K) impedance tube measurement system (see Fig. 58) using “Pulse Materials” software for the analysis of the data acquired.

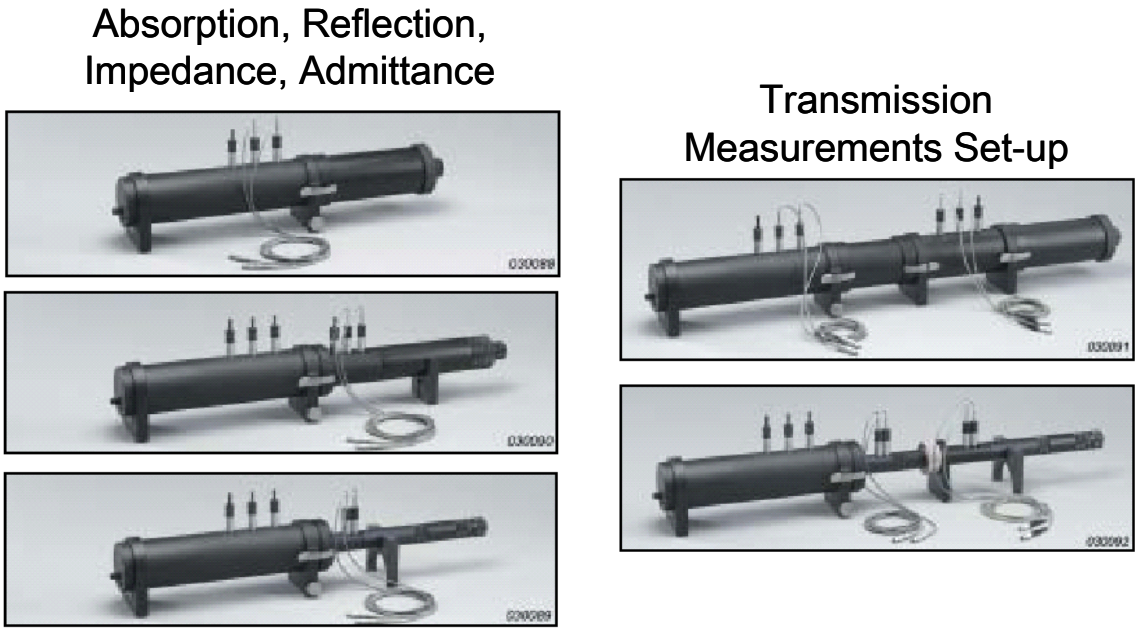

Figure 58. Pictures of the B&K Impedance tube testing system Type 4206T employed in experiments. The tubes of different diameter cover different ranges of frequencies spamming from 60 Hz to 6.4 kHz.

Impedance tubes for characterizing the acoustic properties of materials have been in use for a very long time and several variations exist (Beranek, 1988). The determination of the sound absorption coefficient, impedance ratio, sound pressure reflection factor and transmission factor and admittance has been obtained in various ways. Two major methods have emerged as superior and have achieved standard status: the standing wave method and the transfer function method (ISO-10534-1-2:1998(E)). The B&K system used in this study adopts the transfer function method for all measurements. Two different setups of the impedance tube systems are used for measuring the different properties of the material: the two microphone setup and the four microphone setup (Fig. 59). In the two microphones setup, used for the measurements of acoustic absorption, reflection, impedance and admittance the test sample is mounted at one end of a straight, rigid, smooth and airtight impedance tube (Fig. 59(a) and 60). The four microphones setup, used for transmission loss measurement is described in Fig. 59(b) and Fig. 61. In the two microphones setup plane waves are generated in the tube by a sound source (random, pseudo-random sequence, or chirp), and the sound pressures are measured at two locations near to the sample. The complex acoustic transfer function of the two microphone signals is determined and used to compute the normal-incidence complex reflection factor, the normal-incidence absorption coefficient, and the impedance ratio of the test material. The quantities are determined as functions of the frequency with a frequency resolution which is determined from the sampling frequency and the record length of the digital frequency analysis system used for the measurements.

The usable frequency range depends on the width of the tube and the spacing between the microphone positions. An extended frequency range may be obtained from the combination of measurements with different widths and spacing.

The measurements in this study are performed by employing the two-microphone method (using two microphones in fixed locations). This requires a pre-test or in-test correction procedure to minimize the amplitude and phase difference characteristics between the microphones; however, it combines speed, high accuracy, and ease of implementation.

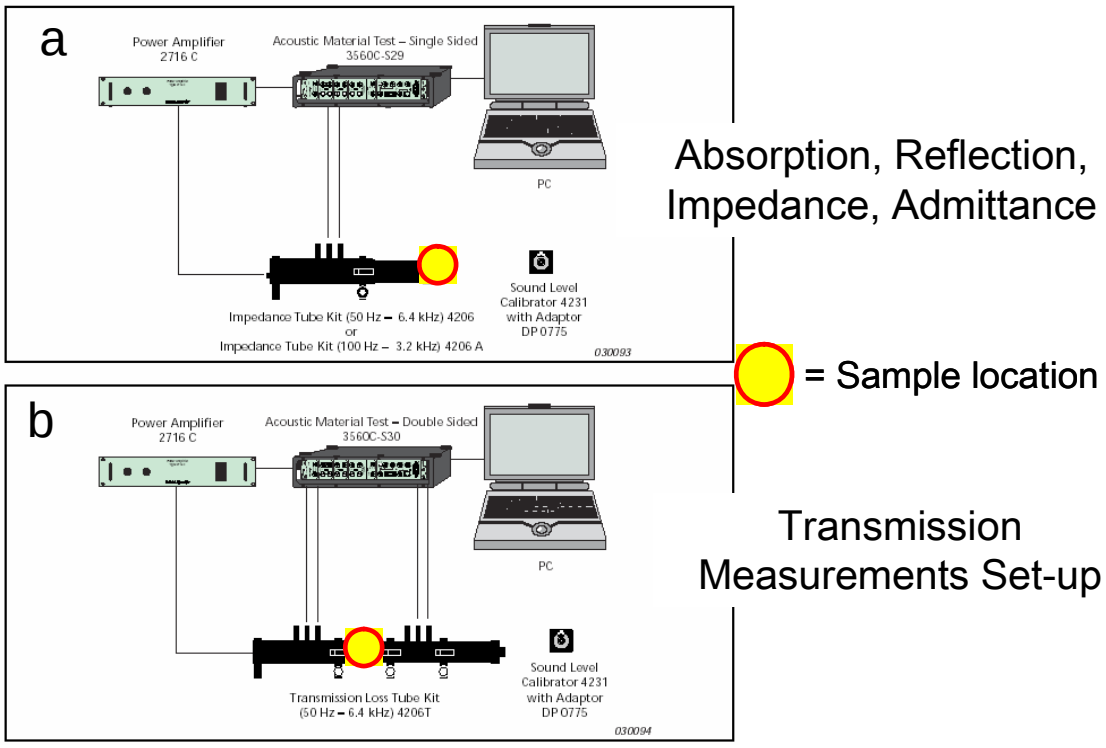

Figure 59. (a) Schematic of the B&K impedance tube setup for measuring sound absorption, reflection Impedance and admittance; (b) Schematic of the transmission loss measurement setup.

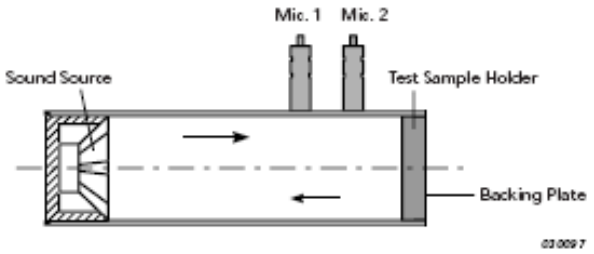

Figure 60. Schematic representation of the experimental setup for the two microphone method for the impedance tube provided by the Manufacturer (Bruel and Kier, 2004).

A specification table for the characteristics of the B&K system can be found in Table 5.

Table 5. Manufacturer (B&K) specifications table for the setup used in the three dimensional experiments.

Specifications – Type 4206, Type 4206 A, 4206 T

FREQUENCY RANGE
Large Tube: 50 Hz to 1.6 kHz
Medium Tube: 100 Hz to 3.2 kHz
Small Tube: 500 Hz to 6.4 kHz

ZERO ABSORPTION
(calculated in 1/3-octave bands)
50 Hz to 4 kHz: < 4%
5 kHz to 6.3 kHz: < 10%

TUBE DIMENSIONS

	Inner Diameter [mm] (in)	Max. Sample Length [mm] (in)
Small Meas. Tube	29 (1.1)	200 (7.9)
Medium Meas. Tube	63.5 (2.5)	200 (7.9)
Large Meas. Tube	100 (3.9)	440 (17.4)
Small Sample Holder	29 (1.1)	200 (7.9)
Medium Sample Holder	63.5 (2.5)	200 (7.9)
Large Sample Holder	100 (3.9)	200 (7.9)
Small Ext. Tubes	29 (1.1)	200 (7.9)
Large Ext. Tubes	100 (3.9)	200 (7.9)
Large TL Tube	100 (3.9)	260 (10.2)
Small TL Tube	29 (1.1)	190 (7.4)
Large TL Sample Holder	100 (3.9)	135 (5.3)
Small TL Sample Holder	29 (1.1)	110 (4.3)

ASSEMBLED SETUP DIMENSIONS
Large Tube (length)*: 700 mm (27.7″)
Medium Tube (length): 910mm (36″)
Small Tube (length)*: 850 mm (33.6″)
TL Large Tube (length): 1170 mm (45.6″)
TL Small Tube (length): 1080 mm (42.1″)
Total Width: 140 mm (5.5″)
Total Height: 240 mm (9.5″)

¼″ CONDENSER MICROPHONE CARTRIDGE TYPE 4187
To optimise the measurement accuracy of Type 4206, the microphones have a non-removable protection grid which forms an airtight front cavity. This gives a coupling between Type 4206 and the microphones that is well-defined with respect to phase
Open-circuit Sensitivity (250 Hz): 4 mV/Pa (–48 ± 3 dB re 1 V/Pa)
Capacitance (250 Hz): 6.4 pF, typical
Frequency Response Characteristic (Flush-mounted) ± 1 dB: 1 Hz to 8 kHz
Polarization Voltage: 200 V

LOUDSPEAKER
Max. Average Power: 10 W at 20°C (68°F)
Max. Pulsed Power: 50 W for 2 s (limited by protection circuit)
Impedance: 4 Ω
Diameter: 80 mm (3.2″)

WEIGHT (WITH ACCESSORIES)
12 kg (26.5 lb.)

* Add 200 mm for each extension tube used

For the measurement of the transmission loss properties (Fig. 59(b)) of our materials we used the Four-microphone Transfer-function Method. Similarly to the two-

microphone method, in this case also, a sound source (loudspeaker) is mounted at one end of the impedance tube and a sample of the material is placed in a holder (see Fig. 61 below).

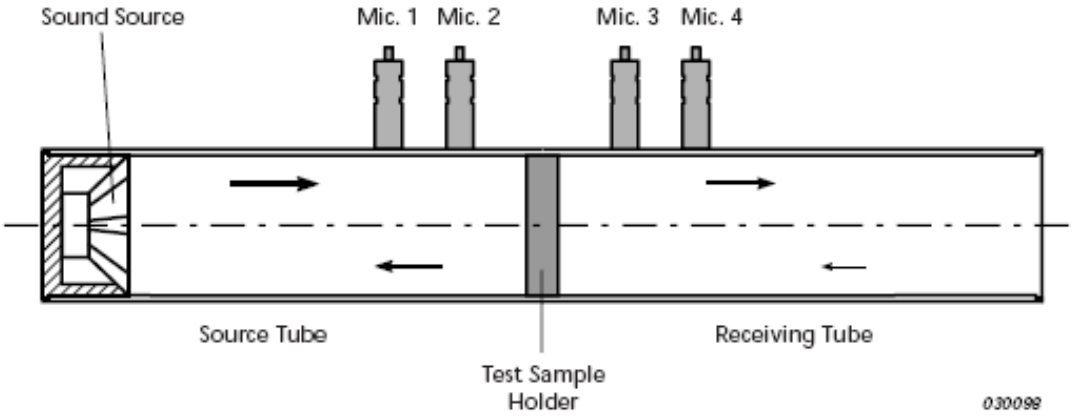

Figure 61. Schematic representation of the experimental setup for the transmission loss measurement tube provided by the Manufacturer (Bruel and Kier, 2004).

The loudspeaker generates broadband, stationary random sound waves that propagate as plane waves. The plane waves hit the sample in the holder with part of the wave reflected back into the source tube, part absorbed by the material, and part passing through the material to the receiving tube. The portion of the plane wave that passes through the material then encounters the end of the receiving tube where some of it is reflected and some exits the tube. By measuring the sound pressure at four fixed locations (two in the source tube and two in the receiving tube) and calculating the complex transfer function using a four-channel digital frequency analyzer, it is possible to determine the transmission loss of the material. The usable frequency range depends on the diameter of the tube and the spacing between the microphone positions.

To better understand the significance of the parameters measured using the described methods a list of definitions provided by ISO standards has been provided:

- *sound absorption coefficient at normal incidence (α)*

The sound absorption coefficient is defined as the ratio of sound power entering the surface of the test object (without return) to the incident sound power for a plane wave at normal incidence (Eq. 20).

$$\alpha = 1 - |r|^2 = 1 - r_r^2 - r_i^2 \tag{20}$$

- *sound pressure reflection factor at normal incidence (r)*

Is defined as the complex ratio of the amplitude of the reflected wave to that of the incident wave in the reference plane for a plane wave at normal incidence (Eq. 21). The measuring method is based on the fact that the sound reflection factor at normal incidence r can be determined from the measured transfer function H_{12} between two microphone positions in front of the tested material.

$$r = |r| e^{j\phi_r} = r_r + j r_i = \frac{H_{12} - H_I}{H_R - H_{12}} e^{2jk_0 x_1} \tag{21}$$

- *normal surface impedance (Z)*

Is the ratio of the complex sound pressure $p(0)$ to the normal component of the complex sound particle velocity $v(0)$ at an individual frequency in the reference plane (Eq. 22).

$$\frac{Z}{\rho c_0} = \frac{R}{\rho c_0} + \frac{jX}{\rho c_0} = \frac{(1+r)}{(1-r)} \tag{22}$$

Where R is the real component, X is the imaginary component and ρc_0 is the characteristic impedance

- *normal surface admittance (G)*

Is the inverse of the normal surface impedance *Z.* Here (Eq. 23) :

$$G\rho\, c_0 = g\rho c_0 - \mathrm{j}b\rho c_0 = \frac{\rho c_0}{Z}\,. \tag{23}$$

Where *g* is the real component and *b* is the imaginary component.

- *sound transmission coefficient (t)*

The sound transmission coefficient of a material is defined as the ratio of the sound power entering the surface of the test object to the sound power exiting the surface of the test object.

Some important concepts necessary to understand the above definitions are provided below:

- The *wave number* (k_0)

  Is a variable defined by $k_0 = \frac{w}{c_0} = \frac{2\pi f}{c_0}$

  Where w is the angular frequency; f is the frequency; c_0 is the speed of sound.

  In general the wave number is complex, so $k_0 = k_0' - jk_0''$.

  Where k_0' is the real component ($k_0' = 2\pi/l_0$); l_0 is the wavelength; k_0'' is the imaginary component which is the attenuation constant, in nepers per metre.

- The *complex sound pressure* (p)

  Is defined as the Fourier Transform of the temporal acoustic pressure

- The *cross spectrum* (S_{12})

  Is defined as the product $p_2 \times p_1^*$, determined from the complex sound pressures p_1 and p_2 at the two microphone positions (* means the complex conjugate).

- The *auto spectrum* (S_{11})

  Is the product $p_1 \times p_1^*$, determined from the complex sound pressure p_1 at microphone position one

- The *transfer function* (H_{12})

  The transfer function from microphone position one to two, is defined by the complex ratio $p_2/p_1 = S_{12}/S_{11}$ or S_{22}/S_{21}, or $[(S_{12}/S_{11})(S_{22}/S_{21})]^{1/2}$.

- The *calibration factor* (*H*c)

  Is the factor used to correct for amplitude and phase mismatches between the microphones

- The *intensity (amplitude)*

  Is defined as the increase or decrease of air pressure associated with sound (dB)

- *Decibel*

  Is the logarithmic measure of the intensity relative to some specified 0dB point (=$2x10^{-4}$ dynes/cm^2)

$$L_p = 20Log_{10}\left(\frac{p}{p_{ref}}\right)$$

Results on the two-microphone based measurements

Preliminary results on absorption measurements on three dimensional systems of various granular materials are provided below. The samples were prepared using a PVC cylindrical holder specifically designed for this application (see Fig. 62) equipped with a millimeter sized rubber pad for needle insertion to allow for precompression via air suction from the inner portion of the sample.

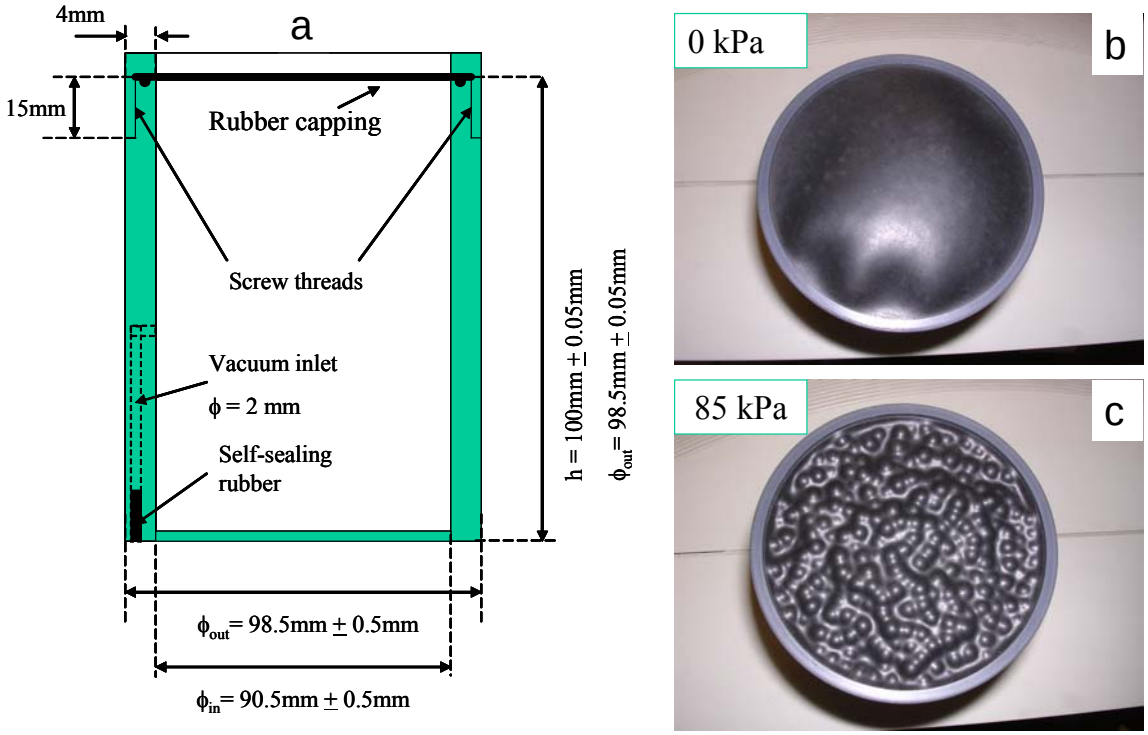

Figure 62. Sample holder designed for measurements in the large impedance tube setup. (a) design of the holder showing the vacuum inlet for precompression of the granular system; (b) uncompressed holder (c) compressed system with at P=85kPa.

To understand the effects of the beads structural configuration on the linear acoustic properties of the medium we designed a PTFE holder with hexagonally arranged

channels to accommodate several chains of beads of different materials (see Fig. 63) that could be easily accommodated in the PVC holder of Fig. 62.

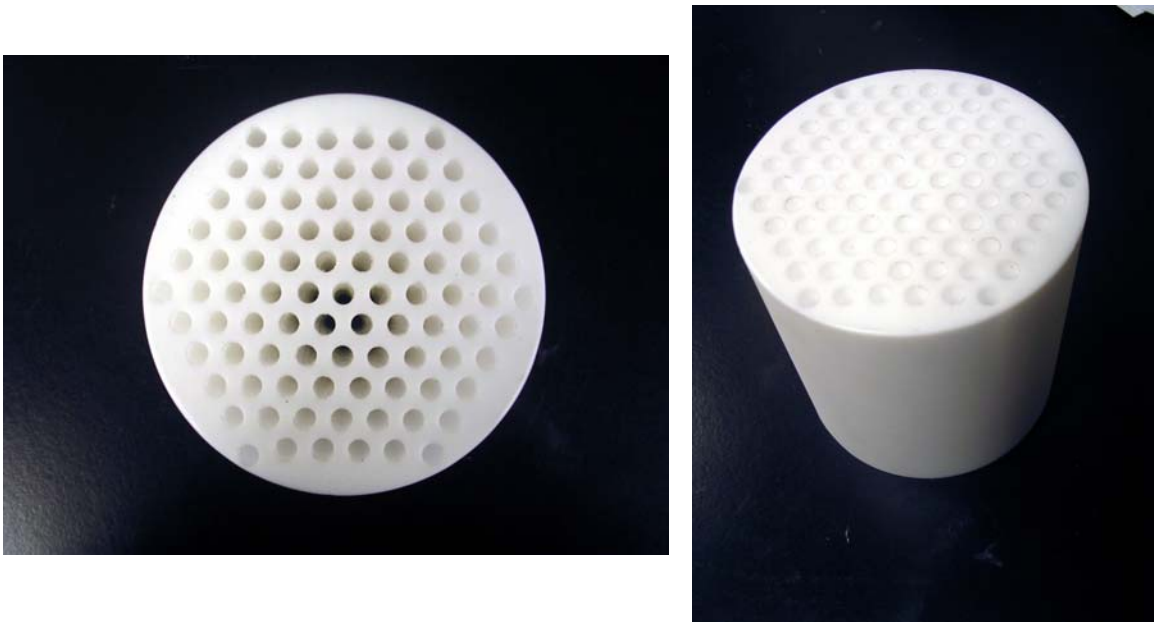

Figure 63. PTFE holder with a set of 91 channels in a hexagonal pattern designed to fit chains of 4.76 mm diameter beads.

The first set of experiments was performed on the two microphone setup of the impedance tube system on uniform PTFE beads and stainless steel beads assemblies. The effect of precompression on the properties of the system was considered to establish the amount of tunability affecting the system. Results for the absorption coefficient for PTFE beads of 4.76 mm diameter and 2.38 mm diameter are presented in Fig. 64. Here it appears evident that the presence of 85 kPa precompression (corresponding curve is indicated by an arrow labeled PC) does have a very well defined effect on the acoustic properties of the material. A frequency shift of ~200 Hz around the 400 Hz peak was

consistently observed under the effect of the added precompression. This shift observed in both, 4.76 mm diameter and 2.38 mm diameter beads, shows that the added precompression allows for a simple and efficient way to tune the absorption (reflection) coefficients. This phenomenon might be explained by the increase on the correlation number (number of contacts) between beads and the increased stiffness of the contrast due to the presence of a precompressive force, similar to the one observed in one dimensional experiments. Further research is necessary to better understand the origin of the phenomenon. To verify the consistency of the experiments and the repeatability of the results even after numerous re-assemblies of the randomly structured beads in the sample, we used as a control data the absorption measurement on the calibration foams provided by the manufacturer (straight lines on the figures). The behavior of the empty PVC holder used for the sample preparation is provided in Fig. 65 as a reference.

To verify if this behavior was consistent also for the stainless steel based assembly, we repeated the absorption measurements on an analogous setup, composed of randomly arranges beads. The results of these experiments are shown in Fig. 66.

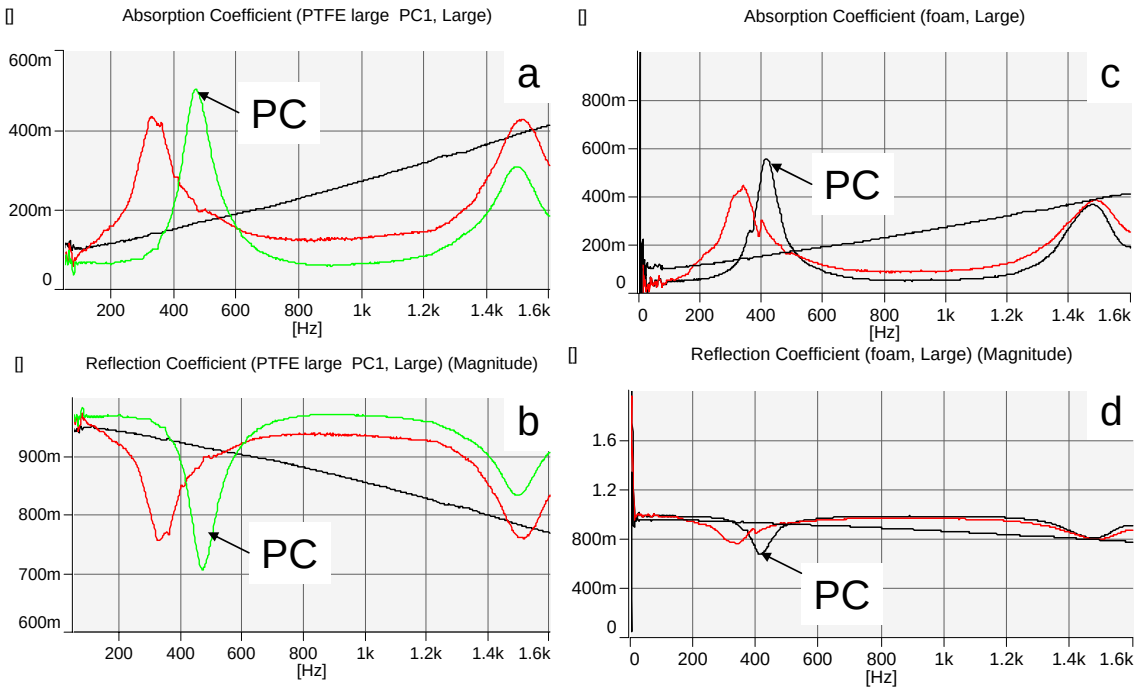

Figure 64. Absorption and reflection coefficients with and without precompression in samples composed of randomly assembled PTFE beads with different diameters. (a) Absorption coefficient as a function of frequency for 4.76 mm beads with and without precompression (PC, indicated by the arrow). (b) Absorption coefficient as a function of frequency for 2.38 mm beads similar to the previous case. (c) Reflection coefficient as a function of frequency for 4.76 mm beads. (d) Reflection coefficient as a function of frequency for 2.38 mm beads. In all figures the straight line represents the absorption of the calibrating foam provided by the manufacturer as a measurement control.

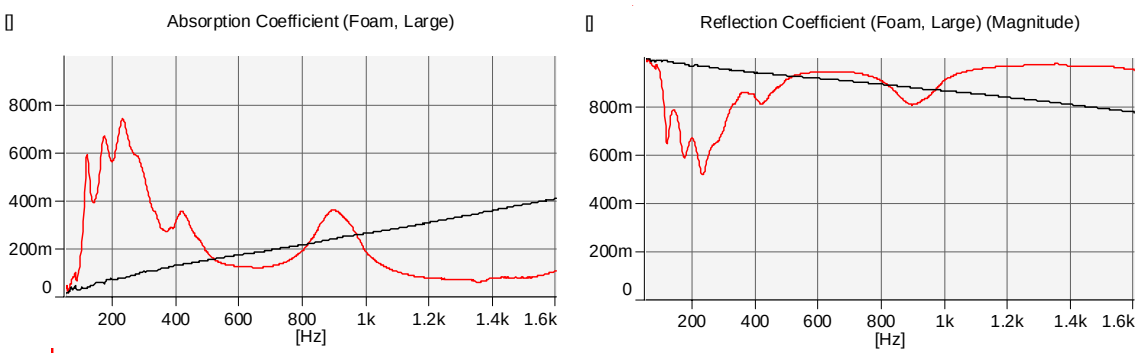

Figure 65. Absorption and reflection coefficient of the PVC sample holder used for the 3D experiments. The straight line represents the same results for the calibrating foam provided by the manufacturer.

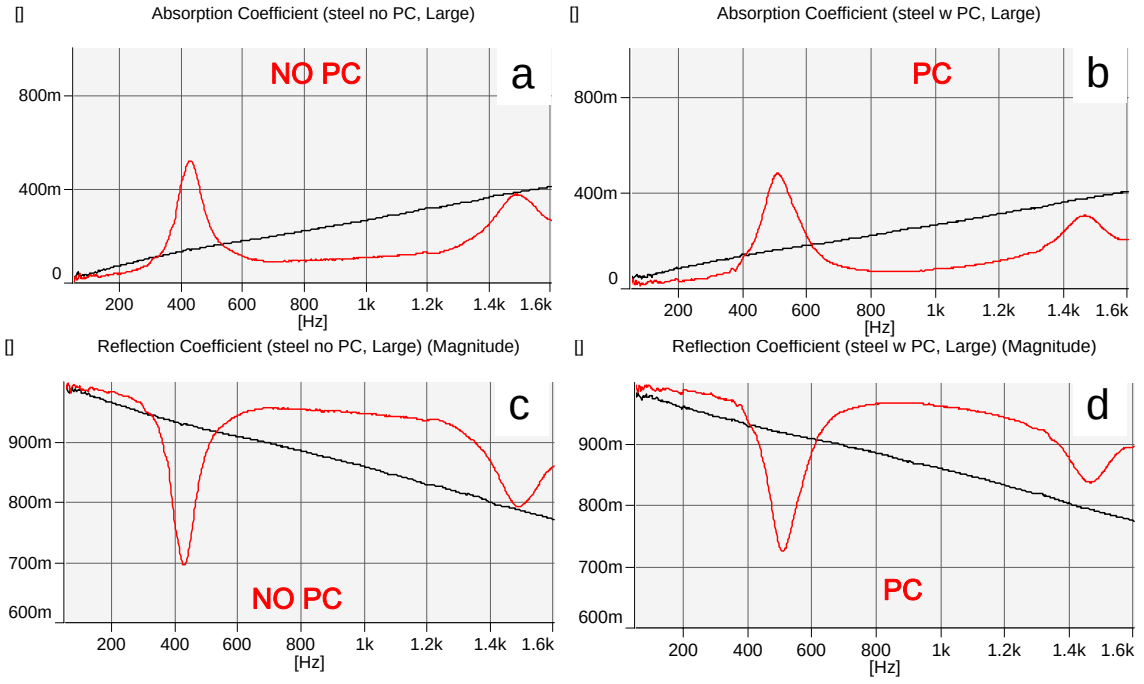

Figure 66. Results of measurements on the randomly assembled 4.76 mm stainless steel beads. (a) Absorption coefficient without precompression (NO PC), (b) with precompression (PC). (c) Reflection coefficient without precompression and (d) with precompression.

From the results on Fig. 66 it is evident that the presence of the 85 kPa precompression on the system causes an analogous shift of the absorption frequencies around the 400 Hz range, similar to the PTFE beads case. In this specific case though the amount of the shifting appears smaller (~80 Hz instead of the ~200 Hz observed earlier).Analogous tunability was observed when testing for the values of the impedance ratio (real and imaginary) and for the admittance ratio (real and imaginary) as it is shown in Fig. 67.

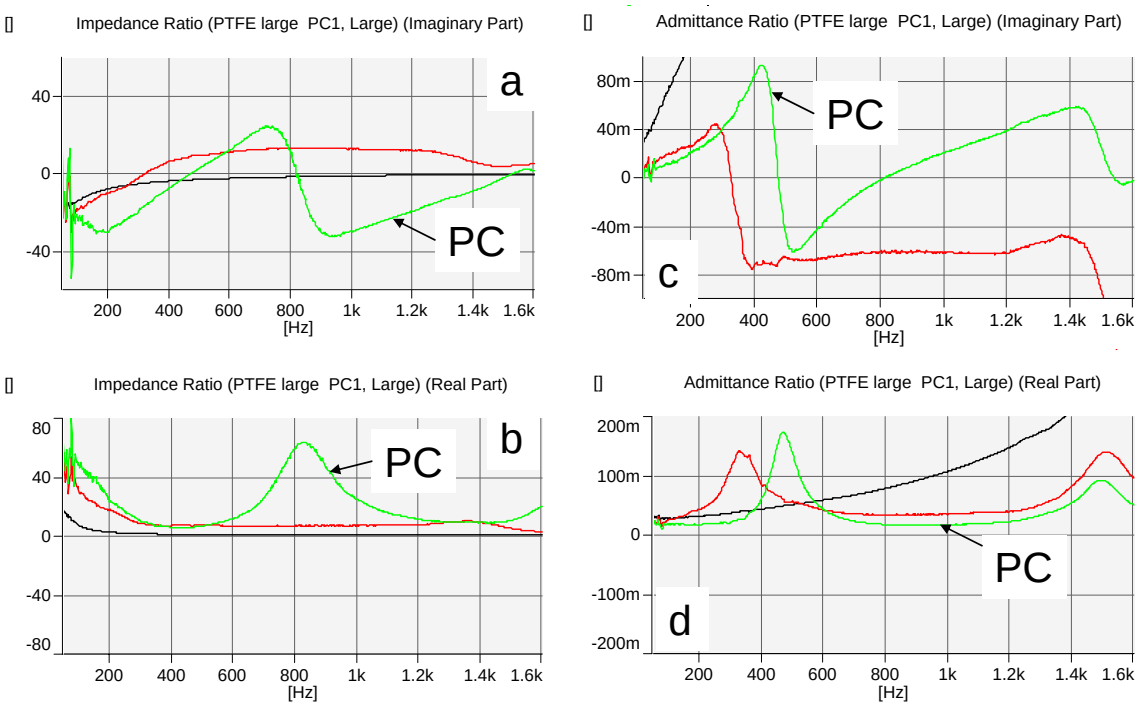

Figure 67. Impedance and admittance ratio measured in the 4.76 PTFE beads, with (PC) and without precompression. (a) Imaginary part of the impedance ratio, (b) real part. (c) Imaginary part of the admittance ratio and (d) real part.

It is evident that even in this case, the presence of the precompression acting on the random granular assemblies varies a lot the properties of the system, dramatically changing the value of the impedance ratio, especially around the 800 Hz frequency range and the admittance ratio around the 400 Hz frequency range. Similar results of tunability of the impedance and admittance ratio were obtained for the 2.38 mm diameter PTFE beads and for the 4.76 mm stainless steel beads. To ease the comparison, results of analogous testing performed on the empty PVC holder, as in the previous case, are provided (see Fig. 68).

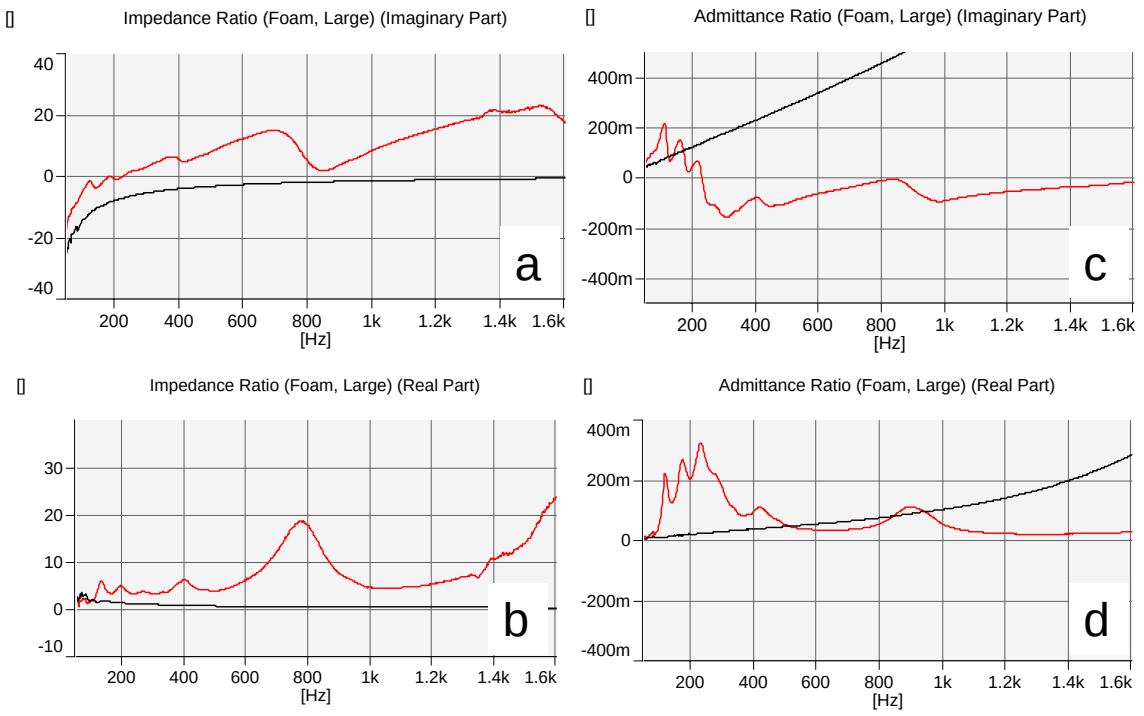

Figure 68. Impedance and admittance ratio measured in the empty PVC holder as compared to the one obtained from the calibration foam provided by the manufacturer. (a) Imaginary part of the impedance ratio, (b) real part. (c) Imaginary part of the admittance ratio and (d) real part.

The results on the absorption coefficient measurements obtained from testing the beads aligned in the hexagonally patterned PTFE holder are presented in Fig. 69 for increasing values of static precompression. It is evident that the increments in static precompression (from 0 to 85 kPa) lead to a fairly regular shift of the absorption peak

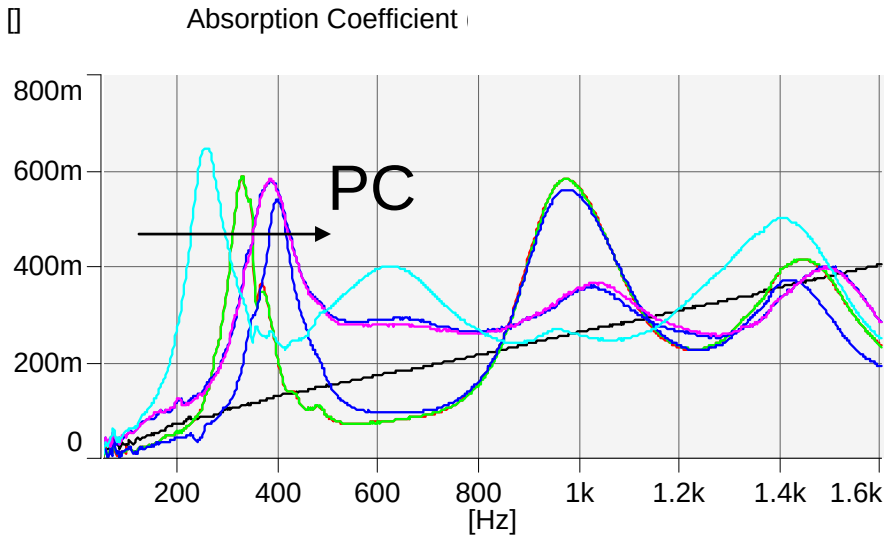

Figure 69. Absorption coefficient measured in the hexagonally patterned PTFE holder filled with 4.76 mm diameter PTFE beads for increasing values of static precompression (PC). The arrow indicates increasing values of precompression.

Analogous data was obtained when testing the 4.76 mm stainless steel beads in the same holder. The results of the impedance and admittance measurements on the 4.76 mm diameter PTFE beads in the hexagonally patterned holder are shown in Fig. 70.

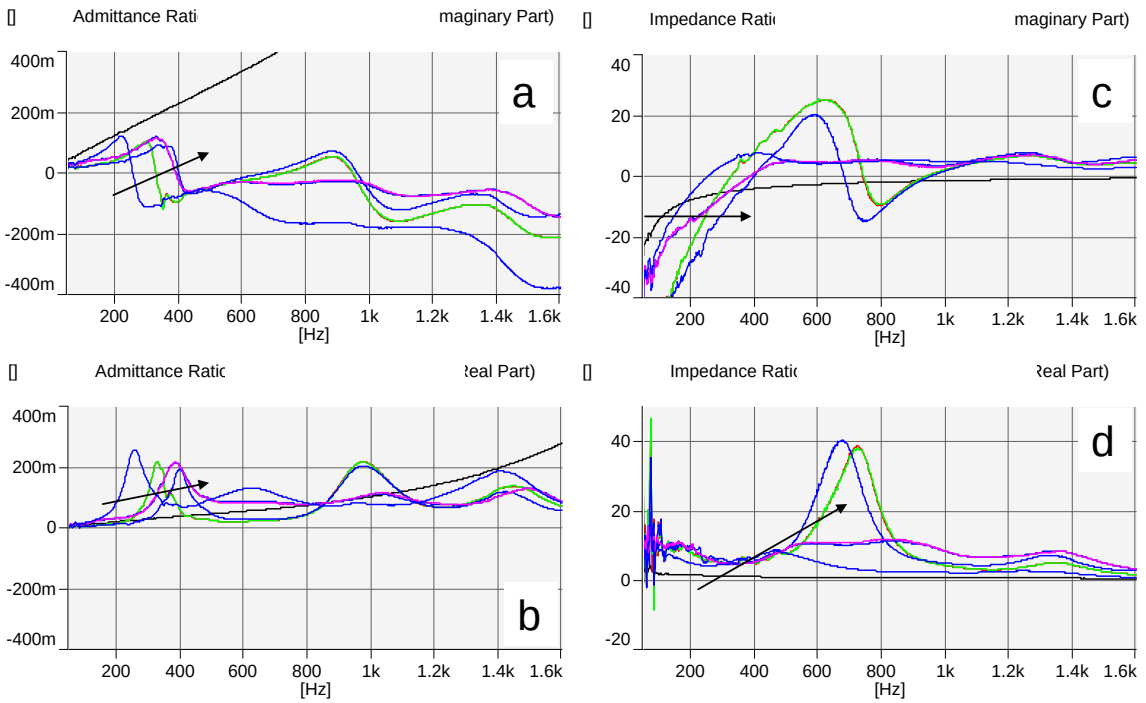

Figure 70. Impedance and admittance ratio measured in the 4.76 PTFE beads, with (PC) and without precompression. (a) Imaginary part of the impedance ratio, (b) real part. (c) Imaginary part of the admittance ratio and (d) real part. The black arrows indicate the increasing static precompression.

Results on the four-microphone based measurements

The four microphones based measurements were performed to calculate the transmission coefficient of the granular assemblies. These measurements are important as a foundation for the possible future design of tunable acoustic lenses. Understanding the amplitude and frequency dependence of the sound power entering the surface of the test object to the sound power exiting the surface of the test object a crucial point in the designing of practical applications.

The preliminary results obtained on the random assemblies of 4.76 mm and 2.38 mm diameter beads are summarized in Fig. 69. The results show a very small influence of the precompression in the behavior of the transmission loss coefficient. Furthermore, almost no difference is noted when comparing the small diameter and large diameter beads behavior. An analogous response was noticed when testing the random assembly of 4.76 mm stainless steel beads I the same container, with and without the presence of the static precompression. Results for these measurements are summarized in Fig. 70. In this case the presence of precompression does not appear to influence the transmission behavior at all. The use of the hexagonally patterned PTFE holder in these measurements did not appear to affect the results on the transmission loss measurements in any way, and behaved similarly to Figs. 71 and 72.

To ease the comparison, results of analogous testing performed on the empty PVC holder, as in the previous case, are provided (see Fig. 73).

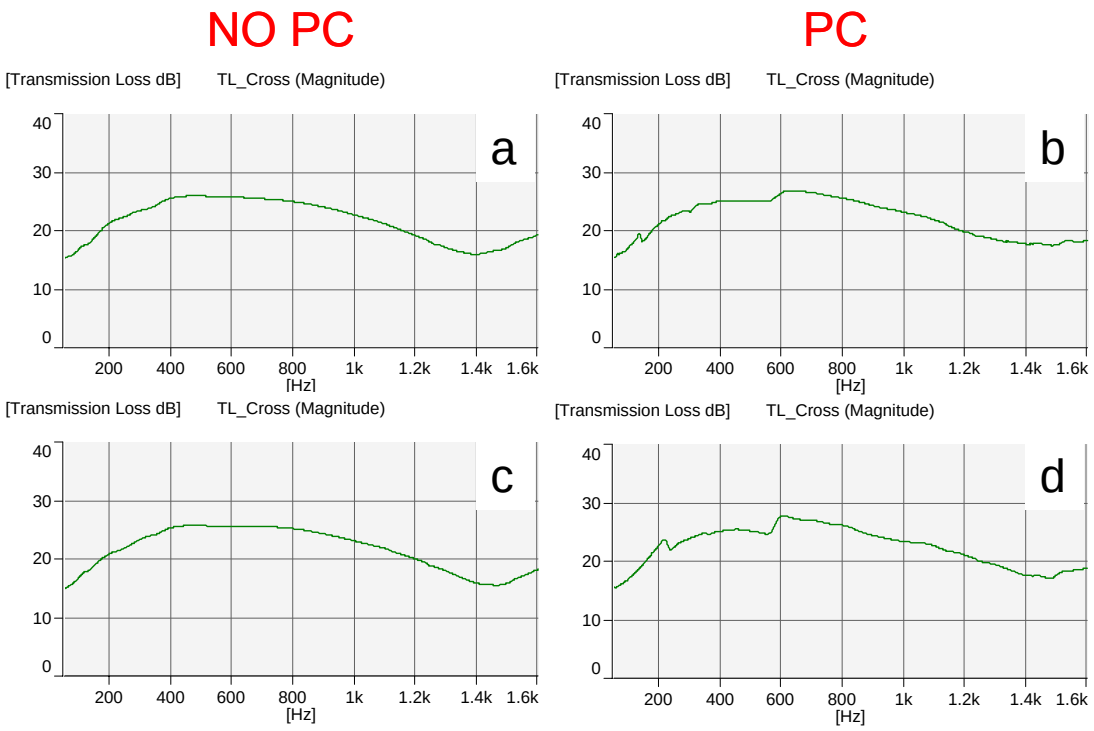

Figure 71. Transmission loss measurements on the granular assemblies composed of 4.76 mm PTFE beads (a) and (b) without and with precompression correspondingly and of 2.38 mm beads (c) and (d) without and with precompression correspondingly.

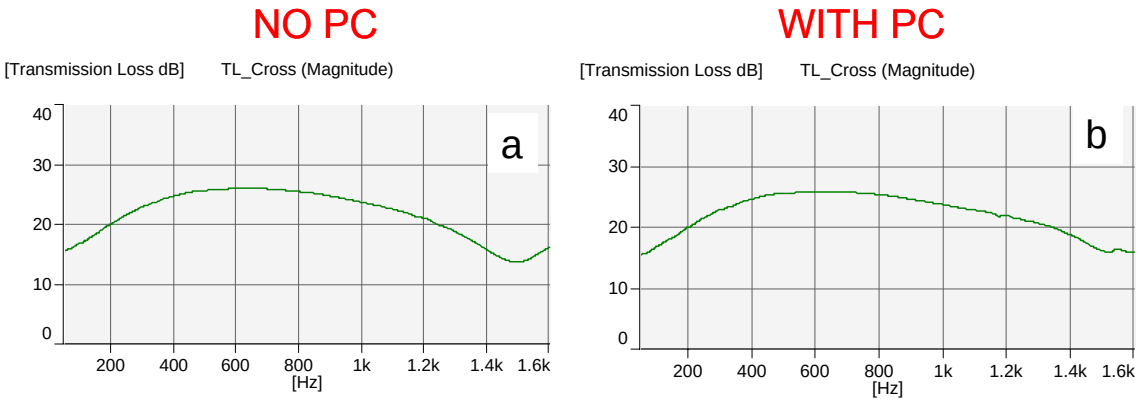

Figure 72. Transmission loss measurements on the granular assemblies composed of 4.76 mm stainless steel beads (a) without and (b) with precompression.

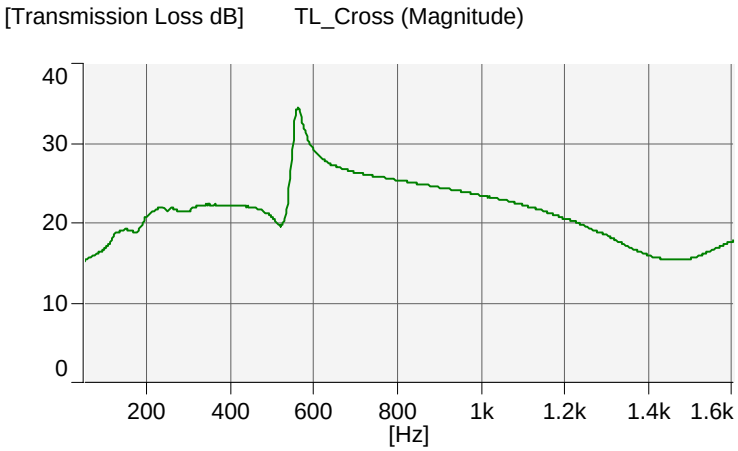

Figure 73. Experimental results obtained in the transmission loss measurements of the empty PVC holder used for experiments.

PART 3

NANOSCALED NONLINEAR CONTACT INTERACTION

The Hertzian type of nonlinear contact interaction characterizing the information propagation in the granular materials is not the only type of nonlinearity enabling the formation of Nesterenko's solitary waves. The strongly nonlinear theory predicts the existence of the so called "compactons" for any power-law interaction with power-law exponent $n>1$ (where n in the Hertzian case is 3/2, Nesterenko, 2001).

It is important to understand that even in the macroscopic systems composed of millimeter-sized grains (like the ones considered in this study) the action of the nonlinear interaction between spheres follows a completely different length-scale, order of magnitude smaller than the diameter of the beads. In particular let's look at the 5 mm diameter stainless steel beads case: the contact interaction area between two adjacent beads calculated using Hertz model for the force amplitudes typical of our experiments had a diameter of ~100 microns. The contact interaction area for signal amplitudes comprised in the acoustic audible range gets even smaller and the surface properties at the nanometer scale start playing a significant role.

To investigate and identify possible alternatives for strongly nonlinear contact interaction between elements in the system, we studied the elastic properties of foam-like forests of carbon nanotubes grown under different conditions. We looked at the elastic and mechanical properties of microwave plasma enhanced CVD grown multi-walled carbon nanotubes (MWCNTs), at DC plasma enhanced CVD grown MWCNTs and

finally at coiled carbon nanotubes (CCNTs) grown on a regular thermal CVD reactor. Understanding the mechanical properties of this films not only could provide an alternative nonlinear layer to ensure the propagation of strongly nonlinear waves in a system but could also provide useful alternatives to protective coating layers for impact reduction in various applications.

The impact response of these forests of carbon nanotubes appeared to be very sensitive to the growth process followed to produce it and showed some very interesting properties in deformation, fracture and response as nonlinear springs accordingly.

Highly nonlinear contact interaction and dynamic energy dissipation by a forest of carbon nanotubes

Mechanical response and energy dissipation of an array of carbon nanotubes under high-strain rate deformation was studied using a simple, drop-ball test with measurement of dynamic force between the ball and forest of nanotubes. This convenient process allows extracting force-displacement curves and evaluating dissipated energy by the nanotubes. The contact force exhibits a strongly nonlinear dependence on displacement being fundamentally different than Hertz law. The forest of vertically aligned nanotubes may be successfully used as a strongly nonlinear spring in discrete systems for monitoring signal propagation speed, and as a novel microstructure for localized energy absorption.

Strongly nonlinear elastic materials are of scientific and technical interest as their unique characteristics can be utilized as an energy-absorbing layered material for noise and shock wave mitigation and as nonlinear phononic crystals. The most famous example of such nonlinearity is the Hertzian interaction law describing forces at one single contact between two linear elastic solids, where the force-displacement relationship has no linear part because of the variation of contact area with the force (Johnson, 1985). Changing contact interaction is crucial for tailoring properties of strongly nonlinear phononic materials for example for the tunability of the speed and shape of propagating signal. Another example of strongly nonlinear behavior can be found in some low-density materials, such as foams, cellular or fibrous materials (Gibson, 1988, Baudequin, 1999). The drawback of these materials is that when large

deformations are involved, damage, crushing, or elastic buckling may dominate the behavior of these materials.

Since their discovery, (Ijima, 1991) carbon nanotubes (CNTs) have been explored for many potential technical applications. The mechanical response of individual nanotubes under axial and radial deformation has been studied extensively using theoretical and molecular-dynamics analysis (Ijima, 1995, Yakobson, 1996, Falvo, 1997, Belytschko, 2002). The elastic modulus (E) has been theoretically calculated in agreement with experimental data to be very high, about 1 TPa (Ru, 2000, Pantano, 2004), showing the superior elastic response and mechanical robustness of the nanotubes. Nonlinear elastic properties, stability, yielding and fracture of CNTs were studied in (Yakobson, 1996, 1997, Falvo, 1997, Belytschko, 2002, Ru, 2000, Arroyo, 2003, Ozaki, 2000, Wei, 2003, Chan, 2003).

Low strain rate mechanical behavior of bundles of nanotubes under pressure was studied in (Chesnokov, 1999, Peters, 2000). Nano-indentation and nonlinear penetration resistance were experimentally investigated for the forest of vertically aligned nanotubes (Qi, 2003). However, neither experimental data on contact resistance of the forest of nanotubes under dynamic conditions nor their ability for energy storage/dissipation at high strain rate deformation is available.

In this analysis we present a new, simple method to determine the high strain rate response and mechanical properties of a forest of vertically aligned CNTs. This allowed measurement and calculation of force-displacement relations for high strain rate penetration process at the level of displacement as small as a few microns. The results of

this work indicate that carbon nanotubes, with their exceptional elastic stiffness combined with excellent resilience under large strain exhibit a strongly nonlinear behavior.

Arrays of carbon nanotubes were grown in a microwave plasma CVD system consisting of a 2.45 GHz microwave power supply and an inductively heated substrate stage (Bower, 2000). Prior to growth, ~5 nm thick film of cobalt metal catalyst was evaporated onto a silicon (100) substrate. The samples were transferred to the growth chamber and heated to 765° C in hydrogen flowing at 200 sccm and held at 20 torr. A 1 kW microwave plasma was subsequently ignited. Ammonia (NH_3) gas was then introduced to completely replace the hydrogen, and acetylene (C_2H_2) was added 2 minutes later to start the nucleation and growth of nanotubes. The growth duration was 50 seconds. The total gas flow rate and pressure was held constant at 200 sccm and 20 torr respectively. The NH_3:C_2H_2 ratio was 3:1. The cobalt catalyst layer breaks up into islands on heating, thus inducing a growth of individual nanotubes. The local electric field in the microwave processing allows aligned growth.

The nanotubes had a narrow diameter distribution around 30 nm and were about 7 μm in average length, although it was observed that a small portion of the nanotubes were much longer than the average. A typical microstructure of vertically aligned carbon nanotubes so obtained is shown in Fig. 74(a). The nanotubes showed slight tangling near the top region, which could be due to their natural mechanical growth configuration or due to Van der Waals force attraction of nearby nanotubes. The presence of such entanglement may help to form a laterally connected nanotubes arrangement structure. The estimated density of the forest of CNTs of the samples is about 100 CNTs/μm^2.

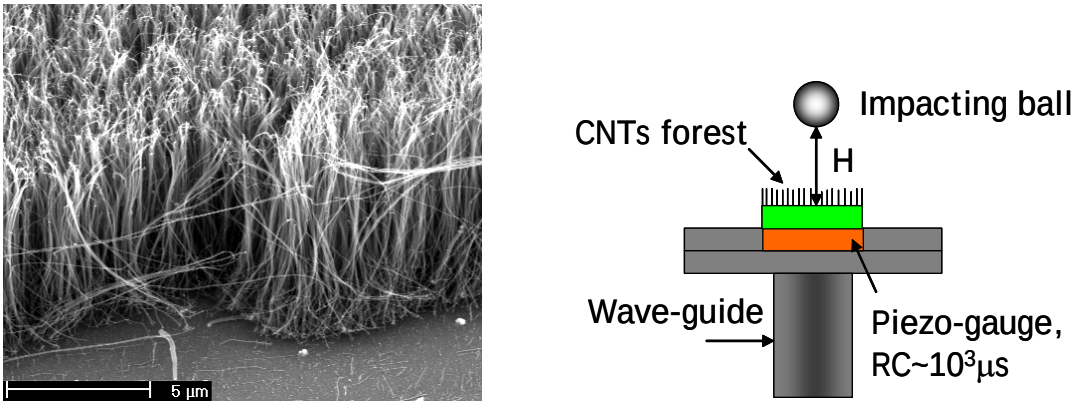

(a) **(b)**

Figure 74. (a) Forest of carbon nanotubes before impact and (b) experimental set-up for measurement of dynamic contact force between the nanotubes and the impacting ball.

The experimental set-up for measurement of mechanical response of the contact between the impacting ball and the array of nanotubes is presented in Fig. 74(b). It includes a calibrated piezo-sensor (RC ~10^3μs) connected to a Tektronix oscilloscope to detect force-time curves during dynamic interaction. Calibration was performed taking into account conservation of linear momentum. A piezo gauge was placed on the top surface of a long, vertical steel rod (wave guide) imbedded at the bottom into a steel block to avoid possible waves reverberation in the system.

High strain rate contact interaction was generated by an impact of a steel ball with 2 mm diameter (mass ~0.03 g) dropped from a height of 2 mm at room temperature. The calculated velocity of the impact was 0.20 m/s, the duration of impact was about 37 microseconds ensuring the strain rate in the interval 10^4 - 10^5 s^{-1}. An essentially similar contact interaction characteristic was observed for other impact velocities of 0.14 and 0.30 m/s. Scanning electron microscopy (SEM) analysis of the morphology of the impact deformed nanotubes was performed in a Phillips SEM operated at 30 kV.

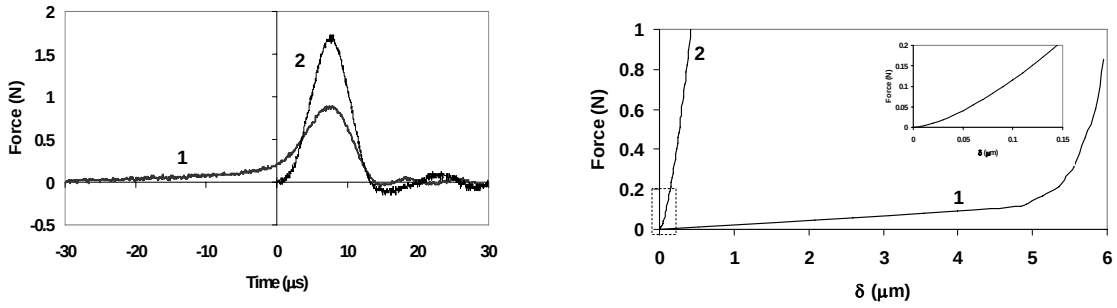

(a) **(b)**

Figure 75. (a) Experimental data for force vs time for contact interaction between the steel ball and the CNTs forest (curve 1) compared to that between the ball and bare Si wafer (curve 2). For convenient comparison curves are centered at their corresponding maximum; (b) Force-displacement curves for contact interaction of a ball with a forest of CNTs (curve 1) and Hertzian contact interaction of a ball with bare Si wafer (curve 2 based on Equation 3).

The measured contact force between the steel ball and the forest of nanotubes versus time is shown in Fig. 75(a), curve 1. Repeated experiments demonstrate identical behavior of contact force. For comparison, the contact response on the bare Si wafer under identical impact conditions was also measured and presented in Fig. 75(a), curve 2. With the presence of nanotubes array, a dramatic change in the slope of contact force is evident in the first part of interaction process. A significant decrease of the maximal force caused by deformation of the forest of nanotubes is also noticeable.

Contact force-displacement curve (F-δ) was constructed based on the measured dependence of force on time. Conservation of linear momentum allows estimation of the ball velocity dependence on time, *u(t),* using Eq. 24:

$$m(u-u_0) = -\int_{t_0}^{t} F(t)dt\,. \tag{24}$$

The velocity of impacting ball *u(t)* can then be used for calculation of its displacement δ (Eq. 25) starting from t_0, which is the beginning of interaction between the ball and the forest of carbon nanotubes (-30 μs in Fig. 75(b), curve 1)

$$\delta = \int_{t_0}^{t} u(t)dt\,. \tag{25}$$

Dependence (F-δ) was obtained by comparison of experimentally detected force F and calculated displacement δ at the same moment t. In calculations the following values of parameters were used: mass m=0.03 g and the initial impact speed u_0=0.20 m/s. The obtained data on contact interaction might be also used for estimating elastic properties of a densified forest of nanotubes.

The resultant force-displacement curve is shown in Fig. 75(b), curve 1. For comparison the Hertzian equation (Johnson, 1985) (Fig. 75(b), curve 2) for ball-silicon wafer contact is also presented as described by the Eq. 26 below

$$F(\delta) = \frac{4E_1 E_2 \sqrt{R}\delta^{3/2}}{3\left[E_2\left(1-\nu_1^2\right)+E_1\left(1-\nu_2^2\right)\right]}, \tag{26}$$

where R is the radius of the ball, δ indicates the displacement during interaction, ν_1 and ν_2 are the Poisson coefficients, and E_1 and E_2 are the Young's moduli for Si and steel, respectively ($\nu_1 = \nu_2$=0.28, E_1=130 GPa, E_2=207 GPa).

It is clear from curves 1 and 2 in Fig. 75 that the nanotube layer exhibits fundamentally different response of contact interactions as compared to the silicon surface. This novel non-Hertzian behavior is revealed by initially weakly nonlinear force dependence on displacement in a relatively wide range of δ = 0-5 microns (compare insert in Fig. 75(b) for Hertz law for small δ and curve 1). At larger displacements contact force (Fig. 75(b), curve 1) starts displaying a strongly nonlinear behavior in the remaining displacement range of 5-6 microns. The initial 5 microns displacement are accompanied by a relatively small increase in force, which might be related to an initial engagement of the ball surface with the taller tubes sticking out of the forest. As the ball continues to penetrate into the nanotubes forest densification and deformation of the forest follows. The dramatic change in force slope observed in the last stage ~1 micron range of ball displacement prior to the peak deformation position. The velocity of the ball is zero at the peak of the *F-t* curves in Fig. 75(a). The slope increase might be related to the continuously increasing volume density of nanotubes as the height of the compressed nanotubes array is decreased further by the impacting ball (this contact behavior is qualitatively different from linear elastic materials which follow Hertz law). It is not clear if this highly nonlinear behavior is connected to the sideway interaction of the bending nanotubes. Another factor to consider is that as the upper part of nanotubes bends sideway, the remaining, still-vertical portion of the same nanotubes gets shorter, thus requiring a much higher stress to deform. The different behavior of the forest of

nanotubes in comparison with linear elastic body causes a qualitatively new contact response than Hertz law. In order to clarify the mechanisms associated with the weakly nonlinear part of interaction, experiments with a very uniform height would be desirable. Strongly nonlinear nanotube materials such as our nanotube forest can be useful as nonlinear springs between inertial elements, and can be utilized to design "sonic vacuum" type devices[1] with possible applications for noise and shock wave mitigation and impact impulse transformation into different wave forms. SEM analysis, Fig. 76(a) and (b), shows bent but not fractured nanotubes in the central heavily affected area of impact (~20 μm in diameter). It is not clear whether some of the observed bending is purely elastic or it contains permanent plastic deformation, for example, involving the formation of pentagon-heptagon type defects (Yakobson, 1998). A schematic picture of interaction of the ball with forest of nanotubes is shown in Fig. 76(c) for different stages of interaction. It is possible that elastic sideway displacements of the nanotubes (from the original vertically aligned position) are retained due to the after-impact entanglement or Van der Waals force type attractions between some of the adjacent, locally contacting nanotubes. From the known average density of the nanotubes, the estimated number of nanotubes in the impacted area (20 μm diameter) is ~$3x10^4$. The overall interacting volume associated with the densely populated nanotubes array of 7 μm height in the deformed region is about $2.2x10^{-15}$ m^3.

The maximum force applied on this area is 0.9 N. The estimation of ball displacement during active rebound stage based on the corresponding force dependence on time (Fig. 75(a), from maximum force to zero in curve 1 gives value about 0.4 microns (Fig. 76(c)).

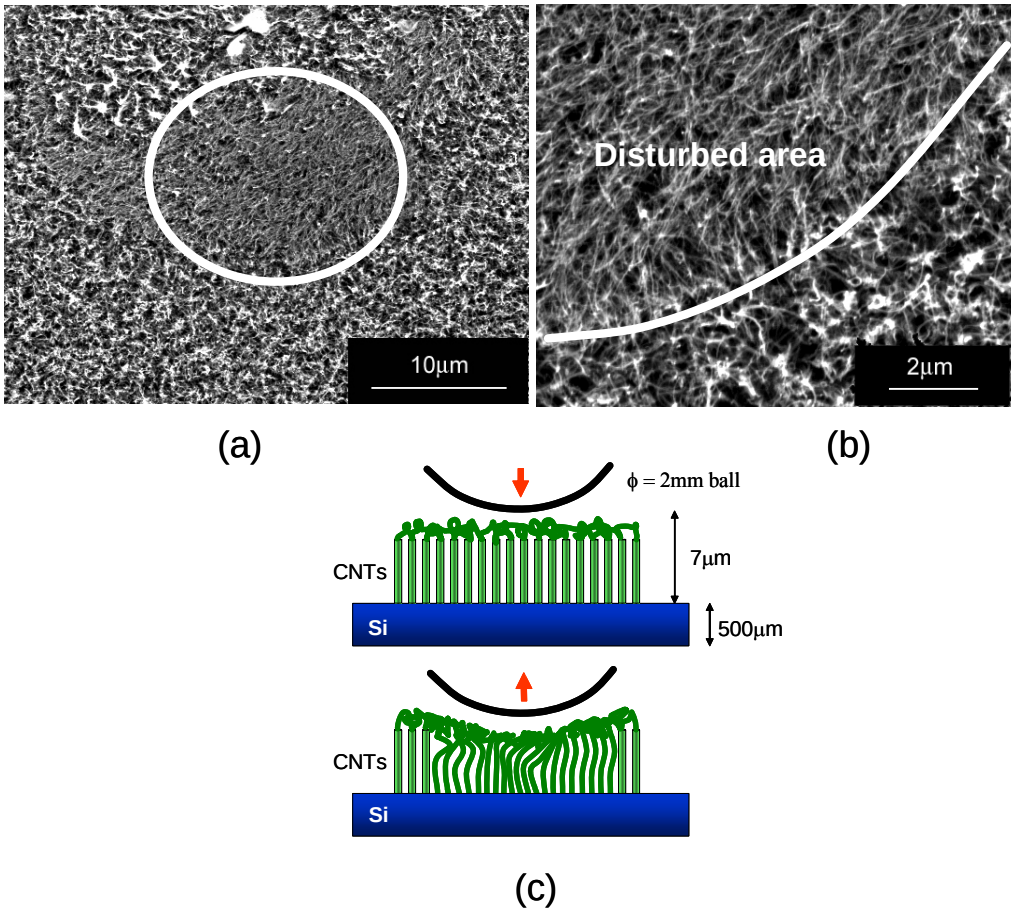

Figure 76. (a) Heavily deformed impacted area shown by white circle; (b) interface between heavily deformed and undeformed region of the Microwave MWCNTs sample; and (c) schematic diagram showing the initial and final stages in the nanotube array on a hard-sphere impact.

The value of the coefficient of restitution (see Appendix III) at impact velocity of 0.20 m/s (e = 0.47) is calculated from the dependence of contact force on time (Fig. 75(a), curve 1) on the first (penetration) and second stages of interaction (rebound). This allows estimate of the energy absorbed by the deformed carbon nanotube forest E_a after impact as (Eq. 27):

$$E_a = \frac{mu_0^2}{2}(1-e^2). \tag{27}$$

Impact with a velocity of 0.20 m/s results in absorbed energy equal to 0.47 μJ or upper limit for volume density 235 MJ/m^3 per initial volume of impacted area of the forest of nanotubes. The corresponding localized energy on each nanotube gives value of 0.015 nJ, which is comparable to (Chesnokov, 1999). This amount of energy can be related to the estimated maximum pressure on the contact (3 GPa) based on the maximal measured force (0.9 N) and diameter of the heavily deformed area (about 20 μm) (Fig. 76(a)). This indicates that the forest of nanotubes can be utilized as a mechanical energy storage device at high strain rate deformation as suggested earlier for reversible quasi-static compression at similar level of pressures.

Preliminary results on a different array of multiwall carbon nanotubes synthesized by DC Plasma CVD (Daraio, 2004) showed a dramatically different behavior. Although the change in slope of the contact force observed was similar to the data presented in Fig. 75(a), curve 1, SEM analysis showed a nano-fragmentation of the individual tubes in uniform segments of 200 nm lengths, instead of the elastic or plastic deformation described in Fig. 76.

In summary, the mechanical response of carbon nanotube forests under conditions of high strain rate deformation was studied using a simple and convenient experimental approach. It is shown that the deformation of vertically aligned nanotubes on vertical impact exhibits a strongly nonlinear, non-Hertzian type contact interaction law, which may be useful for design of strongly nonlinear phononic discrete systems using the nanotube array as nonlinear springs. Such a nonlinear behavior allows tunability of properties of phononic devices due to dramatic change of stiffness of contact interaction

with applied static force. The results also reveal a significant level of energy absorption on high strain rate deformation at high pressures on the order of a few GPa.

Dynamic nanofragmentation of carbon nanotubes

We report a new phenomenon of dynamic nano-fragmentation of carbon nanotubes by high-strain-rate stresses. An impacting sphere on vertically aligned multiwall nanotubes caused them to break up into short segments in just 15 microseconds with a relatively uniform length range of ~100 – 150 nm. The ends of the fragmented nanotubes often exhibit an irregular oval or hexagonal cross-section. Some of the fragments show a sign of plastic bending near the fracture point. The mechanism of multiple-breakup of nanotubes may be tentatively attributed to elastic buckling and fracture at the nodes or weak points, sequential fragmentation due to local bending, or contact interaction of crossed nanotubes. The observed cutting of nanotubes may conveniently be utilized for their resizing and end-opening for a variety of applications such as nanocomposite synthesis, nanoscale and large-surface-area reservoir to store chemical reactants/catalysts, nano carriers for therapeutic drugs/DNAs/proteins, and various other nano-electronics and nano-mechanics applications.

Since their discovery, the processing and properties of carbon nanotubes (CNTs) have been investigated for many different technical applications. While the growth of long nanotubes is relatively easy, controlled cutting of nanotubes into desired short length has not been studied much. For a number of technical applications, cutting of nanotubes (and nanowires in general) into desired short length, preferably of equal or comparable lengths is essential. For example, nanoelectronics, nano circuit interconnections, nano optics (nano laser array), NEMS (nano-electro-mechanical systems) devices including nano manipulators, AFM tips, biomedical applications for interaction with DNAs (Baker,

2002, Gao, 2003), sensors, actuators, and so forth require a controlled and manageable length, rather than the often uncontrollably long nanotube lengths. Some applications require opening of nanotubes especially for filling the inside with other materials or for chemically functionalizing the open ends for advanced composites or for biochemical conjugations. At least one end is usually closed in the as-synthesized nanotubes as the growing nanotube tip is terminated with either a dome or a catalyst particle. Cutting or opening of nanotubes is typically carried out by etching with concentrated acids such as nitric acid, or by mechanical grinding. However, most of these processes result in uncontrolled cut lengths, and often causes structural damages such as amorphization or disrupted nanotube walls (Jia, 1999, Monthioux, 2001). Furthermore, none of these methods allows convenient cutting into nano-scale length of 100-200 nm. A cutting/opening technique for producing short, relatively straight CNTs without damaging the structure of nanotubes is therefore desirable. In this paper we present a new phenomenon of simple, high-strain-rate, head-on impact cutting the length of carbon nanotubes into a multitude of more or less uniform length pieces with open ends, and discuss possible mechanisms for such a phenomenon.

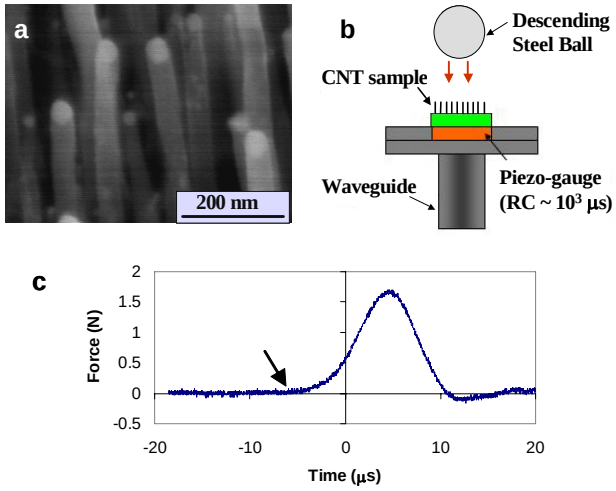

Figure 77. (a) SEM micrograph of the aligned nanotubes, (b) Experimental set-up for measurement of dynamic contact force, (c) Force-Time curve of the vertical impact on the CNT array.

Vertically aligned carbon nanotubes have been demonstrated by various experimental methods, including DC plasma, microwave or thermal CVD (chemical vapor deposition) process (Ren, 1998, Rao, 2000, Teo, 2001, Merkulov, 2001, Bower, 2000, 2002). In the present work, arrays of vertically aligned carbon nanotubes (CNTs) were tip-grown, as shown in Figure 77(a), using a DC plasma enhanced chemical vapor deposition (PECVD). Our array of aligned carbon nanotubes were fabricated by first sputtering a ~5 nm thick Ni film over the surface of an n-type Si (100) substrate. The substrate was then transferred to the CVD chamber. Upon heating to ~700 °C under hydrogen flowing at 150 sccm (standard cubic centimeter per minute) and held at 15 torr, the Ni film breaks up into islands with average diameters ~40 nm which serves as nanotube nucleating islands. The atmosphere was changed to ammonia (NH3) flowing at 150 sccm and held at 3 torr, and a DC bias of 450 V was applied between the anode

above the sample and a cathode which supports the sample. Under the applied voltage, plasma was formed and acetylene (C_2H_2) gas was then added to the chamber flowing at a rate of ~ 30 sccm with the total NH_3 & C_2H_2 pressure held at 3 torr. After ~ 30 minutes of CVD processing, vertically well aligned multiwall nanotubes (MWNTs) were formed. The SEM (scanning electron microscopy) analysis was carried out using Phillips field emission SEM operated at 30kV.

The arrays had a density of ~2 $x10^9$ CNTs/cm^2. The average length of the nanotubes was ~1.5 μm. The SEM micrograph also showed a well-defined tip growth mechanism with the Ni catalyst particles always present at the tip of growing nanotubes. The experimental set-up used here for high strain rate deformation consisted of a bench-top system (Daraio, 2004) (see Figure. 77(b)) which included a free-falling steel sphere and a calibrated piezo-sensor connected to a Tektronix oscilloscope to detect force-time curves to help control the overall dynamic force applied to the forest of CNTs. The use of a sphere allows a reproducible application of large, concentrated force so that each nanotube can be subjected to sufficient impact energy. A steel shock-absorbing rod structure (waveguide) was placed under the sensor to avoid possible reflecting waves from the support bench.

The impact on the aligned nanotubes was generated by dropping a 2 mm diameter steel sphere (0.03 g weight) from a height of 2 mm, which corresponds to a speed of impact of ~ 0.2 m/s. Accordingly the overall strain rate is calculated to be is on the order of 10^4–10^5 s^{-1}. Shown in Fig. 77(c) is a force-time curve for the vertical impact of the descending metal sphere on the nanotube array measured by the set up of Fig. 77(b). The duration of the impact pulse is ~15 μs and the average maximum force applied on the

overall sphere-nanotube contact area is ~1.7 Newton, which corresponds to a force of ~4.3×10^{-5} N/per single CNT. The ball displacement, starting from the point of contact with nanotubes (shown by the arrow (c)) until it comes in contact with the layer of fragmented nanotubes at the bottom, is estimated to be ~1.0 μm, comparable to the average height of the CNTs. The maximum pressure exerted on the impacted area, estimated from the force and the sphere-nanotubes contact area (~50 μm in diameter central portion of the contact area), is very high, amounting to ~8.7 kbar.

The energy used for deformation and fracture of nanotubes derived from the initial kinetic energy of the ball and the calculated coefficient of restitution (e = 0.6) based on experimental data is 0.36 μJ (2.25×10^{12} eV). Assuming that this energy is uniformly distributed among the CNTs in the impacted area, we can derive a localized energy per nanotubes of 9.2×10^{-6} μJ (57.4×10^{6} eV/CNT). This amount of energy is well below the energy necessary to break C-C bonds in the nanotube (C-C binding energy is known to be ~7.4 eV/atom, which is many orders of magnitude larger than the energy supplied here). A possible explanation of the fragmentation phenomena observed at such a low energy level may be due to the inclined graphene walls with respect to the nanotube axis in the DC plasma CVD grown nanotubes (Merkulov, 2001). In this case we may expect breaking of the weaker bonds between graphene layers instead of breaking the strong C-C bonds in the graphene sheet. The impact experiments of Fig. 77(b) were also carried out for different nanotube lengths (1 – 3 μm) and impact velocities in the range of 0.1 – 0.5 m/s, similar mechanical behavior and fragmentation phenomena were observed.

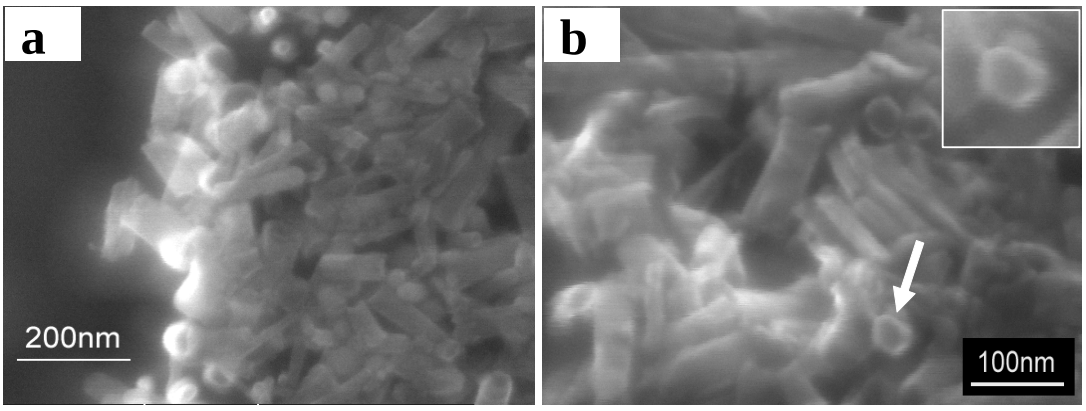

Figure 78. Two examples of nano-fragmented carbon nanotubes (a) lower magnification, (b) higher magnification showing hexagonal or oval cross-section openings formed by impact deformation.

It is seen that the aligned nanotubes of Fig. 77(a) are broken up into many segments (Fig. 78) with a relatively comparable lengths of ~100 – 150 nm on average (although occasional variation of length outside this range is observed). For the ~1.5 μm tall nanotubes, this means a fragmentation of each nanotube into ~10 - 15 segments. As the average diameter is ~40 nm and the nano fragmented length ~100 –150 nm, the aspect ratio (the length to diameter ratio) of each of the short nanotubes is only about 3. This short aspect ratio implies a relatively convenient and easy penetration/incorporation of another material inside these open nanotubes, for example, to prepare new types of nanocomposite materials with unique mechanical, magnetic, electronic, or optical properties. These nanolength, hollow CNTs can also be utilized as a nanoscale and large-surface-area reservoir to store chemical reactants/catalysts or therapeutic drugs/DNAs/proteins to be delivered. The observed phenomenon of nano-scale fragmentation with such a relatively uniform length-distribution is very interesting, as one would normally expect to see a rather random length-distribution of fractured

segments. Such a phenomenon, to the best of our knowledge, has not been reported so far. The open ends of the nanofragmented CNTs often exhibit slightly distorted or oval shape openings as shown in Figs. 78(a) and (b), which was obviously caused by the deformation and fracture process. A relatively well defined hexagon shaped opening was also observed, an example of which is marked by an arrow and inset in Fig. 78(b). The occurrence of a hexagon shaped nanotubes cross section was predicted by Chesnokov et al. on elastic compaction of nanotubes bundles (Chesnokov, 1999). Whether our observation of fractured and permanently hexagon- or oval-shaped nanotube ends is related to Chesnokov prediction is unknown. The non-circular shape of the openings in some of the nano fragmented nanotubes as compared to the originally circular cross-section of as-grown carbon nanotubes implies their plastic deformation during impact. Such plastic deformation is also evident from Figs. 79 (a-c) which shows curved sections near the fragmented ends of the nanotubes. The plastic deformation most likely involves an introduction of crystallographic defects, such as the formation of the well known pentagon and heptagon defects or Stone-Wales pairs (5-7-7-5 defects) on the normally hexagon arrangement of carbon atoms on graphene planes of the carbon nanotubes. Partial fracture of the CNT or bent tubes still partially attached to the remaining vertical segments (about 100 – 200 nm tall) still standing on the substrate were observed in the slightly off-centred region where the curvature of the sphere prevented it from touching the surface of the substrate (Fig. 79(d)). Further study of plastic deformation and fracture behavior of carbon nanotubes on head-on impact might be an interesting area for in-depth research, especially the bending/breaking mechanisms associated with impact deformation.

From the geometry of the 2 mm diameter metal sphere descending and penetrating through the thickness of the carbon nanotube array (~1.5 μm tall), the sphere-nanotube contact area is estimated to be ~90 μm in diameter. Of this contact area, the central region of impact with a diameter of roughly ~50 μm shows essentially completely fractured nanotubes in segments of 100-150 nm in lengths. In this region, the bottom surface of the 2 mm diameter descending sphere is practically flat, with the contact angle between the nanotube tip and the bottom surface of the ball is between 0 and 1.15º. In the noticeably off-centred region just outside this ~50 μm diameter, e.g., an area forming a ~20 μm wide ring around the central part of the impact, most of the nanotubes are also fractured in nano-fragments. The short, bottom sections of nanotubes though are still attached to the substrate. This is because the portion of the sphere contacting this off-centre area is tilted and can not touch the substrate. Such remnant sections of nanotubes with a height of ~100 – 200 nm are shown in Fig. 79(d). Carbon nanotubes are known to have superior mechanical properties (Pantano, 2004), for example a forest of CNTs grown in a microwave plasma system didn't break under similar conditions of impact and can be exploited for strongly nonlinear springs. Mechanisms of fracture and axial and radial deformation of carbon nanotubes have been studied extensively with the aid of theoretical calculations and some in-situ analysis. However, there has been no report on the head-on impact fragmentation behavior of carbon nanotubes such as being described in this work.

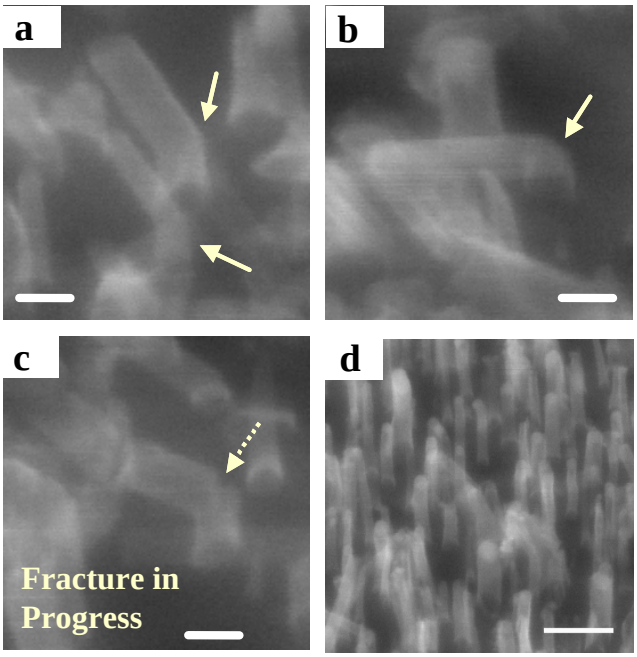

Figure 79. Carbon nanotubes after impact deformation showing local plastic bending (see arrows in (a), (b)) and the onset of fracture (dotted arrow in (c)). The plastic deformation is obvious in the curved sections near some of the fragmented ends of the nanotubes. (d) SEM micrograph showing short remnant nanotubes in the off-centred region after impact fragmentation. Scale bars for (a)-(c) are 50nm, (d) 200nm.

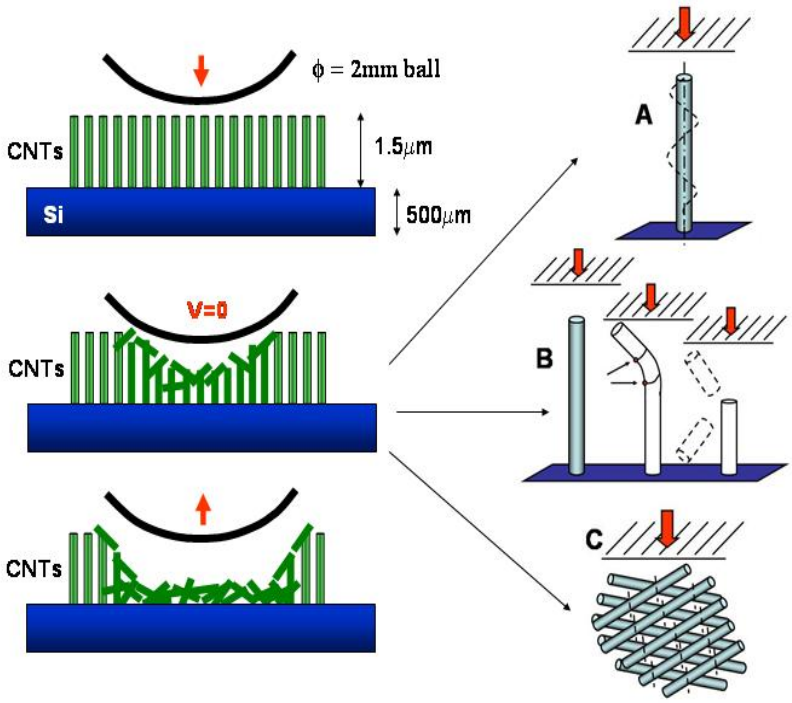

Figure 80. Possible fragmentation mechanisms suggested. (A) Buckling, (B) sequential fragmentation, (C) fracturing of crossed net nanotubes, and/or a combination of any of the above.

Possible mechanisms considered for the observed nano-fragmentation are illustrated schematically in Fig. 80 and are discussed as follows. (A) The ball impact on vertically aligned nanotube generates a critical compression stress resulting in the elastic buckling of nanotube which may be considered as an elastic column fixed at the base and free at the side of impact (Euler instability, Gere, 1990). The theory allows an infinite number of buckled mode shapes (defined by integer n) depending on the applied axial force. In the case of quasi-static loading of single isolated column, the only mode of practical interest is $n = 1$. In the case of dynamic loading on aligned nanotubes a higher order buckling mode is possible (n = 1-20 in our case). There could be a number of other

ways of generating higher order modes, one example being the contact interaction and blocking by neighboring nanotubes. Another alternative is a multiple nucleation of cracks in the first order buckling mode (n =1) and subsequent distributed fracturing originated from all these nucleation sites where stress is exceeding the critical fracture stress. It is conceivable that such multiple nucleation sites can even be purposely introduced during CVD growth via periodic doping, change of deposition parameters, or introduction of lattice or geometrical defects (such as sharp-bending zig-zag nanotubes, AuBuchon, 2004). This mechanism may be supported by the observation of rather uniform and short fragment length. (B) Breaking of the nanotubes due to local bending and fracture progressing from the tip to the base in a sequential manner as the sphere continues to descend, which may be supported by observation of remnant, still vertically attached nanotube segments shown in Fig. 79(d). (C) Each of the nanotubes in the impact area are first broken into a few long pieces (e.g. due to mechanism A or B), which fall on the substrate surface creating a crossed net of overlapping tubes and then fragmented by vertical compression. While the average mesh size of the net, and the subsequent length of the segments, appear to match with estimated density of nanotubes on the substrate, the formation of such a periodically arranged mesh structure in a short time period of ~15 microseconds seems less likely.

Further research is needed to understand the exact mechanism for the observed nano fragmentation of carbon nanotubes. It would be interesting to see if similar nano fragmentation occurs on z-direction impact stressing of other types of aligned nanowires, for example, ZnO, GaN, Si, SiO2, etc. The observed cutting of nanotubes may conveniently be utilized for resizing and end-opening for easier filling of nanotubes with

other materials for synthesis of nanocomposites or nano-carriers of catalysts for chemical reactions, or proteins, DNAs/genes and drugs for biomedical applications, for easier handling of shortened nanotubes or nanowires for other potential applications such as in nano-electronics, nano-interconnections, nanomanipulators, sensors, and actuators.

In summary, a new phenomenon of dynamic nano-fragmentation of CNTs into short lengths has been observed and analyzed for the first time. This rapid technique may conveniently be utilized for resizing and end-opening of nanotubes for a variety of applications.

Impact response by a film of coiled carbon nanotubes

We studied the dynamic response and energy dissipation of a film of coiled carbon nanotubes under high-strain rate deformation using a simple drop-ball test (Daraio, 2004), measuring the dynamic force between the ball and the substrate. The analysis of the film morphology after impact has shown no trace of plastic deformation and a full recovery of the film of coiled carbon nanotubes under various impact velocities. The contact force exhibits a strongly nonlinear dependence on displacement and appears fundamentally different from the response of a forest of straight carbon nanotubes and from the Hertzian type of plane-sphere interaction. "Brittle" fracture of the film is observed after repeated high velocity impacts. Such coiled nanotubes film may be successfully used as a strongly nonlinear spring in discrete systems for monitoring signal propagation speed, and as a novel microstructure for localized energy absorption.

The study of thin structural foams (Gibson, 1988) for cushioning, energy dissipation and protection has recently been receiving increasing attention for several practical applications. Nanotube films have been reported as an excellent alternative, exhibiting a super-compressible foam-like behavior under compressive cycling loads (Cao, 2005). Investigations on the dynamic response of carbon nanotube films of different nature have shown a strongly nonlinear response that appears very suitable for energy-absorbing layered material in noise and shock wave mitigation and as nonlinear phononic crystals.

Carbon nanotubes (CNTs) since their discovery (Iijima, 1991) have been tested for many potential applications. Theoretical and molecular-dynamics analyses have been used extensively to study their individual mechanical response under axial and radial deformation (Iijima, 1995, Yakobson, 1996, Falvo, 1997, Belytschko, 2002). Experimental measurement and theoretical studies have agreed in attributing to CNTs an extremely high elastic modulus (E), about 1TPa, (Ru, 2000, Pantano, 2004) demonstrating their excellent elastic response and mechanical robustness. There has been a number of studies on the nonlinear elastic properties, stability, yielding and fracture of CNTs (Yakobson, 1996, Falvo, 1997, Belytschko, 2002, Ru, 2000, Arroyo, 2003) Ozaki, 2000, Wei, 2003, Chan, 2003) as well as on the low strain rate response of bundles of nanotubes under pressure (Cao, 2005, Peters, 2000, Chesnokov, 1999, Qi, 2003).

In this letter we present the results obtained by drop-ball testing a forest of aligned coiled CNTs. This simple method had been proved in the past to enable determining the high strain rate response to impact of a thin film of nanotubes, allowing measurement and calculation of force-displacement relations for high strain rate penetration processes at displacements as small as a few microns. The results of this work indicate that coiled carbon nanotubes, add a nonlinear spring response to their exceptional elastic stiffness and resilience that makes them suitable for protection of devices from impact.

The elastic contact interaction between a ball and a planar surface is regulated by the Hertzian interaction law describing forces at one single contact between two linear elastic solids. In it the force-displacement relationship has no linear part, therefore Hertz law represents the most famous example of strong nonlinearity Johnson, 1985). Being able to tailor and control the change in contact interaction in composites or layered

materials is a crucial step for achieving proper tuning of the properties of strongly nonlinear phononic materials like, for example, the control of the speed and shape of the propagating signals.

The arrays of carbon nanotubes used in this study were grown as in (Wang, 2005) on bare quartz substrates (~500 μm thick) in a two-stage CVD reactor comprising of liquid and gas injectors. Xylene (C_8H_{10}) and acetylene (C_2H_2) served as the carbon source. Indium isopropoxide ($(i\text{-}C_3H_7O)_3In$) was dissolved in the xylene-ferrocene ($C_{10}H_{10}Fe$) mixture which was continuously injected into the CVD reaction tube (~700°C) at the rate of 1ml/hr. The atomic concentration of Fe in the xylene-ferrocene mixture was held fixed between 0.75-1 at %, and the relative concentration of indium isopropoxide was varied systematically to yield catalyst particles with varying catalysts compositions R=In/(In+Fe). Acetylene at the flow rate of 50 sccm and argon at the flow rate of 800 sccm were fed into the system during the synthesis. After 1 hour reaction, the syringe pump and acetylene injection were shut off and the CVD reactor was allowed to cool to room temperature under flowing argon atmosphere. Various parameters, such as the reactor temperature, gas flow rate, concentration of iron, and indium were adjusted to optimize the synthesis condition. Scanning electron microscopy (SEM) (Philips operated at 20 KV) and transmission electron microscopy (TEM) (Jeol 3010 operated at 300 KV) were employed to explore the structure and morphology of the as-grown coiled structure and of the tested substrates.

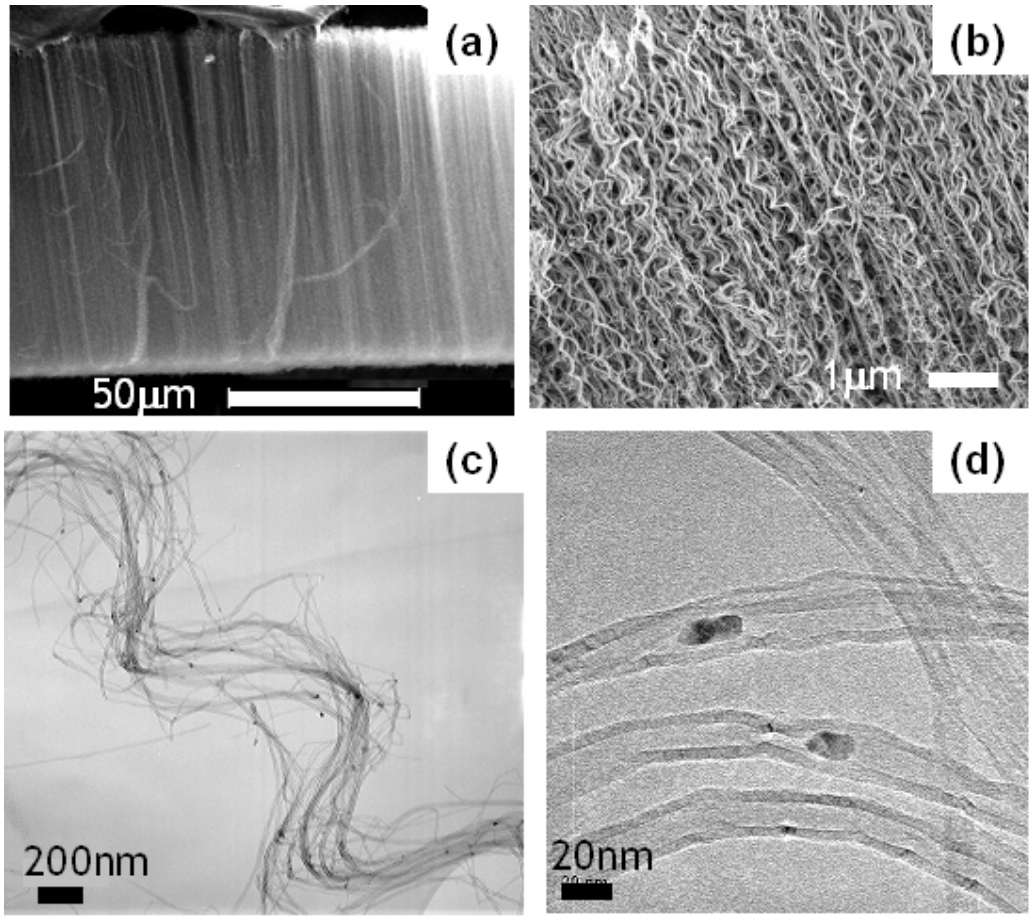

Figure 81. (a)-(b) Low and high magnification SEM pictures showing as grown forest of carbon nanocoils used for the experiments. (c)-(d) Low and high magnification TEM images of a bundle of the coiled carbon nanotubes.

The final film thickness was about 100 μm (Fig. 81(a)). In the forest, the coiled carbon nanotubes are arranged in bundles, probably due to Van der Waals force attraction between them, of ~25 nanocoils with a bundle's diameter ~500 nm (see Fig. 81(b) and (c)). The single coiled nanotubes had a narrow diameter distribution around 20 nm (Fig. 81(d)) with a coiling pitch of ~1 μm. The total density of the carbon nanotubes forest has been estimated at ~100 CNTs/μm^2 from simple geometrical considerations.

The experimental set-up for measuring the mechanical response of the contact between the impacting ball and the array of nanotubes is presented in Fig. 82(a). The quartz substrate with the grown film of coiled nanotubes was cut in pieces of ~25 mm^2 area. This samples were then positioned on top of a calibrated piezo gauge (RC ~$10^3 \mu s$) placed on the top surface of a long, vertical steel rod (wave guide) imbedded at the bottom into a steel block to avoid possible waves reverberation in the system. The sensor, protected by a brass cover plate, was then connected to a Tektronix oscilloscope to detect force-time curves during dynamic interaction. Calibration was performed taking into account conservation of linear momentum.

High strain rate impacts were generated dropping a stainless steel bead (AISI 316L, 2 mm diameter, mass ~0.03 g) from various heights at room temperature. The calculated velocities of the impacts varied between 0.2 m/s and 2.0 m/s. The strain rate for the lower velocity impacts was estimated in the interval 10^4 - 10^5 s^{-1} from the duration of the recorded signal (~40 microseconds). The morphology of the nanotubes forest surface after impact was analyzed with a Phillip scanning electron microscope (SEM) operated at 30 kV and with a Nikon Eclipse optical microscope equipped with digital acquisition camera.

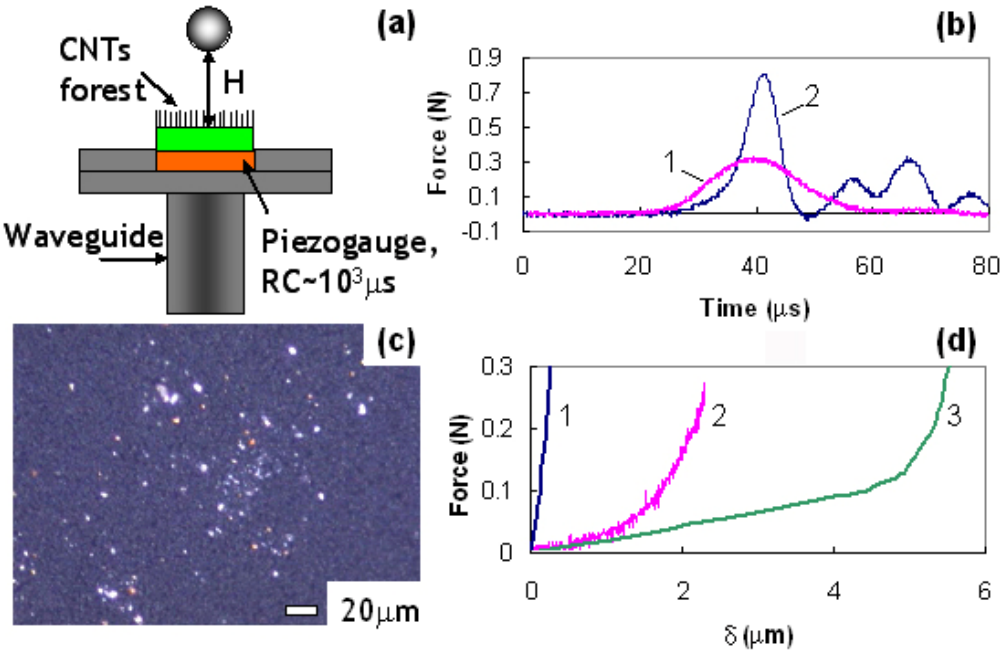

Figure 82. (a) Schematic diagram of the experimental setup used for testing the forest of carbon nanocoils. (b) Force vs. Time response obtained experimentally impacting the coiled carbon nanotubes forest with a 2 mm diameter steel bead (0.02 g) from a height of 2 mm (curve 1) compared to that obtained impacting the bare quartz substrate (curve 2). For convenient comparison curves are time-centered with respect to each other; (c) Forest of the carbon nanocoils after impact observed in an optical microscope. The area of impact is recognizable by the presence of the white "marker particles" left by the striker during impact; (d) Force-displacement curves derived for the Hertzian contact interaction of the striker-ball with the bare quartz wafer (curve 1 based on Eq. 24), for the contact interaction with the forest of coiled carbon nanotubes (curve 2) and, for comparison, with the forest of microwave plasma grown carbon nanotubes under the same impact conditions.

The point of impact area was identified using oxide nanoparticles on the impacting bead's surface as a surface stain. During impact the particles remain trapped by the nanocoils forest and function as a marker on the film surface.

The typical contact force-time response after a small amplitude impact (0.2 m/s striker velocity) on the surface of the film is shown in Fig. 82(b), curve 1. Repeated experiments demonstrate identical behavior of contact force. For comparison, the contact

response on the bare quartz wafer under identical impact conditions was also measured and presented in Fig. 82(b), curve 2. The presence of the coiled carbon nanotubes array appeared to dramatically change the slope of the contact force and attenuate the amplitude of the pulse. The perfectly elastic response is also noticeable from the symmetry of curve 1: the value of the coefficient of restitution (e~1) for the nanocoils film can be calculated from the dependence of the contact force on time on the penetration stage (from the beginning of interaction to the peak of curve 1) and the rebound stage (from the peak to the bottom of curve 1). The image of the forest's surface after impact is shown in Fig. 82(c). It is evident that the forest of nanocoils exhibits a full recovery after the elastic deformation caused by the impact.

The corresponding contact force-displacement curve (F-δ) was constructed based on the measured dependence of force on time and shown in Fig 82(d). We compared F-δ curves obtained for the Hertzian contact interaction of a steel bead with quart (curve 1) with the one for the coiled carbon nanotubes film (curve 2) and with the response of a film composed of aligned straight CNTs grown in a microwave plasma enhanced CVD system (curve 3). Curve 1 was calculated by Eq. 28:

$$F(\delta) = \frac{4E_1 E_2 \sqrt{R}\delta^{3/2}}{3\left[E_2\left(1-\nu_1^2\right)+E_1\left(1-\nu_2^2\right)\right]} \tag{28}$$

where R is the radius of the ball, δ indicates the displacement during interaction, ν_1 and ν_2 are the Poisson coefficients, and E_1 and E_2 are the Young's moduli for quartz and

steel, respectively (ν_1=0.18, ν_2=0.28, E_1= 76.5 GPa, E_2=207 GPa) (Daraio, 2004). Curves 2 and 3 were derived from the conservation of linear momentum, allowing the estimation of the ball velocity dependence on time and the calculation of the displacement δ, obtained by comparison of the experimentally detected force F and the calculated displacement δ at the same moment t. Such data on contact interaction might be also used for estimating the elastic properties of the nanocoils.

It is clear from Fig. 82(d) that the coiled carbon nanotubes layer exhibits a fundamentally different response of the contact interaction as compared to the bare quartz substrate and the aligned CNTs behavior. The total depth of displacement of the striker bead into the nanocoils forest was calculated at ~2 μm, involving an area of interaction with a ~68 μm radius corresponding to a minimum pressure estimated at ~0.2 GPa. From the SEM and Optical microscope analyses (see Fig. 82(c)) no permanent deformation was observed. Analogous responses were detected in the full range of striker velocities tested, demonstrating the huge elastic recovery of the nanocoils. To evaluate the nonlinear response of the film impacted by a striker velocity of 0.2 m/s and compare it with the classical Hertzian behavior, we approximated curve 2 with a power law response, $F=A\delta^m$, and obtained a qualitative match with the value of A=0.028 and m=2.6 measuring the force (F) in Newtons and the displacement (δ) in microns. The values of m for the quartz-steel Hertzian interaction is m=1.5, therefore demonstrating a significant different type of nonlinear behavior. It is not clear if this highly nonlinear behavior is also connected to the sideway interaction of the compressed nanocoils bundles. A schematic diagram

representing the interaction of the ball with the coiled CNTs film is shown in Fig. 83 for the different stages of interaction.

The results of identical impacts on a different array of multiwall CNTs synthesized by microwave plasma enhanced CVD showed a dramatically different behavior (see Curve 3 in Fig. 82(d)). In this case the slope of the F - d curve observed presents a double nonlinearity and a much longer depth of striker penetration. Also, for the forest of straight CNTs, SEM analysis showed a permanent plastic deformation and a densification of the impacted area. Analogous testing performed on DC Plasma grown CNTs under identical impact condition showed again a different response. In this case the individual tubes showed a uniform fragmentation in segments of 200 nm length, instead of the pure elastic response of the nanocoils or the plastic deformation of the straight microwave grown CNTs.

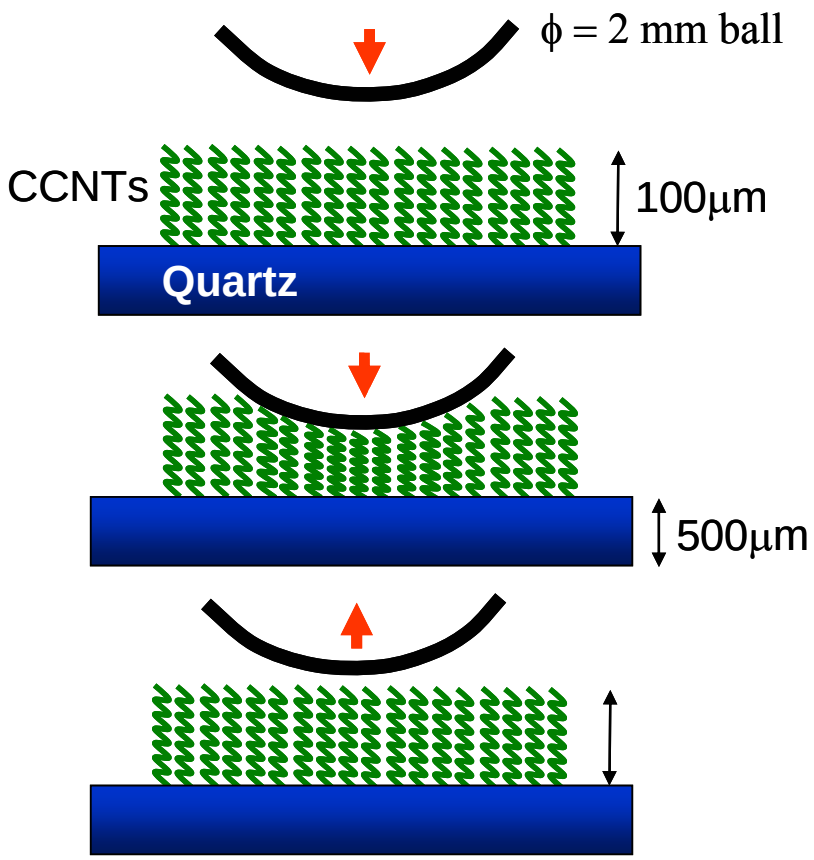

Figure 83. Schematic diagram showing the stages of interaction and full recovery of the coiled carbon nanotubes (CCNT) array during and after the impact.

The differences observed in the dynamic response of the various nanotubes foams in comparison with a linear elastic body cause a qualitatively new contact response than Hertz law. Such novel strongly nonlinear CNTs films as in the case of the coiled nanotubes forest or the other substrates previously tested can be used to create "sonic vacuum" type devices serving as nonlinear springs between inertial elements. Applications can be envisioned for designing noise and shock wave mitigation, for impulse transformation and as mechanical energy storage devices at high strain rate deformation, as suggested earlier for reversible quasi-static compression at similar level

of pressures (Chesnokov, 1999). A similar behavior for a forest of freestanding nanotubes was also reported in (Cao, 2005) for cyclic compressive loading, showing an excellent recovery and a highly resilient nature of the CNTs film even after severe testing conditions. Another set of experiments was performed on the setup described in Fig. 84(a). In this case, we placed the forest of nanocoils upside-down, in direct contact with the sensor's cover-plate to monitor the response of the film under uniform planar impact. The striker bead was dropped directly onto the quartz substrate (rigid plate), which transferred the impulse to the nanocoils. The force (F)-time (t) response of the system to an impact generated by a 2 mm steel bead with an impact velocity 0.2 m/s is presented in Fig. 84(b) curve 1 and compared with the pulse recorded impacting the bare quartz substrate (curve 2) as in Fig. 82(b). Interestingly, here the response of the system appears even more efficient in terms of protection of the bottom wall. The amplitude of the pulse arriving on the sensor when the nanocoils are present is significantly reduced and the pulse length is increased by almost one order of magnitude. The inset of Fig. 84(b) shows a close up of curve 1. It is evident that the shape of the curve is not perfectly symmetric. This may be due to the effect of tangential forces/sliding of the substrate during impact or presence of dirt particles affecting the behavior of the coiled CNTs film. SEM analysis of the foam surface after several small 0.2 m/s impacts showed a complete recovery of the film's structure as in the case observed in Fig. 82. After repeated higher velocity impacts (up to 2 m/s) "brittle" cracking of the film substrate began to be noticeable (see Fig. 84(c)). The cracking was probably related to the detachment of groups of nanocoils bundles from the quartz substrate, forming terraces on the CNTs film. Even after

cracking, the overall elastic response of the film of carbon nanocoils to the planar impacts did not seem to be heavily effected.

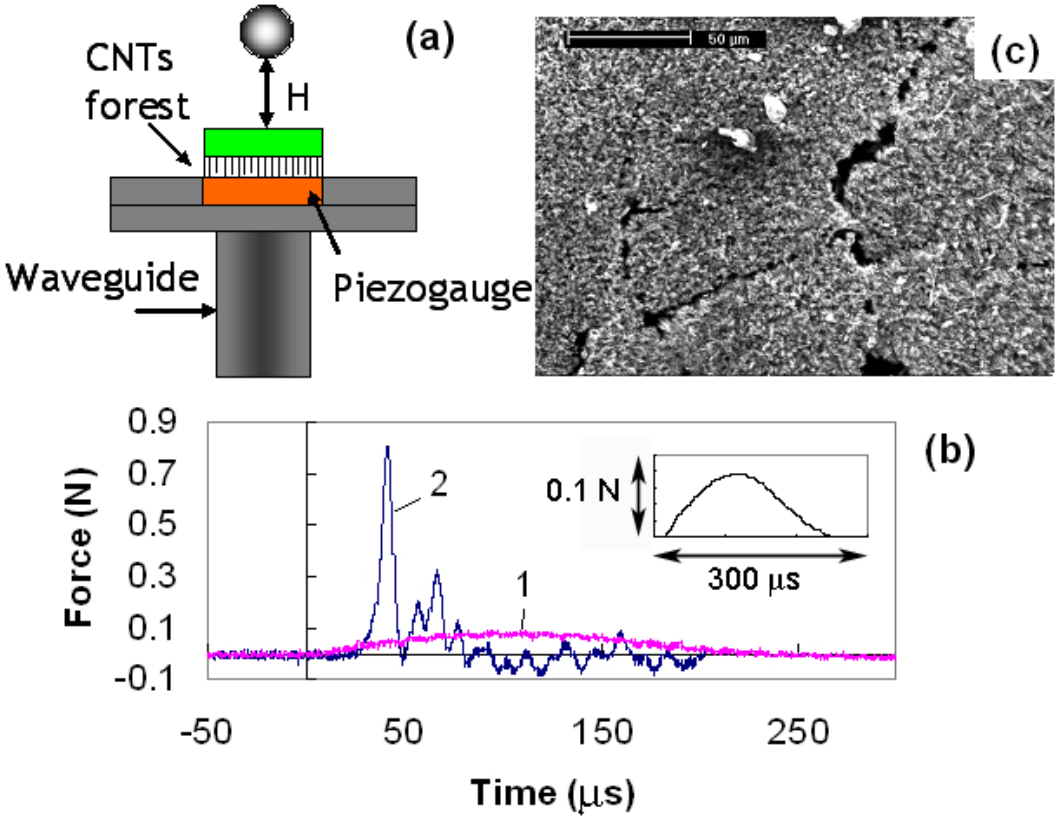

Figure 84. (a) Schematic diagram of the experimental setup used for the inverted testing of the forest of carbon nanocoils; (b) Force vs. Time response obtained experimentally impacting the coiled carbon nanotubes forest from the substrate side with a 2 mm diameter steel bead (0.02 g) from a height of 2 mm (curve 1) compared to that obtained impacting the bare quartz substrate (curve 2). For convenient comparison curves are centered with respect to each other. The inset shows a magnified view of curve 1 for clarity; (c) SEM image showing the fracturing of the surface after repeated high amplitude impacts.

In summary, the mechanical response of a forest of coiled carbon nanotubes under conditions of high strain rate deformation was studied using a simple and convenient

experimental approach. It was shown that the deformation of this open foam-like structure of vertically aligned coiled nanotubes under vertical impacts exhibits a strongly nonlinear, non-Hertzian type contact interaction law, which could allow the design of novel strongly nonlinear phononic devices with tunable properties. The nanocoils responded to dynamic loading as perfect elastic nonlinear springs that fully recover their original lengths under all the impact conditions tested. The results also revealed a significant level of energy absorption on high strain rate deformation at high pressures. Even after repeated high amplitude impacts, the overall structural elastic response appeared to be conserved, despite the formation of partial cracks on the film's surface. Such a resilient system could find applications in micro-/nano- electromechanical systems and actuators as well as coating for protection and energy absorption purposes.

Conclusions on the nanoscaled nonlinear contact interaction analysis

The study on the nonlinear properties of films of different types of carbon nanotubes under high-strain rate deformation has led to the discovery of new and exciting properties of these materials applicable to various fields of engineering. For example, the brittle fracture of DC Plasma grown forests of carbon nanotubes can be exploited as a cheap and easy technique for creating high-aspect-ratio hollow nanostructures to ease fictionalization, filling and discovery of novel optical properties of CNTs. We have developed a very fast, dry technique to cut carbon nanotubes into short segments which may be applicable to a many other types of nanowires and nanotubes. The observed cutting of nanotubes by impact stressing may conveniently be utilized for resizing and end-opening for easier handling and manipulations of nanotubes for a variety of applications such as nano-composite synthesis, nanoscale and large-surface-area reservoir to store chemical reactants/catalysts, nano-carriers for therapeutic drugs/DNAs/proteins, and various other nano-electronics or nano-mechanics related applications. The observed phenomena are likely to stimulate further research work in the nano-materials community. So far, there have been no convenient ways of cutting and opening the long carbon nanotubes other than the tedious wet processing involving concentrated-acid etching, which tends to damage the nanotube structure and results in random, uncontrolled lengths. The phenomenon of nanoscale deformation and fracture is of interest to the broad scientific community. Engineering the shape of CNTs is an important issue for successful applications of nanotubes, e.g., in the nanomechanics, nanoelectronics, nanocomposites, and nano-bio areas.

The films of CCNTs and microwave plasma enhanced CNTs instead, have shown a novel strongly nonlinear dependence on displacement being fundamentally different in comparison with the strongly nonlinear Hertz law. Their ability to absorb energy on impact and act as nonlinear spring, for example in discrete phononic systems, is a proof of exceptional and novel mechanical characteristics. They represent a fascinating new type of interface that can be envisioned in applications in various fields. For example, one could propose the creation of a coating with tunable resilience, obtained by a combinations of various types of CNTs, comprising straight, aligned CNTs, coiled CNTs and Y-shaped or branched CNTs, that will lead to completely different properties and behaviors.

PART 4

ELECTRONIC TRANSPORT IN Y-SHAPED CARBON NANOTUBES

Carbon-nanotube-based electronics offers significant potential as a nanoscale alternative to silicon-based devices for molecular electronics technologies. Here, we show evidence for a dramatic electrical switching behavior in a Y-junction carbon-nanotube (Zhou, 1995, Satishkumar, 2000, Li, 2001) morphology. We observe an abrupt modulation of the current from an on- to an off-state, presumably mediated by defects and the topology of the junction. The mutual interaction of the electron currents (Xu, 2001) in the three branches of the Y-junction is shown to be the basis for a potentially new logic device. This is the first time that such switching and logic functionalities have been experimentally demonstrated in Y-junction nanotubes without the need for an external gate. A class of nanoelectronic architecture and functionality, which extends well beyond conventional field-effect transistor technologies (Baughman, 2002, Xu, 2004) is now possible.

So far, the elucidation of fundamental properties of nanotubes and nanowires (Saito, 1998, Forro, 2001, Kim, 2001, Collins, 2001) and their applicability for electrical devices has mainly focused on adopting the metal-oxide-semiconductor field-effect transistor paradigm (Tans, 1998, Martel, 1998, Javey, 2003) where a nanotube serves as the channel between lithographically fabricated electrodes (namely, source and drain), and an electrically insulated gate modulates the channel conductance. In other demonstrations, cumbersome atomic force microscope manipulations (Postma, 2001) of

nanotube properties have been used. To realize a truly nanoelectronic architecture, it is desirable to have a fully integrated nanotube-based technology, where both devices and interconnects are based on carbon nanotubes (CNTs). Further, it would be attractive in proposing new nanoelectronic elements to harness new functionalities peculiar to novel CNT forms, such as Y-junctions.

Here, we focus on the electrical measurements on a particular multiwalled CNT (MWNT) morphology—the Y-junction—which is grown by a modified chemical vapour deposition (CVD) process (Gothard, 2004). We have observed unique switching behaviour and the promise of using this element as a new type of logic device.

It was derived theoretically (Xu, 2001) and proved experimentally (Shorubalko, 2003) in lithographically patterned two-dimensional electron gases that the ballistic nature of the electron transport and electron–electron interactions in Y-shaped nanostructures result in nonlinear current (I)–voltage (V) characteristics and novel device paradigms (Xu, 2004, Shorubalko, 2002). Current modulation in these structures involves new principles of electron momentum engineering in contrast to the well-known band engineering. An advantage of this approach, over a conventional field-effect transistor, is that the current is only switched between two outputs rather than completely turned on/off (Song, 1998, Palm, 1996), which leads to higher speed and efficiency of operation. Y-junction nanotubes provide a more natural and truly nanoscale alternative avenue to explore this switching behaviour. Branching in nanotubes necessitates the presence of topological defects, to satisfy the local bond order, at the junction region for maintaining a low-energy configuration for the carbon atoms (Andriotis, 2002). Further, there is the inevitable presence of metal catalyst particles introduced at the junction during synthesis

(Gothard, 2004). The delocalization of the electrons over these defects leads to a net charge that acts as a localized scattering centre for modulating the electron-transport characteristics. The consequent gating action from the junction could be responsible for a variety of nonlinear behaviours, which could be exploited for novel applications (Shorubalko, 2002, Csontos, 2003, Xu, 2004), including (i) switching and transistor action, (ii) logic gates and (iii) higher harmonic-frequency generation.

Although existing theoretical work is mostly focused on single-walled nanotubes, similar principles (Andriotis, 2003), namely (i) the formation of an asymmetric scattering centre/quantum dot (Song, 1998) at the junction (Fig. 85(a)), (ii) finite length of the stem and branches connected to metallic leads, (iii) asymmetry of the bias applied/the potential profile (Tian, 1998) across the nanotube and (iv) the Schottky barrier at the nanotube-contact metal leads (Heinze, 2002), would again be important in completely determining the electrical characteristics of the Y-junction devices. The Y-junction can be used as a prototypical nanoelectronic element for a variety of functions such as switching or as a quantum dot, depending on the transmission characteristics of the constituent branches.

The CNT Y-junctions (Fig. 85(b)) were grown on bare quartz or SiO_2/Si substrates through thermal CVD using a carbon feedstock mixture of ferrocene and xylene together with Ti containing precursor gases. The branching, for Y-junction formation, can be introduced at will through the introduction of the Ti precursor. For further details on the growth mechanism and processes, see Gothard, 2004.

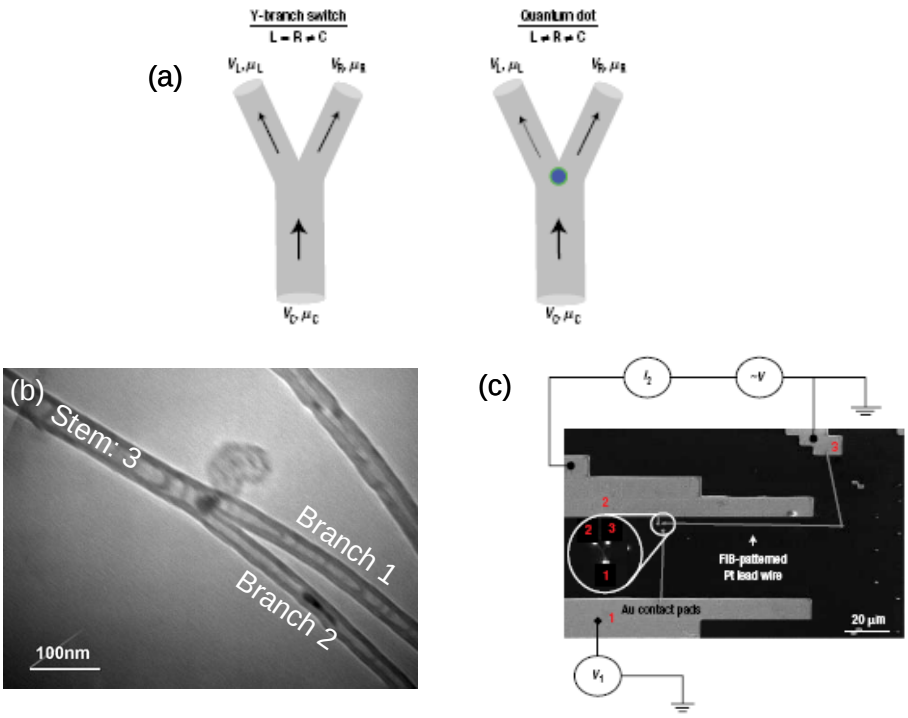

Figure 85. The CNT Y-junction morphology and experimental arrangement for measuring transport properties. (a) L, R and C refer to the left, right and central/stem branches of a Y-junction. (b) A transmission electron microscope (JEOL 3010) image of a typical MWNT Y-junction used in the present measurements. The Fe–Ti catalyst particles formed in the CVD growth along with the presence of topological defects at the junction region can influence the electrical transport characteristics. (c) An SEM micrograph of the overall circuit arrangement used in the measurement of the electrical characteristics, with Au contact pads and an FIB-patterned Pt wire contacting the Au pads and the Y-junction. A configuration is shown where a control d.c. voltage is applied on the stem (terminal 1) of the Y-junction, and the current flow through the other two branches in response to a constant a.c. bias voltage (~V) is monitored. Similarly, control voltages can be applied on branches 2 and 3 for characterizing the Y-junction in detail.

The samples for electrical measurements were prepared by suspending the nanotube Y-junctions in ethanol and depositing them on a SiO_2/Si substrate with patterned Au pads (Fig. 85(c)). Y-junctions, in proximity to the Au contact pads, were then located using a scanning electron microscope (SEM, model FEI Strata 235 M dual beam) equipped with a focused ion beam (FIB). The sample was scanned at 5 kV to

locate the Y-junctions, which results in minimal damage (Crespi, 1996, Banhart, 1999) to the nanotubes. The ion-beam in the FIB-SEM was then used to deposit the Pt lead wires that connect the terminals of the Y-junction to the contact pads (Fig. 85(c) inset) (Gopal, 2004). Special care (Banhart, 1999) was taken to not expose the nanotubes to the ion-beam to prevent radiation damage. A Wentworth probe station, with needle contacts (Heinze, 2002), was used to apply the voltages and measure currents.

The electrical transport properties of the Y-junctions were probed through both two- and three-terminal phase-sensitive lock-in amplifier measurements in air, at room temperature, in the dark. There was little difference in the I−V characteristics between air and vacuum, and a negligible transient response to white light illumination (Forro, 2001). The resistances measured in d.c. were checked to be in accordance with the lock-in measurements. By successively grounding each branch of the Y-junction, we were able to probe the intra-branch (that is 1, 2 and 3) and inter-branch (that is 1–2, 1–3 and 2–3) resistances. If it is assumed that the ohmic contact resistance for all three branches of the Y-junction is identical, this measurement can identify the individual branch's transport characteristics. (It was not possible to determine all four parameters R_1, R_2, R_3 and the contact resistance with three-terminal measurements.) We tested around five samples and obtained reproducible results. When measured pair-wise (that is, 1–2, 1–3 and 2–3) we observe ohmic behaviour, with resistances in the range of 100−400 kΩ. Although MWNTs are expected to have a resistance smaller than around 13 kΩ ($h/2e^2$; where h is the Planck constant and e the electron charge) ideal ohmic contacts through metal evaporation were difficult to achieve. However, reproducible I−V characteristics on a large number of samples would imply that the observed behavior is intrinsic to the Y-

junctions. High-temperature thermal annealing was successful in reducing the contact resistance by an order of magnitude, with similar switching behavior, and is a possible solution to achieving low-resistance contacts in the future. However, local electron exposure (Bachtold, 1998) onto the CNT-ohmic contact did not affect the contact resistance significantly.

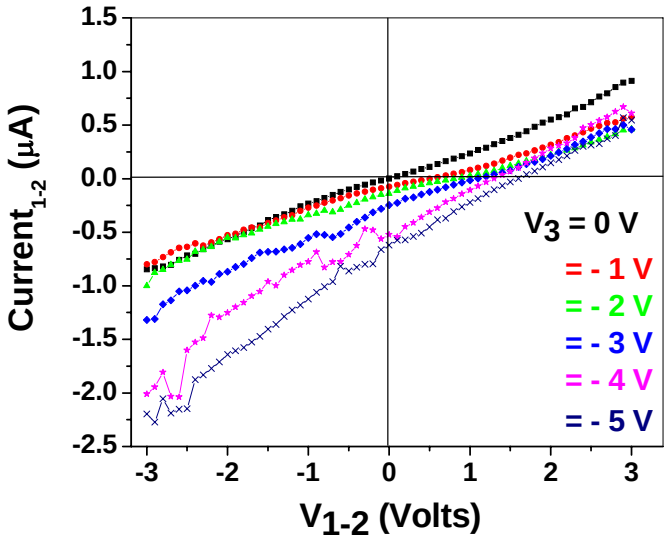

Figure 86. Current (I)–voltage (V) characteristics of a Y-junction. A constant d.c. voltage is applied on the stem (1 in Fig. 85(b)), while the current in branch 2 is monitored as a function of applied voltage (from top to bottom: 0 V; −1 V; −2 V; −3 V; −4 V; −5 V). The gating action of the voltage and the asymmetric response should be noted.

The gating action of the stem (1 in Fig. 85(b)) on the I−V characteristics of the branches in the Y-junction (2 and 3 in Fig. 85(b)) is illustrated in Fig. 86. The asymmetric behavior, where I(+V) ≠ I(−V), had been theoretically predicted earlier (Andriotis, 2001) and this is the first time that the effect of a gate voltage has been experimentally demonstrated. On the basis of these results, we explored the possibility of using the CNT Y-junctions for switching applications, as an electrical inverter, analogous

to earlier (Shorubalko, 2003, Palm, 1996) Y-branch switch studies in lithographically patterned two-dimensional electron gases. In our measurements, a control d.c. voltage was swept on one terminal of the Y-junction and the current through the other two terminals probed under a fixed a.c. bias ranging from 0.1 to 1.0 V. As the d.c. voltage is increased, at a certain point the Y-junction goes from nominally conducting to a pinched-off state (Fig. 87). This switching behavior was observed for all three terminals of the Y-junction, at varying d.c. bias voltages, in different samples. For example, the channel is pinched-off when ~4.6 V is applied to the stem (Fig. 87(a)), to lower than the ~2 V (Fig. 87(b)) needed to observe the pinch-off when the control voltage is applied to the branches (2 and 3). The switching behavior was seen over a wide range of frequencies (Fig. 88), with an upper limit of around 57 kHz being set by the capacitive response of the Y-junction, when the current tends to zero. The transconductance (dI/dVgate) of the Y-junction devices is around 10^{-6} A V^{-1}, which compares well to a single-walled CNT channel transistor (10^{-8} A V^{-1}) (Tans, 1998).

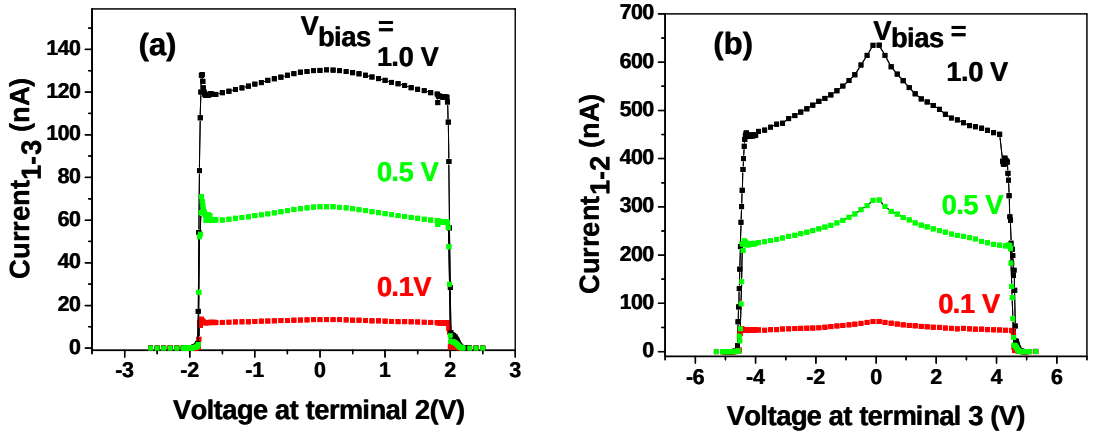

Figure 87. Observation of near-perfect electrical switching in Y-junctions. An abrupt modulation of the electrical current through two branches of the Y-junction is seen on varying the d.c. bias voltage on the third branch. (a) The voltage at which the switching action occurs is ~4.6 V on the stem. (b) The switching on both of the branches occurs at ~2 V. The disparate voltage values could be related to the character, diameter, defects and so on, of the constituents (branch/stem) of the Y-junction.

As the bias voltage applied to our MWNT Y-junction is substantial, it is expected that many walls of the MWNT would contribute (Collins, 2001) to the electronic conduction. The presence of catalyst nanoparticles (see Fig. 85(b)) in the conduction paths would blockade current flow, and their charging could account for the abrupt drop-off of the current. The exact magnitude of the switching voltage would then be related to the exact size of the nanoparticle. This suggests the possibility of nano-engineering the Y-junction to get a variety of switching behaviors. An alternative possibility is that there is inter-mixing of the currents in the Y-junction, where the electron transmission is abruptly cut off owing to the compensation of currents, for example, the current through branches 2 and 3 is cancelled by current leakage through stem 1.

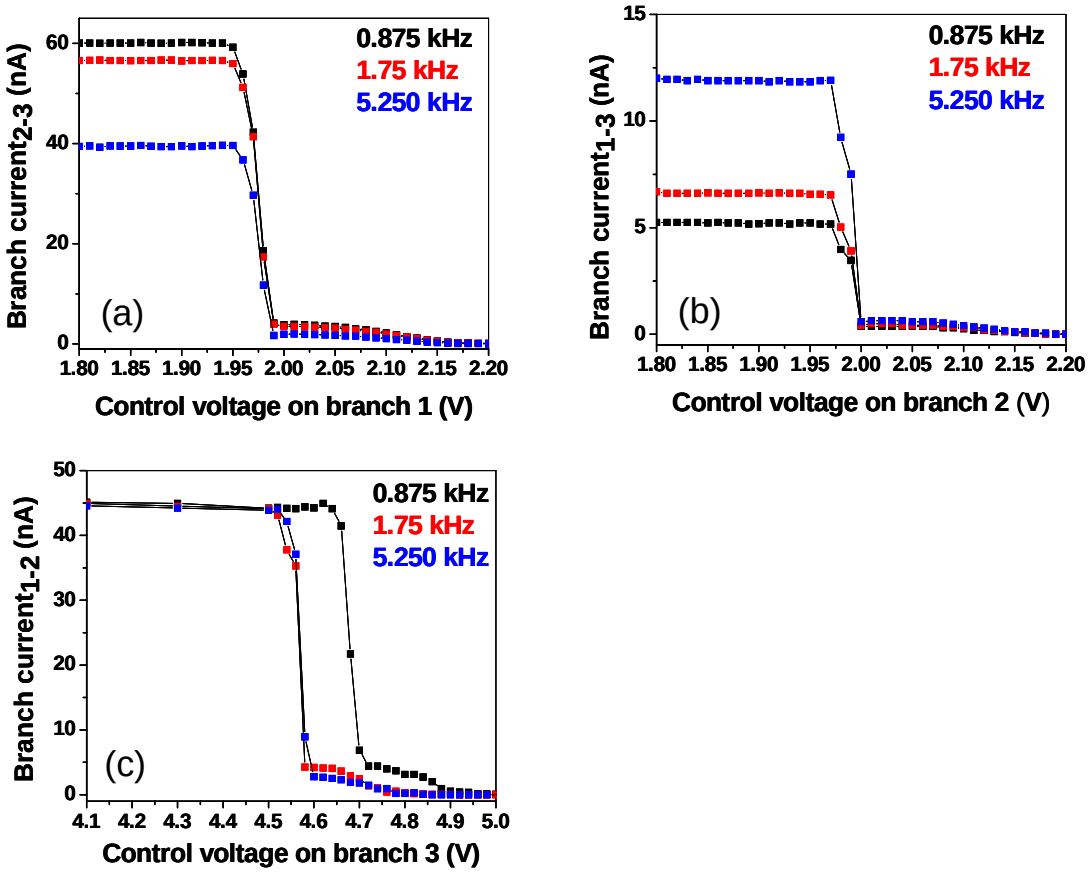

Figure 88. Frequency response of the switching characteristic in the Y-junction. In a, the control voltage is applied on the stem (1) of the Y-junction while the current, under an a.c. bias, is monitored across the other two terminals of the Y-junction. In b and c, a control d.c. voltage is applied on branches 2 and 3. The magnitudes of the current differ owing to the different resistances of the Y-junction constituents.

Further research is needed to clarify the exact mechanisms in these interesting phenomena. When finite voltages are applied to the left and the right branches of a Y-junction, in a push–pull fashion (that is, $V_{left} = -V_{right}$ or vice versa), the voltage output at the stem would have the same sign as the terminal with the lower voltage (Xu, 2001).

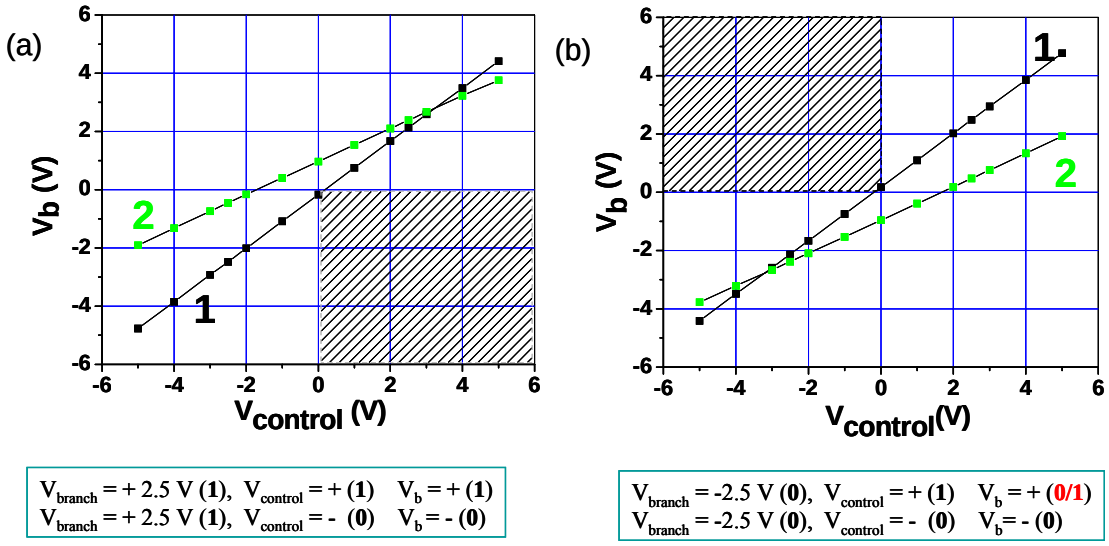

Figure 89. The CNT Y-junction for logic applications. The continuity of the electrochemical potential from one branch of the CNT Y-junction to another (see the text) could be used for the basis for a prototypical logic device. A constant voltage (positive in a and negative in b) is applied on one branch (Vbranch), and the voltage monitored across the second branch (Vb), while a control d.c. voltage (Vcontrol) is swept across the third branch of the Y-junction. The two lines (green and black) refer to the possible permutations of the voltages applied on the two branches (2 and 3 in Fig. 1b). The inter-mixing of the currents between the three branches could be responsible for the partial realization of an AND gate.

This dependence follows from the principle of continuity of electrochemical potential ($\mu=-eV$) in electron transport through a Y-junction and forms the basis for the realization of an AND (Xu, 2004) logic gate, that is, when either of the branch voltages is negative (say, corresponding to a logic state of 0), the voltage at the stem is negative and positive voltage (logic state of 1) at the stem is obtained only when both the branches are at positive biases. We report the results of our measurements in Fig. 89, where a constant voltage (positive/negative) is imposed on one branch, while the voltage across the other branch ($V_{control}$) is swept from −5 to +5 V, and the output voltage from the third branch (V_b) is monitored.

In a naturally formed CNT-based Y-junction, as is the case here, the distinction between stem and branch is not very clear. The deviation from the realization of a perfect AND gate could then be due to inter-mixing between the conduction channels and the currents from the three branches of the Y-junction.

We wish to emphasize that this is the first time that such an abrupt electrical switching behaviour has been seen in CNT Y-junctions. Before this work, only diode-like behaviour (Satishkumar, Papadapoulos, 2000) has been observed. Through this work, we are enabling and adding a new functionality to nanotube electronics that is, switching making overall CNT-based nanoelectronic architecture more complete and feasible. The detailed nature of the abrupt electrical switching behaviour is not completely understood but can be a fertile ground for future research, for example, in defect engineering where one can intentionally modify, mechanically or chemically, the paths of electronic conduction in the Y-junction.

CONCLUSIONS

The work for this thesis was conducted on designing and construction of macro, micro and nano scale structural configurations of materials, and on studies of phononic and electronic behavior of such configurations. Variation of composite arrangements of granular elements with different elastic properties in a linear, chain-of-sphere, or Y-junction configurations led to a variety of novel phononic phenomena and interesting physical properties, which can be potentially useful for security, communications, mechanical and biomedical engineering applications. Phononic, mechanical and electronic properties of carbon nanotubes with different atomic arrangements and microstructures were also investigated. Electronic properties of Y-junction configured carbon nanotubes exhibit an exciting transistor switch behavior which is not seen in linear configuration nanotubes. Strongly nonlinear wave dynamic was first discovered analytically and numerically by Nesterenko in 1983 and represents a completely new form of information propagation in materials, supporting a new type of stationary solitary waves (compactons). The first experimental proof of the strongly nonlinear theoretical model appeared in 1985 in the study of compression waves (acoustic waves) in granular materials. By "granular material" we defined an aggregate of particles in elastic contact with each other, preferably arranged in a linear or network shaped geometry. The unusual feature of this granular state is the negligible linear range of the interaction forces between neighboring particles resulting in the zero sound speed in the uncompressed materials. This specific feature makes the linear and weakly nonlinear continuum approach based on the Korteveg - de Vries equation invalid and places granular materials

in a special class of wave dynamics. This was the reason for the introduction of the concept of "sonic vacuum" - a medium where the traditional wave equation is not a basic equation for wave dynamics and no "classical sound" can propagate.

In this study, strongly nonlinear materials (Nonlinear Tunable Phononic Crystals – NTPCs) were designed, fabricated and tested using novel and innovative concepts. Numerical analysis was performed using MatLab and compared to the corresponding experimental and theoretical data. As in a case of linear phononics, these novel structures also have a periodic structure, which is the reason for the presence of dispersion phenomena and of band gaps observed in the linear case. Strongly nonlinear materials, in facts, exhibit all properties of linear materials in the extreme case of small amplitude of elastic waves or high values of initial static precompression. Due to their unique combination of strong nonlinearity and anisotropic nature, novel wave phenomena have been discovered. Specifically, violations of Snell's law were detected and a new mechanism of wave interaction with interfaces between the assembled NTCPs was established (Nesterenko, 2005). Polymer-based an polymer composite systems were tested under high strain rate impacts for the first time (Daraio, 2005, 2006) and the tunability of the propagating solitary waves speed was demonstrated for various assemblies using a non-contact magnetically induced precompression (Daraio, 2006). New materials with transformed signal propagation speed in the manageable range of 10-100 m/s and signal amplitude typical for audible speech have been developed. Small amplitude solitary waves in these systems broke the "sound barrier" having speed of propagation below sound speed in air (Daraio, 2003, 2005, 2006, Nesterenko, 2005). The enhancing of the mitigation of solitary and shock waves in 1-D chains were demonstrated

and a new type of energy trapping protective medium was designed for practical applications (Daraio, 2006). Two-mass systems were tested for the first time and were found to be in excellent agreement with the theory (Daraio, 2006).

Various types of strongly nonlinear interfaces were investigated under different types of dynamic loading and novel phenomena were discovered. Foam-like carbon nanotube (CNTs) forests were grown on different substrates as interfaces in NTPCs and their nonlinear dynamic properties were studied, leading to the discovery of interesting phenomena as CNTs fragmentation, energy absorption by CNTs and the evaluation of the high strain rate elastic response of coiled nanostructures (Daraio, 2004, 2004, 2006).
1-D (Daraio, 2003, 2004, 2005, 2006, Nesterenko, 2005), 2-D (Daraio, 2006) and 3-D strongly nonlinear system have been analyzed providing a broad impact on the whole area of strongly nonlinear wave dynamics and creating experimental basis for new theories and models. Probable analogy with electrical and optical strongly nonlinear lines can be prompted as a result of this activity. Experimental proof of a traveling insulator-metal transition caused by solitary wave propagation in the 1-D system was also provided.

Potential applications of the NTPCs developed in this work include (1) designing of a sound scrambler/decorder for secure voice communications for military and national security personnel, (2) improving invisibility of submarine to acoustic detection signal, (3) noise and shock wave mitigation for protection of vibration sensitive devices, (4) drastic compression of acoustic signals into centimeter regime impulses for artificial ear implants, hearing aid and devices for ease of conversion to electronic signals and processing, and acoustic delay lines for communication applications.

APPENDIX I

Taylor Expansion for the Derivation of the Anharmonic Approximation for the Strongly Compressed Chains Equation of Motion.

This appendix is aimed to guide the reader to a step-by-step derivation of the anharmonic approximation for the particle equation of motion in a chain of elastic rigid spheres (see Fig. 3). The final result of the derivation is presented in (Nesterenko, 2001, as Eq. 1.5). The general particle equation of motion derived from the Hertz force-displacement relationship is given by:

$$\ddot{u}_i = A(\delta_0 - u_i + u_{i-1})^{3/2} - A(\delta_0 - u_{i+1} + u_i)^{3/2} \qquad (1)$$

$$\text{With } A = \frac{E(2R)^{1/2}}{3(1-\nu^2)m} \text{ and } m = \frac{4}{3}\pi R^3 \rho_0$$

where m is the mass of the particle, E and ρ_0 are the Young's modules and density of particle material, R is the granule radius, ν is the Poisson coefficient. It is assumed that the distance between the particle centers does not exceed $a = 2R$, if particles are spherical and δ_0 is the initial displacement of the beads in the chain caused by the static precompressive force F_0 acting on the system.

Under the assumption of small deformation in the medium for strongly compressed chains, the deformations follow:

$$\left|u_{i-1}-u_i\right| << \delta_0 . \tag{29}$$

As it is well known, Taylor series to the second order decomposes a function following:

$$f(x)=f^{0}(a)+\frac{f'(a)}{1!}(x-a)+\frac{f''(a)}{2!}(x-a)^2 .$$

In view of these assumptions, Eq. (1) can be rewritten as:

$$\ddot{u}_i = A\left[\delta_0\left(1+\frac{-u_i+u_{i-1}}{\delta_0}\right)\right]^{3/2} - A\left[\delta_0\left(1+\frac{-u_{i+1}+u_i}{\delta_0}\right)\right]^{3/2} =$$
$$= A\delta_0^{3/2}\left(1+\frac{-u_i+u_{i-1}}{\delta_0}\right)^{3/2} - A\delta_0^{3/2}\left(1+\frac{-u_{i+1}+u_i}{\delta_0}\right)^{3/2}$$

For simplicity from now on we can call:

$$\mathrm{X}=\frac{-u_i+u_{i-1}}{\delta_0} \qquad \text{and} \qquad \mathrm{Y}=\frac{u_i-u_{i+1}}{\delta_0}$$

From the assumption made (Eq. 25) it follows that X<<1 and Y<<1.

Equation (1) then becomes:

$$\ddot{u}_i = A\delta_0^{3/2}(1+X)^{3/2} - A\delta_0^{3/2}(1+Y)^{3/2} =$$
$$= A\delta_0^{3/2}\left[(1+X)^{3/2} - (1+Y)^{3/2}\right]$$

Applying the 2nd order Taylor/MacLaurin series to the coefficients we obtain:

$$f(x) = f^0(0) + \frac{f'(0)}{1!}(x) + \frac{f''(0)}{2!}(x)^2$$
$$\rightarrow (1+X)^{3/2} = 1 + \frac{3}{2}X + \frac{3X^2}{8}$$
$$\rightarrow (1+Y)^{3/2} = 1 + \frac{3}{2}Y + \frac{3Y^2}{8}$$

Now we can rewrite Eq. (1) as:

$$\ddot{u}_i = A\delta_0^{3/2}\left[1 + \frac{3}{2}X + \frac{3X^2}{8} - \left(1 + \frac{3}{2}Y + \frac{3Y^2}{8}\right)\right] =$$
$$= A\delta_0^{3/2}\left[\frac{3}{2}\left(\frac{-u_i + u_{i-1}}{\delta_0}\right) + \frac{3}{8}\left(\frac{-u_i + u_{i-1}}{\delta_0}\right)^2 - \frac{3}{2}\left(\frac{u_i - u_{i+1}}{\delta_0}\right) - \frac{3}{8}\left(\frac{u_i - u_{i+1}}{\delta_0}\right)^2\right] =$$
$$= A\delta_0^{3/2}\left[\frac{3}{2}\left(\frac{-2u_i + u_{i-1} + u_{i+1}}{\delta_0}\right) + \frac{3}{8}\left(\frac{-2u_i u_{i-1} + u_{i-1}^2 + 2u_i u_{i+1} - u_{i+1}^2}{\delta_0^2}\right)\right] =$$
$$= \frac{3}{2}A\delta_0^{1/2}(-2u_i + u_{i-1} + u_{i+1}) + \frac{3}{8}A\delta_0^{-1/2}\left(u_{i-1}^2 - u_{i+1}^2 - 2u_i(u_{i-1} - u_{i+1})\right) =$$
$$= \alpha(-2u_i + u_{i-1} + u_{i+1}) + \beta(u_{i-1} + u_{i+1} - 2u_i)(u_{i-1} - u_{i+1})$$

With $\alpha = \frac{3}{2}A\delta_0^{1/2}$ and $\beta = \frac{3}{8}A\delta_0^{-1/2}$, as in Eq. 1.5 from Nesterenko, 2001.

APPENDIX II

Extended analysis on the theory of elasticity applied to coated particles

The mathematical steps followed for the theoretical analysis of the Parylene-C coated beads chains is here explained in further details. The purpose of this work was aimed to calculating the maximal stresses and strains acting on the polymer coating during strongly nonlinear wave propagation and to compare them with the maximum strength of the polymer. The analysis was also done to demonstrate the validity of Hertz law in the interaction between two polymer coated particles (Fig. 69).

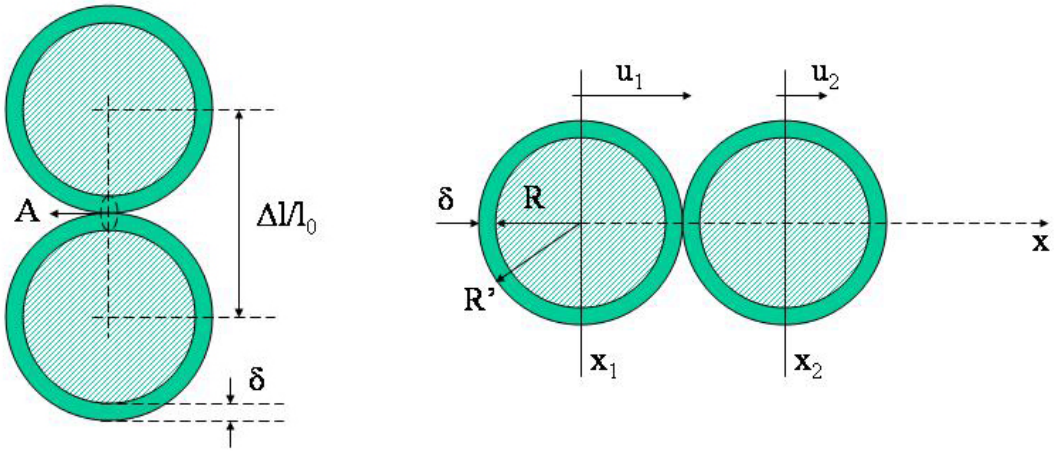

Figure 90. Schematic diagram showing the significant dimensions to be considered in the analysis of the sphere to sphere interaction between to polymer coated beads.

From Eq. 1.3 in (Nesterenko, 2001)

$$\ddot{u}_i = A(\delta_0 - u_i + u_{i-1})^{3/2} - A(\delta_0 - u_{i+1} + u_i)^{3/2}$$
$$m = \frac{4}{3}\pi R^3 \rho_0 \qquad (1)$$
$$A = \frac{E(2R)^{1/2}}{3(1-\nu^2)m}$$

where m is the mass of the particle, E and ρ_0 are the Young's modules and density of particle material, R is the granule radius, ν is the Poisson coefficient. It is assumed that the distance between the particle centers does not exceed $a = 2R$, if particles are spherical and δ_0 is the initial displacement of the beads in the chain caused by the static precompressive force F_0 acting on the system.

In the case of Parylene-C coated baeds (Fig. 69) Eq. 1 becomes:

$$m\ddot{u}_i = \frac{E(2R+2\delta)^{1/2}}{3(1-\nu^2)}(u_{i-1} + u_{i-1} - 2u_i)^{3/2}$$
$$A = \frac{E(2R+2\delta)^{1/2}}{3(1-\nu^2)(\frac{4}{3}\pi R^3 \rho_{ss} + \frac{4}{3}\pi((R+\delta)^3 - R^3)\rho_{polymer})} \qquad (30)$$
$$\xi = -u_x = -\frac{(u_2 - u_1)}{2R'}$$
$$a = 2(R+\delta)$$

where δ is the thickness of the Parylene coating (see Fig. 69), ρ_{ss} is the density of the stainless steel beads, $\rho_{polymer}$ is the density of the Parylene-C coating and R' is the outer radius of the coated particle.

Considering x_1 and x_2 the spatial coordinates of the spherical granules centers and u_1 and u_2 the displacement of the beads relative to their initial position:

$$\begin{aligned} x_1 - x_2 &= 2R' - (u_1 - u_2) \\ \frac{x_1 - x_2}{2R'} &= 1 + \frac{u_2 - u_1}{2R'} = 1 - \xi_{max} \end{aligned} \tag{31}$$

where ξ_{max} is the value of the maximum strain acting on the particles.

Assuming that the particles interaction follows the Hertz Law:

The Force F exchanged between them is:

$$F = \frac{2E}{3(1-\nu^2)}\left(\frac{R+\delta}{2}\right)^{1/2}\left[(2R+2\delta)-(x_2-x_1)\right]^{3/2} \tag{32}$$

From Eq. 27 combined with Eq. 28 it follows:

$$F = \frac{4E}{3(1-\nu^2)}(R+\delta)^2(\xi_{max})^{3/2} \tag{33}$$

Also, from Eq. 1.41 in (Nesterenko, 2001):

$$\xi_{max} = \left(\frac{25}{16}\right)^{1/5} c^{-4/5} v_m^{4/5} \quad \text{and} \quad \begin{aligned} c^2 &= Aa^{5/2} \\ a &= R+\delta \end{aligned} \tag{34}$$

where v_m is the particle velocity corresponding to ξ_{max} and can be considered approximately equivalent to the velocity of the striker (u_s) acting on the system.

The experimental values to plug into these equations for the Parylene-C polymeric coating used are E=2760 MPa, density=1289 Kg/m^3, Poisson's coefficient = 0.388 and density of stainless steel = 8030 Kg/m^3, with a thickness of the coating = 50 μm (values provided by Acraball Inc. manufacturer).

The theory of elasticity for the response to pressure of two spherical bodies in contact (Timoshenko, 1987) estimates the value of α (displacement of the beads centers under the applied force F) as:

$$\alpha = 1.23\sqrt{\frac{2F^2}{E^2(R+\delta)}} \tag{35}$$

To calculate the *limit force* applicable we can rely on the estimation proposed by Coste, 1999. Here (Eq. 32) *b* represents the radius of the maximum contact area between the two beads, F0 is the static precompressive force acting on the system, R' the total outer radius of the beads, P_{av} the mean pressure and P_{max} the maximum pressure on the contact.

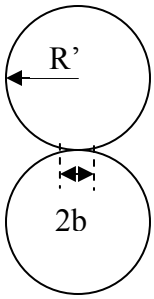

$$
\begin{aligned}
b &= \left(\frac{3F_0R'}{4\theta}\right)^{1/3} \\
P_{av} &= \frac{F_0}{(\pi b)} \\
P_{max} &= \frac{3P_{av}}{2} = \left(\frac{6F_0\theta^2}{\pi^3 R'^2}\right)^{1/3} \\
\theta &= \frac{E}{1-\nu^2}
\end{aligned}
\qquad (36)
$$

According to Coste,1999, the maximum force (F_0) applicable to the system has to respect the yield limit based on the Von Mises criterion by Johnson, 1992, where Y, in Eq. 33, is the Yield stress of the material:

$$
\begin{aligned}
F_0 < F_{limit} &\equiv \frac{(1.6\pi)^3}{6} Y^3 \frac{R'^2}{\theta^2} \\
\theta &= \frac{E}{1-\nu^2} \\
F_0 &= \frac{2\theta}{3}\alpha^{3/2}\sqrt{\frac{R'}{2}}
\end{aligned}
\qquad (37)
$$

APPENDIX III

Coefficient of Restitution

The coefficient of restitution (denoted by the symbol *c* in our formulas) is a measure of the elasticity of the collision between ball and racquet. Elasticity is a measure of how much bounce there is, or in other words, how much of the kinetic energy of the colliding objects before the collision remains as kinetic energy of the objects after the collision. With an inelastic collision, some kinetic energy is transformed into deformation of the material, heat, sound, and other forms of energy, and is therefore unavailable for use in moving.

A perfectly elastic collision has a coefficient of restitution of 1. Example: two diamonds bouncing off each other. A perfectly plastic, or inelastic, collision has $c = 0$. Example: two lumps of clay that don't bounce at all, but stick together. So the coefficient of restitution will always be between zero and one.

The coefficient of restitution is the ratio of the differences in velocities before and after the collision. In other words, the difference in the velocities of the two colliding objects after the collision, divided by the difference in their velocities before the collision. In symbolic language:

$$c = \frac{s_2 - \upsilon_2}{\upsilon_1 - s_1}$$

c = coefficient of restitution

v_1 = linear velocity of the racquet mass center before impact

s_1 = linear velocity of the ball before impact (will be negative according to our convention that away from the player is positive)

v_2 = linear velocity of the racquet mass center after impact

s_2 = linear velocity of the ball after impact

From the coefficient of restitution formula, it follows that:

$s_2 - v_2 = c(v_1 - s_1)$

To find the coefficient of restitution in the case of a falling object bouncing off the floor, or off a racquet on the floor, use the following formula:

$$c = \sqrt{\frac{h}{H}}$$

c = coefficient of restitution (dimensionless)

h = bounce height

H = drop height

Microwave Plasma Grown NTs

From the data obtained impacting the forest of CNTs grown on a microwave plasma system, the values of the coefficients of restitution are:

For a 2mm steel ball, impacting with velocity of 0.30m/s c=0.70

For a 2mm steel ball, impacting with velocity of 0.20m/s c=0.48

For a 2mm steel ball, impacting with velocity of 0.14m/s c=0.47

DC Plasma Grown NTs (Longer run)

From the data obtained impacting the forest of NTs the values of the coefficients of restitution are:

For a 2mm steel ball, impacting with velocity of 0.30m/s c=0.70

For a 2mm steel ball, impacting with velocity of 0.20m/s c=0.55

For a 2mm steel ball, impacting with velocity of 0.14m/s c=0.46

DC Plasma Grown NTs (Short run)

From the data obtained impacting the forest of NTs the values of the coefficients of restitution are:

For a 2mm steel ball, impacting with velocity of 0.30m/s c=0.63

For a 2mm steel ball, impacting with velocity of 0.20m/s c=0.63

For a 2mm steel ball, impacting with velocity of 0.14m/s c=0.53.

APPENDIX IV

Brief history of solitary waves

Solitary waves, localized nonlinear oscillations possessing striking stability properties that allow them to propagate without change and survive massive perturbations in the form of collisions, play an important role in modern physics. They represent the structural basis for viewing and understanding the dynamic behavior of complex nonlinear systems (Remoissenset, 1999). They are present in various forms (solitons, compactons and nanopterons) and exist in different areas of physics, spamming from hydrodynamics, lattice dynamics, and optics to acoustics, like the ones presented in this dissertation. Since their discovery, solitons have been invoked to explain such diverse phenomena as the quantum dark solitons in the Bose-Einstein Condensate, the 'giant red spot' in the highly turbulent Jovian atmosphere, the famous Fermi-Pasta-Ulam paradox, the ion-acoustic waves in a plasma, the energy storage and transfer in proteins via the Davydov soliton and of course, the propagation of short laser pulses in optical fibers over long distances with negligible shape change (Chen, 2006).

The first observation of a soliton and perhaps the best introduction of the concept of a solitary wave to the scientific community is that contained in the Scottish naval engineer J. Scott-Russell's seminal 1844 report to the Royal Society (Russell, 1844). In the less formal scientific writing style of the time, he wrote:

"I was observing the motion of a boat which was rapidly drawn along a narrow channel by a pair of horses, when the boat suddenly stopped - not so the mass of water in the channel which it had put in

motion; it accumulated round the prow of the vessel in a state of violent agitation, then suddenly leaving it behind, rolled forward with great velocity, assuming the form of a large solitary elevation, a rounded smooth and well-defined heap of water, which continued its course along the channel apparently without change of form or diminution of speed. I followed it on horseback, and overtook it still rolling on at a rate of some eight or nine miles an hour, preserving its original figure some thirty feet long and a foot to a foot and a half in height. Its height gradually diminished, and after a chase of one or two miles I lost it in the windings of the channel. Such, in the month of August 1834, was my first chance interview with that singular and beautiful phenomenon ..."

The naturalist John Scott Russell insisted for years that such waves he observed do in facts occur, but several prominent mathematicians, including Stokes, were convinced they were impossible. The wide-spread unbelief stemmed from the apparent contradiction between their existence and the nonlinear shallow water Airy wave theory (that neglected dispersion). It was only after another fifty years that the two Dutchmen, Korteweg and de Vries, in 1895 developed a nonlinear partial differential equation to model the propagation of shallow water waves applicable to situation that Scott-Russell fortuitously witnessed. This famous equation is known simply as the KdV equation. Korteweg and de Vries proved Russell was correct by finding explicit, closed-form, travelling-wave solutions to their equation that moreover decay rapidly and so represent a highly localized moving hump. Both the fact that such a solution to a non-linear equation could exist and the fact that one could write it explicitly were later to be recognized as extremely important, but they went relatively unnoticed at the time. Since then many other equations have been found to be integrable and admit soliton solutions. However, the KdV equation is considered the canonical example, in part because it was the first equation known to have these properties (Kasman, 2006).

For another 50 years ever since, solitary waves remained a rather unimportant curiosity in the mathematical structure of nonlinear wave theory until the beginning of the Fermi, Pasta and Ulam studies on heat-transfer problems (Fermi, 1955), modeled as a one dimensional monoatomic lattice of masses connected by nonlinear springs. In 1955 they observed a nonergodic behavior of such system that was later explained by N. Zabusky and M. Kruskal in 1965 using the solitons solution of the KdV equation. Shortly after that, another remarkable discovery was made concerning the KdV equation: a paper by C. Gardner, J. Greene, M. Kruskal, and R. Miura (1967) demonstrated that it was possible to write many exact solutions to the equation by using ideas from scattering theory. In modern terminology, we would say that they discovered the first integrable non-linear partial differential equation.

These and few other findings sparked fresh interest in the understanding of these nonlinear phenomena. One more step forward was then taken by Zakharov, in 1968, which showed that the time evolution of the envelope of a weekly nonlinear deep water wave train is described by an equation called the nonlinear Schrodinger equation (NLS).

Parallel to this, the discovery of instability of electromagnetic waves propagating in nonlinear dispersive media was brought to the attention of the scientific community by Ostrovskii, 1963. As a result, the existence of optical-envelope solitons was predicted. Furthermore, in 1983, Zvezdin and Popkov predicted theoretically and later experimentally the existence of magnetostatic solitary waves. It was also in 1983 that the strongly nonlinear wave theory came to life (Nesterenko, 1983) and opened up an all new area of physics which will surely stimulate interesting applications in the future.

REFERENCES

AcraBall Manufactoring Co. Product catalogue.

Andriotis, A.N., Menon, M., Srivastava, D. & Chernozatonski, L. (2001). Rectification properties of carbon nanotube "Y-junctions". *Physical Review Letters,* **87**, pp. 066802.

Andriotis, A. N., Menon, M., Srivastava, D. & Chernozatonski, L. (2002). Transport properties of single-wall carbon nanotube Y-junctions. *Physical Review B*, **65**, pp. 165416.

Andriotis, A. N., Srivastava, D. & Menon, M. (2003). Comment on "Intrinsic electron transport properties of carbon nanotube Y-junctions". *Applied Physics Leters*, **83**, pp. 1674-1675.

Arancibia-Bulnes, C.A. and Ruiz-Suarez, J.C. (2002). Broad solitons in homogeneous Hertzian granular chains, *Physica D*, **168**, pp. 159-160.

Arroyo, M. and T. Belytschko (2003). A finite deformation membrane based on inter-atomic potentials for the transverse mechanics of nanotubes. *Mechanics of Materials* **35** (3-6), pp.193-215.

ASM Metals Reference Book, Second Edition, pp. 268.; ASM Metals Handbook, Properties and Selection of Metals, 8th Edition, **1**, 52 (also www.MatWeb.com).

AuBuchon, J.F., Chen, L.H., Gapin, A.I., Kim, D.W., Daraio, C, Jin S. (2004). Multiple sharp bendings of carbon nanotubes during growth to produce zigzag morphology, *Nano Letters*, **4**, 9, pp. 1781-1784.

Bachtold, A. et al. (1998). Contacting carbon nanotubes selectively with low-ohmic contacts for four-probe electric measurements. *Applied Physics Letters,* **73**, pp. 274-276.

Baker, S. E., Cai, W., Lasseter, T. L., Weidkamp, K. P. & Hamers, R. J. (2002). Covalently Bonded Adducts of Deoxyribonucleic Acid (DNA) Oligonucleotides with Single-Wall Carbon Nanotubes: Synthesis and Hybridization, *Nano Letters*, **2**, pp. 1413-1417.

Banhart, F. (1999). Irradiation effects in carbon nanostructures. *Report on Progress in Physics* **62**, pp. 1181-1221.

Banhart, J. (2001). Manufacture, *Characterization and application of cellular metals and metal foams*, Oxford - New York: Pergamon, pp. 632.

Baudequin, M., Ryschenkow, G. and Roux, S. (1999). Non-linear elastic behavior of light fibrous materials, *The European Physical Journal B*, **12**, pp. 157-162.

Baughman, R. H., Zakhidov, A. A. & de Heer,W. A. (2002). Carbon nanotubes-the route toward applications. *Science* **297**, pp. 787-792.

Belytschko, T., Xiao, S.P., Schatz, G.C. and Ruoff, R.S. (2002). Atomistic simulations of nanotube fracture, *Physical Review B,* **65**, pp. 235430 1-8.

Benson, D.J., Nesterenko, V.F. (2001). Anomalous decay of shock impulses in laminated composites, *Journal of Applied Physics*, **89**, pp. 3622-3626.

Beranek, L.L. (1988). Acoustical Measurements. Acoustical Society of America, Woodbury, NY, revised edition.

Bishop, D. J., Jin, S., Ramirez, A. G. (2000). United States Patent No. **6**, 124, 650, Non-volatile MEMS micro-relays using magnetic actuators, issued September 26.

Blair, D.L., Mueggenburg, N.W., Marshall, A.H., Jaeger, H.M., Nagel, S.R. (2001). Force distributions in three-dimensional granular assemblies: Effects of packing order and interparticle friction, *Physical Review E*, **63**, pp. 041304.

Bower, C., O. Zhou, et al. (2000). Nucleation and growth of carbon nanotubes by microwave plasma chemical vapor deposition. *Applied Physics Letters,* **77**, 17, pp. 2767-2769.

Bower, C., W. Zhu, et al. (2000). Plasma-induced alignment of carbon nanotubes. *Applied Physics Letters*, **77**, 6, pp. 830-832.

Bower, C., Zhu, W., Shalom, D., Lopez, D., Chen, L.H., Gammel, P.L. and Jin S. (2002). On-chip vacuum microtriode using carbon nanotube field emitters, *Applied Physics Letters*, **80**, pp. 3820-3822.

Bulgakov, A. A. and Timchenko, A.I. (1984). Propagating of shear acoustic waves in an active periodic structure. *Akusticheskii Zhurnal* **30**, pp. 23-27.

Cao, A., Dickrell, P.L., Sawyer, W.G., Ghasemi-Nejad, M.N., Ajayan, P.M. (2005). Super-Compressible Foamlike Carbon Nanotube Films , *Science*, **310**, pp. 1307-1310.

Carter, W.J. and Marsh, S.P. (1995). Hugoniot Equation of State of Polymers, *Los Alamos Preprint,* LA-13006-MS.

Chan, S.-P., W.-L. Yim, et al. (2003). Carbon Nanotube bundles under high pressure: Transformation to Low-Symmetry Structures. *Physical Review B*, **68**, pp. 075404-1.

Chatterjee, A. (1999). An Asymptotic solution for solitary waves in a chain of elastic spheres. *Physical Review B,* **59**, pp. 5912-5919.

Chen, L.V. (2006). *Advances in Soliton Research.* Nova Science Publishers, Inc., Hauppauge NY.

Chesnokov, S. A., V. A. Nalimova, et al. (1999). Mechanical Energy Storage in Carbon Nanotube Springs. *Physical Review Letters,* **82**, 2, pp. 343-346.

Collins, P.G., Hersam, M., Arnold,M., Martel, R. & Avouris, P. (2001). Current saturation and electrical breakdown in mutiwalled carbon nanotubes. *Physical Review Letters,* **86**, pp. 3128-3131.

Corwin, E.I., Jaeger, H.M. and Nagel, S.R. (2005). Structural signature of jamming in granular media, *Nature*, **435**, pp. 1075-1078.

Coste, C., Falcon, E., and Fauve, S. (1997). Solitary waves in a chain of beads under Hertz contact. *Physical Review E*, **56**, pp. 6104-6117.

Coste, C., and Gilles, B. (1999). On the validity of Hertz contact law for granular material acoustics. *The European Physical Journal B*, **7**, pp. 155-168.

Crespi, V. H., Chopra, N. G., Cohen, M. L., Zettl, A. & Louie, S. G. (1996). Anisotropic electron-beam damage and the collapse of carbon nanotubes. *Physical Review B*, **54**, pp. 5927-5931.

Csontos, D. & Xu, H. Q. (2003). Quantum effects in the transport properties of nanoelectronic three-terminal Y-junction devices. *Physical Review B*, **67**, pp. 235322.

Dash, P.C., and Patnaik, K. (1981). Solitons in nonlinear diatomic lattices. *Progress in Theoretical Physics,* **65**, pp. 526-541.

Daraio, C.; Nesterenko, V.F.; Jin, S. (2003). Strongly nonlinear waves in 3D phononic crystals, *APS - Shock Compression of Condensed Matter*, AIP Conference Proceedings, Portland (OR), pp. 197-200.

Daraio, C.; Nesterenko, V. F.; Aubuchon, J. F.; Jin, S. (2004). Dynamic Nanofragmentation of Carbon Nanotubes. *Nano Letters*; **4**, 10, pp. 1915-1918.

Daraio, C.; Nesterenko, V. F.; Jin, S. (2004). Highly Nonlinear Contact Interaction and Dynamic Energy Dissipation by Forest of Carbon Nanotubes. *Applied Physics Letters,* **85**, 23, pp. 5724-5726.

Daraio, C.; Nesterenko, V.F.; Herbold, E.; Jin, S. (2005). Strongly nonlinear waves in a chain of Teflon beads. *Physical Review E*; **72**, pp. 016603.

Daraio, C.; Nesterenko, V.F.; Herbold, E.; Jin, S. (2006). Energy Trapping and Shock Disintegration in a Composite Granular Medium. *Physical Review Letters*; **96**, pp. 058002.

Daraio, C.; Nesterenko, V.F.; Herbold, E.; Jin, S. (2006). Tunability of solitary wave properties in one dimensional strongly nonlinear phononic crystals. *Physical Review E*; **73**, pp. 026610.

Daraio, C.; Nesterenko, V.F. (2006). Strongly nonlinear waves in a chain of polymer coated steel beads. *Physical Review E*; **73**, pp. 026612.

Daraio, C. and Nesterenko, V.F. (2006). Strongly nonlinear wave propagation in two-dimensional force chains (in progress).

Daraio, C.; Nesterenko, V.F.; Rao, A. M.; Jin, S. (2006). Impact Response by a Forest of Coiled Carbon Nanotubes (submitted).

Daraio, C.; Nesterenko, V.F.; Herbold, E.; Jin, S. (2006). Pulse mitigation by a composite discrete medium. *Journal De Physique IV*, Proceedings DYMAT 2006, Dijon, France (Submitted).

Daraio, C.; Nesterenko, V.F.; Herbold, E.; Jin, S. (2006). Strongly nonlinear waves in polymer based phononic crystals. *APS – Shock Compression of Condensed Matter, AIP Conference Proceedings*, Baltimore (MD), (in press).

Dinda, T. P. and E. Coquet, E. (1990). Periodic structures in a one-dimensional non-linear lattice. *Journal of Physics: Condensed Matter*, **2**, pp. 6953-6963.

DuPont Product Information (2006). Comparison of Different DuPont Fluoropolymers, www.dupont.com/teflon/chemical/.

Ehrenstein, G.W. (2001). Polymeric materials: structure, properties, applications. Munich: Hanser Publishers; Cincinnati, Ohio: Hanser Gardner Publications, pp. 256.

Falvo, M.R., Clary, G. J., Taylor, R.M., Chi, V., Brooks, F. P., Washburn S. and Superfine R. (1997). Bending and buckling of carbon nanotubes under large strain, *Nature* **389**, pp. 582-584.

Fermi, E., Pasta, J.R. and Ulam, S.M. (1965). Studies of Non-Linear Problems. *Technical Report. LA-1940, Los Alamos National Laboratory.* Reprinted in Collected Works of E. Fermi, vol. II. University of Chicago Press, pp. 978-988.

Forro, L. & Schonenberger, C. (2001) in Carbon Nanotubes-Topics in Applied Physics (ed. Avouris, P.) (Springer, Heidelberg, 2001).

Friesecke, G., and Wattis, J.A.D. (1994). Existence theorem for solitary waves on lattices. *Communications in Mathematical Physics*, **161**, pp. 391-418.

Fung, Y.C. (1965). Fundations of Solid Mechanics, Englewood Cliffs, New Jersey: Prentice-Hall.

Gardner, C.S., Greene, J.M., Kruskal, M.D. and Miura, R.M. (1967). Method for solving the Korteweg de Vries equation. *Physical Review Letters,* **19**, pp. 1095-1097.

Gao, H. J., Kong, Y., Cui, D. X. & Ozkan, C. S. (2003). Spontaneous Insertion of DNA Oligonucleotides into Carbon Nanotubes, *Nano Letters*, **3**, 471-473.

Gavrilyuk, S.L. and Nesterenko, V.F. (1993). Stability of periodic excitations for one model of "sonic vacuum". *Prikl. Mekh. Tekh. Fiz.* **6**, pp. 45, 1993 [*Journal of Applied Mechanics and Technical Physics (JAM),* **6**, pp. 784, 1993].

Gere, J. M. & Timoshenko, S. P. (1990). PWS-KENT Publishing Company, Boston, pp. 577

Gibson, L.J. and Ashby, M.F. (1998). *Cellular Solids* (ed. O. Pergamon Press).

Gilles, B., and Coste, C. (2001). Nonlinear elasticity of a 2-D regular array of beads. *Powders and Grains,* Proceedings of the Fourth International Conference on Micromechanics of Granular Media, Sendai, 21 - 25 May.

Goffaux, C. and Vigneron, J.P. (2001). Theoretical study of a tunable phononic band gap system. *Physical Review B* (Condensed Matter and Materials Physics, **64**, pp. 075118/1-5.

Goldenberg, C. and Goldhirsch, I. (2005). Friction enhances elasticity in granular solids, *Nature*, **435**, pp. 188-191.

Gondret, P. Lance, M. Petit, L. (2002). Bouncing motion of spherical particles in fluids. *Physics of Fluids*, **14**, 2, pp. 643-652.

Gopal, V. et al. (2004). Rapid prototyping of site-specific nanocontacts by electron and ion beam assisted direct-write nanolithography. *Nano Letters,* **4**, pp. 2059-2063.

Gothard, N., Daraio, C. et al. (2004). Controlled growth of Y-junction nanotubes using Ti-doped vapor catalyst. *Nano Letters*, **4**, pp. 213-217.

Hascoët, E. and Herrmann, H.J. (2000). Shocks in non-loaded bead chains with impurities. *The European Physical Journal B*, **14**, pp. 183-190.

Heinze, S. et al. (2002). Carbon nanotubes as Schottky barrier transistors. *Physical Review Letters,* **89**, pp. 106801.

Herbold, E.B.; Nesterenko, V. F.; Daraio, C. (2006). Influence of Controlled Viscous Dissipation on the Propagation of Strongly Nonlinear Waves in Stainless Steel Based Phononic Crystals *APS - Shock Compression of Condensed Matter, AIP Conference Proceedings*, Baltimore (MD), (in press).

Hertz, H. (1881). *Journal fur Die Reine und Angewandie Mathematic,* **92**, pp. 156-171.

Hinch, E.J., and Saint-Jean, S. (1999). The Fragmentation of a line of balls by an impact. *Proceedings or the Royal Society of London A*, **455**, pp. 3201-3220.

Hong, J.B. Ji, J.-Y. and Kim, H. (1999). Power Laws in Nonlinear Granular Chain under Gravity. *Physical Review Letters*, **82**, pp. 3058-3061.

Hong, J.B. and Xu, A.G. (2001). Effects of gravity and nonlinearity on the waves in the granular chain, *Physical Review* E, **63**, pp. 061310.

Hong, J.B. (2005). Universal Power-Law Decay of the Impulse Energy in Granular Protectors. *Physical Review Letters,* **94**, pp. 108001.

Hou, P., Gong, Y. (2001). Detecting nonlinearity in the radiated noise of underwater targets. *Acta Acustica*, **26**, pp. 135-139.

Iijima, S. (1991). Helical microtubules of graphitic carbon, *Nature*, **354**, pp. 56-58.

Iijima, S., Brabec, C., Maiti A. and Bernholc, J. (1996). Structural flexibility of carbon nanotubes, *Journal of Chemical Physics*, **104**, pp. 2089-2092.

Javey, A., Guo, J.,Wang, Q., Lundstrom, M. & Dai, H. (2003). Ballistic carbon nanotube field-effect transistors. *Nature,* **424**, pp. 654-657.

Jia, Z. J., Wang, Z. Y., Liang, J., Wei, B. Q. & Wu, D. H. (1999). Production of short multi-walled carbon nanotubes, *Carbon*, **37**, pp. 903-906.

Jin, S., Mavoori, H., Espindola, R. P., and Strasser, T. A. (1999). Broad-Range latchable reconfiguration of bragg wavelength in optical gratings. *Applied Physics Letters 74,* pp. 2259-2261.

Jin, S., Espindola, R. P., Mavoori, H., Strasser, T. A. and DeMarco, J. J. (1998) Magnetically programmable fiber Bragg gratings. *Electron. Lett.,* **34***,* pp. 2158-2159.

Jin, S., Sherwood, R.C., Mottine, J.J., Tiefel, T.H., Opila, R.L., and Fulton, J.A., (1988). Z-Direction anisotropically conductive composites. *Journal of Applied Physics*, **64**, pp. 6008-6010.

Jin, S., Tiefel, T.H., Wolfe, R., Sherwood, R.C., and Mottine, J.J.(1992). Optically transparent, electrically conductive composite medium. *Science*, **255**, pp. 446-448.

Jin, S., Tiefel, T.H., Wolfe, R., Chen, L-H., and Dahringer, D.W. (1993). Anisotropically conductive Polymer Films with a uniform dispersion of particles. *IEEE Transactions on Components, Hybrids, and Manufacturing Technology*, **16**, pp. 972-977.

Jin, S., and McCormack, M. (1994). Dispersoid additions to a Pb-free solder for suppression of microstructural coarsening, *Journal of Electronic Materials*, **23**, pp. 735-739.

Job, S., Melo, F., Sen S. and Sokolow, A. (2005). How Hertzian Solitary Waves Interact with Boundaries in a 1D Granular Medium, *Physical Review Letters*, **94**, pp. 178002.

Johnson, K.L. (1985). *Contact Mechanics* (Cambridge University Press).

Kasman, A. (2006) *The History and Significance of the KdV Equation*, web publication http://math.cofc.edu/kasman/SOLITONPICS/kdv.html

Kastner, M. (2004). Energy Thresholds for Discrete Breathers, *Physical Review Letters*, **92**, pp. 104301.

Kastner, M.(2004). Dimension dependent energy thresholds for discrete Breathers, *Nonlinearity,* **17**, pp. 1923-1939.

Kafesaki, M., Sigalas, M. M., and Garcia, N. (2000). Frequency modulation in the transmittivity of wave guides in elasticwave band-gap materials. *Physical Review Letters*, **85,** pp. 4044-4047.

Kim, P., Shi, L.,Majumdar, A. & McEuen, P. L. (2001). Thermal transport measurements of individual multiwalled nanotubes. *Physical Review Letters,* **87**, pp. 215502

Kinra, V. K. and Ker, E. L.(1983). An experimental investigation of pass bands and stop bands in two periodic particulate composites. *International Journal of Solids and Structures*, **19,** pp. 393-410.

Korteweg, D.J., and de Vries, G. (1895). On the change of form of long waves advancing in a rectangular canal, and on a New type of long stationary Waves. *London, Edinburgh and Dublin Philosophical Magazine and Journal of Science*, ser. 5, **39**, pp. 422-443.

Lambert, R. F. and Tesar, J.S. (1984). Acoustic structure and propagation in highly porous, layered, fibrous materials. *Journal of the Acoustical Society of America,* **76**, pp. 1231-1237.

Landau, L.D., and Lifshitz E.M. (1995)., *Theory of Elasticity.* Translated from Russian by J.B. Sykes and W.H. Reid, 3rd English ed. Revised and enlarged by E.M. Lifshitz, A.M. Kosevich, and L.P. Pitaevskii. Butterworth, Oxford; Heinemann, Boston.

Lazaridi, A.N., and Nesterenko, V.F. (1985). Observation of a new type of solitary waves in a one-dimensional granular medium. *Journal of Applied Mechanics and Technical Physics (JAM),* **26, 3**, pp. 405-408.

Li, W. Z.,Wen, J.G. & Ren, Z. F. (2001). Straight carbon nanotube Y junctions. *Applied Physics Letters,* **79**, pp. 1879-1881.

Lian-Jie, H. and Mora, P. (1994). The phononic lattice solid with fluids for modelling non-linear solid-fluid interactions. *Geophysical Journal International,* **117**, pp. 529-538.

Lisina, S.A., Potapov, A.I., and Nesterenko, V.F. (2001). A Nonlinear granular medium with particle rotation: A onedimensional Model, *Acoustical Physics,* **47**, pp. 598-606.

Liu, Z., Zhang, X., Mao, Y., Zhu, Y., Yang, Z., Chan, C., and Sheng, P. (2000). Locally resonant sonic materials, *Science*, **289**, pp. 1734-1736.

Majmudar, T.S. and Behringer, R.P. (2005). Contact force measurements and stress-induced anisotropy in granular materials, *Nature*, **435**, pp. 1079-1082.

Manciu, M., Sen, S., and Hurd, A.J. (1999). The propagation and backscattering of soliton-like pulses in a chain of quartz beads and related problems (I). Propagation. *Physica A,* **274**, pp. 588-606.

Manciu, M., Sen, S., and Hurd, A.J. (1999). The propagation and backscattering of soliton-like pulses in a chain of quartz beads and related problems. (II). Backscattering *Physica A,* **274**, pp. 607-618.

Manciu, F.S., Manciu, M., and Sen, S. (2000). Possibility of controlled ejection of ferrofluid grains from a magnetically ordered ferrofluid using high frequency non-linear acoustic pulses. A particle dynamical study. *J. Magnetism and Magnetic Materials*, **220**, pp. 285-292.

Manciu, M., Sen, S. and Hurd, A.J. (2001). Impulse propagation in dissipative and disordered chains with power-law repulsive potentials. *Physica D*, **157**, pp.226-240.

Manciu, M., Sen, S. and Hurd, A.J. (2001). Crossing of identical solitary waves in a chain of elastic beads. *Physical Review E,* **63**, pp. 016614.

Manciu, F.S.and Sen, S. (2002). Secondary solitary wave formation in systems with generalized Hertz interactions, *Physical Review E*, **66**, pp. 016616-1-11.

Martel, R., Schmidt, T., Shea, H. R., Hertel, T. & Avouris, P. (1998). Single- and multi-wall carbon nanotube field-effect transistors. *Applied Physics Letters*, **73**, pp. 2447–2449.

Merkulov, V. I., Melechko, A. V., Guillorn, M. A., Lowndes, D. H. & Simpson, M. L. (2001). Alignment mechanism of carbon nanofibers produced by plasma-enhanced chemical-vapor deposition, *Applied Physics Letters*, **79**, pp. 2970-2972.

Monthioux, M. et al. (2001). Sensitivity of single-wall carbon nanotubes to chemical processing: an electron microscopy investigation, *Carbon,* **39**, pp. 1251-1272.

Musienko, A.I., Manevich, L.I. (2004). Classical mechanical analogs of relativistic effects, *Physics*-Uspekhi **47**, pp. 797.

Nesterenko, V.F., (1984). Propagation of nonlinear compression pulses in granular media. *Prikl. Mekh. Tekh. Fiz.* **5**, 136, 1983 and *Journal of Applied Mechanics and Technical Physics (JAM),* **24**, pp. 733-743.

Nesterenko, V.F. (1992). *High-Rate Deformation of Heterogeneous Materials*. Nauka, Novosibirsk, Ch. 2, pp. 51-80 (in Russian).

Nesterenko, V.F., (1994). Solitary waves in discrete media with anomalous compressibility and similar to Sonic Vacuum, *Journal De Physique IV,* Colloque C8, supplement au *Journal de Physique III*, **4**, pp. C8-72-C8-734.

Nesterenko, V.F., (1995). Continuous approximation for wave perturbations in a nonlinear discrete medium. *Explosion, Combustion and Shock Waves,* **31**, pp. 116-119.

Nesterenko, V.F., Lazaridi, A.N., and Sibiryakov, E.B. (1995). The decay of soliton at the contact of two Acoustic Vacuums. *Journal of Applied Mechanics and Technical Physics (JAM),* **36**, pp. 166-168.

Nesterenko, V.F. (2000). Solitons, Shock waves in strongly nonlinear particulate media. In: *Shock Compression of Condensed Matter.1999* (Edited by M.D. Furnish, L.C. Chabildas, and R.S. Hixson). AIP, New York, pp. 177-180.

Nesterenko, V.F., Indrakanti, S.S., Brar, S and Gu, Y. (2000). Ballistic performance of hot isostatically pressed (Hiped) Ti-based targets, in *Key Engineering Materials*, Trans Tech Publications Ltd. Switzerland**,** 177-180, pp. 243-248.

Nesterenko, V.F., Indrakanti, S.S., Brar, S and Gu, Y. (2000). Long rod penetration test of hot isostatically pressed Ti-based targets, in *Shock Compression of Condensed Matter-1999*, Edited by M.D. Furnish, L.C. Chabildas, and R.S. Hixson, AIP, pp. 419-422.

Nesterenko, V.F. (2001). New wave dynamics in granular state. In: *Granular State, Materials Research Society Symposium Proceedings* (Edited by S.Sen and M.L. Hunt). Materials Research Society, Warrendale, Pennsylvania, pp. BB3.1.1-BB.3.1.12.

Nesterenko, V.F. (2001). *Dynamics of heterogeneous materials*, Springer-Verlag, NY, Chapter 1.

Nesterenko, V.F. (2003). Shock (Blast) Mitigation by "Soft" Condensed Matter in "Granular Material-Based Technologies", MRS Symp. Proc., 729 (MRS, Pittsburgh, PA), pp. MM4.3.1- 4.3.12.

Nesterenko, V.F.; Daraio, C.; Herbold, E.B.; Jin, S. (2005). Anomalous wave reflection at the interface of two strongly nonlinear granular media, *Physical Review Letters*, **95**, pp. 158702.

Ostrovskii, L.A. (1963). Electromagnetic waves in nonlinear media with dispersion, *Zh. Tek. Fiz.*, **33**, pp. 905-908. [(1964) *Sov. Phys. Thech. Phys.* **8**, pp. 679-681].

Ozaki, T., Iwasa, Y. and Mitani, T. (2000). Stiffness of Single-Walled Carbon Nanotubes under Large Strain. *Physical Review Letters,* **84**, pp. 1712-1715.

Page, J. H. and McCulloch, R.D. (1986). Ultrasound propagation in sintered metal powder: Evidence for a crossover from phonons to fractons. *Physical Review Letters* **57**, pp. 1324-1327.

Palm, T. & Thylen, L. (1996). Designing logic functions using an electron waveguide Y-branch switch. *Journal of Applied Physics*, **79**, pp. 8076-8081.

Pantano, A., Parks D.M. and Boyce, M.C. (2004). Mechanics of deformation of single- and multi-wall carbon nanotubes, *Journal of the Mechanics and Physics of Solids,* **52**, pp. 789-821.

Papadapoulos, C., Rakitin, A., Li, J., Vedeneev, A. S. & Xu, J. M. (2000). Electronic transport in Y-junction carbon nanotubes. *Physical Review Letters,* **85**, pp. 3476-3479.

Parmley, S., Zobrist, T., Clough, T., Perez-Miller, A., Makela, M, and Yu, R. (1995). Phononic band structure in a mass chain. *Applied Physics Letters* **67**, pp. 777-779.

Peters, M. J., McNeil, L. E., et al. (1999). Structural phase transition in carbon nanotube bundles under pressure. *Physical Review B*, **61**, 9, pp. 5939-5944.

Postma, H.W. C., Teepen, T., Yao, Z., Grifoni, M. & Dekker, C. (2001). Carbon nanotube single-electron transistors at room temperature. *Science,* **293**, pp. 76-79.

Qi, H. J., K. B. K. Teo, et al. (2003). Determination of mechanical properties of carbon nanotubes and vertically aligned carbon nanotube forests using nanoindentation. *Journal of the Mechanics and Physics of Solids* **51**, 11-12, pp. 2213-2237.

Rao, A.M., Jacques, D., Haddon, R.C., Zhu, W., Bower, C., Jin, S. (2000). *Applied Physics Letters*, In situ-grown carbon nanotube array with excellent field emission characteristics, **76**, pp. 3813-3815.

Reigada, R., Samiento, A. and Lindenberg, K. (2003). Breathers and thermal relaxation in Fermi–Pasta–Ulam arrays, *Chaos*, **13**, 2, pp. 646-656.

Remoissenet, M. (1999). *Waves called solitons (Concepts and Experiments)*. 3rd revised and enlarged edition. Springer-Verlag, Berlin.

Ren, Z.F., Huang, Z.P., Xu, J.W., Wang, J. H., Bush, P., Siegal, M.P., Provencio, P.N. (1998). Synthesis of Large Arrays of Well-Aligned Carbon Nanotubes on Glass *Science*, **282**, pp. 1105-1107.

Rice, H. J., Torrance, and Eikelman, G. A.(1998). A model of stiffness non-linearity in fibrous material dynamics. *Journal of Sound and Vibration,* **212**, pp. 375-381.

Rosas, A. and Lindenberg, K. (2003). Pulse dynamics in a chain of granules with friction, *Physical Review E,* **68**, pp. 041304.

Rosas, A. and Lindenberg, K. (2004). Pulse velocity in a granular chain. *Physical Review E*, **69**, pp. 037601.

Ru, C.Q. (2000). Effective bending stiffness of carbon nanotubes, *Physical Review B*, **62**, pp. 9973-9976.

Russel, J.S. (1844). Report on Waves, *Report of the 14th Meeting of the British Association for the Advancement of Science,* York, pp. 311.

Sadeghipour, K., Chen, W., Baran, G. (1994). Spherical micro-indentation process of polymer based materials: a finite element study. *Journal of Physics D: Applied Physics,* **27**, pp. 1300.

Saito, R., Dresselhaus, G. & Dresselhaus, M. S. (1998) Physical Properties of Carbon Nanotubes (Imperial College Press, London, 1998).

Satishkumar, B. C., Thomas, P. J., Govindaraj, A. & Rao, C. N. R. (2000). Y-junction carbon nanotubes. *Applied Physics Letters*. **77**, pp. 2530-2532.

Sen, S., Manciu, M., and Wright, J.D. (1998). Solitonlike pulses in perturbed and driven Hertzian chains and their possible applications in detecting buried impurities. *Physical Review E,* **57**, pp. 2386-2397.

Sen, S., Manciu, M., and Manciu, F.S. (1999). Ejection of ferrofluid grains using nonlinear acoustic impulses.a particle dynamical study. *Applied Physics Letters,* **75**, pp. 1479-1481.

Sen, S., and Manciu, M. (1999). Discrete Hertzian chains and solitons. *Physica A,* **268**, pp. 644-649.

Sen, S. and Manciu, M.(2001). Solitary wave dynamics in generalized Hertz chains: An improved solution of the equation of motion, *Physical Review E*, **64**, pp. 056605.

Sen, S., Manciu, M. Sinkovits, R.S. and Hurd, A.J. (2001). Nonlinear acoustics in granular assemblies *Granular Matter,* **3**, pp. 33-39.

Sen, S., Chakravarti, S., Visco, D.P., Wu, D.T., Nakagawa, M., and Agui, J.H. Jr. (2003). Modern Challenges in Statistical Mechanics, edited by V.M. Kenkre and K.Lindenberg, *AIP Conf. Proc.* No. **658** (AIP, Melville, NY, 2003), pp. 357.

Shih, C.S., Harder, T.A., Tai, Y.C. (2004). Yield strength of thin-film parylene-C, *Microsystem Technologies,* **10**, pp. 407-411.

Shorubalko, I. et al. (2002). A novel frequency-multiplication device based on three-terminal ballistic junction. *IEEE Electron Device Letters,* **23**, pp. 377-379.

Shorubalko, I., Xu, H. Q., Omling, P. & Samuelson, L. (2003). Tunable nonlinear current-voltage characteristics of three-terminal ballistic nanojunctions. *Applied Physics Letters*, **83**, pp. 2369-2371.

Shukla, A., Sadd, M.H., Xu, Y., and Tai, Q.M. (1993). Influence of loading pulse duration on dynamic load transfer in a simulated granular medium. *Journal of the Mechanics and Physics of Solids*, **41**, pp. 1795-1808.

Sinkovits, R.S., and Sen, S. (1996). Sound propagation in impure granular columns. *Physical Review E,* **54**, pp. 6857-6865.

Sokolow, A., Bittle, E.G. and Sen, S. (2005). (Submitted to Phys. Rev. E).

Song, A. M. et al. (1998). Nonlinear electron transport in an asymmetric microjunction: A ballistic rectifier. *Physical Review Letters*, **80**, pp. 3831-3834.

Tans, S. J., Verschueren, A. R.M.&Dekker, C. (1998). Room-temperature transistor based on a single carbon nanotube. *Nature* **393**, pp. 49-52.

Teo, K. B. K. et al. (2001). Uniform patterned growth of carbon nanotubes without surface carbon, *Applied Physics Letters*, **79**, pp. 1534-1536.

Tian, W. et al. (1998). Conductance spectra of molecular wires. *Journal of Chemical Physics,* **109**, pp. 2874-2882.

Timoshenko S.P. and Goodier J.N. (1987). *Theory of Elasticity*, 3rd ed. McGraw-Hill, New York, pp. 414.

Tournat, V., Gusev, V.E., Castagnede, B. (2004). Subharmonics and noise excitation in transmission of acoustic wave through unconsolidated granular medium, *Physics Letters A*, **326**, pp. 340-348.

Vasseur, J. O. and Deymier, P. A. (1997). Propagation of acoustic waves in periodic and random two-dimensional composite media. *Journal of Materials Research* **12**, pp. 2207-2212.

Vergara, L. (2005). Scattering of Solitary Waves from Interfaces in Granular Media, *Physical Review Letters*, **95**, pp. 108002.

Wang W. and Rao, A.M. (2005). Bulk Synthesis of Helical Coiled Carbon Nanostructures, *MRS Conference proceedings*, 2004 Fall meeting, Symposium HH Functional Carbon Nanotubes, Editors: D.L. Carroll, B. Weisman, S. Roth, A. Rubio, **858E**, pp. HH.2.8.1-6.

Wei, C., K. Cho, et al. (2003). Tensile Yielding of Multiwall Carbon Nanotubes. *Applied Physics Letters,* **82**, 15, pp. 2512-2514.

Wright, T.W. (1984).Weak shocks and steady waves in a nonlinear elastic rod or granular material. *Int. J. Solids Structures*, pp. 911-919.

Xu, H. Q. (2001). Electrical properties of three-terminal ballistic junctions. *Applied Physics Letters*. **78**, pp. 2064-2066.

Xu, H. Q. et al. (2004). Novel nanoelectronic triodes and logic devices with TBJs. IEEE *Electron Device Letters*, **25**, pp. 164-166.

Yakobson, B.I., Brabec C.J. and Bernholc, J. (1996). Nanomechanics of Carbon Tubes: Instabilities beyond Linear Response, *Physical Review Letters,* **76**, pp. 2511-2514.

Yakobson, B.I. ,Campbell, M.P., Brabec, C.J., Bernholc, J. (1997). High strain rate fracture and C-chain unraveling in carbon nanotubes. *Computational Materials Science*, **8**, pp. 341-348.

Yakobson, B. I. (1998). "Mechanical relaxation and "intramolecular plasticity" in carbon nanotubes." *Applied Physics Letters,* **72**, 8, pp. 918-920.

Yang, S., Page, J. H., Liu, Z., Cowan, M.L., Chan, C.T., Sheng, P. (2002). Ultrasound tunneling through 3D phononic crystals. *Physical Review Letters*, **88**, pp.104301/1-4.

Zabusky, N. and Kruskal, M. (1965). Interaction of solitons in a collisionless plasma and the recurrence of initial states. *Physical Review Letters*, **15**, pp. 240-143.

Zakharov, V.E. (1968). Stability of periodic waves of finite amplitude on the surface of a deep fluid. *Journal of Applied Mechanics and Technical Physics (JAM),* **9**, pp. 86-94.

Zerilli, F.J. and Armstrong, R.W. (2002). Thermal activation constitutive model for polymers applied to plytetrafluoroethylene, CP620, *Shock Compression of Condensed Matter,* CP620, Edited by M.D. Furnish, N.N. Thadhani and Y. Horie, pp. 657-660.

Zhou, D. & Seraphin, S. (1995) Complex branching phenomena in the growth of carbon nanotubes. *Chemical Physics Letters,* **238**, pp. 286-289.

Zhu, Y., Shukla, A., and Sadd, M.H. (1996). The effect of microstructural fabric on dynamic load transfer in twodimensional assemblies of elliptical particles. *Journal of the Mechanics and Physics of Solids*, **44**, pp. 1283-1303.

Zhu, Y., Sienkiewicz, F., Shukla, A., Sadd, M. (1997). Propagation of Explosive Pulses in Assemblies of Disks and Spheres, *Journal of Engineering Mechanics*, **123,** 10, pp. 1050-1059.

Zvezdin, A. K. and Popkov (1983). On the nonlinear theory of magnetostatic spin waves, *Sov. Phys. JETP*, **57**, pp. 350-362.